Award Number: W81XWH-12-1-0255

TITLE: Genetic Networks Activated by Blast Injury to the Eye

PRINCIPAL INVESTIGATOR: Eldon E. Geisert

CONTRACTING ORGANIZATION:
Emory University
Atlanta GA 30322

REPORT DATE: March 2018

TYPE OF REPORT: Final

PREPARED FOR: U.S. Army Medical Research and Materiel Command

Fort Detrick, Maryland, 21702-5012

REPORT DOCUMENTATION PAGE

Form Approved
OMB No. 0704-0188

1. REPORT DATE	2. REPORT TYPE	3. DATES COVERED
March 2018	Final	15Jul2012 - 14Dec2017

4. TITLE AND SUBTITLE
Genetic Networks Activated by Blast Injury to the Eye

5a. CONTRACT NUMBER

5b. GRANT NUMBER
W81XWH-12-1-0255

5c. PROGRAM ELEMENT NUMBER

6. AUTHOR(S)
Eldon E. Geisert

E-Mail: egeiser@emory.edu

5d. PROJECT NUMBER

5e. TASK NUMBER

5f. WORK UNIT NUMBER

7. PERFORMING ORGANIZATION NAME(S) AND ADDRESS(ES)
Department of Ophthalmology
Emory University
1365B Clifton Road NE
Atlanta, GA 30322

8. PERFORMING ORGANIZATION REPORT

9. SPONSORING / MONITORING AGENCY NAME(S) AND ADDRESS(ES)

U.S. Army Medical Research and Materiel Command
Fort Detrick, Maryland 21702-5012

10. SPONSOR/MONITOR'S ACRONYM(S)

11. SPONSOR/MONITOR'S REPORT NUMBER(S)

12. DISTRIBUTION / AVAILABILITY STATEMENT

Approved for Public Release; Distribution Unlimited

13. SUPPLEMENTARY NOTES

14. ABSTRACT

The present grant proposes to look at the effects of blast on the eye of the mouse looking at phenotypic changes in the eye and in the changes in gene expression following a 50psi blast. We are using these data to define biomarkers to predict the severity of the injury and to predict eventual outcomes. We have examined the phenotypic changes in the eye in the BXD strains before and 5 days after a 50psi blast and have observed no strain specific change in either the cornea or the IOP. We have completed the normal retina database containing 222 microarrays from 58 strains of mice. The data was presented in a publication in Molecular Vision. We have collected 213 retinas from 54 strains 5 days after a 50psi blast. The RNA from the retinas was processed and was run on microarray. The database is complete and the manuscript describing the results is published in Frontiers in Genetics. We have found two good markers for retinal injury: SOX11 involved in the abortive regeneration response and POU6F2 which marks reginal ganglion cells that are very susceptible to injury. We continue to examine the involvement of the immune system in the response of the retina to injury. The

15. SUBJECT TERMS

Nothing listed

16. SECURITY CLASSIFICATION OF:			17. LIMITATION OF ABSTRACT	18. NUMBER OF PAGES	19a. NAME OF RESPONSIBLE PERSON
a. REPORT	b. ABSTRACT	c. THIS PAGE			USAMRMC
Unclassified	Unclassified	Unclassified	UU	173	19b. TELEPHONE NUMBER *(include area code)*

Table of Contents

1. INTRODUCTION

In a collaboration with Dr. Tonia Rex we developed a mouse model of blast injury to the eye, which accurately mimics the traumatic blast injury increasingly suffered by warriors under current battlefield conditions (Hines-Beard et al., 2012). Using this mouse model in combination with a powerful combination of systems biology, microarray analysis, expression genetics, and bioinformatics, we are defining the genetic networks activated by the ocular blast injury. At the heart of our approach is a genetic reference panel of mice, the unique resource of BXD recombinant inbred (RI) strain set. The set of RI strains was produced from a genetic cross between the C57BL/6J mouse and the DBA/2J mouse. Using 60 BXD strains provides a new and powerful method to defining elements in the genome regulating the response of the eye to blast injury. This allows us to generate specific, testable hypotheses to define the pathways that regulate the response of the eye to blast injury and reactive responses in the retina. As more diverse gene expression data sets become available, comparison of gene expression and regulation in different biological contexts will help identify the regulatory elements controlling the injury response of the eye and the retina. We are have identified genetic networks activated by blast injury and the genomic regions controlling these networks. One of the key networks activated following blast injury involves the innate immune system. We have defined a number of markers for retinal injury and potential targets for therapeutic intervention, including two neuronal genes, Sox11 and Pou6f2.

2. KEY WORDS

Mouse Genomics, Blast Injury, Eye, Retina, Gene Expression, Microarray

3. ACCOMPLISHMENTS

Major Goals:

Task 1) Quantify the strain-to-strain differences in the severity of blast-induced ocular pathologies, using a set of 60 BXD RI mouse strains and map the genomic loci that regulate the response of the eye to blast injury. In this Task we were measuring intraocular pressure (IOP), central corneal thickness (CCT) and visual acuity.

Task 2) Define the genetic networks activated by blast injury in the eye and in the retina, using transcriptome-wide profiling across the BXD RI strain set. We are using the Affymetrix GeneChip Gene 2.0 ST Mouse Array to characterize the changes occurring following a blast injury to the eye in 60 BXD strains. There were several major benefits to using the new Affymetrix array. Specifically, there are probes for 7,000 non-coding RNAs (RNA that is not converted to protein but does affect the functioning of the cell). We are now finding out that many of these non-coding RNAs play extremely important roles in the body. Within these 7,000 probes, 588 encode microRNAs (small RNAs that regulate protein expression). We are creating an entire normal retina dataset using the Affymetrix GeneChip Gene 2.0 Mouse Array and comparing this data set to a dataset from retinas 5 days after a 50psi blast injury to the eye.

Task 3) Define biomarkers that can predict the severity of injury and eventual outcomes.

This portion of our study was to begin in the latter years of the grant (Months 40 to 48). We are using this to characterize the 50-psi blast injury in advance of resuming the blast microarray study on the BXD RI strain set. Immunostaining sections of retina revealed that SOX11 was upregulated in the neurons of the inner retina following blast. SOX11 labeled cells in the ganglion cell layer and the inner nuclear layer. In the ganglion cell layer SOX11 labeled a majority of the cells, indicating that it was labeling most ganglion cells and displaced amacrine cells. Once the datasets are fully implemented, we will be able to accurately define the changes occurring within the injured retina. In addition, we have found a second transcription factor, Pou6f2, that marks ganglion cells that are particularly susceptible to injury.

Accomplishments Under These Goals:

Task1:

We have measured IOP and central corneal thickness in over 50 strains of mice before and after a 50psi blast injury to the eye. When we run a student t test on the data there was no significant difference in CCT or IOP before and after blast in the control eyes. This is expected. We also did not see a significant difference in either CCT or IOP 5 days after a 50psi blast to the experimental eye. This is unexpected. The lack of corneal damage and changes in IOP may be directly related to the use of Avertin for anesthesia. Recent studies by the Anderson group (PMID: 26222692) reveal that the corneal damage that occurs following blast injury can be directly related to the use of Ketamine/Xylazine for anesthesia.

Task 2.

A) We have completed the construction of the DoD CDMRP Normal Retinal Dataset. Using the Affymetrix Mouse Gene 2.0 ST array and the Microarray data following a 50psi blast injury to the eye. The data bases interrogate all exons of traditional protein coding genes, non-coding RNAs and microRNAs. These data are presented in a highly interactive database within the GeneNetwork website. In the Normal Retina Database, we quantified mRNA levels of the transcriptome from retinas using the Affymetrix Mouse Gene 2.0 ST array. The Normal Retina Database consists of gene expression data from male and female mice. The dataset includes a total of 55 BXD RI strains, the parental strains (C57Bl/6J and DBA/2J), and a reciprocal cross. In combination with GeneNetwork, the DoD (Department of Defense) CDMRP (Congressionally Directed Medical Research Programs) Normal Retina Database provides a large resource for mapping, graphing, analyzing, and testing complex genetic networks. Protein-coding and non-coding RNAs can be used to map quantitative trait loci (QTLs) that contribute to expression differences among the BXD strains and to establish links between classical ocular phenotypes associated with differences in genomic sequence. With this resource we are able to extract transcriptome signatures for retinal cells and to define genetic networks associated with the maintenance of the normal retina. Ultimately, we will use this database to define changes occurring following blast injury to the retina. The DoD CDMRP Normal Retina Database uses the Affymetrix MouseGene 2.0 ST Array (May 15 2015). The RMA analysis and scaling was conducted by Arthur Centeno. This data set consists of 55 BXD strains, C57BL/6J, DBA/2J, an F1 cross between C57BL/6J and DBA/2J. A total of 58 strains were quantified. There is a total of 222 microarrays. All of the data from each of the microarrays used in this dataset is publically available on GeneNetwork.org.

Mice were killed by rapid cervical dislocation. Retinas were removed immediately and placed in 1 ml of 160 U/ml Ribolock for 1 min at room temperature. The retinas were removed from the eye and placed in Hank's Balanced Salt solution with RiboLock in 50µl RiboLock (Thermo Scientific RiboLock RNase #EO0381 40U/µl 2500U) and stored in -80°C. The RNA was isolated using a QiaCube. All RNA samples were checked for quality before running microarrays. The samples were analyzed using the Agilent 2100 Bioanalyzer. The RNA integrity values ranged from 7.0 to 10. Our goal was to obtain data for independent biological sample pools from both sexes for most lines of mice. The four batches of arrays included in this final data set collectively represent a reasonably well-balanced sample of males and females, in general without within-strain-by-sex replication.

The data is presented using the Affymetrix Mouse Gene 2.0 ST Array. These expression arrays have been designed with a median of 22 unique probes per transcript. Each unique probe is 25 bases in length, which means that the array measures a median of 550 bases per transcript. The arrays provide comprehensive transcriptome coverage with over 30,000 coding and non-coding transcripts. In addition, there is coverage for over 600 microRNAs. The dataset for the normal retina is DoD CDMRP Retina Affy MoGene 2.0

ST (May15) RMA Gene and Exon Level, and the dataset for the retina injured by blast is DoD TATRC Retina Blast Affy MoGene 2.0 ST RMA. Both sets of data are complete and open to the public on GeneNetwork.org.

Publication:

King R, Lu L, Williams RW and **Geisert EE**. Transcriptome networks in the mouse retina: an improved BXD RI database Molecular Vision 2015 21: 1235-1251. PMCID: PMC4626778

Felix L. Struebing, Richard K. Lee, Robert W. Williams and **Eldon E. Geisert**, Genetic Networks in Mouse Retinal Ganglion Cells. Frontiers in Genetics 2016 7:169-182. PMCID: PMC5039302

Struebing FL, King R, Li Y, Chrenek MA, Lyuboslavsky PN, Sidhu CS, Iuvone PM, **Geisert EE**, Transcriptional Changes in the Mouse Retina Following Ocular Blast Injury: A Role for the Immune System. J Neurotrauma 2017 [Epub ahead of print] PMID: 28599600

Task 3) We have identified a list of potential biomarkers for injury to the retinal ganglion cells Sox11 and Pou6f2. The best marker is SOX11 (manuscript being revised). We are using this to characterize the 50psi blast injury in advance of resuming the blast microarray study on the BXD RI strain set. Immunostaining sections of retina revealed that SOX11 was upregulated in the neurons of the inner retina following blast. SOX11 labeled cells in the ganglion cell layer and the inner nuclear layer. In the ganglion cell layer SOX11 labeled a majority of the cells, indicating that it was labeling most ganglion cells and displaced amacrine cells. Amacrine cells in the inner nuclear layer were also lightly labeled by SOX11. On immunoblots there was approximately a 2-fold increase in the intensity of the SOX11 band. The second marker, Pou6f2, identifies cells that are particularly susceptible to injury and represent an early marker for dying retinal ganglion cells.

Publication:

Felix L. Struebing1, Jiaxing Wang1, Ying Li1, Rebecca King1, Olivia C. Mistretta2, Arthur W. English2, **Eldon E. Geisert1** Differential Expression of Sox11 and Bdnf mRNA Isoforms in the Injured and Regenerating Nervous Systems. Frontiers in Molecular Neuroscience (2017) Nov 2; 10:354 PMID: 29209164.

Diana Zhou, Ye Lu, Rebecca King, Claire Simpson, Wenbo Zhang, Byron Jones, **Eldon E. Geisert**. Lu Lu, The genetic dissection of Myo7a gene expression in the retina of BXD mice. (2018) Mol. Vis (In Press)

Rebecca King, Felix L. Struebing, Ying Li, Jiaxing Wang, Allison Ashley Koch, Jessica Cooke Bailey, Puya Gharahkhani, International Glaucoma Genetics Consortium, NEIGHBORHOOD consortium, Stuart MacGregor, R. Rand Allingham, Michael A. Hauser, Janey L. Wiggs, and **Eldon E. Geisert**, Genomic Locus Modulating Corneal Thickness in the Mouse Identifies *POU6F2* as a Potential Risk of Developing Glaucoma. (2018) Plos Genetics PMID 29370175.

Struebing FL, R King, Y Li, J N Cooke Bailey, NEIGHBORHOOD consortium, J L Wiggs, and **E E Geisert**, Genomic loci modulating ganglion cell death following elevated IOP in the mouse. Exp. Eye Res. 2018 (In press).

Rebecca King, Ying Li, Jiaxing Wang, Felix L. Struebing and **Eldon E. Geisert** Genomic Locus Modulating IOP in the BXD RI Strains of Mice.
BioRxiv 202937; doi: https://doi.org/10.1101/202937

Felix L. Struebing, Steven G. Hart, and **Eldon E. Geisert** (2017) Upregulation of SOX11 in Retinal Ganglion Cells Following Injury. (In preparation).

Training and Professional Development Opportunities:

Nothing to Report

Dissemination of Results:

Meeting Presentations:

Hart, Steven G; Wang, XiangDi; Rex, Tonia S.; **Geisert, Eldon E**. Biomarkers for Neuronal Injury Following Blast Trauma to the Eye. Poster abstract submitted for the Association for Research in Vision and Ophthalmology (ARVO) Annual Meeting, May 5-9, 2013, Seattle, Washington.

Geisert E.E., Tonia S Rex, Ocular Blast Trauma in the DBA/2J Mouse, Poster abstract submitted for the Association for Research in Vision and Ophthalmology (ARVO) Annual Meeting, May 5-9, 2013, Seattle, Washington.

Geisert E.E., Joe Caron, XiangDi Wang, SOX11 Marks injured retinal ganglion cells. Association for Research in Vision and Ophthalmology (ARVO) Orlando Florida 2014.

Struebing FL, King R, Ashley-Koch AE, Hauser MA, Allingham RR, **Geisert EE**: "Interval mapping reveals a quantitative trait locus controlling retinal ganglion cell number in mice", The Association for Research in Vision and Ophthalmology (ARVO) annual meeting, Denver 2015.

Geisert EE, Struebing FL, King R, Pasquale LR, Ashley-Koch AE, Hauser MA, Allingham RR, Wiggs JL: "Genomic loci modulating ganglion cell death following elevated IOP in the mouse", The Association for Research in Vision and Ophthalmology (ARVO) annual meeting, Denver 2015.

Sidhu C, Lyuboslavsky P, Chrenek MA, Struebing FL, Sellers JT, Setterholm NA, McDonals FE, Boatright JH, **Geisert EE**, Iuvone PM: "Traumatic Blast-Induced Closed Globe Injury Reduces Visual Function in Retinal Ganglion Cells of Thy1-CFP mice: Mitigation by a Small Molecule TrkB Activator", The Association for Research in Vision and Ophthalmology (ARVO) annual meeting, Denver 2015.
King R., M.A. Hauser, L.R. Pasquale, J.L. Wiggs, A.A. Koch, R.R. Allingham and

Michael Iuvone, P., Lyuboslavsky, Polina, Sidhu, Curran, He, Li., Boatright, Jeffrey H. **Geisert, Eldon E**. Protection from blast-induced vision loss by the N-acetylserotonin derivative HIOC through a BDNF/TrkB receptor mechanism (ARVO) annual meeting, Seattle 2016.

Li, Ying, King, Rebecca, Struebing, Felix L., Iuvone, P. Michael, and **Geisert, Eldon E.** Activation of the immune system following blast injury to the eye (ARVO) annual meeting, Seattle 2016.

Iuvone P.M., Dhakal S., Lyuboslavsky P., He L., Struebing F.L., Boatright J.H., **Geisert E.E**., HIOC, a TrkB receptor activator, for the treatment of blast-induced vision loss. (ISER) Semiannual Meeting, Tokyo 2016

Geisert, Eldon, Li, Ying; King, Rebecca; Struebing, Felix L.; Iuvone, P. Michael Activation of the innate and acquired immune system following blast injury to the eye. (ISER) Semiannual Meeting, Tokyo 2016

P. Michael Iuvone, Susov Dhakal, Polina N. Lyuboslavksy, Li He, and **Eldon E. Geisert**, Loss of visual function following blast-induced ocular trauma and TBI: Protection by HIOC through a BDNF/TrkB receptor mechanism. 6th Military vision Symposium on Ocular and Vision Injury, March 2017 Boston, MA.

Struebing FL, and **E.E. Geisert**. Regulatory element networks underlying QTLs and disease loci: Towards a better understanding of non-coding variations in complex traits. Complex Trait Consortium, June 2017 Memphis TN.

Eldon E. Geisert, Rebecca King, Felix L. Struebing, Ying Li, Jiaxing Wang, Allison Ashley Koch, Jessica Cooke Bailey, Puya Gharahkhani, International Glaucoma Genetics Consortium, NEIGHBORHOOD consortium, Stuart MacGregor, R. Rand Allingham, Michael A. Hauser, and Janey L. Wiggs, Genomic locus modulating corneal thickness in the mouse identifies *Pou6f2* as a potential risk of developing glaucoma. ISER Glaucoma Meeting, Atlanta GA (2017).

Rebecca King, Ying Li, Jiaxing Wang, Felix L. Struebing, Janey L. Wiggs, and **Eldon E.**

Geisert. Genomic Locus Modulating IOP in the BXD RI Mouse Strains. ISER Glaucoma Meeting, Atlanta GA (2017).

Felix L. Struebing, Ying Li, Rebecca King, and **Eldon E. Geisert**. Genomic Loci Modulating Retinal Ganglion Cell Death Following Elevated IOP in the Mouse. ISER Glaucoma Meeting, Atlanta GA (2017).

Jiaxing Wang, Ying Li, Rebecca King, Felix L. Struebing and **Eldon E. Geisert.** Genomic modulation of optic nerve regeneration in mice. ISER Glaucoma Meeting, Atlanta GA (2017).

Ying Li, Felix L. Struebing, Rebecca King, Jiaxing Wang, **Eldon E. Geisert.** POU6F2 labels subset of retinal ganglion cells in mouse. ISER Glaucoma Meeting, Atlanta GA (2017).

Publication:

1. King R, Lu L, Williams RW and **Geisert EE**. Transcriptome networks in the mouse retina: an improved BXD RI database Molecular Vision (2015) 21: 1235-1251. PMCID: PMC4626778

2. Felix L. Struebing, Richard K. Lee, Robert W. Williams and **Eldon E. Geisert**, Genetic Networks in Mouse Retinal Ganglion Cells. Frontiers in Genetics (2016) 7:169-182. PMCID: PMC5039302

3. Struebing FL, King R, Li Y, Chrenek MA, Lyuboslavsky PN, Sidhu CS, Iuvone PM, **Geisert EE**, Transcriptional Changes in the Mouse Retina Following Ocular Blast Injury: A Role for the Immune System. J Neurotrauma (2017) [Epub ahead of print] PMID: 28599600

4. Felix L. Struebing1, Jiaxing Wang1, Ying Li1, Rebecca King1, Olivia C. Mistretta2, Arthur W. English2, **Eldon E. Geisert1** Differential Expression of Sox11 and Bdnf mRNA Isoforms in the Injured and Regenerating Nervous Systems. Frontiers in Molecular Neuroscience (2017) Nov 2; 10:354 PMID: 29209164.

5. Diana Zhou, Ye Lu, Rebecca King, Claire Simpson, Wenbo Zhang, Byron Jones, **Eldon E. Geisert**. Lu Lu, The genetic dissection of Myo7a gene expression in the retina of BXD mice. (2018) Mol. Vis (In Press)

6. Rebecca King, Felix L. Struebing, Ying Li, Jiaxing Wang, Allison Ashley Koch, Jessica Cooke Bailey, Puya Gharahkhani, International Glaucoma Genetics Consortium, NEIGHBORHOOD consortium, Stuart MacGregor, R. Rand Allingham, Michael A. Hauser, Janey L. Wiggs, and **Eldon E. Geisert**, Genomic Locus Modulating Corneal Thickness in the Mouse Identifies *POU6F2* as a Potential Risk of Developing Glaucoma. (2018) Plos Genetics PMID 29370175.

7. Struebing FL, R King, Y Li, J N Cooke Bailey, NEIGHBORHOOD consortium, J L Wiggs, and **E E Geisert**. Genomic loci modulating ganglion cell death following elevated IOP in the mouse. Exp. Eye Res. 2018 (In Press).

8. Jiaxing Wang, Ying Li, Rebecca King, Felix L. Struebing and **Eldon E. Geisert**. Optic Nerve Regeneration in the Mouse is a Complex Trait Modulated by Genetic Background. (2017) bioRxiv 204842; doi: https://doi.org/10.1101/204842.

9. Rebecca King, Ying Li, Jiaxing Wang, Felix L. Struebing and **Eldon E. Geisert** Genomic Locus Modulating IOP in the BXD RI Strains of Mice. (2017) bioRxiv 202937; doi: https://doi.org/10.1101/202937.

10. Felix L. Struebing, Steven G. Hart, and **Eldon E. Geisert** (2017) Upregulation of SOX11 in Retinal Ganglion Cells Following Injury. (In preparation).

Book Chapters:

HE Grossniklaus, **EE Geisert** and JM Nickerson (2015) Intorduction to the Retina. Prog. Mol Giol Transl Sci 134: 383-396.

FL Strubing and **EE Geisert** (2015) What Animal Models Can Tell Us About Glaucoma. Prog. Mol Giol Transl Sci 134: 365-380.

Invited Talks:

2013 An innate Immune Genetic Network Defined in the Mouse Retina: Relevance to CNS injury and Disease. Medical College of Georgia (Augusta), Center for Biotechnology and Genomic Medicine

2014 Genetic Network of Innate Immunity in the Retina: Relevance to CNS Injury and Alzheimer's Disease, Department of Neurology, Emory University Atlanta GA.

2014 Genetic Network of Innate Immunity in the Retina: Relevance to CNS Injury and Disease VA Atlanta GA.

2014 Genetic Network of Innate Immunity in the Retina: Relevance to CNS Injury and Disease Department of Molecular Physiology and Biophysics University of Iowa.

2015 Genetic Network Looking at Innate Immunity in the Retina: Relevance to CNS Injury and Alzheimer's Disease, Department of Cell Biology, Emory University Atlanta GA.

2015 Innate Immunity in the Retina: Relevance to CNS Injury and Alzheimer's Disease, Frontiers in Neuroscience Seminar Series, Emory University Atlanta GA.

2015 Innate Immunity in the Retina: Relevance to CNS Injury and Disease, Neurology Grand Rounds, Emory University Atlanta GA.

2015 Innate immunity in the Retina: Relevance to AMD and Glaucoma, University of North Texas Health Science Center Eye Research institute, Fort Worth TX.

2016 A systems Approach to Retinal Injury and Disease Using the BXD RI Mouse Strains and GeneNetwork. Department of Human Genetics, Emory University.

Website and Databases:

GeneNetwork

http://www.genenetwork.org/webqtl/main.py

Databases:

DoD Retina Normal Affy MoGene 2.0 ST (May15) RMA Gene Level
DoD Retina Normal Affy MoGene 2.0 ST (May15) RMA Exon Level
DoD Retina After Blast Affy MoGene 2.0 ST (Mar16) RMA Gene Level
DoD Retina Blast vs Normal Retina Affy MoGene 2.0 ST (Apr16) RMA Gene Level
DoD Retina After Blast Affy MoGene 2.0 ST (Mar16) RMA Exon Level

Plans for Next Reporting Period to Accomplish the Goals:

1) Prepare manuscript describing the Markers of Blast injury.

Press Releases:

EurekaAlert! AAAS: Study finds genetic link between thinner corneas and increased risk of glaucoma. January 25, 2018.

Science News: Genetic link between thinner corneas and increased risk of glaucoma. January 25, 2018.

ScienceDaily: Genetic link between thinner corneas and increased risk of glaucoma. January 25, 2018.

MedicalResearch.com: Genetic link between corneas and risk of glaucoma. January 25, 2018.

Business Standard: Thinner corneas linked to high risk of eye disease. January 26, 2018

EyeWireToday: Study Finds Genetic Link Between Thinner Corneas and Increased Risk of Glaucoma, January 26, 2018

4. IMPACT

Impact on the Development of the Principal Discipline of the Project:

Once the proposed studies are completed they will provide a comprehensive analysis of the molecular pathways activated in the retina by blast injury to the eye. Furthermore, we have identified two markers for retinal ganglion cell injury: Sox11 and Pou6f2. The POU6F2 positive retinal ganglion cells are particularly sensitive to injury including blast injury. This first paper is receiving a considerable amount of press (see above) and will hopefully stimulate interest in the molecular pathway responsible for this injury response.

Impact on Other Disciplines:

When developing Biomarkers for retinal injury, our microarray dataset will provide a means to determine if any specific biomarker could have originated from the retinal injury itself.

Impact on Society Beyond Science and Technology:

Nothing to Report

5) Changes/Problems

Changes in Approach and Reasons for Change:
None

Actual or Anticipated Problems or Delays and Actions or Plans to Resolve Them:
None

Changes that had Significant Impact on Expenditures:
None

Significant Changes in the Use or Care of Human Subjects Vertebrate Animals Biohazards, or Select Agents:
None

6. PRODUCTS

Conference Papers:

Hart, Steven G; Wang, XiangDi; Rex, Tonia S.; **Geisert, Eldon E**. Biomarkers for Neuronal Injury Following Blast Trauma to the Eye. Poster abstract submitted for the Association for Research in Vision and Ophthalmology (ARVO) Annual Meeting, May 5-9, 2013, Seattle, Washington.

Geisert E.E., Tonia S Rex, Ocular Blast Trauma in the DBA/2J Mouse, Poster abstract submitted for the Association for Research in Vision and Ophthalmology (ARVO) Annual Meeting, May 5-9, 2013, Seattle, Washington.

Geisert E.E., Joe Caron, XiangDi Wang, SOX11 Marks injured retinal ganglion cells. Association for Research in Vision and Ophthalmology (ARVO) Orlando Florida 2014.

Struebing FL, King R, Ashley-Koch AE, Hauser MA, Allingham RR, **Geisert EE**: "Interval mapping reveals a quantitative trait locus controlling retinal ganglion cell number in mice", The Association for Research in Vision and Ophthalmology (ARVO) annual meeting, Denver 2015.

Geisert EE, Struebing FL, King R, Pasquale LR, Ashley-Koch AE, Hauser MA, Allingham RR, Wiggs JL: "Genomic loci modulating ganglion cell death following elevated IOP in the mouse", The Association for Research in Vision and Ophthalmology (ARVO) annual meeting, Denver 2015.

Sidhu C, Lyuboslavsky P, Chrenek MA, Struebing FL, Sellers JT, Setterholm NA, McDonals FE, Boatright JH, **Geisert EE**, Iuvone PM: "Traumatic Blast-Induced Closed Globe Injury Reduces Visual Function in Retinal Ganglion Cells of Thy1-CFP mice: Mitigation by a Small Molecule TrkB Activator", The Association for Research in Vision and Ophthalmology (ARVO) annual meeting, Denver 2015.
King R., M.A. Hauser, L.R. Pasquale, J.L. Wiggs, A.A. Koch, R.R. Allingham and

Michael Iuvone, P., Lyuboslavsky, Polina, Sidhu, Curran, He, Li., Boatright, Jeffrey H. **Geisert, Eldon E**. Protection from blast-induced vision loss by the N-acetylserotonin derivative HIOC through a BDNF/TrkB receptor mechanism (ARVO) annual meeting, Seattle 2016.

Li, Ying, King, Rebecca, Struebing, Felix L., Iuvone, P. Michael, and **Geisert, Eldon E.** Activation of the immune system following blast injury to the eye (ARVO) annual meeting, Seattle 2016.

Iuvone P.M., Dhakal S., Lyuboslavsky P., He L., Struebing F.L., Boatright J.H., **Geisert E.E**., HIOC, a TrkB receptor activator, for the treatment of blast-induced vision loss. (ISER) Semiannual Meeting, Tokyo 2016

Geisert, Eldon, Li, Ying; King, Rebecca; Struebing, Felix L.; Iuvone, P. Michael Activation of the innate and acquired immune system following blast injury to the eye. (ISER) Semiannual Meeting, Tokyo 2016

P. Michael Iuvone, Susov Dhakal, Polina N. Lyuboslavksy, Li He, and **Eldon E. Geisert**, Loss of visual function following blast-induced ocular trauma and TBI: Protection by HIOC through a BDNF/TrkB receptor mechanism. 6th Military vision Symposium on Ocular and Vision Injury, March 2017 Boston, MA.

Struebing FL, and **E.E. Geisert**. Regulatory element networks underlying QTLs and disease loci: Towards a better understanding of non-coding variations in complex traits. Complex Trait Consortium, June 2017 Memphis TN.

Eldon E. Geisert, Rebecca King, Felix L. Struebing, Ying Li, Jiaxing Wang, Allison Ashley Koch, Jessica Cooke Bailey, Puya Gharahkhani, International Glaucoma Genetics Consortium, NEIGHBORHOOD consortium, Stuart MacGregor, R. Rand Allingham, Michael A. Hauser, and Janey L. Wiggs, Genomic locus modulating corneal thickness in the mouse identifies *Pou6f2* as a potential risk of developing glaucoma. ISER Glaucoma Meeting, Atlanta GA (2017).

Rebecca King, Ying Li, Jiaxing Wang, Felix L. Struebing, Janey L. Wiggs, and **Eldon E. Geisert**. Genomic Locus Modulating IOP in the BXD RI Mouse Strains. ISER Glaucoma Meeting, Atlanta GA (2017).

Felix L. Struebing, Ying Li, Rebecca King, and **Eldon E. Geisert**. Genomic Loci Modulating Retinal Ganglion Cell Death Following Elevated IOP in the Mouse. ISER Glaucoma Meeting, Atlanta GA (2017).

Jiaxing Wang, Ying Li, Rebecca King, Felix L. Struebing and **Eldon E. Geisert.** Genomic modulation of optic nerve regeneration in mice. ISER Glaucoma Meeting, Atlanta GA (2017).

Ying Li, Felix L. Struebing, Rebecca King, Jiaxing Wang, **Eldon E. Geisert.** POU6F2 labels subset of retinal ganglion cells in mouse. ISER Glaucoma Meeting, Atlanta GA (2017).

Invited Talks:

2013 An innate Immune Genetic Network Defined in the Mouse Retina: Relevance to CNS injury and Disease. Medical College of Georgia (Augusta), Center for Biotechnology and Genomic Medicine

2014 Genetic Network of Innate Immunity in the Retina: Relevance to CNS Injury and Alzheimer's Disease, Department of Neurology, Emory University Atlanta GA.

2014 Genetic Network of Innate Immunity in the Retina: Relevance to CNS Injury and Disease VA Atlanta GA.

2014 Genetic Network of Innate Immunity in the Retina: Relevance to CNS Injury and Disease Department of Molecular Physiology and Biophysics University of Iowa.

2015 Genetic Network Looking at Innate Immunity in the Retina: Relevance to CNS Injury and Alzheimer's Disease, Department of Cell Biology, Emory University Atlanta GA.

2015 Innate Immunity in the Retina: Relevance to CNS Injury and Alzheimer's Disease, Frontiers in Neuroscience Seminar Series, Emory University Atlanta GA.

2015 Innate Immunity in the Retina: Relevance to CNS Injury and Disease, Neurology Grand Rounds, Emory University Atlanta GA.

2015 Innate immunity in the Retina: Relevance to AMD and Glaucoma, University of North Texas Health Science Center Eye Research institute, Fort Worth TX.

2016 A systems Approach to Retinal Injury and Disease Using the BXD RI Mouse Strains and GeneNetwork. Department of Human Genetics, Emory University.

Publication:

1. King R, Lu L, Williams RW and **Geisert EE**. Transcriptome networks in the mouse retina: an improved BXD RI database Molecular Vision (2015) 21: 1235-1251. PMCID: PMC4626778

2. Felix L. Struebing, Richard K. Lee, Robert W. Williams and **Eldon E. Geisert**, Genetic Networks in Mouse Retinal Ganglion Cells. Frontiers in Genetics (2016) 7:169-182. PMCID: PMC5039302

3. Struebing FL, King R, Li Y, Chrenek MA, Lyuboslavsky PN, Sidhu CS, Iuvone PM, **Geisert EE**, Transcriptional Changes in the Mouse Retina Following Ocular Blast Injury: A Role for the Immune System. J Neurotrauma (2017) [Epub ahead of print] PMID: 28599600

4. Felix L. Struebing1, Jiaxing Wang1, Ying Li1, Rebecca King1, Olivia C. Mistretta2, Arthur W. English2, **Eldon E. Geisert1** Differential Expression of Sox11 and Bdnf mRNA Isoforms in the Injured and Regenerating Nervous Systems. Frontiers in Molecular Neuroscience (2017) Nov 2; 10:354 PMID: 29209164.

5. Diana Zhou, Ye Lu, Rebecca King, Claire Simpson, Wenbo Zhang, Byron Jones, **Eldon E. Geisert**. Lu Lu, The genetic dissection of Myo7a gene expression in the retina of BXD mice. (2018) Mol. Vis (In Press)

6. Rebecca King, Felix L. Struebing, Ying Li, Jiaxing Wang, Allison Ashley Koch, Jessica Cooke Bailey, Puya Gharahkhani, International Glaucoma Genetics Consortium, NEIGHBORHOOD consortium, Stuart MacGregor, R. Rand Allingham, Michael A. Hauser, Janey L. Wiggs, and **Eldon E. Geisert**, Genomic Locus Modulating Corneal Thickness in the Mouse Identifies *POU6F2* as a Potential Risk of Developing Glaucoma. (2018) Plos Genetics PMID 29370175.

7. Struebing FL, R King, Y Li, J N Cooke Bailey, NEIGHBORHOOD consortium, J L Wiggs, and **E E Geisert**. Genomic loci modulating ganglion cell death following elevated IOP in the mouse. Exp. Eye Res. 2018 (In Press).

8. Jiaxing Wang, Ying Li, Rebecca King, Felix L. Struebing and **Eldon E. Geisert**. Optic Nerve Regeneration in the Mouse is a Complex Trait Modulated by Genetic Background. (2017) bioRxiv 204842; doi: https://doi.org/10.1101/204842.

9. Rebecca King, Ying Li, Jiaxing Wang, Felix L. Struebing and **Eldon E. Geisert** Genomic Locus Modulating IOP in the BXD RI Strains of Mice. (2017) bioRxiv 202937; doi: https://doi.org/10.1101/202937.

10. Felix L. Struebing, Steven G. Hart, and **Eldon E. Geisert** (2017) Upregulation of SOX11 in Retinal Ganglion Cells Following Injury. (In preparation).

Book Chapters:

HE Grossniklaus, **EE Geisert** and JM Nickerson (2015) Intorduction to the Retina. Prog. Mol Giol Transl Sci 134: 383-396.

FL Strubing and **EE Geisert** (2015) What Animal Models Can Tell Us About Glaucoma. Prog. Mol Giol Transl Sci 134: 365-380.

Website(s) or Other Internet site(s):
The DoD CDMRP Retina Affy MoGene 2.0 ST Database and the DoD TATRC Retina Affy MoGene 2.0 ST Exon Level Database are hosted on GeneNetwork.org. This database was made pu public in 2015. These datasets describe gene expression in the normal retina in the BXD Strains. Both databases can be found under Mice, BXD, retina and then either DoD CDMRP Retina Affy MoGene 2.0 ST Database or DoD CDMRP Retina Affy MoGene 2.0 ST Exon Level Database.

The DoD TATRC Retina Blast Affy MoGene 2.0 ST RMA Exon Level Database are hosted on GeneNetwork.org. The databases describe the changes thatin gene expression that occur following a 50 psi blast injury to the eye. This database was open to the public in 2017. The databases can be found under Mice, BXD, retina and then either DoD TATRC Retina Blast Affy MoGene 2.0 ST RMA Database or DoD TATRC Retina Blast Affy MoGene 2.0 ST RMA Exon Level Database.

Both the normal and blast databases are presented on the multiple websites:

GeneNetwork **Time Machine**: Full versions from 2009 to 2016 (mm9); UTHSC Genome Browser **Classic** and **Newest**; UTHSC **Galaxy** Service; UTHSC **Bayesian Network Web Server**; GeneNetwork Classic on **Amazon Cloud**; GeneNetwork Classic Code on **GitHub**; GeneNetwork 2.0 Development Code on **GitHub**; and **GeneNetwork 2.0** Development.

Technologies or techniques:
None

Inventions, patent applications, and/or licenses:
None

Other products:
None

7. PARTICIPANTS & OTHER COLLABORATING ORGANIZATIONS

What individuals have worked on the project?

At Emory University (7/15/14 to present):

Becky King, Research Technician (50% effort)
Eldon E. Geisert, Principal Investigator (25% effort)

We have been collaborating with Dr. Mike Iuvone to construct and test a new blast gun. We are currently in the process of writing a manuscript describing the effects of a 50psi blast to the mouse eye.

Has there been a change in the other active support of the PD/PI(s) or senior/key personnel since the last reporting period?

No.

What other organizations have been involved as partners?
None

8. SPECIAL REPORTING REQUIREMENTS

None

9. APPENDICES

A) Transcriptome networks in the mouse retina: an improved BXD RI database.

B) Genetic Networks in Mouse Retinal Ganglion Cells.

C) Transcriptional changes in the mouse retina following ocular blast injury: A Role for the Immune System.

D) Differential expression of Sox11 and Bdnf mRNA isoforms in the injured and regenerating nervous systems.

E) Genomic Locus Modulating Corneal Thickness in the Mouse Identifies *POU6F2* as a Potential Risk of Developing Glaucoma

F) Genomic loci modulating ganglion cell death following elevated IOP in the mouse.

G) Optic Nerve Regeneration in the Mouse is a Complex Trait Modulated by Genetic Background.

H) Press releases concerning POU6F2.

Appendix A

Molecular Vision 2015; 21:1235-1251 <http://www.molvis.org/molvis/v21/1235>
Received 7 July 2015 | Accepted 22 October 2015 | Published 26 October 2015

Transcriptome networks in the mouse retina: An exon level BXD RI database

Rebecca King,[1] Lu Lu,[2] Robert W. Williams,[2] Eldon E. Geisert[1]

[1]Department of Ophthalmology and Emory Eye Center, Emory University, Atlanta, GA; [2]Department of Anatomy and Neurobiology and Center for Integrative and Translational Genomics, University of Tennessee Health Science Center, Memphis, TN

Purpose: Differences in gene expression provide diverse retina phenotypes and may also contribute to susceptibility to injury and disease. The present study defines the transcriptome of the retina in the BXD RI strain set, using the Affymetrix Mouse Gene 2.0 ST array to investigate all exons of traditional protein coding genes, non-coding RNAs, and microRNAs. These data are presented in a highly interactive database on the GeneNetwork website.
Methods: In the Normal Retina Database, the mRNA levels of the transcriptome from retinas was quantified using the Affymetrix Mouse Gene 2.0 ST array. This database consists of data from male and female mice. The data set includes a total of 52 BXD RI strains, the parental strains (C57BL/6J and DBA/2J), and a reciprocal cross.
Results: In combination with GeneNetwork, the Department of Defense (DoD) Congressionally Directed Medical Research Programs (CDMRP) Normal Retina Database provides a large resource for mapping, graphing, analyzing, and testing complex genetic networks. Protein-coding and non-coding RNAs can be used to map quantitative trait loci (QTLs) that contribute to expression differences among the BXD strains and to establish links between classical ocular phenotypes associated with differences in the genomic sequence. Using this resource, we extracted transcriptome signatures for retinal cells and defined genetic networks associated with the maintenance of the normal retina. Furthermore, we examined differentially expressed exons within a single gene.
Conclusions: The high level of variation in mRNA levels found among the BXD RI strains makes it possible to identify expression networks that underline differences in retina structure and function. Ultimately, we will use this database to define changes that occur following blast injury to the retina.

Large-scale sequencing initiatives have led to a new era in understanding gene and genome functions [1-5]. There is now an acute need for powerful approaches that integrate and analyze massive proteomics/genomics data sets. In vision research, many single gene variants are known to cause vision loss, including retinitis pigmentosa [6-9], Usher syndrome [10,11], and some forms of glaucoma [12]. However, many ocular diseases have a complex genetic basis with multiple chromosomal loci contributing to differences in the susceptibility and severity of the disease. Two prominent examples are glaucoma [13-15] and age-related macular degeneration [16,17]. In addition, the response of the eye and the retina to trauma is driven by a host of different genes expressed in a large number of different cell types.

Until recently, it was extremely difficult to define the genetic and molecular basis of complex diseases or to adequately monitor the response of the eye and the retina to injury. We used a novel and powerful approach that relies on systems biology and a mouse genetic reference panel, the BXD family of recombinant inbred (RI) strains. This resource is particularly well suited to define complex genetic networks that are also active in human diseases. This approach allows us to not only identify specific gene variants involved in retinal disease and response to injury but also place corresponding molecular changes in a global context in the eye and the retina.

The initial efforts of our group explored the genetic diversity of the BXD family of strains to define the genetic networks active in the eye (see data sets and refs [18] and [19]). In this study, we created a new mouse retinal database that offers a more complete description of the mouse transcriptome. This resource uses the genetic covariance of expression across a panel of 52 BXD strains to identify cellular signatures and genetic networks within the mouse retina. The array we used provides expression profiling at the exon level for 26,191 well-established annotated transcripts, as well as 9,049 non-coding RNAs, including more than 600 microRNAs. Using the bioinformatics tools located on GeneNetwork, we examined the cellular signature of RPE cells. We also analyzed a genetic and molecular network involved in neuronal development and axon growth. In both examples, we highlight the specific benefits of the new

Correspondence to: Eldon E. Geisert, Department of Ophthalmology, Emory University, 1365B Clifton Road NE, Atlanta, GA, 30322; Phone: (404) 778-4239; FAX: (404) 778 4111; email: egeiser@emory.edu

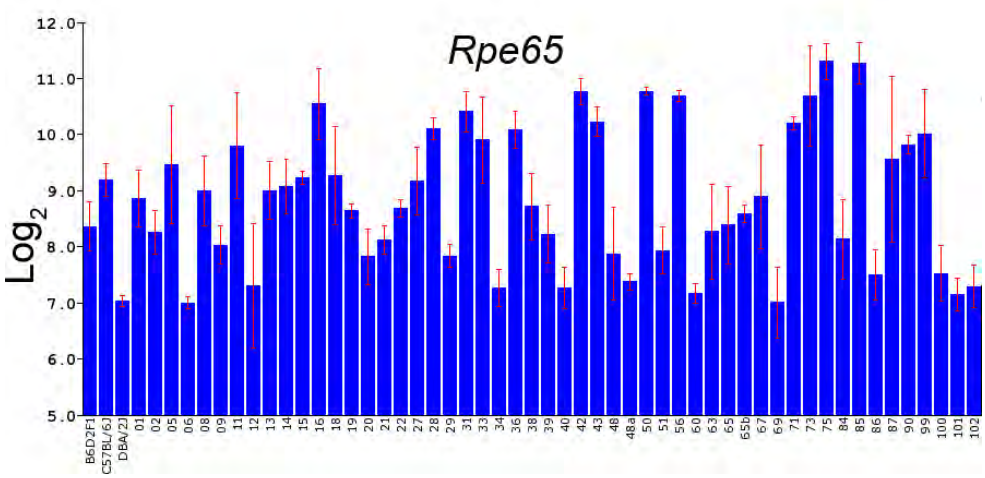

Figure 1. The expression at the gene level of *Rpe65* across the BXD strains in the DoD CDMRP Normal Retina Database. The expression levels of *Rpe65* are shown for many of the BXD strains as the mean expression and the standard error of the mean. The individual strain identifications are shown along the bottom, and the scale is $\log_2$. Notice the low levels of *Rpe65* in some stains (DBA/2J, BXD5 BXD12, BXD34, BXD40, BXD48a, BXD60, BXD69, BXD100, BXD101, and BXD102) and the eightfold higher levels of expression in other strains (BXD16, BXD31, BXD42, BXD43, BXD50, BXD56, BXD75, and BXD85). Most of the high expressing strains were isolated at 2 h after light on and the low expressing strains had retinas isolated at least 4 h after light on.

database with a special emphasis on microRNAs, non-coding RNAs, and the exon level data available with the Affymetrix MouseGene 2.0 ST array.

METHODS

All of the procedures used involving mice were approved by IACUC at the Emory University and adhered to the ARVO Statement for the Use of Animals in Research. The Department of Defense (DoD) Congressionally Directed Medical Research Programs (CDMRP) Normal Retina Database uses the Affymetrix MouseGene 2.0 ST Array (May 15, 2015). Robust multiarray average (RMA) analysis and scaling were conducted by Arthur Centeno. This data set consists of 52 BXD strains, C57BL/6J, DBA/2J, and an F1 cross between C57BL/6J and DBA/2J. A total of 55 strains were quantified. There is a total of 222 microarrays. All data from each microarray used in this data set is publicly available on GeneNetwork.

These are RMA expression data that have been normalized using what we call a 2*z*+8 scale, but without corrections for batch effects. The data for each strain were computed as the mean of four samples per strain. The expression values on the $\log_2$ scale ranged from 3.81 to 14.25 (10.26 units), a nominal range of approximately 1,000-fold. After taking the $\log_2$ of the original non-logged expression estimates, we converted the data within an array to a z-score. We then multiplied the z-score by 2. Finally, we added 8 units to ensure that no values were negative. The result was a scale with the mean expression of the probes on the array of 8 units and a standard deviation of 2 units. A twofold difference in expression is equivalent to roughly 1 unit on this scale. The lowest level of expression was 3.81 (*Olfr1186*) from the DoD CDMRP (the Normal Retina Database uses the Affymetrix MouseGene 2.0 ST Array, May 15, 2015). The highest level of expression was rhodopsin for *17462036* (Rho). The highest single value was 14.25.

Cases used to generate this data set: Almost all animals were young adults between 60 and 100 days of age. We measured expression in conventional inbred strains, BXD recombinant inbred (RI) strains, and reciprocal F1s between C57BL/6J and DBA/2J.

BXD strains: The first 32 of the strains were from the Taylor series of BXD strains generated at the Jackson Laboratory (Bar Harbor, ME) by Benjamin A. Taylor. BXD1 through BXD32 were started in the late 1970s, whereas BXD33 through 42 were started in the 1990s. BXD43 and higher were bred by Lu Lu, Jeremy Peirce, Lee M. Silver, and Robert W. Williams starting in 1997 using B6D2 generation 10 advanced intercross progeny. This modified breeding protocol doubles the number of recombinations per BXD strain and improves the mapping resolution [20]. All of the Taylor series of BXD strains and many of the new BXD strains are available from The Jackson Laboratory. Several strains were specifically excluded from the data set. For BXD43 and higher, the DBA/2J parent carried the *Tyrp1b* mutation and the *GpnmbR150X* mutation; these two mutations produce pigment dispersion glaucoma. Mice that carried these two mutations were not included in the data set: BXD53, BXD55, BXD62, BXD66, BXD68, BXD74, BXD77, BXD81, BXD88, BXD89, BXD95, and BXD98. In addition, BXD24 was omitted, since it developed a spontaneous mutation, *rd16* (*Cep290*) that resulted in retinal degeneration and was

Table 1. The list of genes with similar expression patterns across the BXD strains as RPE65.

Symbol	Description	Location (Chr: Mb)	Mean Expr	Sample r
Rpe65	retinal pigment epithelium 65	Chr3: 159.262145	8.84	1.00
Rgr	retinal G protein coupled receptor	Chr14: 37.850676	10.66	0.98
Pon1	paraoxonase 1	Chr6: 5.118090	7.61	0.98
Ttr	transthyretin	Chr18: 20.823751	10.86	0.95
Ermn	ermin, ERM-like protein	Chr2: 57.897524	7.17	0.94
Lrat	lecithin-retinol acyltransferase	Chr3: 82.696501	8.19	0.93
Rdh5	retinol dehydrogenase 5	Chr10: 128.350646	8.76	0.92
Slc6a20a	solute carrier family 6	Chr9: 123.545240	8.36	0.92
Trf	transferrin	Chr9: 103.106331	10.66	0.89
Slc26a7	solute carrier family 26, member 7	Chr4: 14.429577	7.98	0.89
Car12	carbonic anyhydrase 12	Chr9: 66.561493	7.90	0.89
Clstn1	calsyntenin 1	Chr4: 148.960577	12.74	-0.88
Camk2b	calcium	Chr11: 5.869645	8.98	-0.88
Pkm	pyruvate kinase, muscle	Chr9: 59.504175	13.46	-0.88
Thbs1	thrombospondin 1	Chr2: 117.937612	8.37	0.88
Snora17	small nucleolar RNA, H/ACA box 17	Chr2: 26.494759	6.27	0.87
Abl1	c-abl oncogene 1, non-receptor tyrosine kinase	Chr2: 31.543896	8.80	-0.87
Itgb8	integrin beta 8	Chr12: 120.396495	9.95	0.87
Rrh	retinal pigment epithelium derived rhodopsin homolog	Chr3: 129.507326	10.40	0.87
Tiam1	T-lymphoma invasion and metastasis-inducing	Chr16: 89.787356	9.16	-0.87
Chchd3	coiled-coil-helix-coiled-coil-helix domain containing 3	Chr6: 32.740976	10.72	0.87
Gm5567	predicted gene 5567	Chr6: 40.060252	9.84	-0.87
Hdac5	histone deacetylase 5	Chr11: 102.086139	10.80	-0.87
Cntn2	contactin 2	Chr1: 134.406002	8.84	-0.87
Olfr875	olfactory receptor 875	Chr9: 37.580222	7.60	0.87
Gm19522	predicted gene, 19522	Chr16: 42.884483	7.57	0.87
Gm19272	predicted gene, 19272	Chr6: 7.251908	6.40	-0.87
Sez6l2	seizure related 6 homolog like 2	Chr7: 134.094049	10.14	-0.86
Nrxn2	neurexin II	Chr19: 6.418731	10.14	-0.86
Olfr726	olfactory receptor 726	Chr14: 50.703389	7.14	0.86
Sv2a	synaptic vesicle glycoprotein 2 a	Chr3: 95.985074	12.28	-0.86
Tmem161b	transmembrane protein 161B	Chr13: 84.361901	10.91	0.86
Pdcd5	programmed cell death 5	Chr1: 191.101187	11.26	0.86

Symbol	Description	Location (Chr: Mb)	Mean Expr	Sample r
Fap	fibroblast activation protein	Chr2: 62.339000	7.19	0.86
Cacna1g	calcium channel, voltage-dependent,	Chr11: 94.269705	9.95	-0.86
Rapgef1	Rap guanine nucleotide exchange factor (GEF) 1	Chr2: 29.475240	10.50	-0.86
Nsmce2	non-SMC element 2 homolog	Chr15: 59.205753	10.91	0.86
Plxna1	plexin A1	Chr6: 89.266307	10.09	-0.86
Ube2b	ubiquitin-conjugating enzyme E2B	Chr11: 51.798648	11.28	0.86
Aacs	acetoacetyl-CoA synthetase	Chr5: 125.956184	9.52	-0.86
Acsf3	acyl-CoA synthetase family member 3	Chr8: 125.299405	9.51	-0.86
Slc17a7	solute carrier family 17	Chr7: 52.419291	13.14	-0.86
Srebf2	sterol regulatory element binding factor 2	Chr15: 81.977696	11.31	-0.86
Epb4.9	erythrocyte protein band 4.9	Chr14: 71.001070	9.98	-0.86
Vapa	vesicle-associated membrane protein, associated protein A	Chr17: 65.929392	12.32	0.85
Slc12a5	solute carrier family 12, member 5	Chr2: 164.786302	12.12	-0.85
Card9	caspase recruitment domain family, member 9	Chr2: 26.207696	7.65	-0.85
Cfh	complement component factor h	Chr1: 141.982432	8.59	0.85
Dagla	diacylglycerol lipase, alpha	Chr19: 10.319755	9.57	-0.85
Pde4dip	phosphodiesterase 4D interacting protein	Chr3: 97.493751	9.55	-0.85
Ank1	ankyrin 1, erythroid	Chr8: 24.085316	9.54	-0.85
Zcchc14	zinc finger, CCHC domain containing 14	Chr8: 124.122603	10.39	-0.85
Ssr3	signal sequence receptor, gamma	Chr3: 65.186870	6.09	0.85
Mterfd1	MTERF domain containing 1	Chr13: 67.007904	9.55	0.85
G3bp2	GTPase activating protein (SH3 domain) binding protein 2	Chr5: 92.052145	8.76	0.85
Apba1	amyloid beta (A4) precursor protein binding	Chr19: 23.833366	10.55	-0.85
Acot13	acyl-CoA thioesterase 13	Chr13: 24.909817	10.63	0.85
Rbl1	retinoblastoma-like 1 (p107)	Chr2: 156.971629	9.07	0.85
Cpxm2	carboxypeptidase X 2 (M14 family)	Chr7: 139.234493	8.07	0.85
Mir467h	microRNA 467h	Chr9: 115.291078	6.80	0.85
Ret	ret proto-oncogene	Chr6: 118.101766	10.23	-0.85
Mospd1	motile sperm domain containing 1	ChrX: 50.698185	10.71	0.85
Lrp3	low density lipoprotein receptor-related protein 3	Chr7: 35.984852	9.10	-0.85

The gene symbol and name are listed, along with the chromosomal location, mean expression and correlation to *Rpe65*.

Molecular Vision 2015; 21:1235-1251 <http://www.molvis.org/molvis/v21/1235>

Table 2. The predicted targets from the top 500 correlates of *Rpe65* are listed in columns below for each of the five microRNAs found to correlate themselves with *Rpe65*.

Rpe65	Mir98	Mir449a	mir301b	mir28b
Camk2b	–	–	–	Camk2b
Atp2b2	–	–	Atp2b2	–
Cfl2	–	–	Cfl2	–
Dlc1	–	–	Dlc1	–
Eif2c1	Eif2c1	–	Eif2c1	–
Nptx1	Nptx1	Nptx1	Nptx1	–
Pitpnm2	–	–	Pitpnm2	–
Ppp6r1	–	–	Ppp6r1	–
Psap	–	–	Psap	–
Slc17a7	–	–	Slc17a7	–
Snx2	–	–	Snx2	–
Sub1	–	–	Sub1	–
Tet3	–	–	Tet3	–
Zbtb4	–	–	Zbtb4	–
Zcchc14	–	–	Zcchc14	–
2610507B11Rik	2610507B11Rik	2610507B11Rik	–	–
Abr	Abr	Abr	–	–
Ahsa2	Ahsa2	Ahsa2	–	–
Cacna2d2	Cacna2d2	Cacna2d2	–	–
Cntn2	Cntn2	Cntn2	–	–
Dcaf7	Dcaf7	Dcaf7	–	–
E2f5	E2f5	E2f5	–	–
Fbxo10	Fbxo10	Fbxo10	–	–
Mgat5b	Mgat5b	Mgat5b	–	–
Ndst1	Ndst1	Ndst1	–	–
Nrxn2	Nrxn2	Nrxn2	–	–
Pvrl1	Pvrl1	Pvrl1	–	–
Ret	Ret	Ret	–	–
Slc6a1	Slc6a1	Slc6a1	–	–
Tfdp2	Tfdp2	Tfdp2	–	–
Trim67	Trim67	Trim67	–	–
Usp31	Usp31	Usp31	–	–

Molecular Vision 2015; 21:1235-1251 <http://www.molvis.org/molvis/v21/1235>

Rpe65	Mir98	Mir449a	mir301b	mir28b
Agap1	Agap1	–	–	–
Apba1	Apba1	–	–	–
Bsn	Bsn	–	–	–
Fbxl14	Fbxl14	–	–	–
Insr	Insr	–	–	–
Kcnc1	Kcnc1	–	–	–
Nsmce2	Nsmce2	–	–	–
Slc7a14	Slc7a14	–	–	–
Srebf2	Srebf2	–	–	–
Syt7	Syt7	–	–	–
Thbs1	Thbs1	–	–	–

Molecular Vision 2015; 21:1235-1251 <http://www.molvis.org/molvis/v21/1235>

Table 3. The probes for each of the exons of Col18a1 are presented.

Probe ID	Symbol	Description	Location (Chr, Mb)	Mean Expr	Max LRS
17,242,233	Col18a1	collagen, type XVIII, alpha 1	Chr10: 76.515054	7.706218147	12.8
17,242,235	Col18a1	collagen, type XVIII, alpha 1	Chr10: 76.516921	7.824909037	12.5
17,242,236	Col18a1	collagen, type XVIII, alpha 1	Chr10: 76.517574	7.407200033	11.2
17,242,238	Col18a1	collagen, type XVIII, alpha 1	Chr10: 76.521455	9.306981902	18.4
17,242,239	Col18a1	collagen, type XVIII, alpha 1	Chr10: 76.521899	8.679945391	11.9
17,242,242	Col18a1	collagen, type XVIII, alpha 1	Chr10: 76.523117	6.338236349	12
17,242,246	Col18a1	collagen, type XVIII, alpha 1	Chr10: 76.529745	6.939890905	14.2
17,242,248	Col18a1	collagen, type XVIII, alpha 1	Chr10: 76.531176	5.754218162	13.7
17,242,250	Col18a1	collagen, type XVIII, alpha 1	Chr10: 76.532565	9.958654568	176.3
17,242,251	Col18a1	collagen, type XVIII, alpha 1	Chr10: 76.532696	9.252999965	12.1
17,242,254	Col18a1	collagen, type XVIII, alpha 1	Chr10: 76.534773	7.823781802	19.3
17,242,255	Col18a1	collagen, type XVIII, alpha 1	Chr10: 76.536490	6.731690944	15.9
17,242,256	Col18a1	collagen, type XVIII, alpha 1	Chr10: 76.537103	8.810418181	14.5
17,242,259	Col18a1	collagen, type XVIII, alpha 1	Chr10: 76.540499	5.251781802	12.4
17,242,260	Col18a1	collagen, type XVIII, alpha 1	Chr10: 76.540746	6.876309109	10.9
17,242,261	Col18a1	collagen, type XVIII, alpha 1	Chr10: 76.541023	6.412472682	12
17,242,264	Col18a1	collagen, type XVIII, alpha 1	Chr10: 76.543517	9.105672802	14.4
17,242,266	Col18a1	collagen, type XVIII, alpha 1	Chr10: 76.548057	9.839090885	7
17,242,267	Col18a1	collagen, type XVIII, alpha 1	Chr10: 76.550127	10.48203631	11.3
17,242,269	Col18a1	collagen, type XVIII, alpha 1	Chr10: 76.552081	6.064109126	9
17,242,270	Col18a1	collagen, type XVIII, alpha 1	Chr10: 76.559097	9.295490941	9.2
17,242,271	Col18a1	collagen, type XVIII, alpha 1	Chr10: 76.575355	8.399236367	17.5
17,242,272	Col18a1	collagen, type XVIII, alpha 1	Chr10: 76.575935	8.588909123	17.4
17,242,273	Col18a1	collagen, type XVIII, alpha 1	Chr10: 76.576553	7.142545466	12.7
17,242,274	Col18a1	collagen, type XVIII, alpha 1	Chr10: 76.629063	8.688581805	8.5
17,242,275	Col18a1	collagen, type XVIII, alpha 1	Chr10: 76.629242	8.288054553	10.3

Notice that most of the probes have LRS ranging from 7 to 19. However one probe (17242250) has an LRS of 176.3. This latter exon is differentially spliced.

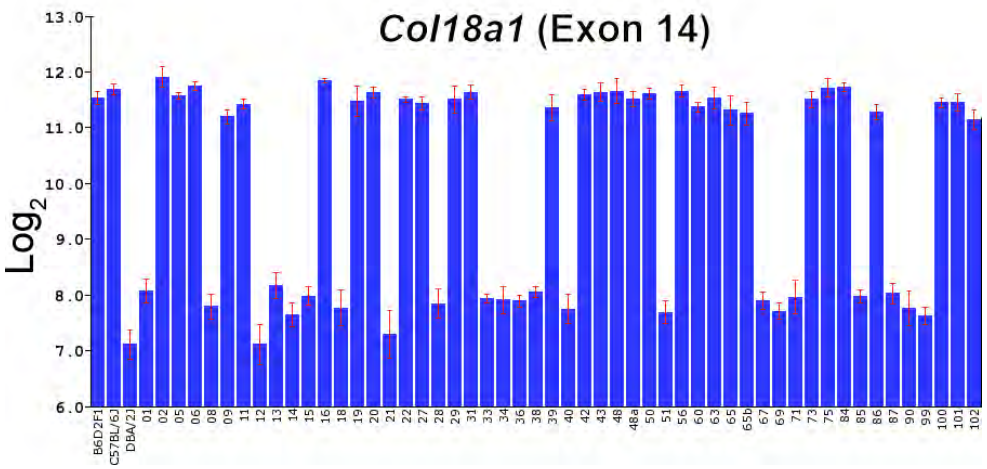

Figure 2. Expression of *Col18a1* (Exon 14) is illustrated across the BXD strains in the DoD CDMRP Normal Retina Exon Level DataSet. The expression levels of *Col18a1* at exon 14 are shown for many of the BXD strains as the mean expression and the standard error of the mean. The individual strain identifications are shown along the bottom, and the scale is $\log_2$ This difference in expression reflects the differential splicing of this exon.

renamed BXD24b/TyJ [21]. Several additional strains were excluded due to abnormally high *Gfap* levels observed in the Full HEI Retina (April 2010) data set: BXD32, BXD49, BXD70, BXD83, and BXD89.

Tissue preparation protocol: The mice were killed by rapid cervical dislocation. The retinas were removed immediately by placing the globe under pressure and cutting the cornea. The lens burst out of the opening in the cornea followed by the retina. In this process, no specific procedures were used to include or exclude the RPE. The retina was placed immediately in 1 ml of 160 U/ml RiboLock (Thermo Scientific Waltham, MA) for 1 min at room temperature. The retina was then transferred to Hank's Balanced Salt solution with RiboLock in 50 µl RiboLock (Thermo Scientific, RiboLock RNase #EO0381 40 U/µl 2500U) and stored in −80 °C. The RNA was isolated using a QiaCube (Hilden, Germany) and the in-column DNase procedure. All RNA samples were checked for quality before the microarrays were run. The samples were analyzed using the Agilent 2100 Bioanalyzer (Agilent, Santa Clara, CA). The RNA integrity values ranged from 7.0 to 10. Our goal was to obtain data from independent biologic sample pools for both sexes of each BXD strain. The four batches of arrays included in this final data set collectively represented a reasonably well-balanced sample of males and females.

Affymetrix gene array: In the present study, we used the Affymetrix Mouse Gene 2.0 ST Array. The array was designed with a median of 22 unique probes per transcript. Each probe is 25 bases in length. The arrays provide comprehensive transcriptome coverage with more than 30,000 coding and non-coding transcripts. In addition, there is coverage for more than 600 microRNAs. For some arrays, the RNA was pooled from two retinas, and other arrays were run on a single retina. Dr. XiangDi Wang (University of Tennessee, Health Science Center) was involved in the retinal extractions and isolation of RNA. The Affymetrix arrays were run by two research core laboratories: the Molecular Resource Center at UTHSC (Dr. William Taylor, director) and the Integrated Genomics Core at Emory University by Robert B. Isett (Dr. Michael E. Zwick, director). In a separate set of experiments, we tested a set of arrays from C57BL/6J retinas run at each facility to determine if there were batch effects or other confounding differences in the results. We did not detect any significant difference in the arrays run at UTHSC or at Emory University. Thus, we included both sets of data in the analysis.

RESULTS

The DoD CDMRP Retina Database presents the retinal transcriptome profiles of 52 BXD RI strains on a highly interactive website, GeneNetwork. There are two separate presentations of the microarray data. The first is at the gene level (DoD CDMRP Retina Affymetrix Mouse Gene 2.0 ST (May 15, 2015) RMA Gene-Level Database), and the same data is presented at the exon level (DoD CDMRP Retina Affymetrix Mouse Gene 2.0 ST (May 15, 2015) RMA Exon-Level Database). For analyzing these data sets, a suite of bioinformatics tools is integrated in the GeneNetwork website. These tools identify genes that vary across the BXD RI strains, construct genetic networks that control the development of the mouse retina, and identify the genomic loci that underlie complex traits in the retina. In this paper, we present these two new data sets and illustrate their use with three examples. The first was to identify the genetic signatures of the RPE. The second identified genes that are differentially spliced between the C57BL/6J retina and the DBA/2J retina. In the third

example, we looked at the genetic network associated with roundabout homolog 2 (*Robo2*) gene and the modulation of axonal growth.

Cellular signature of the RPE in the DoD CDMRP Retina Database: The DoD CDMRP Retina Database has a unique signature for RPE cells. When looking at the expression of the RPE marker *Rpe65*, there was an almost biphasic distribution of expression (Figure 1). Many of the strains expressed low levels of *Rpe65* (approximately 7 units on our scale) while other strains had high levels of expression ranging from two- to eightfold higher (8 to 11 units). We believe that this difference is due to the time of day that the retinas were removed from the eye. Many of the retinas were isolated at the University of Tennessee Health Science Center where isolation started at approximately 10:00 a.m. and lights on in the animal colony occurred at 6:00 a.m. These retinas were isolated approximately 4 h after the lights came on. At Emory University, the retinas were isolated starting at 9:00 a.m., and lights on occurred at 7:00 a.m. These later sets of retinas were removed at approximately 2 h after the lights came on in the animal colony. The mean expression level of *Rpe65* in the samples isolated at the University of Tennessee was 8.3, and the mean for the samples isolated at Emory University was 10.2, roughly a fourfold difference in expression. This difference in expression between the samples isolated at the different locations was significant using a Student *t* test ($p<0.01$). If we examine the correlation between these differences in *Rpe65* expression and the genes' associated circadian rhythm, several genes correlate with the expression of *Rpe65* across the data set, including cytochrome 2 (*Cry2*, $r = -0.75$) and period homolog 2 (*Per2*, $r = -0.65$).

When this data set is used, it is important to remember the difference in *Rpe65* expression due to the time of day the retinas were isolated. However, if one is interested in defining a molecular signature of RPE cells and if the level of *Rpe65* is directly associated with the number of cells that adhere to the retina, then we can use the level of *Rpe65* in each strain to define a set of genes that covary with *Rpe65* across the BXD strain set. When we examined the data set for genes with a similar expression pattern across the BXD strains, a list of genes uniquely expressed in RPE was observed (Table 1). This cellular signature represents genes that are expressed within the RPE, including retinal G protein coupled receptor (*Rgr*), lecithin-retinol acyltransferase (*Lrat*), retinol dehydrogenase 5 (*Rdh5*), transferrin (*Trf*), and retinal pigment epithelium derived rhodopsin homolog (*Rrh*). This signature can also be thought of as the result of genetic networks that drive gene expression within a given cell type.

With the MouseGene 2.0 ST Affymetrix chip, we found not only protein-coding genes that correlate with *Rpe65* but also microRNAs and non-coding RNAs. When we examined the top 500 correlates of *Rpe65* (all of which have a correlation higher than 0.8 with *Rpe65*), five microRNAs were present: *Mir98*, *Mir666*, *Mir449a*, *Mir301b,* and *Mir28b* (Table 2). Using the bioinformatics tools on TargetScan (Targetscan.org) [22-24], we predicted targets for each microRNA from the top 500 correlates of *Rpe65*. One microRNA, *Mir666*, did not appear on the TargetScan website. The remaining four microRNAs appeared on the website. When the microRNAs were scanned for targets, *Mir98* had 29 targets in the RPE signature, *Mir449a* had 14 targets, *Mir301b* had 13 targets, and *Mir28b* had one target. This type of analysis may be one approach to constructing and understanding microarray networks within a specific cell type such as the mouse RPE.

For many Affymetrix probes, there is minimal annotation. For example, within the top 100 correlates of *Rpe65*,

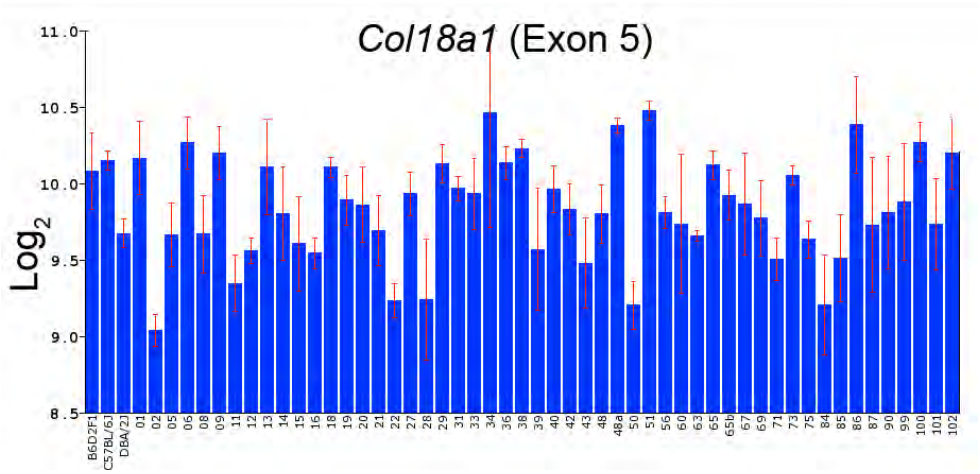

Figure 3. Expression of *Col18a1* (Exon 5) is illustrated across the BXD strains in the DoD CDMRP Normal Retina Exon Level Database. The expression levels of *Col18a1* are shown for many of the BXD strains as the mean expression and the standard error of the mean. The individual strain identifications are shown along the bottom, and the scale is $\log_2$. Thus, this exon is not differentially spliced across the BXD RI strains.

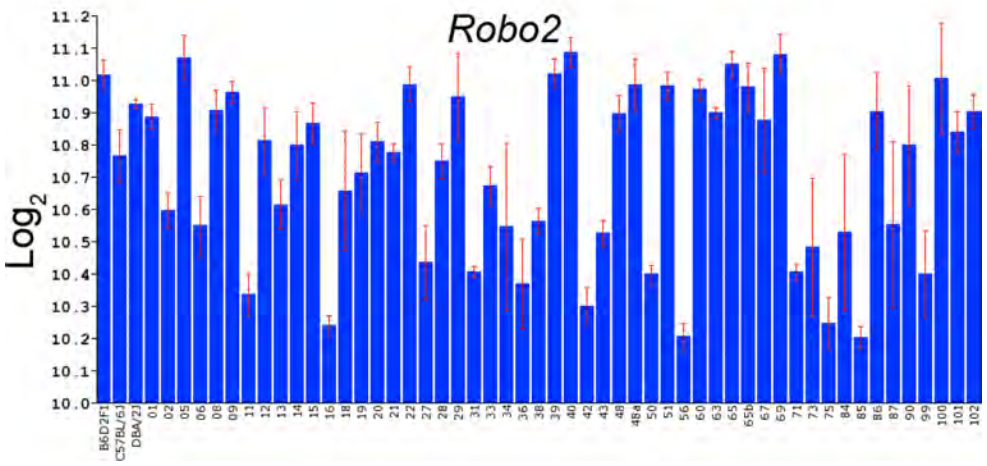

Figure 4. Expression of *Robo2* across the BXD strains in the DoD CDMRP Normal Retina Database. The expression levels of *Robo2* are shown for many of the BXD strains as the mean expression and the standard error of the mean. The individual strain identifications are shown along the bottom of the plot, and the scale is $\log_2$. This variability from strain to strain indicates that the gene is differentially regulated by multiple genomic elements.

17 Affymetrix probes are present that have minimal annotation furnished by Affymetrix. For two of these probes, Affy_17203447 and Affy_17204181, there is no annotation from Affymetrix, including the sequence of the probe itself. Thus, for these two probes, no further analysis can be conducted until Affymetrix furnishes sequence data. For the remaining 15 Affymetrix probes, the expression within the retinal transcriptome is low, ranging from 4.6 to 8.8. The sequences of these probes can be related to the mouse genome using the Verify Tool on the probe's Trait Data and Analysis page on GeneNetwork. The three probes with expression levels higher than 8 all aligned with the mouse genome. Affy_17241598 aligns to a sequence on chromosome 10 that is a predicted protein with no further annotation. Affy_17414264 aligns with a sequence on chromosome 4 that is a non-protein coding gene or gene fragment. Affy_17527409 aligns with a sequence on chromosome 9 that is a predicted protein. When the role of these transcripts in the network associated with Rpe65 is considered, these data are far from informative. Unfortunately, for many of the probes on the Affymetrix Mouse Gene 2.0 ST Array, this is the current state of annotation. We are beginning to improve the annotation, and the identification of probes associated with microRNAs is due to the efforts of members of the Rob Williams group. With time, we believe that the annotation will improve allowing investigators to include these probes in functional genetic networks.

Analysis of differentially spliced genes using the exon dataset: One of the extended features of the Affymetrix MouseGene 2.0 ST Array is its extensive coverage of gene expression at the exon level, and these data are presented in the DoD CDMRP Retina Affymetrix Mouse Gene 2.0 ST (May 15) RMA Exon-Level Database. At the present time, we do not have specific bioinformatic tools that fully investigate the exon-level data set. However, this database can be used to identify genes that are differentially spliced in the DBA/2J mouse and the C57BL/6J mouse. If an exon is expressed in one strain of mouse and not the other strain, the exon will have a large and significant likelihood ratio statistic (LRS) score across the BXD RI strain set. Basically, that individual exon will function like a Mendelian trait being either highly expressed or expressed at a low level. Therefore, to begin the analysis, we identified the exons with LRS scores higher than 60. We identified 2,314 exons, and the highest LRS score was 250. Then we reasoned that if an exon had a significant LRS score and at the gene level there was not a high LRS score, then the selected exon(s) was behaving differently from the other exons within the gene. Of the 2,314 exons with an LRS score above 60, 1,569 exons were part of a gene that did not have a high LRS score. An extensive evaluation of all these exons is beyond the scope of the present paper. Therefore, the top ten exons with LRS scores ranging from 165 to 202 were selected for further analysis. These exons were from ten genes: *Cyb5r3, Hmgn2, Kif22, Col18a1, Uba2, Wdtc1, Haus5, Sdc2, Poc5*, and *Cntn1*. In every case, at least one exon was differentially expressed between the C57BL/6J mouse and the DBA/2J mouse. To illustrate the differential splicing seen in these genes, we examined *Col18a1* in depth. In the exon data set, there are 26 separate probes for the exons in the *Col18a1* gene (see Table 3). Most of the probes have an associated LRS score ranging from 7 to 19. However, one probe (17242250) had an LRS score of 176.3. When we examined the distribution of the expression of this exon across the BXD RI strains, we saw that it is highly expressed in the C57BL/6J mouse retina relative to the DBA/2J retina (Figure 2). In other exon probes for *Col18a1*, there is a similar level of expression between the C57BL/6J mouse retina and the DBA/2J mouse

Table 4. A list of genes that are highly correlated to *Robo2*.

Symbol	Description	Location (Chr: Mb)	Mean Expr	Sample r
Robo2	roundabout homolog 2 (Drosophila)	Chr16: 73.892551	10.72	1.00
Cask	calcium	ChrX: 13.094206	10.91	0.94
Ncam2	neural cell adhesion molecule 2	Chr16: 81.200942	9.95	0.93
Gria3	glutamate receptor, ionotropic, AMPA3	ChrX: 38.754305	10.25	0.92
Lphn3	latrophilin 3	Chr5: 81.450227	10.25	0.92
Cnksr2	connector enhancer of kinase suppressor of Ras 2	ChrX: 154.259368	10.37	0.92
Clstn2	calsyntenin 2	Chr9: 97.344814	10.00	0.92
Gnaq	guanine nucleotide binding protein	Chr19: 16.207321	10.63	0.92
Dnajc6	DnaJ (Hsp40) homolog, subfamily C, member 6	Chr4: 101.169253	11.97	0.92
Slc8a1	solute carrier family 8 (sodium	Chr17: 81.772445	9.45	0.91
Dpysl2	dihydropyrimidinase-like 2	Chr14: 67.421701	13.25	0.91
Plch1	phospholipase C, eta 1	Chr3: 63.500156	10.96	0.91
Gria1	glutamate receptor, ionotropic, AMPA1 (alpha 1)	Chr11: 56.824889	9.77	0.91
Fam165b	family with sequence similarity 165, member B	Chr16: 92.301531	10.04	−0.91
Ncam1	neural cell adhesion molecule 1	Chr9: 49.310243	12.95	0.90
B4galt6	UDP-Gal:betaGlcNAc beta 1,4-galactosyltransferase	Chr18: 20.843100	10.76	0.90
Odz1	odd Oz	ChrX: 40.677132	8.81	0.90
Sort1	sortilin 1	Chr3: 108.087009	11.52	0.90
Ubqln2	ubiquilin 2	ChrX: 149.932775	11.29	0.90
Mtmr9	myotubularin related protein 9	Chr14: 64.142447	11.71	0.90
Gabbr2	gamma-aminobutyric acid (GABA) B receptor, 2	Chr4: 46.675190	11.04	0.90

The gene symbol, name of the gene, chromosome location, mean expression and correlation to Robo2 are listed across the top of the table.

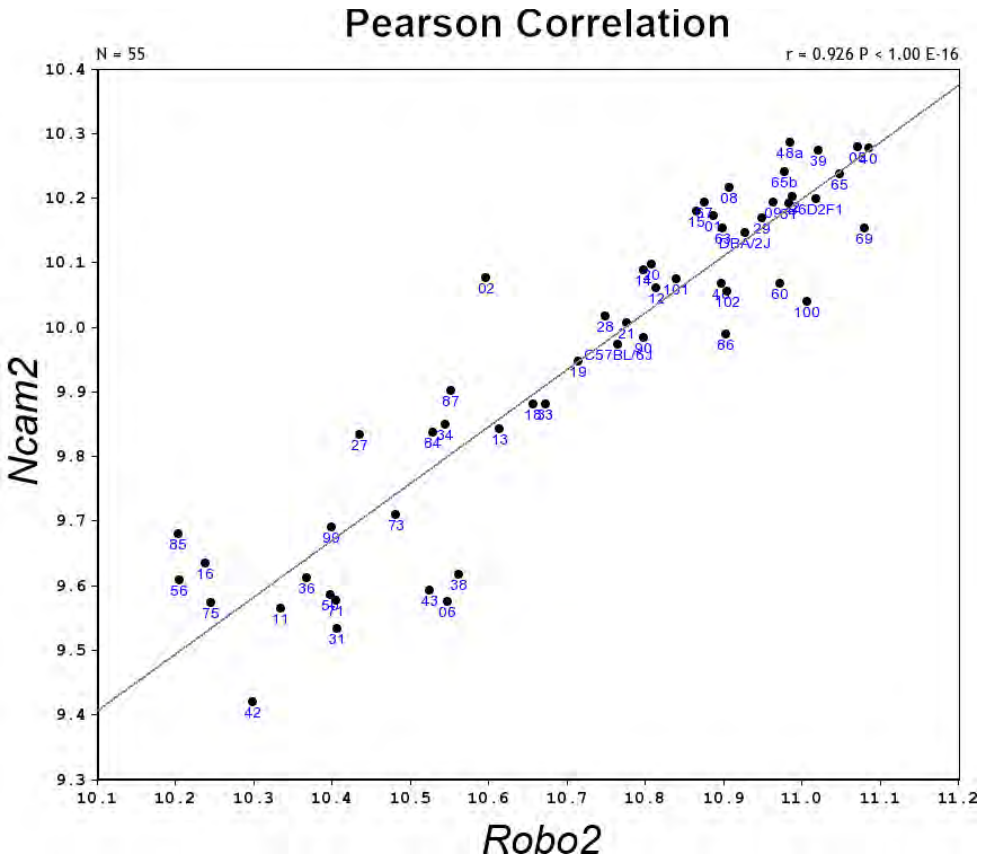

Figure 5. The Pearson correlation between *Robo2* and *Ncam2*. *Ncam2* was the second highest correlate to *Robo2* in the Department of Defense (DoD) Congressionally Directed Medical Research Programs (CDMRP) Normal Retina Database. These data indicate that these two genes are co-regulated with across the BXD strain set. When one gene is high in a strain the other gene is also expressed at a high level.

retina, as well as the remaining BXD strains (Figure 3). It is possible that these differences in probe binding could be due to sequence variants between the C57BL/6J mouse and the DBA/2J. To test this hypothesis, we examined the sequence of the exons with high LRS scores to define the sequence differences between the two strains. Of the ten exons examined, five had single nucleotide polymorphisms (SNPs) within the region recognized by the Affymetrix probe. For these five exons, the difference in expression could be explained by differences in probe binding and not by differential splicing. For the remaining five exons, including that of *Col18a1*, the sequence in the C57BL/6J mouse was identical to that of the DBA/2J mouse. This type of analysis appears to identify differentially spliced genes in the retina of the BXD RI strain set. Our group is in the process of developing bioinformatic tools to take full advantage of the data from the Affymetrix exon chips. In the near future, this type of analysis may be as simple as a single query on the Trait Data and Analysis page of GeneNetwork.

Example of a functional network in the DoD CDMRP Retina Database: To illustrate the features of the new DoD CDMRP Retina Database, we chose a specific gene, *Robo2* (roundabout homolog 2) and used it to demonstrate the analytical powers of the database and the bioinformatics tools associated with GeneNetwork. *Robo2* is highly expressed in the retina with a mean value of 10.7 across the BXD strain set. The expression within individual strains varies from a low of 10.2 to a high of 11.1. This is a $\log_2$ scale and represents approximately a twofold difference in expression (Figure 4). When we examined the database for genes with a similar pattern of expression across the BXD strain set, we found a group of genes that are highly correlated with the expression pattern of *Robo2* (Table 4). One example is the third correlate on the list, *Ncam2* (Figure 5) with a value of 0.926. Even the 100th correlate on the list (*Git1*) has a high correlation (r=0.873) with *Robo2* (see Supplemental Table 1).

To define the regions of the genome that modulate the expression of *Robo2,* we plotted a genome-wide scan for *Robo2* (Figure 6). This plot defines regions of the genome that correlate with the level of *Robo2* expression, a quantitative trait locus (QTL). In this interval map, there is one significant QTL on chromosome 16 (notice the peak reaches the red line on the scan, p=0.05), and there are two suggestive peaks on chromosome 1 and chromosome 17 (above the gray line, p=0.63). The expression of *Robo2* is modulated by genomic elements on chromosome 16. Two types of elements could

affect the expression of *Robo2*: a cis-QTL or a gene with a nonsynonymous SNP. When we examined the significant QTL on chromosome 16 (21–27 Mb), we found there were no significant cis-QTLs at the gene level. With the DoD CDMRP Retina Database, it is now possible to look at the individual probes in exons and introns. When we checked the DoD CDMRP Retina Exon Level Database, we found one probe (Affy_17329472) that lies within the *Leprel1* gene. When we checked the location of the probe with the Verify function on GeneNetwork, the probe lies in an intron and may be a non-coding RNA. However, when we examined the RNA-seq data from GeneNetwork, it appeared that this probe was detected in an RNA-seq analysis of the hippocampus and thus may be part of *Leprel1* gene itself. Nonetheless, this probe marks a candidate for modulating the expression of *Robo2*. The second approach was to examine this region for nonsynonymous SNPs. Using the SNP browser in GeneNetwork, we looked at chromosome 16 (21–27 Mb) and found four known genes with nonsynonymous SNPs: *Kng2*, *Kng1*, *BC106179*, and *Masp1*. This analysis provided us with five candidates for modulating the expression of *Robo2*.

To determine whether this highly correlated set of genes in the *Robo2* network have functional relationship(s), we used WebGestalt (WEB-based GEne SeT AnaLysis Toolkit) to examine the top 500 correlates of *Robo2* to determine if there were specific functional transcript enrichments. The list of the top 500 correlates of *Robo2* was enriched for several biologic processes (nervous system development, synaptic transmission, and neuron differentiations); molecular functions (enzyme binding, post synaptic density [PDZ] domain binding, inorganic cation transmembrane transporter, and metal ion transmembrane transporter activity); and cellular components (cell projection part, neuron projection, intracellular part, and axon genes). This type of analysis plays a critical role in many genetic networks, defining the functional role of the network. In this specific case, the analysis indicates that the *Robo2* network is involved in axonal growth and neuronal development.

DISCUSSION

This article announces the release of two new BXD retina databases on GeneNetwork. The first is at the gene level (DoD CDMRP Retina Affymetrix Mouse Gene 2.0 ST (May 15) RMA Gene-Level Database). The second data set is an exon-level analysis of the data presented in the first data set (DoD CDMRP Retina Affymetrix Mouse Gene 2.0 ST (May 15) RMA Exon-Level Database). Here, we emphasize some of the special aspects of these two data sets, including exon-level analysis and the inclusion of microRNAs and many non-coding RNAs. To illustrate many of these new features, we presented three approaches for analysis using the data sets.

The first was an examination of a cell signature within the data set. Within the DoD CDMRP Retina Database, there is a pronounced RPE signature. Some strains demonstrate low levels of expression of *RPE65* while other strains have more than 16-fold higher levels of expression. This difference could not be due to differences in expression within the RPE. We believe that this difference is due to differences in the time of

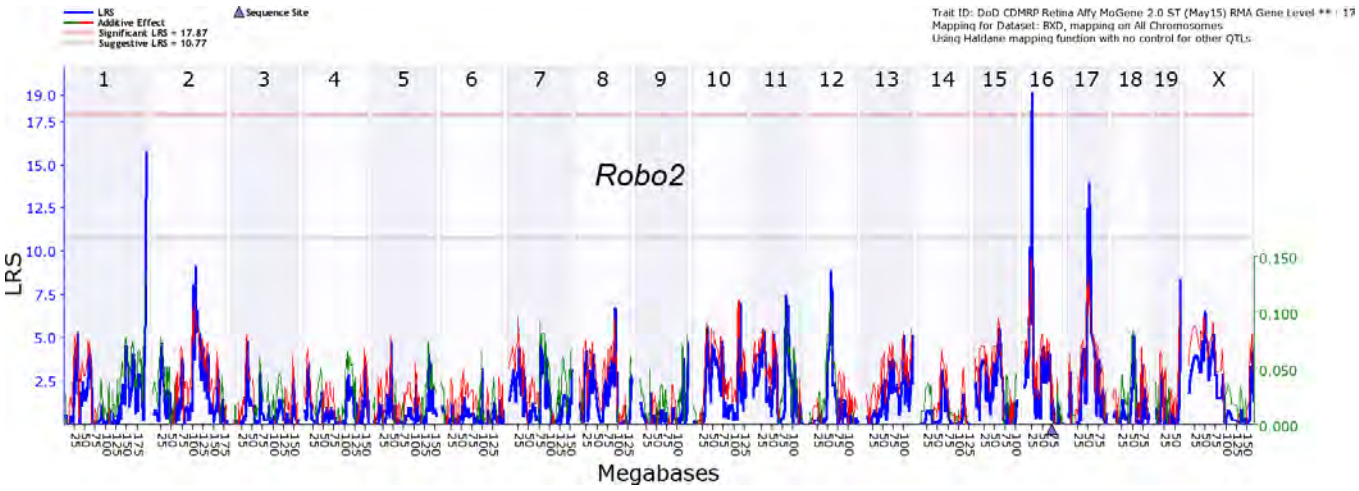

Figure 6. Genome-wide Interval Map of *Robo2*. This genome-wide graph displays the quantitative trait loci (QTL) distribution across the Department of Defense (DoD) Congressionally Directed Medical Research Programs (CDMRP) Normal Retina Database. The x-axis plots the locations of the QTLs that control the transcript expression. Positions are measured in megabases from chromosome 1 to chromosome X (1–2,600 Mb). The *y*-axis plots the "likelihood ratio statistic" (LRS). The significant levels of individual QTLs are color-coded. The red line represents a genome-wide significance level (p=0.05), and the gray line is suggestive. Notice the significant QTL on chromosome 16.

day when the retinas were isolated. The retinal samples were collected at two locations. At the University of Tennessee, the samples were usually isolated starting at 10:00 a.m., and lights were turned on in the animal colony at 6:00 a.m. Thus, the retinas were isolated at least 4 h after the lights came on. At Emory University, the retinas were isolated starting at 9:00 a.m., and lights on occurred at 7:00 a.m. (2 h after the lights came on in the animal colony). These differences in the time of day the retinas were isolated may be related to the number of RPE cells that adhered to the retinal samples [25].

Several bioinformatics tools are available to the vision research community. These tools include the NEI Bank project, which provides transcriptome profiling of the tissues of the eye, including mouse and human [26]. The Cepko group at Harvard, Boston, MA has provided the mouse retina serial analysis of gene expression (SAGE) library that includes gene expression of the embryonic and postnatal retina [27,28]. Daiger and his group at the University of Texas Health Science Center, Houston TX have lists of mapped loci and cloned genes associated with inherited retinal disease on the RetNet website. The Gene Expression Nervous System Atlas (GENSAT) now has a section devoted to the Retina Project [29] at GENSAT. The cell-specific labeling in the retina for different genes was illustrated using BAC transgenic mice [30]. The pattern of labeling in the retina defines the retinal cell types that express specific genes. This cellular localization aids in defining the localization of genetic networks in the retina. Finally, we posted the data from the study of glaucoma by Howell et al. [31] on the GeneNetwork website under the BXD eye database. These data are helpful in understanding the role of specific genetic networks in glaucoma (for example, see Templeton et al. [32]).

In conclusion, the DoD CDMRP Retina Database offered on GeneNetwork is a new resource for the vision community, in the ever-expanding variety of bioinformatics tools available. Previously, we offered several BXD microarray databases on GeneNetwork to the vision science community: the transcriptome of the whole eye (Eye M430v2 (September 2008) RMA Database) described in detail by Geisert et al. [18], a normal retina database (Normal Retina (April 2010) RankInv Database) described in detail by Freeman et al. [19], and the retina 2 days after optic nerve crush (ONC Retina (April 2012) RankInv Database) described by Templeton et al. [33]. This new data set offers a unique look at expression at the exon level. In addition, many non-protein coding transcripts are represented in the data set. The bioinformatics tools offered on GeneNetwork and these new databases are a unique resource for the vision research community.

APPENDIX 1. TOP 100 CORRELATES OF *ROBO2*.

To access these data, click or select the words "Appendix 1".

ACKNOWLEDGMENTS

This work was supported by DoD CDMRP Grant W81XWH1210255 from the USA Army Medical Research & Materiel Command and the Telemedicine and Advanced Technology (EEG), NIH Grant R01EY017841 (EEG), Vision Core Grant P30EY006360 (P. Michael Iuvone), and Unrestricted Funds from Research to Prevent Blindness (Emory University). We thank XiangDi Wang and Arthur Centeno for their technical assistance in this project. This study was supported in part by the Emory Integrated Genomics Core (EIGC), which is subsidized by the Emory University School of Medicine and is one of the Emory Integrated Core Facilities.

REFERENCES

1. Consortium EP, Birney E, Stamatoyannopoulos JA, Dutta A, Guigo R, Gingeras TR, Margulies EH, Weng Z, Snyder M, Dermitzakis ET, Thurman RE, Kuehn MS, Taylor CM, Neph S, Koch CM, Asthana S, Malhotra A, Adzhubei I, Greenbaum JA, Andrews RM, Flicek P, Boyle PJ, Cao H, Carter NP, Clelland GK, Davis S, Day N, Dhami P, Dillon SC, Dorschner MO, Fiegler H, Giresi PG, Goldy J, Hawrylycz M, Haydock A, Humbert R, James KD, Johnson BE, Johnson EM, Frum TT, Rosenzweig ER, Karnani N, Lee K, Lefebvre GC, Navas PA, Neri F, Parker SC, Sabo PJ, Sandstrom R, Shafer A, Vetrie D, Weaver M, Wilcox S, Yu M, Collins FS, Dekker J, Lieb JD, Tullius TD, Crawford GE, Sunyaev S, Noble WS, Dunham I, Denoeud F, Reymond A, Kapranov P, Rozowsky J, Zheng D, Castelo R, Frankish A, Harrow J, Ghosh S, Sandelin A, Hofacker IL, Baertsch R, Keefe D, Dike S, Cheng J, Hirsch HA, Sekinger EA, Lagarde J, Abril JF, Shahab A, Flamm C, Fried C, Hackermuller J, Hertel J, Lindemeyer M, Missal K, Tanzer A, Washietl S, Korbel J, Emanuelsson O, Pedersen JS, Holroyd N, Taylor R, Swarbreck D, Matthews N, Dickson MC, Thomas DJ, Weirauch MT, Gilbert J, Drenkow J, Bell I, Zhao X, Srinivasan KG, Sung WK, Ooi HS, Chiu KP, Foissac S, Alioto T, Brent M, Pachter L, Tress ML, Valencia A, Choo SW, Choo CY, Ucla C, Manzano C, Wyss C, Cheung E, Clark TG, Brown JB, Ganesh M, Patel S, Tammana H, Chrast J, Henrichsen CN, Kai C, Kawai J, Nagalakshmi U, Wu J, Lian Z, Lian J, Newburger P, Zhang X, Bickel P, Mattick JS, Carninci P, Hayashizaki Y, Weissman S, Hubbard T, Myers RM, Rogers J, Stadler PF, Lowe TM, Wei CL, Ruan Y, Struhl K, Gerstein M, Antonarakis SE, Fu Y, Green ED, Karaoz U, Siepel A, Taylor J, Liefer LA, Wetterstrand KA, Good PJ, Feingold EA, Guyer MS, Cooper GM, Asimenos G, Dewey CN, Hou M, Nikolaev S, Montoya-Burgos JI, Loytynoja A, Whelan S, Pardi F, Massingham T, Huang H, Zhang NR, Holmes I, Mullikin JC, Ureta-Vidal A, Paten B, Seringhaus M, Church D, Rosenbloom K, Kent WJ, Stone EA, Program NCS.

Baylor College of Medicine Human Genome Sequencing C, Washington University Genome Sequencing C, Broad I, Children's Hospital Oakland Research I, Batzoglou S, Goldman N, Hardison RC, Haussler D, Miller W, Sidow A, Trinklein ND, Zhang ZD, Barrera L, Stuart R, King DC, Ameur A, Enroth S, Bieda MC, Kim J, Bhinge AA, Jiang N, Liu J, Yao F, Vega VB, Lee CW, Ng P, Shahab A, Yang A, Moqtaderi Z, Zhu Z, Xu X, Squazzo S, Oberley MJ, Inman D, Singer MA, Richmond TA, Munn KJ, Rada-Iglesias A, Wallerman O, Komorowski J, Fowler JC, Couttet P, Bruce AW, Dovey OM, Ellis PD, Langford CF, Nix DA, Euskirchen G, Hartman S, Urban AE, Kraus P, Van Calcar S, Heintzman N, Kim TH, Wang K, Qu C, Hon G, Luna R, Glass CK, Rosenfeld MG, Aldred SF, Cooper SJ, Halees A, Lin JM, Shulha HP, Zhang X, Xu M, Haidar JN, Yu Y, Ruan Y, Iyer VR, Green RD, Wadelius C, Farnham PJ, Ren B, Harte RA, Hinrichs AS, Trumbower H, Clawson H, Hillman-Jackson J, Zweig AS, Smith K, Thakkapallayil A, Barber G, Kuhn RM, Karolchik D, Armengol L, Bird CP, de Bakker PI, Kern AD, Lopez-Bigas N, Martin JD, Stranger BE, Woodroffe A, Davydov E, Dimas A, Eyras E, Hallgrimsdottir IB, Huppert J, Zody MC, Abecasis GR, Estivill X, Bouffard GG, Guan X, Hansen NF, Idol JR, Maduro VV, Maskeri B, McDowell JC, Park M, Thomas PJ, Young AC, Blakesley RW, Muzny DM, Sodergren E, Wheeler DA, Worley KC, Jiang H, Weinstock GM, Gibbs RA, Graves T, Fulton R, Mardis ER, Wilson RK, Clamp M, Cuff J, Gnerre S, Jaffe DB, Chang JL, Lindblad-Toh K, Lander ES, Koriabine M, Nefedov M, Osoegawa K, Yoshinaga Y, Zhu B, de Jong PJ. Identification and analysis of functional elements in 1% of the human genome by the ENCODE pilot project. Nature 2007; 447:799-816. [PMID: 17571346].

2. Lander ES, Linton LM, Birren B, Nusbaum C, Zody MC, Baldwin J, Devon K, Dewar K, Doyle M, FitzHugh W, Funke R, Gage D, Harris K, Heaford A, Howland J, Kann L, Lehoczky J, LeVine R, McEwan P, McKernan K, Meldrim J, Mesirov JP, Miranda C, Morris W, Naylor J, Raymond C, Rosetti M, Santos R, Sheridan A, Sougnez C, Stange-Thomann N, Stojanovic N, Subramanian A, Wyman D, Rogers J, Sulston J, Ainscough R, Beck S, Bentley D, Burton J, Clee C, Carter N, Coulson A, Deadman R, Deloukas P, Dunham A, Dunham I, Durbin R, French L, Grafham D, Gregory S, Hubbard T, Humphray S, Hunt A, Jones M, Lloyd C, McMurray A, Matthews L, Mercer S, Milne S, Mullikin JC, Mungall A, Plumb R, Ross M, Shownkeen R, Sims S, Waterston RH, Wilson RK, Hillier LW, McPherson JD, Marra MA, Mardis ER, Fulton LA, Chinwalla AT, Pepin KH, Gish WR, Chissoe SL, Wendl MC, Delehaunty KD, Miner TL, Delehaunty A, Kramer JB, Cook LL, Fulton RS, Johnson DL, Minx PJ, Clifton SW, Hawkins T, Branscomb E, Predki P, Richardson P, Wenning S, Slezak T, Doggett N, Cheng JF, Olsen A, Lucas S, Elkin C, Uberbacher E, Frazier M, Gibbs RA, Muzny DM, Scherer SE, Bouck JB, Sodergren EJ, Worley KC, Rives CM, Gorrell JH, Metzker ML, Naylor SL, Kucherlapati RS, Nelson DL, Weinstock GM, Sakaki Y, Fujiyama A, Hattori M, Yada T, Toyoda A, Itoh T, Kawagoe C, Watanabe H, Totoki Y, Taylor T, Weissenbach J, Heilig R, Saurin W, Artiguenave F, Brottier P, Bruls T, Pelletier E, Robert C, Wincker P, Smith DR, Doucette-Stamm L, Rubenfield M, Weinstock K, Lee HM, Dubois J, Rosenthal A, Platzer M, Nyakatura G, Taudien S, Rump A, Yang H, Yu J, Wang J, Huang G, Gu J, Hood L, Rowen L, Madan A, Qin S, Davis RW, Federspiel NA, Abola AP, Proctor MJ, Myers RM, Schmutz J, Dickson M, Grimwood J, Cox DR, Olson MV, Kaul R, Raymond C, Shimizu N, Kawasaki K, Minoshima S, Evans GA, Athanasiou M, Schultz R, Roe BA, Chen F, Pan H, Ramser J, Lehrach H, Reinhardt R, McCombie WR, de la Bastide M, Dedhia N, Blocker H, Hornischer K, Nordsiek G, Agarwala R, Aravind L, Bailey JA, Bateman A, Batzoglou S, Birney E, Bork P, Brown DG, Burge CB, Cerutti L, Chen HC, Church D, Clamp M, Copley RR, Doerks T, Eddy SR, Eichler EE, Furey TS, Galagan J, Gilbert JG, Harmon C, Hayashizaki Y, Haussler D, Hermjakob H, Hokamp K, Jang W, Johnson LS, Jones TA, Kasif S, Kaspryzk A, Kennedy S, Kent WJ, Kitts P, Koonin EV, Korf I, Kulp D, Lancet D, Lowe TM, McLysaght A, Mikkelsen T, Moran JV, Mulder N, Pollara VJ, Ponting CP, Schuler G, Schultz J, Slater G, Smit AF, Stupka E, Szustakowski J, Thierry-Mieg D, Thierry-Mieg J, Wagner L, Wallis J, Wheeler R, Williams A, Wolf YI, Wolfe KH, Yang SP, Yeh RF, Collins F, Guyer MS, Peterson J, Felsenfeld A, Wetterstrand KA, Patrinos A, Morgan MJ, de Jong P, Catanese JJ, Osoegawa K, Shizuya H, Choi S, Chen YJ. International Human Genome Sequencing C. Initial sequencing and analysis of the human genome. Nature 2001; 409:860-921. [PMID: 11237011].

3. Pennisi E. Genomics. ENCODE project writes eulogy for junk DNA. Science 2012; 337:1159-61. [PMID: 22955811].

4. Rubin GM, Yandell MD, Wortman JR, Gabor Miklos GL, Nelson CR, Hariharan IK, Fortini ME, Li PW, Apweiler R, Fleischmann W, Cherry JM, Henikoff S, Skupski MP, Misra S, Ashburner M, Birney E, Boguski MS, Brody T, Brokstein P, Celniker SE, Chervitz SA, Coates D, Cravchik A, Gabrielian A, Galle RF, Gelbart WM, George RA, Goldstein LS, Gong F, Guan P, Harris NL, Hay BA, Hoskins RA, Li J, Li Z, Hynes RO, Jones SJ, Kuehl PM, Lemaitre B, Littleton JT, Morrison DK, Mungall C, O'Farrell PH, Pickeral OK, Shue C, Vosshall LB, Zhang J, Zhao Q, Zheng XH, Lewis S. Comparative genomics of the eukaryotes. Science 2000; 287:2204-15. [PMID: 10731134].

5. Venter JC, Adams MD, Myers EW, Li PW, Mural RJ, Sutton GG, Smith HO, Yandell M, Evans CA, Holt RA, Gocayne JD, Amanatides P, Ballew RM, Huson DH, Wortman JR, Zhang Q, Kodira CD, Zheng XH, Chen L, Skupski M, Subramanian G, Thomas PD, Zhang J, Gabor Miklos GL, Nelson C, Broder S, Clark AG, Nadeau J, McKusick VA, Zinder N, Levine AJ, Roberts RJ, Simon M, Slayman C, Hunkapiller M, Bolanos R, Delcher A, Dew I, Fasulo D, Flanigan M, Florea L, Halpern A, Hannenhalli S, Kravitz S, Levy S, Mobarry C, Reinert K, Remington K, Abu-Threideh J, Beasley E, Biddick K, Bonazzi V, Brandon R, Cargill M, Chandramouliswaran I, Charlab R, Chaturvedi K, Deng Z, Di Francesco V, Dunn P, Eilbeck K, Evangelista C, Gabrielian AE, Gan W, Ge W, Gong F, Gu Z, Guan P, Heiman TJ, Higgins ME, Ji RR, Ke Z, Ketchum KA, Lai Z, Lei Y, Li Z, Li J, Liang Y, Lin X, Lu F, Merkulov GV, Milshina N, Moore HM, Naik AK, Narayan VA, Neelam B, Nusskern D, Rusch DB, Salzberg S, Shao W,

Shue B, Sun J, Wang Z, Wang A, Wang X, Wang J, Wei M, Wides R, Xiao C, Yan C, Yao A, Ye J, Zhan M, Zhang W, Zhang H, Zhao Q, Zheng L, Zhong F, Zhong W, Zhu S, Zhao S, Gilbert D, Baumhueter S, Spier G, Carter C, Cravchik A, Woodage T, Ali F, An H, Awe A, Baldwin D, Baden H, Barnstead M, Barrow I, Beeson K, Busam D, Carver A, Center A, Cheng ML, Curry L, Danaher S, Davenport L, Desilets R, Dietz S, Dodson K, Doup L, Ferriera S, Garg N, Gluecksmann A, Hart B, Haynes J, Haynes C, Heiner C, Hladun S, Hostin D, Houck J, Howland T, Ibegwam C, Johnson J, Kalush F, Kline L, Koduru S, Love A, Mann F, May D, McCawley S, McIntosh T, McMullen I, Moy M, Moy L, Murphy B, Nelson K, Pfannkoch C, Pratts E, Puri V, Qureshi H, Reardon M, Rodriguez R, Rogers YH, Romblad D, Ruhfel B, Scott R, Sitter C, Smallwood M, Stewart E, Strong R, Suh E, Thomas R, Tint NN, Tse S, Vech C, Wang G, Wetter J, Williams S, Williams M, Windsor S, Winn-Deen E, Wolfe K, Zaveri J, Zaveri K, Abril JF, Guigo R, Campbell MJ, Sjolander KV, Karlak B, Kejariwal A, Mi H, Lazareva B, Hatton T, Narechania A, Diemer K, Muruganujan A, Guo N, Sato S, Bafna V, Istrail S, Lippert R, Schwartz R, Walenz B, Yooseph S, Allen D, Basu A, Baxendale J, Blick L, Caminha M, Carnes-Stine J, Caulk P, Chiang YH, Coyne M, Dahlke C, Mays A, Dombroski M, Donnelly M, Ely D, Esparham S, Fosler C, Gire H, Glanowski S, Glasser K, Glodek A, Gorokhov M, Graham K, Gropman B, Harris M, Heil J, Henderson S, Hoover J, Jennings D, Jordan C, Jordan J, Kasha J, Kagan L, Kraft C, Levitsky A, Lewis M, Liu X, Lopez J, Ma D, Majoros W, McDaniel J, Murphy S, Newman M, Nguyen T, Nguyen N, Nodell M, Pan S, Peck J, Peterson M, Rowe W, Sanders R, Scott J, Simpson M, Smith T, Sprague A, Stockwell T, Turner R, Venter E, Wang M, Wen M, Wu D, Wu M, Xia A, Zandieh A, Zhu X. The sequence of the human genome. Science 2001; 291:1304-51. [PMID: 11181995].

6. Redmond TM, Yu S, Lee E, Bok D, Hamasaki D, Chen N, Goletz P, Ma JX, Crouch RK, Pfeifer K. Rpe65 is necessary for production of 11-cis-vitamin A in the retinal visual cycle. Nat Genet 1998; 20:344-51. [PMID: 9843205].

7. Allikmets R, Shroyer NF, Singh N, Seddon JM, Lewis RA, Bernstein PS, Peiffer A, Zabriskie NA, Li Y, Hutchinson A, Dean M, Lupski JR, Leppert M. Mutation of the Stargardt disease gene (ABCR) in age-related macular degeneration. Science 1997; 277:1805-7. [PMID: 9295268].

8. Nathans J, Hogness DS. Isolation and nucleotide sequence of the gene encoding human rhodopsin. Proc Natl Acad Sci USA 1984; 81:4851-5. [PMID: 6589631].

9. Swaroop A, Wang QL, Wu W, Cook J, Coats C, Xu S, Chen S, Zack DJ, Sieving PA. Leber congenital amaurosis caused by a homozygous mutation (R90W) in the homeodomain of the retinal transcription factor CRX: direct evidence for the involvement of CRX in the development of photoreceptor function. Hum Mol Genet 1999; 8:299-305. [PMID: 9931337].

10. Bork JM, Peters LM, Riazuddin S, Bernstein SL, Ahmed ZM, Ness SL, Polomeno R, Ramesh A, Schloss M, Srisailpathy CR, Wayne S, Bellman S, Desmukh D, Ahmed Z, Khan SN, Kaloustian VM, Li XC, Lalwani A, Riazuddin S, Bitner-Glindzicz M, Nance WE, Liu XZ, Wistow G, Smith RJ, Griffith AJ, Wilcox ER, Friedman TB, Morell RJ. Usher syndrome 1D and nonsyndromic autosomal recessive deafness DFNB12 are caused by allelic mutations of the novel cadherin-like gene CDH23. Am J Hum Genet 2001; 68:26-37. [PMID: 11090341].

11. Adato A, Weil D, Kalinski H, Pel-Or Y, Ayadi H, Petit C, Korostishevsky M, Bonne-Tamir B. Mutation profile of all 49 exons of the human myosin VIIA gene, and haplotype analysis, in Usher 1B families from diverse origins. Am J Hum Genet 1997; 61:813-21. [PMID: 9382091].

12. Stone EM, Fingert JH, Alward WL, Nguyen TD, Polansky JR, Sunden SL, Nishimura D, Clark AF, Nystuen A, Nichols BE, Mackey DA, Ritch R, Kalenak JW, Craven ER, Sheffield VC. Identification of a gene that causes primary open angle glaucoma. Science 1997; 275:668-70. [PMID: 9005853].

13. Crooks KR, Allingham RR, Qin X, Liu Y, Gibson JR, Santiago-Turla C, Larocque-Abramson KR, Del Bono E, Challa P, Herndon LW, Akafo S, Wiggs JL, Schmidt S, Hauser MA. Genome-wide linkage scan for primary open angle glaucoma: influences of ancestry and age at diagnosis. PLoS ONE 2011; 6:e21967-[PMID: 21765929].

14. Ulmer M, Li J, Yaspan BL, Ozel AB, Richards JE, Moroi SE, Hawthorne F, Budenz DL, Friedman DS, Gaasterland D, Haines J, Kang JH, Lee R, Lichter P, Liu Y, Pasquale LR, Pericak-Vance M, Realini A, Schuman JS, Singh K, Vollrath D, Weinreb R, Wollstein G, Zack DJ, Zhang K, Young T, Allingham RR, Wiggs JL, Ashley-Koch A, Hauser MA. Genome-wide analysis of central corneal thickness in primary open-angle glaucoma cases in the NEIGHBOR and GLAUGEN consortia. Invest Ophthalmol Vis Sci 2012; 53:4468-74. [PMID: 22661486].

15. Aung T, Ozaki M, Mizoguchi T, Allingham RR, Li Z, Haripriya A, Nakano S, Uebe S, Harder JM, Chan AS, Lee MC, Burdon KP, Astakhov YS, Abu-Amero KK, Zenteno JC, Nilgun Y, Zarnowski T, Pakravan M, Safieh LA, Jia L, Wang YX, Williams S, Paoli D, Schlottmann PG, Huang L, Sim KS, Foo JN, Nakano M, Ikeda Y, Kumar RS, Ueno M, Manabe S, Hayashi K, Kazama S, Ideta R, Mori Y, Miyata K, Sugiyama K, Higashide T, Chihara E, Inoue K, Ishiko S, Yoshida A, Yanagi M, Kiuchi Y, Aihara M, Ohashi T, Sakurai T, Sugimoto T, Chuman H, Matsuda F, Yamashiro K, Gotoh N, Miyake M, Astakhov SY, Osman EA, Al-Obeidan SA, Owaidhah O, Al-Jasim L, Al Shahwan S, Fogarty RA, Leo P, Yetkin Y, Oguz C, Kanavi MR, Beni AN, Yazdani S, Akopov EL, Toh KY, Howell GR, Orr AC, Goh Y, Meah WY, Peh SQ, Kosior-Jarecka E, Lukasik U, Krumbiegel M, Vithana EN, Wong TY, Liu Y, Koch AE, Challa P, Rautenbach RM, Mackey DA, Hewitt AW, Mitchell P, Wang JJ, Ziskind A, Carmichael T, Ramakrishnan R, Narendran K, Venkatesh R, Vijayan S, Zhao P, Chen X, Guadarrama-Vallejo D, Cheng CY, Perera SA, Husain R, Ho SL, Welge-Luessen UC, Mardin C, Schloetzer-Schrehardt U, Hillmer AM, Herms S, Moebus S, Nothen MM, Weisschuh N, Shetty R, Ghosh A, Teo YY, Brown MA, Lischinsky I. Blue Mountains Eye Study GT, Wellcome Trust Case Control C, Crowston JG,

Coote M, Zhao B, Sang J, Zhang N, You Q, Vysochinskaya V, Founti P, Chatzikyriakidou A, Lambropoulos A, Anastasopoulos E, Coleman AL, Wilson MR, Rhee DJ, Kang JH, May-Bolchakova I, Heegaard S, Mori K, Alward WL, Jonas JB, Xu L, Liebmann JM, Chowbay B, Schaeffeler E, Schwab M, Lerner F, Wang N, Yang Z, Frezzotti P, Kinoshita S, Fingert JH, Inatani M, Tashiro K, Reis A, Edward DP, Pasquale LR, Kubota T, Wiggs JL, Pasutto F, Topouzis F, Dubina M, Craig JE, Yoshimura N, Sundaresan P, John SW, Ritch R, Hauser MA, Khor CC. A common variant mapping to CACNA1A is associated with susceptibility to exfoliation syndrome. Nat Genet 2015; 47:387-92. [PMID: 25706626].

16. Scheetz TE, Fingert JH, Wang K, Kuehn MH, Knudtson KL, Alward WL, Boldt HC, Russell SR, Folk JC, Casavant TL, Braun TA, Clark AF, Stone EM, Sheffield VC. A genome-wide association study for primary open angle glaucoma and macular degeneration reveals novel Loci. PLoS ONE 2013; 8:e58657-[PMID: 23536807].

17. Grassi MA, Folk JC, Scheetz TE, Taylor CM, Sheffield VC, Stone EM. Complement factor H polymorphism p.Tyr402His and cuticular Drusen. Arch Ophthalmol 2007; 125:93-7. [PMID: 17210858].

18. Geisert EE, Lu L, Freeman-Anderson NE, Templeton JP, Nassr M, Wang X, Gu W, Jiao Y, Williams RW. Gene expression in the mouse eye: an online resource for genetics using 103 strains of mice. Mol Vis 2009; 15:1730-63. [PMID: 19727342].

19. Freeman NE, Templeton JP, Orr WE, Lu L, Williams RW, Geisert EE. Genetic networks in the mouse retina: growth associated protein 43 and phosphatase tensin homolog network. Mol Vis 2011; 17:1355-72. [PMID: 21655357].

20. Peirce JL, Lu L, Gu J, Silver LM, Williams RW. A new set of BXD recombinant inbred lines from advanced intercross populations in mice. BMC Genet 2004; 5:7-[PMID: 15117419].

21. Chang B, Khanna H, Hawes N, Jimeno D, He S, Lillo C, Parapuram SK, Cheng H, Scott A, Hurd RE, Sayer JA, Otto EA, Attanasio M, O'Toole JF, Jin G, Shou C, Hildebrandt F, Williams DS, Heckenlively JR, Swaroop A. In-frame deletion in a novel centrosomal/ciliary protein CEP290/NPHP6 perturbs its interaction with RPGR and results in early-onset retinal degeneration in the rd16 mouse. Hum Mol Genet 2006; 15:1847-57. [PMID: 16632484].

22. Garcia DM, Baek D, Shin C, Bell GW, Grimson A, Bartel DP. Weak seed-pairing stability and high target-site abundance decrease the proficiency of lsy-6 and other microRNAs. Nat Struct Mol Biol 2011; 18:1139-46. [PMID: 21909094].

23. Grimson A, Farh KK, Johnston WK, Garrett-Engele P, Lim LP, Bartel DP. MicroRNA targeting specificity in mammals: determinants beyond seed pairing. Mol Cell 2007; 27:91-105. [PMID: 17612493].

24. Lewis BP, Burge CB, Bartel DP. Conserved seed pairing, often flanked by adenosines, indicates that thousands of human genes are microRNA targets. Cell 2005; 120:15-20. [PMID: 15652477].

25. Ruggiero L, Sarang Z, Szondy Z, Finnemann SC. alphavbeta5 integrin-dependent diurnal phagocytosis of shed photoreceptor outer segments by RPE cells is independent of the integrin coreceptor transglutaminase-2. Adv Exp Med Biol 2012; 723:731-7. [PMID: 22183400].

26. Wistow G. The NEIBank project for ocular genomics: data-mining gene expression in human and rodent eye tissues. Prog Retin Eye Res 2006; 25:43-77. [PMID: 16005676].

27. Blackshaw S, Harpavat S, Trimarchi J, Cai L, Huang H, Kuo WP, Weber G, Lee K, Fraioli RE, Cho SH, Yung R, Asch E, Ohno-Machado L, Wong WH, Cepko CL. Genomic analysis of mouse retinal development. PLoS Biol 2004; 2:E247-[PMID: 15226823].

28. Blackshaw S, Fraioli RE, Furukawa T, Cepko CL. Comprehensive analysis of photoreceptor gene expression and the identification of candidate retinal disease genes. Cell 2001; 107:579-89. [PMID: 11733058].

29. Siegert S, Scherf BG, Del Punta K, Didkovsky N, Heintz N, Roska B. Genetic address book for retinal cell types. Nat Neurosci 2009; 12:1197-204. [PMID: 19648912].

30. Gong S, Doughty M, Harbaugh CR, Cummins A, Hatten ME, Heintz N, Gerfen CR. Targeting CRE recombinase to specific neuron populations with Bacterial Artificial Chromosome constructs J Neurosci 2007; 27:9817-23. [PMID: 17855595].

31. Howell GR, Macalinao DG, Sousa GL, Walden M, Soto I, Kneeland SC, Barbay JM, King BL, Marchant JK, Hibbs M, Stevens B, Barres BA, Clark AF, Libby RT, John SW. Molecular clustering identifies complement and endothelin induction as early events in a mouse model of glaucoma. J Clin Invest 2011; 121:1429-44. [PMID: 21383504].

32. Templeton JP, Freeman NE, Nickerson JM, Jablonski MM, Rex TS, Williams RW, Geisert EE. Innate immune network in the retina activated by optic nerve crush. Invest Ophthalmol Vis Sci 2013; 54:2599-606. [PMID: 23493296].

33. Templeton JP, Wang X, Freeman NE, Ma Z, Lu A, Hejtmancik F, Geisert EE. A crystallin gene network in the mouse retina. Exp Eye Res 2013; 116:129-40. [PMID: 23978599].

Articles are provided courtesy of Emory University and the Zhongshan Ophthalmic Center, Sun Yat-sen University, P.R. China. The print version of this article was created on 26 October 2015. This reflects all typographical corrections and errata to the article through that date. Details of any changes may be found in the online version of the article.

Appendix B

frontiers in Genetics

ORIGINAL RESEARCH
published: 28 September 2016
doi: 10.3389/fgene.2016.00169

Genetic Networks in Mouse Retinal Ganglion Cells

Felix L. Struebing[1], *Richard K. Lee*[2], *Robert W. Williams*[3] *and Eldon E. Geisert*[1]*

[1] Department of Ophthalmology, Emory University School of Medicine, Atlanta, GA, USA, [2] Bascom Palmer Eye Institute, University of Miami Miller School of Medicine, Miami, FL, USA, [3] Department of Genetics, Genomics and Informatics, University of Tennessee Health Science Center, Memphis, TN, USA

Retinal ganglion cells (RGCs) are the output neuron of the eye, transmitting visual information from the retina through the optic nerve to the brain. The importance of RGCs for vision is demonstrated in blinding diseases where RGCs are lost, such as in glaucoma or after optic nerve injury. In the present study, we hypothesize that normal RGC function is transcriptionally regulated. To test our hypothesis, we examine large retinal expression microarray datasets from recombinant inbred mouse strains in GeneNetwork and define transcriptional networks of RGCs and their subtypes. Two major and functionally distinct transcriptional networks centering around *Thy1* and *Tubb3* (Class III beta-tubulin) were identified. Each network is independently regulated and modulated by unique genomic loci. Meta-analysis of publically available data confirms that RGC subtypes are differentially susceptible to death, with alpha-RGCs and intrinsically photosensitive RGCs (ipRGCs) being less sensitive to cell death than other RGC subtypes in a mouse model of glaucoma.

Keywords: retinal ganglion cells, gene regulatory networks, transcription factors, recombinant inbred strain, subtypes

OPEN ACCESS

Edited by:
Igor Ponomarev,
University of Texas at Austin, USA

Reviewed by:
Claudio V. Mello,
Oregon Health & Science University, USA
Michael F. Miles,
Virginia Commonwealth University, USA

***Correspondence:**
Eldon E. Geisert
egeiser@emory.edu

Specialty section:
This article was submitted to Neurogenomics, a section of the journal Frontiers in Genetics

Received: *01 June 2016*
Accepted: *06 September 2016*
Published: *28 September 2016*

Citation:
Struebing FL, Lee RK, Williams RW and Geisert EE (2016) Genetic Networks in Mouse Retinal Ganglion Cells. Front. Genet. 7:169. doi: 10.3389/fgene.2016.00169

INTRODUCTION

The retinal ganglion cell (RGC) is the final output neuron of the retina, projecting through the optic nerve to the brain, where it targets a number of functionally distinct areas: for visual perception, RGC axons travel to the lateral geniculate nucleus (Chalupa and Günhan, 2004); for the regulation of circadian rhythms, they pass through the suprachiasmatic nucleus (Guido et al., 2010); for eye movements, a group of RGC axons terminates in the superior colliculus (Triplett et al., 2014); and for the pupillary light reflex, RCG axons terminate in the pretectal area (Young and Lund, 1998). Each of these areas receives input from distinct subtypes of RGCs with unique morphological and molecular signatures. At the present time, over 30 subtypes of RGCs (Baden et al., 2016) are estimated to exist. They all receive inputs from other types of retinal neurons (bipolar cells and amacrine cells), and most of them express similar groups of genes that may serve as general RGC markers (Raymond et al., 2008; Rodriguez et al., 2014). Identifying gene expression patterns in RGCs and their subtypes is currently an active area of research, as demonstrated by the discovery of new subtypes of ganglion cells based on gene expression (Macosko et al., 2015; Sanes and Masland, 2015).

The death of RGCs in glaucoma or after injury eventually leads to loss of vision (Templeton et al., 2009; Zode et al., 2011; Munguba et al., 2014; Nuschke et al., 2015). However, the susceptibility of RGC subtypes to death differs among the distinct subtypes. Some RGCs are resistant to injury, while others appear to be more sensitive to insult, indicating differential gene expression and response to injury among subtypes (Chang et al., 2013; Duan et al., 2015; Puyang et al., 2015). The present

study focuses on transcriptional networks within RGCs of the mouse, using gene expression data measured across 55 strains of recombinant inbred BXD mice (King et al., 2015) as well as the bioinformatic tools from GeneNetwork (Williams and Mulligan, 2012). The analysis begins by examining genes correlated with two relatively general RGC markers, *Thy1* and *Tubb3*. Each of these markers forms a unique network of genes that appears to function independently across many of the RGC subtypes. These networks are functionally different to the point of having distinct transcription factor binding sites. Subtype-specific networks partially overlapping with the *Thy1*-network are also present. In a meta-analysis of previously published data from a microarray study of a mouse glaucoma model (Howell et al., 2011), we examine the differential effects of this disease state on transcriptional networks in RGC subtypes and confirm intrinsically photosensitive RGCs (ipRGCs) and alpha-RGCs as more resistant to cell death (Duan et al., 2015).

The systems genetics and bioinformatics approach used in the present study demonstrates how signatures of RGCs and their subtypes can be extracted from a complex neural tissue such as the retina.

RESULTS

RGC Markers Segregate into Two Major Correlation Networks

The present study examines the correlation of gene expression in the retina across the BXD recombinant inbred strain set to define gene networks active in RGCs. The BXD strain set is derived from two parental strains, the C57BL/6J mouse and the DBA/2J mouse. Natural variation in gene expression across strains can be used to identify co-regulated genes with a similar expression pattern, allowing for the construction of genetic networks (Williams et al., 2001; Geisert et al., 2009; Templeton et al., 2013a; Keeley et al., 2014).

The data used in this study consist of whole retinal samples collected from 55 BXD strains. They can be found on www.genenetwork.org under the identifier "DoD Retina Normal Affy MoGene 2.0 ST (May15) RMA Gene Level". Two features of this dataset enhance the quality of the analysis: The first is that the retina is a tissue that can be consistently isolated with minimal contamination by other tissues. The second is the quality of the RNA with an average RNA Integrity Score of 9.43 and a standard error of 0.037 across the 220 samples isolated for this dataset.

The analysis began with two well-characterized markers for RGCs, *Thy1* and *Tubb3*, as they both exhibited substantial variability in mRNA expression levels across BXD strains (**Figure 1**). Expression of *Thy1* ranged from 10.39 in BXD42 to 11.45 in BXD15 (this data is presented on a $\log_2$ scale and the difference in expression is equivalent to an over 2-fold change). A similar variability in gene expression was observed for *Tubb3*, with expression levels ranging from 9.68 (BXD6) to 10.74 (BXD2). When correlations for *Thy1* and *Tubb3* were made across all microarray data, both produced a highly correlated group of genes. For *Thy1*, the top 100 correlates had an absolute *r*-value (Pearson) greater than 0.89 (Bonferroni-adjusted $p < 1e^{-12}$) and the top 2000 correlates all had an absolute *r*-value greater than 0.77 (adj. $p < 1e^{-8}$). If we examine the Pearson correlation values above 0.60, which corresponds to an adjusted *p*-value of 0.02, then *Thy1* has a total of 8596 correlates. This tightly correlated list of genes forms a potential network, and indicates that the genes in this network are co-regulated across the BXD strains (King et al., 2015). Within the list of the top 2000 *Thy1*-correlates, we found several other well-characterized RGC markers, including *Rbfox3* (producing NeuN, Neuronal Nuclei), *Pou4f1* (producing BRN3A), and *Pou4f2* (producing BRN3B) (**Table 1**). Interestingly, the *Thy1* correlate list did not contain other known RGC markers, including *Tubb3*.

For *Tubb3*, the top 100 genes had an absolute *r* value greater than 0.71 (adj. $p < 1e^{-6}$), and the top 2000 genes showed values greater than 0.52 (adj. $p = 0.12$) and did not contain *Thy1*, *Pou4f1*, *Pou4f2*, or *Rbfox3*. This was also true for the 1387 correlates with Pearson $r > 0.60$ (equal to a significant Bonferroni-adjusted *p*-value of 0.02). However, other RGC markers were present in the *Tubb3* correlation list, including the newly described *Rbpms* (RNA binding protein with multiple splicing) as well as *Calb2* (Calbindin 2) and *Chrna6* (Cholinergic receptor nicotinic alpha 6).

These two networks are relatively independent, with minimal overlap. When examining the correlates of the *Thy1*-network relative to the *Tubb3*-network, only one gene is shared within their top 100 correlations (1%), 31 genes (1.55%) are present in the top 2000 correlations, and 51 genes (0.05%) are in common with the 9982 genes found in both the *Thy1* (8596 genes) and the *Tubb3* (1386 genes) correlation lists with a Pearson correlation above 0.6.

The basis for the segregation of genes into two distinct networks is illustrated by plotting the correlations for combinations of genes from both networks. In **Figure 2**, the expression of *Thy1*, *Pou4f1*, *Tubb3,* and *Rbpms* across BXD strains is displayed in scatterplots. These plots demonstrate the tight correlation for *Thy1*-*Pou4f1* (**Figure 2A**) and *Tubb3*-*Rbpms* (**Figure 2C**). They further show the lack of correlation between *Thy1* and *Tubb3* (**Figure 2B**) as well as *Tubb3* and *Pou4f1* (**Figure 2D**). The presence of additional RGC markers in the correlation lists of *Thy1* and *Tubb3* together with the minimal overlap of genes indicated the presence of at least two RGC-specific transcriptional networks in mouse RGCs.

Since we selected *Thy1* and *Tubb3* to serve as primary RGC markers for this analysis based upon literature evidence, we wondered if an alternative unbiased approach would validate our findings. As an independent examination of these networks, we performed weighted gene correlation network analysis (WGCNA) on the whole microarray dataset (Langfelder and Horvath, 2008). This method relies on unsupervised clustering of co-expressed genes across all of the BXD RI strains into so-called modules or eigengenes and thus represents an unbiased approach to test the assumption that *Thy1*- and *Tubb3*- networks exist independently from each other. WGCNA created 18 modules of co-expressed genes. Module #1 contained 1741 of the top 2000 *Thy1* correlates, whereas only 131 genes from the top 2000

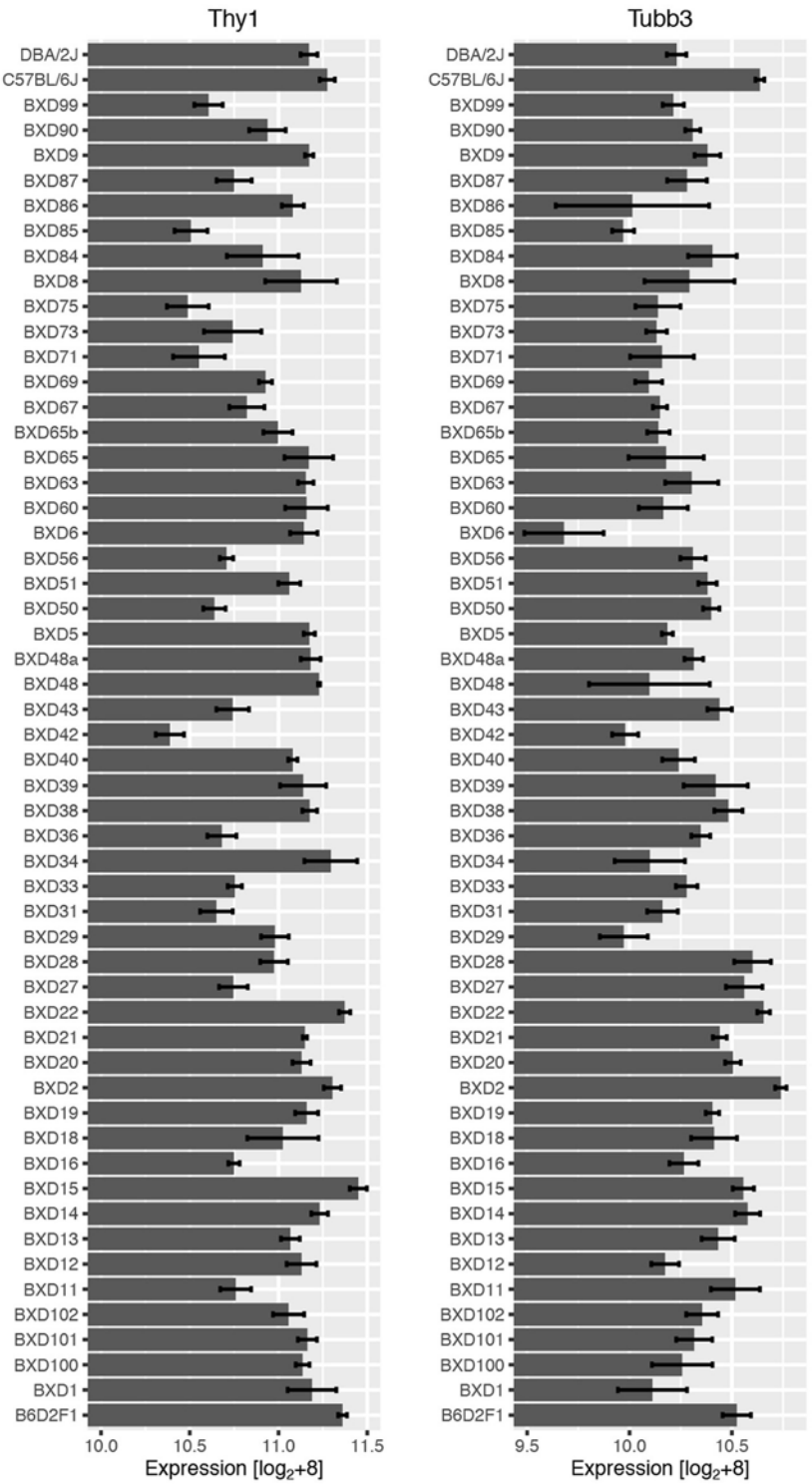

FIGURE 1 | RNA expression across the BXD RI strain set for *Thy1* (left) and *Tubb3* (right) with the means and standard errors. There was an approximately 2-fold difference in mean expression levels for both genes. This data is given as raw expression values on a $\log_2$ scale +8.

Tubb3 correlates were assigned to this module. The majority of the *Tubb3* correlates belonged to modules #4 ($n = 279$), #5 ($n = 886$), and #6 ($n = 327$), none of which contained any of the *Thy1* correlates. This minor overlap in module affiliation between genes of both networks reaffirms our finding that the *Thy1*- and *Tubb3*-network function individually.

TABLE 1 | List of all RGC marker genes used in this manuscript.

Symbol	RGC Subtype Labeled	References
Thy1	pan-RGC	Barnstable and Drager, 1984; Raymond et al., 2008
Rbfox3 (NeuN)	pan-RGC	Wolf et al., 1996; Schlamp et al., 2013; Kim et al., 2014
Pou4f2 (Brn3b)	RGC (about 50–60% of total population) ipRGCs (71% of all Melanopsin-positive cells)	Xiang et al., 1993; Erkman et al., 1996; Jain et al., 2012
Pou4f1 (Brn3a)	RGC (about 60–70% of total population)	Erkman et al., 1996; Jain et al., 2012
Tubb3 (class III beta-tubulin)	pan-RGC	Mellough et al., 2004
Rbpms (Retina binding protein with multiple splicing)	pan-RGC	Piri et al., 2006; Rodriguez et al., 2014
Nefl (Neurofilament light)	RGC (∼85% of all RGCs)	Ruiz-Ederra et al., 2004
Chrna6	RGC	Mackey et al., 2012; Munguba et al., 2013
Slc17a6 (Vglut2)	RGC	Bai et al., 2001; Mimura et al., 2002; Wässle et al., 2006
Nrn1	RGCs	Picard et al., 2014; Sharma et al., 2015
Calb2	pan-RGC (87% of all RGCs) transient OFF α-RGCs (tOFF-αRGCs, Huberman et al., 2008)	Huberman et al., 2008; Mojumder et al., 2008; Haverkamp et al., 2009
Sncg (gamma-synuclein)	RGC	Buckingham et al., 2008
Opn4 (Melanopsin)	ipRGC	Semo et al., 2005
Jam2	J-RGC (5% of all RGCs)	Daniele et al., 2007; Kim et al., 2008
Spp1 (Osteopontin)	alpha-RGC	Ju et al., 2000; Sanes and Masland, 2015
Kcng4	alpha-RGC	Duan et al., 2014; Sanes and Masland, 2015
Cartpt	ooDSGC	Adams et al., 1999; Kay et al., 2011
Hoxd10	ON-DSGC	Dhande et al., 2013

To define the genomic location of upstream modulators for both the *Thy1*- and the *Tubb3*-network, we examined interval maps for the 7 RGC marker genes found in both correlation lists (*Thy1*, *Rbfox3*, *Pou4f2*, *Pou4f1*, *Tubb3*, *Calb2*, and *Rbpms*). When we investigated each marker's signature quantitative trait locus (QTL), we found that *Thy1*, *Rbfox3*, *Pou4f2,* and *Pou4f1,* had similar interval maps. The same was true for *Tubb3*, *Calb2,* and *Rbpms*. To further investigate this phenomenon, we plotted multiple interval maps as heat maps for each marker and its 20 highest correlated genes (**Figure 3**). In these heat maps, rows correspond to the QTL curve of a single correlated gene plotted across the entire genome. Two color gradients were used to characterize differential expression between strains: A yellow to red gradient identified a transcript whose expression was higher in strains with a B haplotype (allele origin from C57BL/6J), whereas a green to blue gradient represented a transcript whose expression was higher in strains with the D haplotype (allele origin from DBA/2J). The linkage significance (LRS or LOD-score) increased with color intensity. In other words: A deeply colored vertical line characterized a genomic locus that may contain a regulatory element responsible for the differential expression of these genes.

These bands are thought to identify a genomic locus modulating the expression of the genes in the network across the BXD RI strains. Likely candidates for modulating gene expression include transcription factors, micro RNAs or long noncoding RNAs (Geisert et al., 2009; Templeton et al., 2013b; Williams and Auwerx, 2015). Since the analysis is only correlational in nature, we cannot exclude the possibility that loci for individual networks do not have regulatory roles, as they could just be co-regulated with the other identified networks. When comparing heat maps for both networks, no overlap in patterns was observed. Thus, the RGC marker genes segregated into two independently regulated gene networks. From here on, we will refer to these networks as the *Thy1*-network and the *Tubb3*-network. This is an arbitrary nomenclature, mirroring the most prominent RGC marker for each of both networks. For the *Thy1*-network, the strongest modulatory signature was localized at the distal end of Chromosome 1. For members of the *Tubb3*- network, the most prominent genomic signature was on mid-distal Chromosome 13. Several candidate genes exist in those loci; a comprehensive analysis is attached as Supplemental Material (Supplemental Tables 1, 2).

There are three potential scenarios that would allow two specific genetic networks to exist within a single cell population. The first is that the mRNA levels of each marker differ across the entire retina. The second explanation is that their mRNA expression levels differ in specific RGC subtypes, leading to unique expression of each protein within each RGC subtype. The third potential mechanism involves differences in the percentage of each of the RGC subtypes from strain to stain. To further examine this, we immunostained retinas with THY1 and Class III beta tubulin. In these retinal whole mounts, the more than 90% of labeled cells were double-labeled of RGCs were both THY1- and Class III beta tubulin- positive (**Figure 4**), indicating that the two markers are co-localized and expressed in the same cell. Despite their protein co-expression, their mRNA level may differ from cell to cell. When examining the double stained cells, the intensity of each stain varied from ganglion cell to ganglion cell. Some cells had approximately equal labeling for THY1 and Class III beta

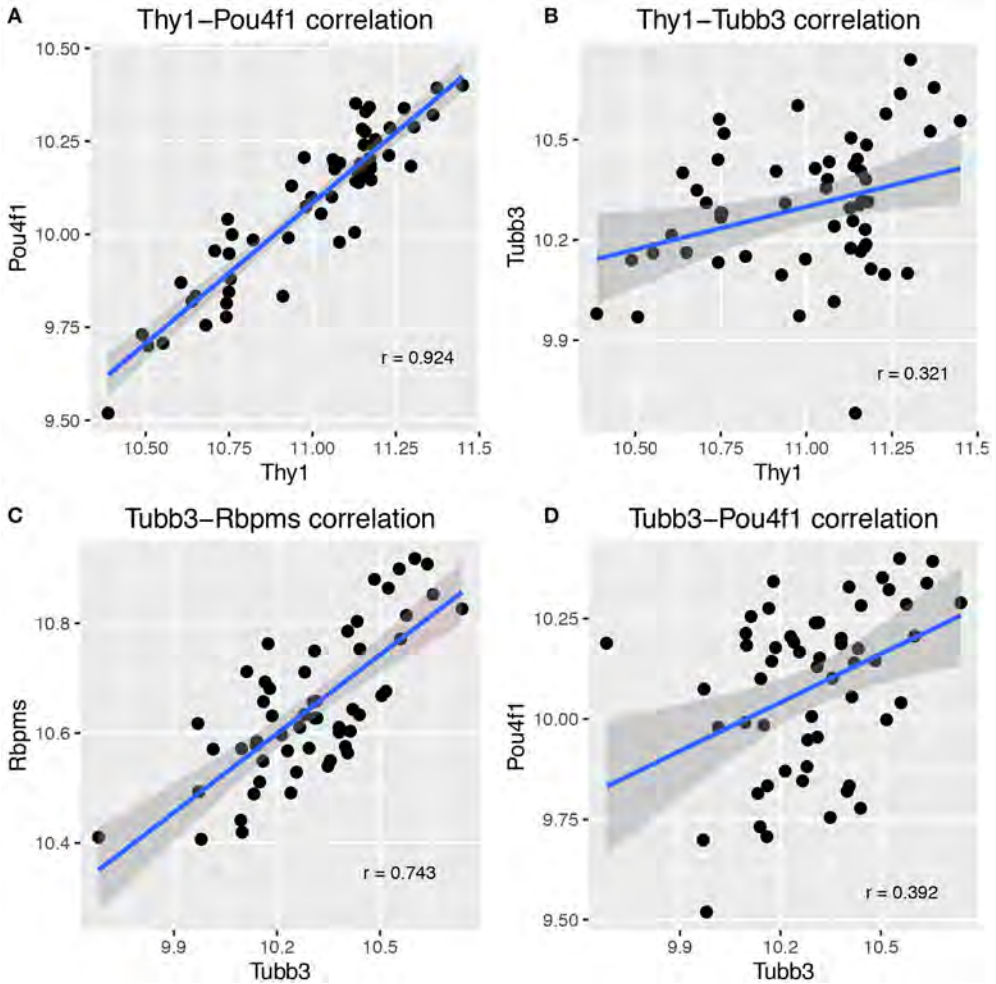

FIGURE 2 | Scatterplots illustrating the correlation between major RGC markers. There was a tight correlation between *Thy1* and *Pou4f1* **(A)**, which are part of the same network. Correlation dropped greatly for *Thy1* and *Tubb3* **(B)**, which are not part of the same network. Similarly, *Tubb3* correlated well with Rbpms **(C)** but not with *Pou4f1* **(D)**. Pearson's correlation coefficient is given in each plot on the lower right half. Each dot represents one BXD RI strain, and the confidence interval for the smoothing function (dark gray areas surrounding the blue line) is 0.95.

tubulin, while in other cells THY1 staining was more intense than Class III beta tubulin. In a few cells, the labeling of Class III beta tubulin was more intense. It also appeared that some cells were labeled by only one of the two markers. Thus, even though both markers are co-expressed in many RGCs, their expression levels do not consistently correlate with each other, corroborating that their expression is independently regulated.

Since multiple subtypes of RGCs are known to exist, one could predict that there are also multiple genetic networks within each of these subtypes. We compiled an extended list of RGC markers from the literature. This list consisted of 17 proteins and their respective genes, 6 of which are known to be relatively specific for a single RGC subtype (**Table 1**). Calculating the correlation in expression across the BXD RI strain set and displaying these relations in a network graph revealed that indeed two major network hubs formed around *Thy1* and *Tubb3* based on the highest correlations surrounding these two markers (**Figure 5**). The only significant connection between *Thy1* and *Tubb3* existed through 2 of their respective correlates, *Slc17a6* (VGLUT2), and *Chrna6*. Except for *Hoxd10* (a marker of ON-directionally selective RGCs), all the other RGC markers had a direct connection to either *Thy1* or *Tubb3*.

Functional Differences of RGC Networks

Following the identification of two gene networks related to normal RGC function, we asked whether both networks had any functional differences.

In order to facilitate this analysis, we grouped genes with a similar heat map pattern belonging to the same network into one "synthetic trait" using principal component analysis. These "synthetic traits" provide for more robust functional network analysis than a single marker gene, and they can be used to generate correlation lists specific to a group of genes by reducing

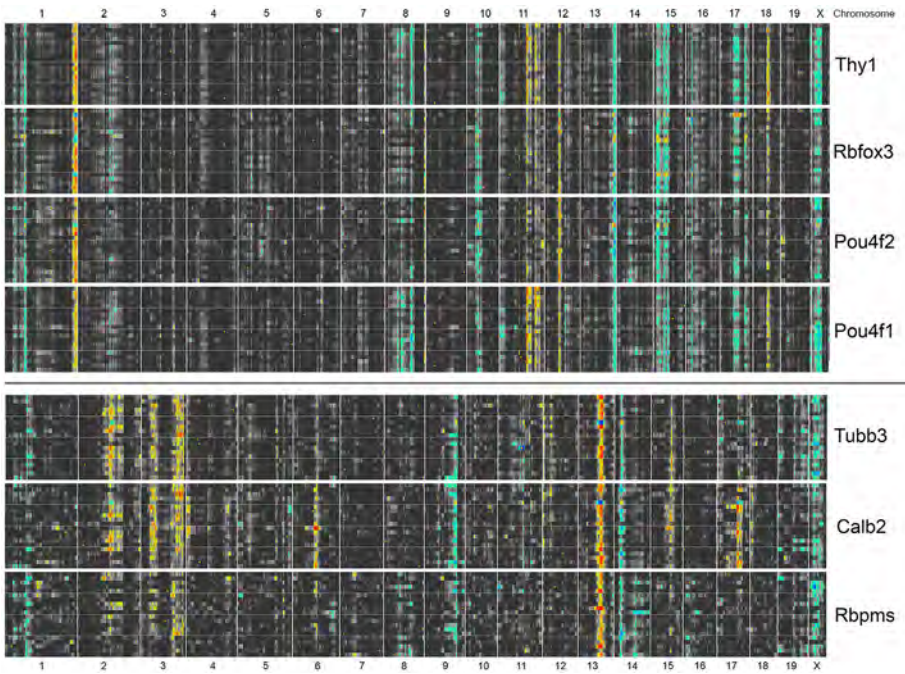

Gene	Network	Pearson r
9130221H12Rik	Rbfox3	0.87
9130221H12Rik	Pou4f2	0.83
Arhgap44	Thy1	0.92
Arhgap44	Pou4f1	0.89
Cnnm1	Thy1	0.93
Cnnm1	Rbfox3	0.86
Fam115a	Thy1	0.92
Fam115a	Pou4f1	0.87
Fam117b	Rbfox3	0.89
Fam117b	Pou4f2	0.81
Jup	Thy1	0.92
Jup	Pou4f1	0.87
Ndn	Thy1	0.95
Ndn	Pou4f1	0.87
Pou4f1	Thy1	0.92
Pou4f1	Pou4f2	0.81
Scrt1	Thy1	0.92
Scrt1	Pou4f1	0.87
Slc6a17	Thy1	0.93
Slc6a17	Rbfox3	0.87
Tmem130	Thy1	0.94
Tmem130	Pou4f1	0.88
Ube2ql1	Rbfox3	0.87
Ube2ql1	Pou4f2	0.85

Gene	Network	Pearson r
Prune	Calb2	0.72
Prune	Rbpms	0.70
Rab4b	Tubb3	0.82
Rab4b	Calb2	0.72
Tubb3	Calb2	0.74
Tubb3	Rbpms	0.74

FIGURE 3 | RGC markers segregate into two major correlation networks. For each of the general RGC markers on the right, the eQTL curve for the 20 highest correlated genes was plotted as a heat map. In these, the LRS/LOD score is given in pseudocolors: A yellow to red gradient identifies a transcript whose expression is higher in strains with a B haplotype at that locus (allele origin from C57BL/6J), whereas a green to blue gradient represents a transcript whose expression is higher in strains with the D haplotype (allele origin from DBA/2J). There are several strong and sharp trans-bands extending across *Thy1*, *Rbfox3*, *Pou4f2,* and *Pou4f1*, such as on distal Chromosome 1 or 13. There are also trans-bands extending across *Tubb3*, *Calb2,* and *Rbpms* on mid Chr. 13 and proximal Chr. 14. No overlap is present between the genes separated by the black line, indicating that RGC markers segregate into two major independently regulated gene networks. The panel on the right lists genes that are found in more than one of the top 20 correlations. For example, *Arhgap44* is present in the 20 highest correlates for both *Thy1* and *Pou4f1*.

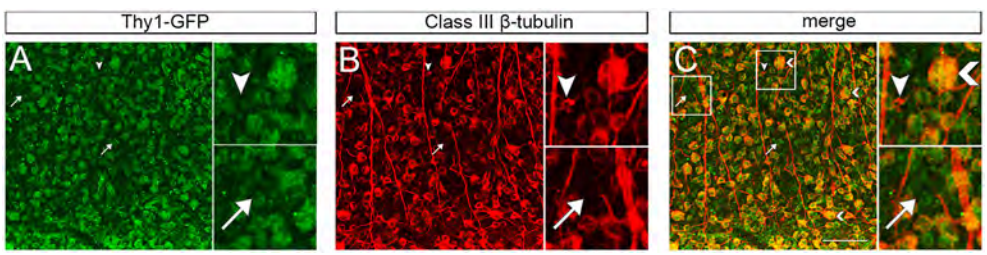

FIGURE 4 | Maximum intensity projections of confocal z-stacks taken from retinal whole-mounts showing the co-localization of THY1 (A) and Class III beta-tubulin (B) in the retinal ganglion cell layer from a C57BL/6 mouse. Most cells were double-stained for both RGC markers **(C)**, but some cells only expressed Class III beta-tubulin (arrowhead) or THY1 (arrow). Furthermore, the staining intensity was different across cells, and some cells had large somata and were more intensely stained than others (large arrowhead in "merge"). Staining with the secondary antibodies only did not result in unspecific fluorescence (data not shown). Scale bar in C = 100 μm.

the dimensionality of the data (Yin et al., 2012; Vanderlinden et al., 2013; Graybeal et al., 2014).

The synthetic trait for the *Thy1*-network was constructed using *Thy1* and its direct correlates *Rbfox3*, *Pou4f1,* and *Pou4f2*, while the *Tubb3*-network was constructed using *Tubb3*, *Calb2,* and *Rbpms*. When we compared the correlations of these networks using WebGestalt-based gene ontology (GO) analysis (Wang et al., 2013), each of the two synthetic traits was enriched in genes with very different molecular and cellular functions. The *Thy1*-network was significantly enriched in genes involved in neuron development, synaptic transmission, cation transmembrane transporter activity and voltage-gated channel activity (adj. $p < 0.0000001$ for all), strongly indicating that this network was highly neuron-specific (Supplemental Figure S1). Some examples of the genes associated with neuronal development and synaptic transmission included: *Tnr*, *NeuroD2*, *L1cam*, *Syn2*, *Grn4*, and *Gabbr1* (see Supplemental Table 3 for the whole list). A close examination of the highest ($r > 0.9$) correlates

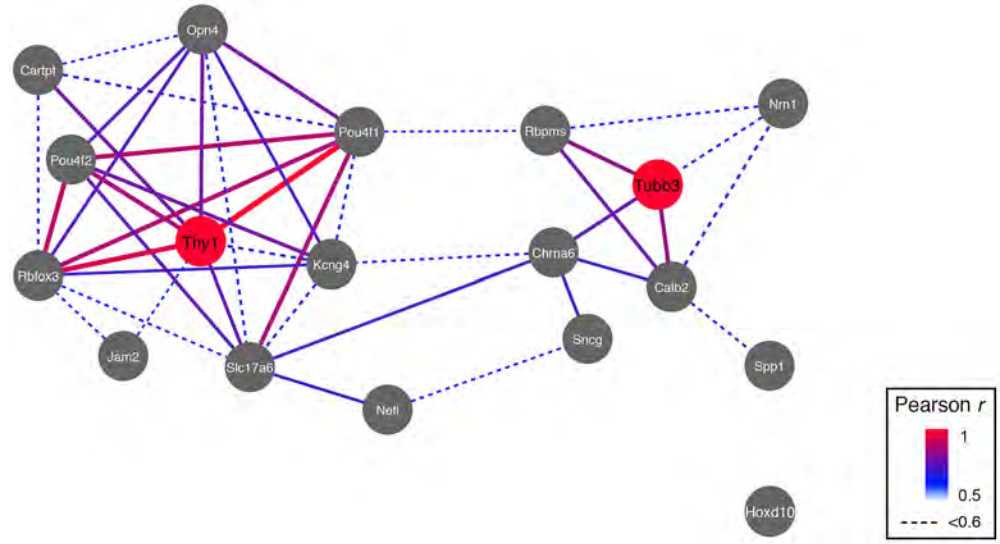

FIGURE 5 | RGC markers segregate into two networks, and two major hubs are formed around *Thy1* and *Tubb3*. The only connection between the *Thy1*- and the *Tubb3*-network is through two of their correlates, *Slc17a6* and *Chrna6*. Pearson's correlation coefficient was mapped to line color and thickness (high correlation = thicker and red bars).

also revealed that at least 6 genes (*Gsk3a*, *Srgap1*, *Arhgap44*, *Ncdn*, *L1cam*, and *Lrrc4b)* were functionally associated with neurite outgrowth.

The *Tubb3* synthetic network contained genes that were associated with completely different biological functions (Supplemental Figure S2). Several members of the tubulin family of proteins were at the top of the correlation list, such as *Tubg2*, *Tuba4a*, *Tubg1*, *Tubb5*, and *Tuba1b*. Gene Ontology analysis revealed enrichment in GO terms "guanyl nucleotide binding" and "protein polymerization" (both with adj. $p < 0.001$), including the genes *Rab11b*, *Bab8a*, *Tufm*, *Rabb1b*, *Arf6,* and *Rab4b*. The highest correlates of the *Tubb3* synthetic trait were two genes encoding proteins from the Rab family (*Rab15* and *Rab4b*).

TABLE 2a | Transcription factor binding site enrichment for genes of the *Thy1*-network.

Transcription Factor	Enrichment probability (fold) vs. Tubb3	Matched promoters *p*-value
P53	3.6921	1.17E-04
TBP	4.7405	2.47E-03
PPARgamma:RXR-alpha	1.1771	1.07E-02
PPAR direct repeat	1.7507	1.34E-02
LXR, PXR, CAR, COU	1.9258	1.93E-02
DEC1	4.4442	2.11E-02
FOXJ1	4.4442	2.11E-02
AP-1	1.2523	3.47E-02
SP1	1.1402	4.62E-02
ER-alpha	2.4295	5.18E-02

Distinct Groups of Transcription Factor Binding Sites Are Associated with the Two RGC networks

Since the *Thy1*- and the *Tubb3*-network were functionally enriched for distinct GO terms, we asked if this difference would be reflected in their transcription factor binding site (TFBS) distribution. We searched the promoter sequences for genes in the *Thy1*-network using the TRANSFAC FMatch algorithm (Matys et al., 2006) for over-represented TFBS in comparison to the *Tubb3*-network and vice versa (**Tables 2a,b**). Genes of the *Thy1*-network were ~4 times more enriched in TFBS for *p53* and *Dec1*, two master regulators of cell cycle progression (Qian et al., 2012). The *Thy1*-network was also more enriched in TFBS for PPAR gamma and estrogen receptor alpha as well as effectors SP1 and AP1. In contrast, the promoters of genes in the *Tubb3*-network were significantly enriched in TFBS of developmental origin, such as *Pax6*, *Six6*, proteins of the *Sox* and *Oct* family, as well as *Pou4f1*.

Genomic Regulation of Subtype-Specific RGC Markers

Since our analysis revealed two distinct molecular networks governing normal RGC function, we hypothesized that subtype-specific RGC markers would contain regulatory signatures from either one or both RGC networks.

Thus, we generated heat maps of the highest correlates of each subtype-specific marker (*Cartpt2*, *Jam2*, *Kcng4*, *Opn4*, *Spp1,* and *Hoxd10*, see **Figure 5**). This comprehensive analysis revealed that two pairs of genes were regulated in a similar fashion: *Cartpt* and *Jam2* as well as *Kcng4* and *Opn4* showed very similar heat maps to each other. When we compared the heat maps

TABLE 2b | Transcription factor binding site enrichment for genes of the *Tubb3*-network.

Transcription Factor	Enrichment probability (fold) vs. Thy1	Matched promoters *p*-value
Pax-6	1.3845	2.13E-05
OTX	1.8106	5.81E-05
SRY	1.428	3.26E-04
Oct1	1.6876	2.71E-03
FOXO1	1.1574	3.08E-03
Sox1	3.0377	3.10E-03
Nkx6-2	1.3845	3.16E-03
Tst-1	1.2976	3.55E-03
Oct4 (POU5F1)	1.8934	3.90E-03
Foxc1	1.0931	4.14E-03
Foxm1	1.0472	5.44E-03
SIX6 secondary motif	1.6129	5.65E-03
NF-AT	1.2657	6.66E-03
Pitx3	1.2304	7.34E-03
Brn-2	1.6214	9.59E-03
POU4F1	4.219	9.66E-03
c-Myc:Max	1.8081	1.14E-02
Bach1	10.1255	1.25E-02
Dlx2	1.4746	1.36E-02
POU2F1	1.1806	1.45E-02

for these 4 subtype-specific markers, we found that some of their bands were at identical loci as bands observed in the *Thy1*-network (**Figure 6**). While *Cartpt*/*Jam2* had the distinct band from distal Chromosome 1, *Kcng4*/*Opn4* shared a band on distal Chromosome 13. It was also noticed that the allelic distribution of correlates for *Cartpt*/*Jam2* seen as a blue line on distal Chromosome 1 was diametrical to the original *Thy1*-correlates, where the line was mostly yellow-red (see **Figure 3**). This simply implies that the top 20 correlates of *Cartpt* and *Jam2* are in fact correlated inversely to *Cartpt* or *Jam2* itself, whereas the top 20 correlates of *Thy1* are positively correlated to *Thy1* itself.

Hoxd10 had very distinct trans-QTL bands that were not found elsewhere, and its correlates also did not contain any RGC-enriched genes. Since no connection of *Hoxd10* to either the *Thy1*- or the *Tubb3*-network (see **Figure 3**) was observed, the lack of overlap with RGC-enriched genes casts doubt on the specificity of this marker for the identification of RGC subtypes based on gene expression. The eQTL pattern of *Spp1* was the most complex of all markers, as it lacked any clearly detectable *trans*-band.

Overlap of Correlates of Subtype-Specific Markers with the *Thy1*-network and the *Tubb3*-network

When we took the top 2000 correlates (an arbitrary cut-off) of each of the six subtype specific markers (*Cartpt*, *Jam2*, *Kcng4*, *Opn4*, *Hoxd10,* and *Spp1*) and examined the distributions of these markers across the *Thy1*- and the *Tubb3*-networks, we were able to see the relative interplay between these networks (**Table 3**). For *Spp1* and *Hoxd10*, the majority of the overlap was seen with genes from the *Tubb3*-network. The picture was quite different for the remaining subtype-specific markers. For *Cartpt*, *Opn4*, *Kcng4,* and *Jam2,* the overlap was dominated by similarities with the *Thy1*-network. This analysis was also conducted using only the genes with a Pearson correlation value above 0.6 (adj. $p < 0.02$) and it displayed a similar trend (**Table 3**). Taken together these data indicate that each of the RGC subtypes has a unique interplay with the *Thy1*- and the *Tubb3*-networks. The dramatic differences in overlap between correlates may reflect the differential expression of the *Thy1*- and *Tubb3*-networks in different RGC subtypes. These relationships can also be seen in the network map (**Figure 5**).

Susceptibility of RGC Marker Genes to Glaucomatous Nerve Damage

The identification of RGC subtypes has raised the question whether or not there is a difference in susceptibility to nerve damage, subsequent cell survival, or axon regeneration. In order to test this hypothesis on a transcriptional level, we used publicly available microarray data generated from DBA/2J glaucomatous eyes (Howell et al., 2011) and correlated glaucoma severity score (GSS) with expression levels of RGC markers (**Figure 7**). As expected, expression levels of all general RGC markers decreased as nerve damage increased (implicated by the negative correlation between GSS and RGC markers in **Figure 7**, dashed blue line). This was also the case for two subtype-specific markers, *Jam2* and *Cartpt*. Interestingly, expression levels of markers for alpha-RGCs (*Kcng4* and *Spp1*) and ipRGCs (*Opn4*) did not correlate to GSS (cutoff $r < 0.6$), suggesting that these two RGC subtypes are differentially susceptible to nerve damage.

DISCUSSION

Using the DoD CDMRP Retina expression microarray dataset to examine correlates of known RGC markers across the BXD RI strain set, this study revealed two distinct gene networks regulating normal RGC function. Detecting these transcriptional networks with high statistical power required tissue from 55 RI strains with 4 biological replicates per strain. The bioinformatic tools on GeneNetwork allowed us to extract gene networks from a complex structure such as the mouse retina (Geisert et al., 2009; Keeley et al., 2014). Interestingly, almost all of the general RGC markers described in the literature (see **Table 1**) selectively group with one of two genetic networks, the *Thy1*-network or the *Tubb3*-network. Both *Thy1* (Barnstable and Drager, 1984) and *Tubb3* (Snow and Robson, 1994) are believed to be generalized markers for RGCs. Nonetheless, these markers segregate into two distinct genetic networks. Two scenarios could explain the biological basis of correlated genes that are co-regulated in BXD RI mice: (I) differences in cell number of each RGC subtype across the BXD strains, or (II), differences in gene expression within individual RGC subtypes (Geisert et al., 2009; Keeley et al., 2014). Currently, we are not able

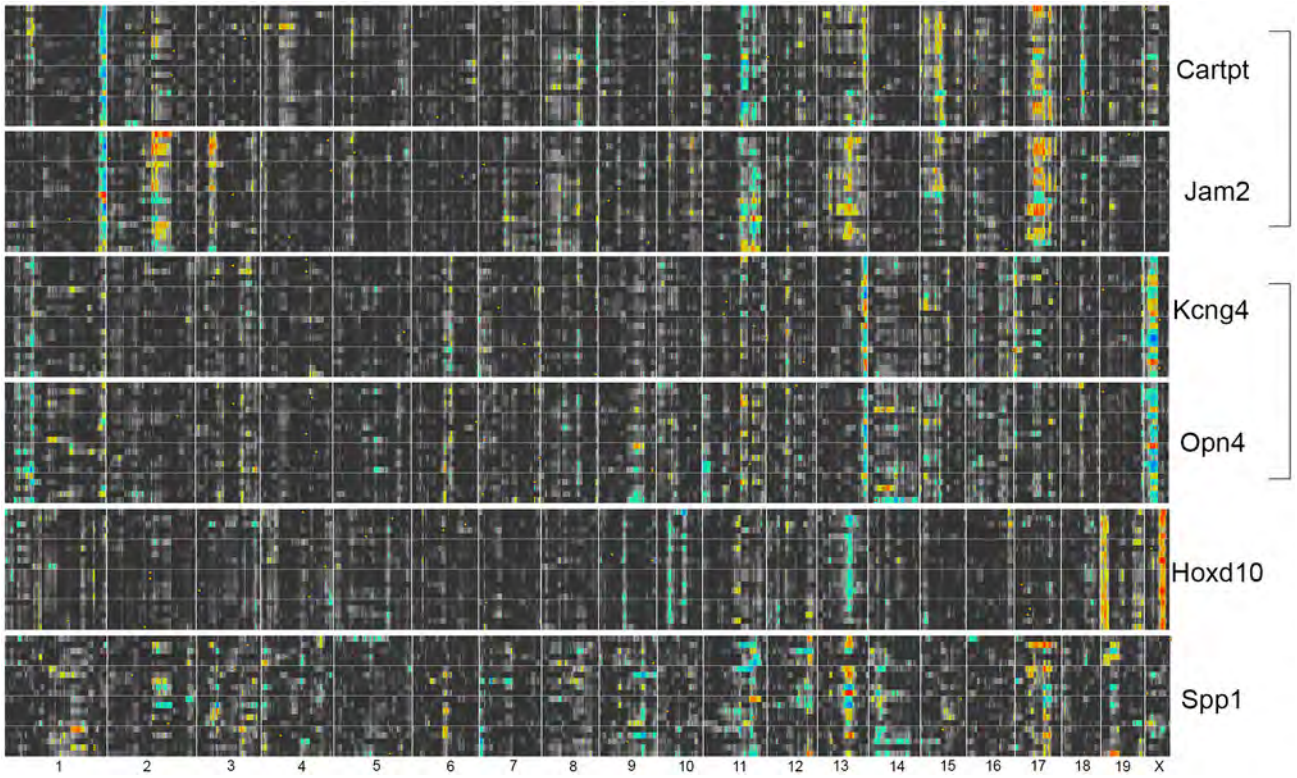

FIGURE 6 | Heat maps for RGC subtype-specific marker genes. *Cartpt/Jam2* share the trans-band on distal Chromosome 1 with the *Thy1*-network, whereas *Kcng4/Opn4* share the *Thy1*-network trans-band from Chromosome 13. There is no obvious overlap of trans-bands with either network for *Hoxd10*. For *Spp1*, no obvious trans-bands can be appreciated, suggesting that this gene is not part of a transcriptional network in its normal state.

to distinguish between these two potential explanations. Our analysis also revealed that these networks have unique biological functions.

Both the *Thy1*- and the *Tubb3*-networks contained large groups of genes that were consistent with a neuronal phenotype. However, they were each enriched in distinct functional roles. The *Thy1*-network appeared to be functionally involved in neuronal development and maintenance, as well as axon guidance. Some of the highest correlates of this network (*Gsk3a*, *Srgap1*, *Arhgap44*, *Ncdn*, *L1cam,* and *Lrrc4b)* were all previously reported to affect dendrite or axon pathfinding and outgrowth (Schwaibold and Brandt, 2008; Cherry et al., 2011; Ip et al., 2011; Galic et al., 2014). Therefore, this network could be directly involved in RGC process extension, potentially including dendrites and axons projecting to the brain. Furthermore, the network was enriched in transmembrane ion transporters. This included several calcium- and sodium-gated channel subunits, all of which have been previously localized to RGCs (Lipton and Tauck, 1987; Farrell et al., 2014).

The *Tubb3*-network contained genes that differed in function from those of the *Thy1*-network. The biological processes enriched in this group included protein polymerization and organic substrate metabolic processes. Under molecular processes, the *Tubb3*-network was enriched for GTP binding proteins and GTPase activity, two mechanisms known to be essential for cellular transport involving the cytoskeleton (Roychowdhury and Rasenick, 2008; Schappi et al., 2014). The highest two correlates of the Tubb3-network were *Rab15* and *Rab4b*, two G-proteins that are known to play an important role in endosome formation and vesicle movement along actin and tubulin networks (Zuk and Elferink, 2000; Falk et al., 2014). Several other genes in this list were associated with intracellular trafficking, such as sorting nexin 32 (*Snx32*, a molecule that links transport vesicles to dynactin (Wassmer et al., 2009), vesicle associated membrane protein 1 (*Vamp1*, a SNARE protein important for linking vesicles to the target membrane; Hasan et al., 2010), *Pigu* (a GPI anchor protein; Guo et al., 2004), and *Tmem9* (part of the lysosomal membrane; Kveine et al., 2002). These genes were highly correlated with and specific to the *Tubb3*-network.

These findings suggest that the *Tubb3*-network is functionally associated with cytoskeleton and vesicle transport in RGCs. Since neurons are known for the significant amount of cytoskeletal proteins necessary to maintain dendritic and axonal integrity (Kevenaar and Hoogenraad, 2015), it can be hypothesized that the *Tubb3*-network is involved in maintenance of these structural elements.

Taken together, this analysis indicates that each network has distinct molecular functions and that both of these networks can exist independently within a single RGC.

The functional differences between networks were mirrored by the transcription factor binding site (TFBS) analysis for promoters of their respective genes. Members of the *Thy1*-network showed significant enrichment in TFBS for proteins regulating cell cycle, growth and apoptosis (Tu et al., 2013). Genes belonging to the *Tubb3*-network, however, showed an over-representation of TFBS for transcription factors known to establish cell fate decisions during development, particularly in later stages. Proteins such as OTX1, PAX6, SIX6, or POU4F1 belonged to the latter group (Zagozewski et al., 2014). *Pou4f1* was not originally found in the correlates of the *Tubb3*-network, which might seem surprising. A possible explanation for this is that the *Thy1*-network, which correlates well with the expression of *Pou4f1* across the BXD strains, acts upstream of the *Tubb3*-network. In a developmental sense, this could suggest that members of the *Thy1*-network establish expression of *Pou4f1*, which can then bind to members of the *Tubb3*-network to influence their transcription. Because *Pou4f1* was originally not found to be part of the *Tubb3*-network but the *Thy1*-network instead, we hypothesize here that basic cell cycle tasks such as survival decisions are managed by members of the *Thy1*-network, while members of the *Tubb3*-network regulate the fine-tuning of RGC development, possibly even influencing subtype commitments.

TABLE 3 | Overlap of subtype-specific RGC markers with genes from the *Thy1*- and the *Tubb3*-network.

Subtype Marker	Top 2000		
	Thy1	***Tubb3***	**Total Overlap (of 4000)**
Cartpt	1022	54	1076 (27%)
Jam2	382	25	407 (10.2%)
Kcng4	326	241	567 (14.2%)
Opn4	713	185	898 (22.5%)
Hoxd10	10	19	29 (0.7%)
Spp1	29	756	1785 (19.6%)
Subtype Marker	**Pearson $r > 0.6$**		
	Thy1	***Tubb3***	**Total Overlap (of 9982)**
Cartpt	2482	0	2482 (24.9%)
Jam2	1030	3	1033 (10.3%)
Kcng4	886	207	1093 (10.9%)
Opn4	1086	56	1142 (11.4%)
Hoxd10	4	17	21 (0.2%)
Spp1	13	9	22 (0.2%)

For the top table, the top 2000 correlates of both networks served as comparison, whereas a Pearson r cutoff of >0.6 was chosen for the lower table, corresponding to a Bonferroni-corrected value of $p < 0.02$.

The identification of neuronal subtypes has gained a considerable amount of attention in neuroscience across a variety of scientific disciplines (Hoshino, 2012; Russ and Kaltschmidt, 2014). This is especially the case for RGC subtypes (Kay et al., 2011; Dhande et al., 2013; Sanes and Masland, 2015). The establishment of transgenic mouse models has recently transformed the field, and new paradigms are starting to emerge. For example, it is becoming increasingly evident that RGC subtypes seem to be differentially susceptible to nerve injury to the point of having different chances of survival or regeneration (Kay et al., 2011; Dhande et al., 2013; Pérez de Sevilla Müller et al., 2014; Duan et al., 2015; Sanes and Masland, 2015). In order to develop new therapeutic approaches to nerve regeneration,

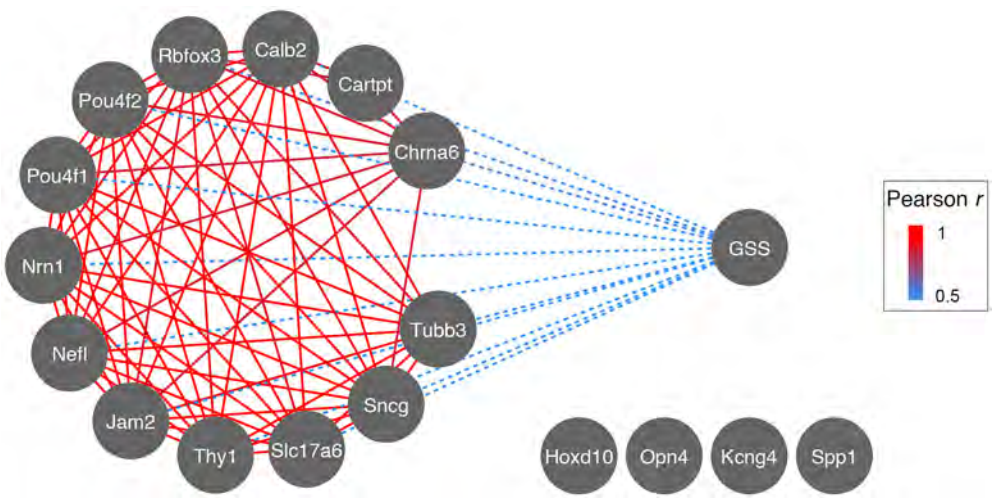

FIGURE 7 | Correlation network of Glaucoma Severity Score (GSS) to RGC markers during glaucoma progression. The GSS is a visual grading system identifying axonal damage in the optic nerve and consists of 4 stages: no damage, light, medium, and severe damage. These stages are inversely correlated (dashed blue) to the expression levels of most RGC markers, suggesting that as RGCs die and axonal damage increases, mRNA expression of RGC marker genes decreases (most likely due to decrease in RGC number). The decrease of RGC marker gene expression is strongly correlated across glaucoma stages (red, *r* for all >0.9). Markers for ipRGCs (*Opn4*) and alpha-RGCs (*Kcng4* and *Spp1*) do not correlate to GSS, possibly indicating their preferential survival.

it may be necessary to tease apart the transcriptional programs of injury-susceptible and non-susceptible RGC subtypes.

When we investigated the heat maps of subtype-specific gene correlates, we found that two pairs—*Kcng4*/*Opn4*, or *Jam2*/*Cartpt*—showed similarity to two different heat map bands from the *Thy1*-network. *Kcng4* marks alpha-RGCs, while *Opn4* marks ipRGCs, and these two subtypes were recently found to be most resistant to optic nerve crush (Pérez de Sevilla Müller et al., 2014; Duan et al., 2015). Since the regulatory pattern of those two gene pairs was very similar based on heat map analysis of their co-varying genes, it would be interesting to systematically investigate if these upstream modulatory loci are responsible for increased neuronal survival or regeneration. Bioinformatic analysis of RGC marker susceptibility to glaucomatous nerve damage supported the notion that alpha-RGCs and ipRGCs were also most resistant to neurodegeneration. The decrease in mRNA expression of alpha-RGC markers (*Kcng4*, *Spp1*) and ipRCG markers (*Opn4*) did not correlate with GSS (a visual grading scale for optic nerve axon damage), whereas the overwhelming majority of RGC markers did.

Interestingly, the discovery of *Spp1* marking a particular RGC subtype had only been made after crush injury to the optic nerve in a mouse model (Pérez de Sevilla Müller et al., 2014; Duan et al., 2015). In this study, it was found that alpha-RGCs secreting Osteopontin (the protein made from the gene *Spp1*) were most resistant to optic nerve crush among all RGC subtypes, and that this protective effect was due to Osteopontin. We were not able to identify putative upstream modulatory loci for this gene due to the lack of distinct trans-QTL bands. This suggests that *Spp1* is part of a genetic network that needs to be activated by neuronal injury before it can be co-regulated in a more RGC-specific way. This phenomenon has been observed elsewhere for other genes following retinal injury (Templeton et al., 2013b).

In summary, we have identified multiple loci modulating RGC function in the BXD mouse strain set, and we have provided *in silico* evidence for the differential susceptibility of RGC subtypes to neurodegeneration and cell death. One caveat of this study is the fact that the performed analysis is only a correlative one. Proving a biological cause will require experimental manipulation of the mentioned genes and examination of the effects *in vivo* or *in vitro*. Nevertheless, our findings enhance the understanding of the RGC's normal transcriptome, as they are the first to describe gene regulatory networks for some of their subtypes. They may serve others and us as a reference for future studies on RGC subtype identification and their susceptibility to injury.

MATERIALS AND METHODS

Animals

All of the procedures involving mice were approved by IACUC at Emory University and adhered to the ARVO Statement for the Use of Animals in Research.

Microarray Datasets

Two microarray datasets were used in this project as part of a comprehensive meta-analysis.

(i) The Department of Defense (DoD) Normal Retina Database (May2015). This is the most comprehensive retina microarray dataset and creation is described in King et al. (2015). The DoD Normal Retina Dataset consists of 222 microarrays from 55 different strains BXD mice, the parental strain C57BL/6J, the parental strain DBA/2J and an F1 cross.

(ii) The Howell et al. (2011), DBA/2J Glaucoma Retina M430 2.0 (Sep11) RMA database. This dataset consists of retinal tissue dissected from 40 DBA/2J mouse eyes at 10.5 months of age showing varying levels of RGC damage due to naturally occuring glaucoma in this mouse strain (as graded by visual inspection of the optic nerve). Twenty eyes served as negative controls. The generation of this dataset is described in Howell et al. (2011).

All of the used datasets are publicly accessible through www.genenetwork.org.

Statistical Analysis and Plot Generation

GeneNetwork provided the platform for correlation analysis, principal component generation, and linkage analysis. In general, datasets were queried for gene symbols, downloaded from GeneNetwork, and additional analysis was performed in R whenever necessary. *P*-values mentioned in relation to Pearson's coefficient throughout this paper are based on pair-wise comparisons. All *p*-values were Bonferroni-adjusted for 36,012 genes, which is equal to the number of genes captured on the microarray after accounting for replicated and wrongly annotated probes. Plots were generated with R and the dplyr and ggplot2 packages. Cytoscape version 3.2.1 was used to generate gene network graphs.

Gene Ontology Analysis

GO analysis was performed using WebGestalt (Wang et al., 2013). The top 500 genes of each network were used to compile a gene list and duplicates were removed. GO term enrichment was calculated using Affymetrix MouseGene 2.0 ST probe set IDs against a background dataset from the same chip. GO trees are appended as expanded view data. All *p*-values presented in the GO analysis are corrected for multiple comparisons using the Bonferroni method.

Candidate Gene Analysis

A list of candidate genes for putative upstream modulators of both networks was created by extracting genes with cis-QTLs from the loci showing trans-bands. For a cis-QTL considered to be a good candidate gene, it should fulfill three conditions: (i) be expressed above background, (ii) correlate well with the trait used to create the trans-bands, and (iii) have a nucleotide variation that alters either protein structure or other regulatory elements (such as promoters or enhancers). These lists are appended as Supplemental Tables.

Transcription Factor Binding Site Analysis

Gene lists including the top 500 correlated genes in each network were compiled, duplicates were removed, and uploaded to BIOBASE. The TRANSFAC FMatch algorithm was used to search for overrepresented neuron-specific transcription factor binding sites in the gene lists using the "best supported promoter" model for each gene (Matys et al., 2006). As a background dataset for both networks, the opposite network was chosen. Resulting *p*-values were Bonferroni-adjusted. The enrichment window for a gene's promoter was chosen to be −5000 to +100 bp of its best supported transcription start site. "Minimize false positives" was selected as cut-off method. The TRANSFAC data version was 2016.2, and only high-quality matrices were used for the analysis.

WGCNA Analysis

Weighted gene network analysis was performed using the WGCNA package in the R environment (Langfelder and Horvath, 2008). A soft thresholding power of 10 was used to calculate the adjacency matrix based on the criterion of scale-free topology (Zhang and Horvath, 2005). Modules were identified using the following parameters for the blockwiseModules function: minimum module size of 100, merge cut height of 0.25, and maximum block size of 2000. The top 2000 correlates of *Thy1* and *Tubb3* were then each merged with their module affiliation by Affymetrix Probe Set ID and the resulting list was checked for overlaps.

Immunohistochemistry

Two 60 day-old Thy1-CFP C57BL/6 transgenic mouse (Jax identifier B6.Cg-Tg(Thy1-CFP)23Jrs/J) were deeply anesthetized with a mixture of 13 mg/kg of xylazine and 87 mg/kg of ketamine and intracardially perfused with 0.9% saline followed by 4% paraformaldehyde. Retinas were dissected and flat-mounted on glass slides following a standard protocol. Retinas were blocked in 4% bovine serum albumin in PBS overnight. One retina was stained with anti-TUJ1 (a gift from Anthony Frankforter, dilution 1:1000) and anti-GFP (Invitrogen, 1:500) antibodies overnight and then labeled with appropriate Alexa Fluor-conjugated secondary antibodies. One retina served as negative secondary antibody control (data not shown). High-resolution Z-stacks were captured on a Nikon confocal microscope with the Nikon C1 software throughout the entire ganglion cell layer only. Z-stacks were collapsed using FiJi (Schindelin et al., 2012) and the whole image was adjusted for contrast and brightness using Adobe Photoshop.

ACCESSIBILITY OF DATA

The data presented in this article is publicly available under www.genenetwork.org and can be downloaded under http://genenetwork.org/webqtl/main.py?FormID=sharinginfo&GN_AccessionId=709.

AUTHOR CONTRIBUTIONS

FS, EG provided the initial design of the study. FS performed experiments and bioinformatic analyses with assistance from EG. FS, EG wrote the paper with input from RW and RL. RW supplied the datasets through the GeneNetwork platform and is responsible for its maintenance. RL has provided intellectual framework for this project as part of an ongoing collaborative effort between his laboratory and the laboratories of EG, RW.

ACKNOWLEDGMENTS

This work was supported by DoD CDMRP Grant W81XWH1210255 from the USA Army Medical Research & Materiel Command and the Telemedicine and Advanced Technology (to EG), NIH Grant R01EY017841 (to EG), Vision Core Grant P30EY006360 (to P. Michael Iuvone), and Unrestricted Funds and a Stein Innovation Award from Research to Prevent Blindness (to the Ophthalmology Department at Emory University, the University of Tennessee Health Science Center, and the Bascom Palmer Eye Institute, University of Miami Miller School of Medicine). FS is supported by the institutional training grant T32EY007092-30 (to P. Michael Iuvone). The authors would like to thank Rebecca King for technical assistance with the retinal flat mounts and Dr. John Nickerson for his comments on the manuscript.

SUPPLEMENTARY MATERIAL

The Supplementary Material for this article can be found online at: http://journal.frontiersin.org/article/10.3389/fgene.2016.00169

REFERENCES

Adams, L. D., Gong, W., Vechia, S. D., Hunter, R. G., and Kuhar, M. J. (1999). CART: from gene to function. *Brain Res.* 848, 137–140. doi: 10.1016/S0006-8993(99)01907-1

Baden, T., Berens, P., Franke, K., Román Rosón, M., Bethge, M., and Euler, T. (2016). The functional diversity of retinal ganglion cells in the mouse. *Nature* 529, 345–350. doi: 10.1038/nature16468

Bai, L., Xu, H., Collins, J. F., and Ghishan, F. K. (2001). Molecular and functional analysis of a novel neuronal vesicular glutamate transporter. *J. Biol. Chem.* 276, 36764–36769. doi: 10.1074/jbc.M104578200

Barnstable, C. J., and Dräger, U. C. (1984). Thy-1 antigen: a ganglion cell specific marker in rodent retina. *Neuroscience* 11, 847–855. doi: 10.1016/0306-4522(84)90195-7

Buckingham, B. P., Inman, D. M., Lambert, W., Oglesby, E., Calkins, D. J., Steele, M. R., et al. (2008). Progressive ganglion cell degeneration precedes neuronal loss in a mouse model of glaucoma. *J. Neurosci.* 28, 2735–2744. doi: 10.1523/JNEUROSCI.4443-07.2008

Chalupa, L. M., and Günhan, E. (2004). Development of On and Off retinal pathways and retinogeniculate projections. *Prog. Retin. Eye Res.* 23, 31–51. doi: 10.1016/j.preteyeres.2003.10.001

Chang, Z. Y., Yeh, M. K., Chiang, C. H., Chen, Y. H., and Lu, D. W. (2013). Erythropoietin protects adult retinal ganglion cells against NMDA-, trophic factor withdrawal-, and TNF-alpha-induced damage. *PLoS ONE* 8:e55291. doi: 10.1371/journal.pone.0055291

Cherry, T. J., Wang, S., Bormuth, I., Schwab, M., Olson, J., and Cepko, C. L. (2011). NeuroD factors regulate cell fate and neurite stratification in the developing retina. *J. Neurosci.* 31, 7365–7379. doi: 10.1523/JNEUROSCI.2555-10.2011

Daniele, L. L., Adams, R. H., Durante, D. E., Pugh, E. N. Jr., and Philp, N. J. (2007). Novel distribution of junctional adhesion molecule-C in the neural retina and retinal pigment epithelium. *J. Comp. Neurol.* 505, 166–176. doi: 10.1002/cne.21489

Dhande, O. S., Estevez, M. E., Quattrochi, L. E., El-Danaf, R. N., Nguyen, P. L., Berson, D. M., et al. (2013). Genetic dissection of retinal inputs to brainstem nuclei controlling image stabilization. *J. Neurosci.* 33, 17797–17813. doi: 10.1523/JNEUROSCI.2778-13.2013

Duan, X., Krishnaswamy, A., De la Huerta, I., and Sanes, J. R. (2014). Type II cadherins guide assembly of a direction-selective retinal circuit. *Cell* 158, 793–807. doi: 10.1016/j.cell.2014.06.047

Duan, X., Qiao, M., Bei, F., Kim, I. J., He, Z., and Sanes, J. R. (2015). Subtype-specific regeneration of retinal ganglion cells following axotomy: effects of osteopontin and mTOR signaling. *Neuron* 85, 1244–1256. doi: 10.1016/j.neuron.2015.02.017

Erkman, L., McEvilly, R. J., Luo, L., Ryan, A. K., Hooshmand, F., O'Connell, S. M., et al. (1996). Role of transcription factors Brn-3.1 and Brn-3.2 in auditory and visual system development. *Nature* 381, 603–606. doi: 10.1038/381603a0

Falk, J., Konopacki, F. A., Zivraj, K. H., and Holt, C. E. (2014). Rab5 and Rab4 regulate axon elongation in the Xenopus visual system. *J. Neurosci.* 34, 373–391. doi: 10.1523/JNEUROSCI.0876-13.2014

Farrell, S. R., Sargoy, A., Brecha, N. C., and Barnes, S. (2014). Modulation of voltage-gated Ca2+ channels in rat retinal ganglion cells by gabapentin. *Vis. Neurosci.* 31, 47–55. doi: 10.1017/S0952523813000588

Galic, M., Tsai, F. C., Collins, S. R., Matis, M., Bandara, S., and Meyer, T. (2014). Dynamic recruitment of the curvature-sensitive protein ArhGAP44 to nanoscale membrane deformations limits exploratory filopodia initiation in neurons. *Elife* 3:e03116. doi: 10.7554/elife.03116

Geisert, E. E., Lu, L., Freeman-Anderson, N. E., Templeton, J. P., Nassr, M., Wang, X., et al. (2009). Gene expression in the mouse eye: an online resource for genetics using 103 strains of mice. *Mol. Vis.* 15, 1730–1763. Available online at: http://www.molvis.org/molvis/v15/a185

Graybeal, C., Bachu, M., Mozhui, K., Saksida, L. M., Bussey, T. J., Sagalyn, E., et al. (2014). Strains and stressors: an analysis of touchscreen learning in genetically diverse mouse strains. *PLoS ONE* 9:e87745. doi: 10.1371/journal.pone.0087745

Guido, M. E., Garbarino-Pico, E., Contin, M. A., Valdez, D. J., Nieto, P. S., Verra, D. M., et al. (2010). Inner retinal circadian clocks and non-visual photoreceptors: novel players in the circadian system. *Prog. Neurobiol.* 92, 484–504. doi: 10.1016/j.pneurobio.2010.08.005

Guo, Z., Linn, J. F., Wu, G., Anzick, S. L., Eisenberger, C. F., Halachmi, S., et al. (2004). CDC91L1 (PIG-U) is a newly discovered oncogene in human bladder cancer. *Nat. Med.* 10, 374–381. doi: 10.1038/nm1010

Hasan, N., Corbin, D., and Hu, C. (2010). Fusogenic pairings of vesicle-associated membrane proteins (VAMPs) and plasma membrane t-SNAREs–VAMP5 as the exception. *PLoS ONE* 5:e14238. doi: 10.1371/journal.pone.0014238

Haverkamp, S., Inta, D., Monyer, H., and Wassle, H. (2009). Expression analysis of green fluorescent protein in retinal neurons of four transgenic mouse lines. *Neuroscience* 160, 126–139. doi: 10.1016/j.neuroscience.2009.01.081

Hoshino, M. (2012). Neuronal subtype specification in the cerebellum and dorsal hindbrain. *Dev. Growth Differ.* 54, 317–326. doi: 10.1111/j.1440-169X.2012.01330.x

Howell, G. R., Macalinao, D. G., Sousa, G. L., Walden, M., Soto, I., Kneeland, S. C., et al. (2011). Molecular clustering identifies complement and endothelin induction as early events in a mouse model of glaucoma. *J. Clin. Invest.* 121, 1429–1444. doi: 10.1172/JCI44646

Huberman, A. D., Manu, M., Koch, S. M., Susman, M. W., Lutz, A. B., Ullian, E. M., et al. (2008). Architecture and activity-mediated refinement of axonal projections from a mosaic of genetically identified retinal ganglion cells. *Neuron* 59, 425–438. doi: 10.1016/j.neuron.2008.07.018

Ip, B. K., Bayatti, N., Howard, N. J., Lindsay, S., and Clowry, G. J. (2011). The corticofugal neuron-associated genes ROBO1, SRGAP1, and CTIP2 exhibit an anterior to posterior gradient of expression in early fetal human neocortex development. *Cereb. Cortex* 21, 1395–1407. doi: 10.1093/cercor/bhq219

Jain, V., Ravindran, E., and Dhingra, N. K. (2012). Differential expression of Brn3 transcription factors in intrinsically photosensitive retinal ganglion cells in mouse. *J. Comp. Neurol.* 520, 742–755. doi: 10.1002/cne.22765

Ju, W. K., Kim, K. Y., Cha, J. H., Kim, I. B., Lee, M. Y., Oh, S. J., et al. (2000). Ganglion cells of the rat retina show osteopontin-like immunoreactivity. *Brain Res.* 852, 217–220. doi: 10.1016/S0006-8993(99)02140-X

Kay, J. N., De la Huerta, I., Kim, I. J., Zhang, Y., Yamagata, M., Chu, M. W., et al. (2011). Retinal ganglion cells with distinct directional preferences differ in molecular identity, structure, and central projections. *J. Neurosci.* 31, 7753–7762. doi: 10.1523/JNEUROSCI.0907-11.2011

Keeley, P. W., Whitney, I. E., Madsen, N. R., St John, A. J., Borhanian, S., Leong, S. A., et al. (2014). Independent genomic control of neuronal number across retinal cell types. *Dev. Cell* 30, 103–109. doi: 10.1016/j.devcel.2014.05.003

Kevenaar, J. T., and Hoogenraad, C. C. (2015). The axonal cytoskeleton: from organization to function. *Front. Mol. Neurosci.* 8:44. doi: 10.3389/fnmol.2015.00044

Kim, I. J., Zhang, Y., Yamagata, M., Meister, M., and Sanes, J. R. (2008). Molecular identification of a retinal cell type that responds to upward motion. *Nature* 452, 478–482. doi: 10.1038/nature06739

Kim, K. K., Yang, Y., Zhu, J., Adelstein, R. S., and Kawamoto, S. (2014). Rbfox3 controls the biogenesis of a subset of microRNAs. *Nat. Struct. Mol. Biol.* 21, 901–910. doi: 10.1038/nsmb.2892

King, R., Lu, L., Williams, R. W., and Geisert, E. E. (2015). Transcriptome networks in the mouse retina: an exon level BXD RI database. *Mol. Vis.* 21, 1235–1251. Available online at: http://www.molvis.org/molvis/v21/1235

Kveine, M., Tenstad, E., Døsen, G., Funderud, S., and Rian, E. (2002). Characterization of the novel human transmembrane protein 9 (TMEM9) that localizes to lysosomes and late endosomes. *Biochem. Biophys. Res. Commun.* 297, 912–917. doi: 10.1016/S0006-291X(02)02228-3

Langfelder, P., and Horvath, S. (2008). WGCNA: an R package for weighted correlation network analysis. *BMC Bioinformat.* 9:559. doi: 10.1186/1471-2105-9-559

Lipton, S. A., and Tauck, D. L. (1987). Voltage-dependent conductances of solitary ganglion cells dissociated from the rat retina. *J. Physiol.* 385, 361–391. doi: 10.1113/jphysiol.1987.sp016497

Mackey, E. D., Engle, S. E., Kim, M. R., O'Neill, H. C., Wageman, C. R., Patzlaff, N. E., et al. (2012). alpha6∗ nicotinic acetylcholine receptor expression and function in a visual salience circuit. *J. Neurosci.* 32, 10226–10237. doi: 10.1523/JNEUROSCI.0007-12.2012

Macosko, E. Z., Basu, A., Satija, R., Nemesh, J., Shekhar, K., Goldman, M., et al. (2015). Highly parallel genome-wide expression profiling of individual cells using nanoliter droplets. *Cell* 161, 1202–1214. doi: 10.1016/j.cell.2015.05.002

Matys, V., Kel-Margoulis, O. V., Fricke, E., Liebich, I., Land, S., Barre-Dirrie, A., et al. (2006). TRANSFAC and its module TRANSCompel: transcriptional gene regulation in eukaryotes. *Nucleic Acids Res.* 34: D108–D110. doi: 10.1093/nar/gkj143

Mellough, C. B., Cui, Q., Spalding, K. L., Symons, N. A., Pollett, M. A., Snyder, E. Y., et al. (2004). Fate of multipotent neural precursor cells transplanted into mouse retina selectively depleted of retinal ganglion cells. *Exp. Neurol.* 186, 6–19. doi: 10.1016/j.expneurol.2003.10.021

Mimura, Y., Mogi, K., Kawano, M., Fukui, Y., Takeda, J., Nogami, H., et al. (2002). Differential expression of two distinct vesicular glutamate transporters in the rat retina. *Neuroreport* 13, 1925–1928. doi: 10.1097/00001756-200210280-00019

Mojumder, D. K., Wensel, T. G., and Frishman, L. J. (2008). Subcellular compartmentalization of two calcium binding proteins, calretinin and calbindin-28 kDa, in ganglion and amacrine cells of the rat retina. *Mol. Vis.* 14, 1600–1613. Available online at: http://www.molvis.org/molvis/v14/a190

Munguba, G. C., Galeb, S., Liu, Y., Landy, D. C., Lam, D., Camp, A., et al. (2014). Nerve fiber layer thinning lags retinal ganglion cell density following crush axonopathy. *Invest. Ophthalmol. Vis. Sci.* 55, 6505–6513. doi: 10.1167/iovs.14-14525

Munguba, G. C., Geisert, E. E., Williams, R. W., Tapia, M. L., Lam, D. K., Bhattacharya, S. K., et al. (2013). Effects of glaucoma on Chrna6 expression in the retina. *Curr. Eye Res.* 38, 150–157. doi: 10.3109/02713683.2012.724512

Nuschke, A. C., Farrell, S. R., Levesque, J. M., and Chauhan, B. C. (2015). Assessment of retinal ganglion cell damage in glaucomatous optic neuropathy: axon transport, injury and soma loss. *Exp. Eye Res.* 141, 111–124. doi: 10.1016/j.exer.2015.06.006

Pérez de Sevilla Müller, L., Sargoy, A., Rodriguez, A. R., and Brecha, N. C. (2014). Melanopsin ganglion cells are the most resistant retinal ganglion cell type to axonal injury in the rat retina. *PLoS ONE* 9:e93274. doi: 10.1371/journal.pone.0093274

Picard, N., Leslie, J. H., Trowbridge, S. K., Subramanian, J., Nedivi, E., and Fagiolini, M. (2014). Aberrant development and plasticity of excitatory visual

cortical networks in the absence of cpg15. *J. Neurosci.* 34, 3517–3522. doi: 10.1523/JNEUROSCI.2955-13.2014

Piri, N., Kwong, J. M., Song, M., and Caprioli, J. (2006). Expression of hermes gene is restricted to the ganglion cells in the retina. *Neurosci. Lett.* 405, 40–45. doi: 10.1016/j.neulet.2006.06.049

Puyang, Z., Chen, H., and Liu, X. (2015). Subtype-dependent morphological and functional degeneration of retinal ganglion cells in mouse models of experimental Glaucoma. *J. Nat. Sci.* 1, e103.

Qian, Y., Jung, Y. S., and Chen, X. (2012). Differentiated embryo-chondrocyte expressed gene 1 regulates p53-dependent cell survival versus cell death through macrophage inhibitory cytokine-1. *Proc. Natl. Acad. Sci. U.S.A.* 109, 11300–11305. doi: 10.1073/pnas.1203185109

Raymond, I. D., Vila, A., Huynh, U.-C. N., and Brecha, N. C. (2008). Cyan fluorescent protein expression in ganglion and amacrine cells in a thy1-CFP transgenic mouse retina. *Mol. Vis.* 14, 1559–1574. Available online at: http://www.molvis.org/molvis/v14/a186

Rodriguez, A. R., de Sevilla Müller, L. P., and Brecha, N. C. (2014). The RNA binding protein RBPMS is a selective marker of ganglion cells in the mammalian retina. *J. Comp. Neurol.* 522, 1411–1443. doi: 10.1002/cne.23521

Roychowdhury, S., and Rasenick, M. M. (2008). Submembraneous microtubule cytoskeleton: regulation of microtubule assembly by heterotrimeric Gproteins. *FEBS J.* 275, 4654–4663. doi: 10.1111/j.1742-4658.2008.06614.x

Ruiz-Ederra, J., García, M., Hicks, D., and Vecino, E. (2004). Comparative study of the three neurofilament subunits within pig and human retinal ganglion cells. *Mol. Vis.* 10, 83–92. Available online at: http://www.molvis.org/molvis/v10/a12/

Russ, J. B., and Kaltschmidt, J. A. (2014). From induction to conduction: how intrinsic transcriptional priming of extrinsic neuronal connectivity shapes neuronal identity. *Open Biol.* 4:140144. doi: 10.1098/rsob.140144

Sanes, J. R., and Masland, R. H. (2015). The types of retinal ganglion cells: current status and implications for neuronal classification. *Annu. Rev. Neurosci.* 38, 221–246. doi: 10.1146/annurev-neuro-071714-034120

Schappi, J. M., Krbanjevic, A., and Rasenick, M. M. (2014). Tubulin, actin and heterotrimeric G proteins: coordination of signaling and structure. *Biochim. Biophys. Acta* 1838, 674–681. doi: 10.1016/j.bbamem.2013.08.026

Schindelin, J., Arganda-Carreras, I., Frise, E., Kaynig, V., Longair, M., Pietzsch, T., et al. (2012). Fiji: an open-source platform for biological-image analysis. *Nat. Methods* 9, 676–682. doi: 10.1038/nmeth.2019

Schlamp, C. L., Montgomery, A. D., Mac Nair, C. E., Schuart, C., Willmer, D. J., and Nickells, R. W. (2013). Evaluation of the percentage of ganglion cells in the ganglion cell layer of the rodent retina. *Mol. Vis.* 19, 1387–1396. Available online at: http://www.molvis.org/molvis/v19/1387

Schwaibold, E. M., and Brandt, D. T. (2008). Identification of Neurochondrin as a new interaction partner of the FH3 domain of the Diaphanous-related formin Dia1. *Biochem. Biophys. Res. Commun.* 373, 366–372. doi: 10.1016/j.bbrc.2008.06.042

Semo, M., Muñoz Llamosas, M., Foster, R. G., and Jeffery, G. (2005). Melanopsin (Opn4) positive cells in the cat retina are randomly distributed across the ganglion cell layer. *Vis. Neurosci.* 22, 111–116. doi: 10.1017/S0952523805001069

Sharma, T. P., Liu, Y., Wordinger, R. J., Pang, I. H., and Clark, A. F. (2015). Neuritin 1 promotes retinal ganglion cell survival and axonal regeneration following optic nerve crush. *Cell Death Dis.* 6, e1661. doi: 10.1038/cddis.2015.22

Snow, R. L., and Robson, J. A. (1994). Ganglion cell neurogenesis, migration and early differentiation in the chick retina. *Neuroscience* 58, 399–409. doi: 10.1016/0306-4522(94)90046-9

Templeton, J. P., Freeman, N. E., Nickerson, J. M., Jablonski, M. M., Rex, T. S., Williams, R. W., et al. (2013a). Innate immune network in the retina activated by optic nerve crush. *Invest. Ophthalmol. Vis. Sci.* 54, 2599–2606. doi: 10.1167/iovs.12-11175

Templeton, J. P., Nassr, M., Vazquez-Chona, F., Freeman-Anderson, N. E., Orr, W. E., Williams, R. W., et al. (2009). Differential response of C57BL/6J mouse and DBA/2J mouse to optic nerve crush. *BMC Neurosci.* 10:90. doi: 10.1186/1471-2202-10-90

Templeton, J. P., Wang, X., Freeman, N. E., Ma, Z., Lu, A., Hejtmancik, F., et al. (2013b). A crystallin gene network in the mouse retina. *Exp. Eye Res.* 116, 129–140. doi: 10.1016/j.exer.2013.08.001

Triplett, J. W., Wei, W., Gonzalez, C., Sweeney, N. T., Huberman, A. D., Feller, M. B., et al. (2014). Dendritic and axonal targeting patterns of a genetically-specified class of retinal ganglion cells that participate in image-forming circuits. *Neural Dev.* 9:2. doi: 10.1186/1749-8104-9-2

Tu, C. C., Kumar, V. B., Day, C. H., Kuo, W. W., Yeh, S. P., Chen, R. J., et al. (2013). Estrogen receptor alpha (ESR1) over-expression mediated apoptosis in Hep3B cells by binding with SP1 proteins. *J. Mol. Endocrinol.* 51, 203–212. doi: 10.1530/JME-13-0085

Vanderlinden, L. A., Saba, L. M., Kechris, K., Miles, M. F., Hoffman, P. L., and Tabakoff, B. (2013). Whole brain and brain regional coexpression network interactions associated with predisposition to alcohol consumption. *PLoS ONE* 8:e68878. doi: 10.1371/journal.pone.0068878

Wang, J., Duncan, D., Shi, Z., and Zhang, B. (2013). WEB-based GEne SeT AnaLysis Toolkit (WebGestalt): update 2013. *Nucleic Acids Res.* 41, W77–W83. doi: 10.1093/nar/gkt439

Wässle, H., Regus-Leidig, H., and Haverkamp, S. (2006). Expression of the vesicular glutamate transporter vGluT2 in a subset of cones of the mouse retina. *J. Comp. Neurol.* 496, 544–555. doi: 10.1002/cne.20942

Wassmer, T., Attar, N., Harterink, M., van Weering, J. R., Traer, C. J., Oakley, J., et al. (2009). The retromer coat complex coordinates endosomal sorting and dynein-mediated transport, with carrier recognition by the trans-Golgi network. *Dev. Cell* 17, 110–122. doi: 10.1016/j.devcel.2009.04.016

Williams, E. G., and Auwerx, J. (2015). The convergence of systems and reductionist approaches in complex trait analysis. *Cell* 162, 23–32. doi: 10.1016/j.cell.2015.06.024

Williams, R. W., Gu, J., Qi, S., and Lu, L. (2001). The genetic structure of recombinant inbred mice: high-resolution consensus maps for complex trait analysis. *Genome Biol.* 2, RESEARCH0046

Williams, R. W., and Mulligan, M. K. (2012). Genetic and molecular network analysis of behavior. *Int. Rev. Neurobiol.* 104, 135–157. doi: 10.1016/B978-0-12-398323-7.00006-9

Wolf, H. K., Buslei, R., Schmidt-Kastner, R., Schmidt-Kastner, P. K., Pietsch, T., Wiestler, O. D., et al. (1996). NeuN: a useful neuronal marker for diagnostic histopathology. *J. Histochem. Cytochem.* 44, 1167–1171. doi: 10.1177/44.10.8813082

Xiang, M., Zhou, L., Peng, Y. W., Eddy, R. L., Shows, T. B., and Nathans, J. (1993). Brn-3b: a POU domain gene expressed in a subset of retinal ganglion cells. *Neuron* 11, 689–701. doi: 10.1016/0896-6273(93)90079-7

Yin, L., Unger, E. L., Jellen, L. C., Earley, C. J., Allen, R. P., Tomaszewicz, A., et al. (2012). Systems genetic analysis of multivariate response to iron deficiency in mice. *Am. J. Physiol. Regul. Integr. Comp. Physiol.* 302, R1282–R1296. doi: 10.1152/ajpregu.00634.2011

Young, M. J., and Lund, R. D. (1998). The retinal ganglion cells that drive the pupilloconstrictor response in rats. *Brain Res.* 787, 191–202. doi: 10.1016/S0006-8993(97)01473-X

Zagozewski, J. L., Zhang, Q., Pinto, V. I., Wigle, J. T., and Eisenstat, D. D. (2014). The role of homeobox genes in retinal development and disease. *Dev. Biol.* 393, 195–208. doi: 10.1016/j.ydbio.2014.07.004

Zhang, B., and Horvath, S. (2005). A general framework for weighted gene co-expression network analysis. *Stat. Appl. Genet. Mol. Biol.* 4:17. doi: 10.2202/1544-6115.1128. Available online at: http://dibernardo.tigem.it/files/papers/2008/zhangbin-statappsgeneticsmolbio.pdf

Zode, G. S., Kuehn, M. H., Nishimura, D. Y., Searby, C. C., Mohan, K., Grozdanic, S. D., et al. (2011). Reduction of ER stress via a chemical chaperone prevents disease phenotypes in a mouse model of primary open angle glaucoma. *J. Clin. Invest.* 121, 3542–3553. doi: 10.1172/JCI58183

Zuk, P. A., and Elferink, L. A. (2000). Rab15 differentially regulates early endocytic trafficking. *J. Biol. Chem.* 275, 26754–26764. doi: 10.1074/jbc.m000344200

Conflict of Interest Statement: The authors declare that the research was conducted in the absence of any commercial or financial relationships that could be construed as a potential conflict of interest.

Appendix C

JOURNAL OF NEUROTRAUMA 35:118–129 (January 1, 2018)

DOI: 10.1089/neu.2017.5104

Transcriptional Changes in the Mouse Retina after Ocular Blast Injury: A Role for the Immune System

Felix L. Struebing, Rebecca King, Ying Li, Micah A. Chrenek, Polina N. Lyuboslavsky, Curran S. Sidhu, P. Michael Iuvone, and Eldon E. Geisert

Abstract

Ocular blast injury is a major medical concern for soldiers and explosion victims due to poor visual outcomes. To define the changes in gene expression following a blast injury to the eye, we examined retinal ribonucleic acid (RNA) expression in 54 mouse strains 5 days after a single 50-psi overpressure air wave blast injury. We observe that almost 40% of genes are differentially expressed with a false discovery rate (FDR) of <0.001, even though the nominal changes in RNA expression are rather small. Moreover, we find through machine learning approaches that genetic networks related to the innate and acquired immune system are activated. Accompanied by lymphocyte invasion into the inner retina, blast injury also results in progressive loss of visual function and retinal ganglion cells (RGCs). Collectively, these data demonstrate how systems genetics can be used to put meaning to the transcriptome changes following ocular blast injury that eventually lead to blindness.

Keywords: axon injury; ocular blast injury; ocular immune system; systems genetics; transcriptome

Introduction

Since the introduction of improvised explosive devices into modern warfare, the incidence rate of ocular trauma has increased dramatically from 0.65% of all battle injuries to about 13%.[1] Based on severity, these can be subdivided into penetrating or open-globe and closed-globe injuries. Whereas open-globe injuries usually require immediate medical attention, closed-globe injuries can go unnoticed. However, the latter can also lead to decreased vision.[2] For example, boxers, who frequently sustain blunt trauma to the eye, report decreasing visual function in almost half of cases.[3] Similarly, patients suffering from paintball ocular injuries show a visual acuity less than 20/200 in almost 60% of all reported cases.[4] The decline in vision is gradual and might not be apparent at initial examination. Recent experimental data suggest subtle axonal damage underlying the deleterious short- and long-term effects of ocular blast trauma in rodents.[5–7] The short-term (hours to days) effects include diminished pupillary reflex to red and blue light, increased cell death pathway markers, and reactive gliosis. Visual function declines after a month post-blast, accompanied by gradual thinning of the nerve fiber layer and chronic pattern electroretinogram (ERG) deficits.[5] Exposure to one single blast wave is sufficient to lead to decreased axon density and glial scarring in the optic nerve observable as late as 10 months after injury, indicating that the late-onset decline in visual function is partly due to degeneration of optic nerve axons and retinal ganglion cell (RGC) damage.[6] These rodent data are consistent with a report on visual dysfunction in veterans, which was strongly associated with blast injury one year after injury.[8] Thus, there seems to be a subacute phase during which retinal ganglion cells slowly degenerate, paving the way for gradual vision loss. Despite these findings, no study has systematically investigated the transcriptional changes during this sensitive time.

The present study was designed to define the influence of closed-globe blast injury on the retinal transcriptome. We examined gene expression in 52 BXD recombinant inbred (RI) mouse strains and their parental strains C57BL/6J and DBA/2J 5 days after exposure to a single 50-psi blast wave directed to the eye. Microarray analysis was carried out at both gene and exon level, whereas the use of RI strains allowed for the discovery of gene regulatory networks by linking deoxyribonucleic acid (DNA) sequence variants to corresponding differences in gene expression. The result is a system-wide map of gene interactions that take place 5 days after blast injury. Comparing these data with a naive control group reveals several co-expression modules, among which we find an unexpected cross talk of innate and acquired immune systems. Even though the nominal changes in messenger RNA (mRNA) expression are subtle, the mutual correlation of immune-system–related genes increases, in some cases drastically, suggesting activation of genetic networks.

Methods

Animals: Strains, sex, and age

The DoD Retina Blast (Mar16) dataset contains the data of 213 Affymetrix® Mouse Gene 2.0 ST microarrays. With a total of 52

Department of Ophthalmology, Emory University, Atlanta, Georgia.

BXD strains and 2 parental strains (C57BL/6J and DBA/2J), this dataset is genotypically identical to our previously published DoD Normal Retina (May15) dataset and allows for strain-to-strain comparison. Almost all strains are represented by four independent biological samples usually comprising retinas from two male and two female mice between 66 and 114 days of age with a median of 76 days (Supplementary Fig. 1; see online supplementary material at http://www.liebertpub.com). Animals were maintained on a 12-h light–12-h dark cycle in a parasite-free facility with food and water *ad libitum*. All procedures involving animals were approved by the Animal Care and Use Committee of Emory University, Animal Use and Care Review Office (ACURO) of the U.S. Army Medical Research and Materiel Command (USAMRMC), and were in accordance with the Association for Research in Vision and Ophthalmology (ARVO) Statement for the Use of Animals in Ophthalmic and Vision Research.

Ocular blast injury procedure

Ocular blast injury was performed using a previously described model.[6] Briefly, animals were deeply anesthetized with 67 mg/kg tribromoethanol and secured with tape on a semi-open plastic tube sleigh. The head was safely positioned between Styrofoam nuggets to minimize blast exposure to the brain. The sleigh was then inserted into a hollow plastic cylinder with the right eye of the mouse directly facing a 7-mm-wide hole, which was then placed in front of a custom short airgun barrel. Before every blast procedure, the output pressure was checked at the position of the eye with a pressure sensor (Honeywell; Morris Plains, NJ) and recalibrated, if necessary, to an output of 49 ± 1 psi (Supplementary Fig. 1). The pressure sensor was fixed in place and placed flush against the tube opening. Because the thickness of the outer and inner tube (~ 6 mm), it was not possible to position the eye closer toward the tip of the barrel than 6 mm as this would have resulted in inappropriate pressure on the eye due to squeezing it out of its orbit. Thus, there was an approximately 6-mm difference in distance of the pressure transducer and the eye to the gun barrel tip. Following a single blast, eyes were carefully investigated for signs of macroscopic damage. Eyes were lubricated with GenTeal® and mice were allowed to wake up on a heating pad. There was an overall mortality rate of 5% associated with the blast procedure. Of the 240 mice in the blast experiment, 10 died under anesthesia or during recovery. After recovery from anesthesia, 2 mice died the following day.

Functional assessment and Thy1-*CFP* flat mounts

Thy1-CFP mice (n = 4–7 per group) bred on a C57BL/6 background were subjected to blast and their eyes were fixed in Z-FIX (Anatech Ltd.; Battlecreek, MI), and washed 3 times in phosphate-buffered saline (PBS). Retinas were dissected, mounted on slides with rails in Vectashield Hardset (Vector Laboratories; Burlingame, CA), and coverslipped.

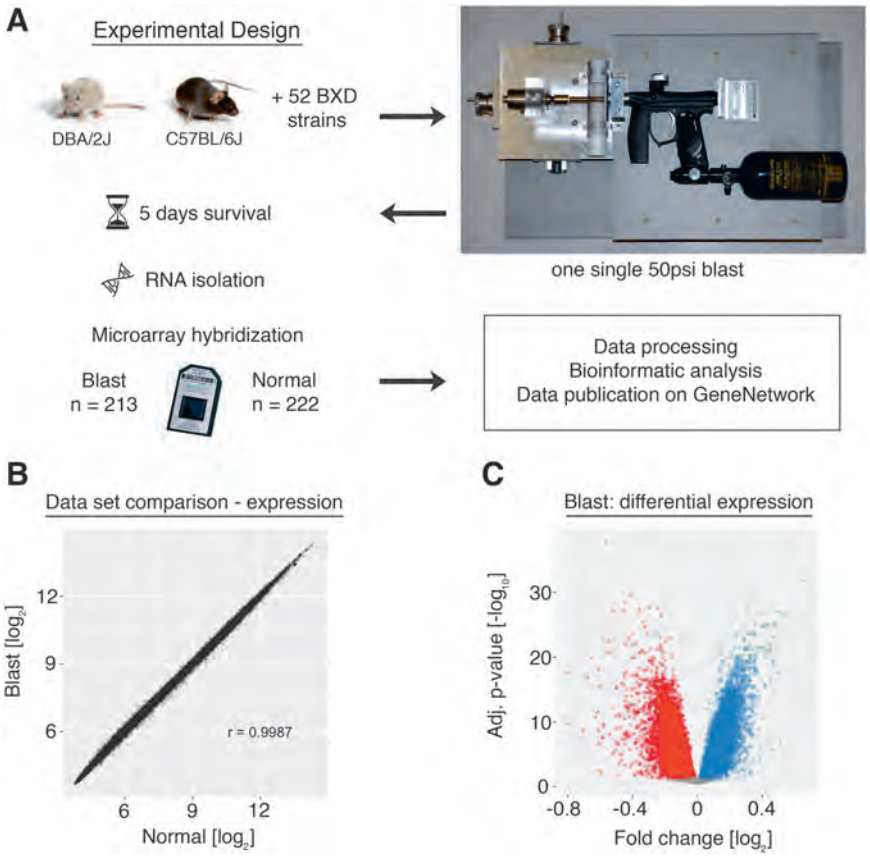

FIG. 1. **(A)** Experimental design. Mice were subjected to a single ocular 50-psi blast wave in the apparatus depicted on the right. Ribonucleic acid (RNA) was isolated 5 days after injury and hybridized to the Affymetrix GeneChip®Mouse Gene ST 2.0 microarray. **(B)** Correlation of microarray probes between the blast and the normal dataset. In this scatterplot, each dot represents one unique microarray probe. The total correlation (Pearson's *r*) is 0.999. **(C)** Volcano plot showing fold-change after blast and its associated logarithmic *p*-value after adjustment for multiple comparisons using a false discovery rate (FDR) of 0.001. Each dot represents one microarray probe. Red: downregulated probes. Blue: upregulated probes. Gray: no significant change at FDR <0.001. Color image is available online at www.liebertpub.com/neu

Thy1-*CFP* fluorescence, RGC counting, and soma size assessment

Total fluorescence of *Thy1*-CFP flat mounts was measured by quantifying green channel intensity using Photoshop CS5 without applying any further image enhancements (control $n=3$; blast $n=4$). Retinal ganglion cell (RGC) soma size was automatically measured in square pixels using a custom script in CellProfiler in two single frames (outer and inner) per retinal quadrant each, resulting in approximately 2000 to 4000 RGCs identified per animal.[9] RGCs were counted using flat mounted retinas from *Thy1*-CFP mice. Briefly, each flat mount was divided into 8 regions, such that regions 1 through 4 were close to the optic nerve head (ONH) and regions 5 through 8 were toward the periphery of each flat mount. Each region consisted of a ''cutbox,'' which was 636.5 μm $\times$ 636.5 μm in dimension and was prepared in Adobe Photoshop. Representative regions for each flat mount were selected and the number of CFP-positive RGC bodies were counted manually using the count tool in Photoshop. Data were averaged per group (blast, control) and determined to be significant if $p<0.05$ (Welch's t test).

Optokinetic tracking

Contrast sensitivity and visual acuity thresholds were measured by optokinetic tracking (OptoMotry, CerebralMechanics. Inc.; Lethbridge, Alberta).[10] Briefly, the mouse was placed on a central elevated platform in the optometry chamber surrounded by four monitors projecting a virtual rotating cylinder with sinusoidal gratings of vertical light and dark bars. A video camera mounted on the top of the chamber tracked the behavior of the mouse, which followed the moving gratings by turning its head, allowing for determination of spatial frequency (''acuity'') and contrast thresholds. Contrast sensitivity function data are expressed as the inverse of the contrast thresholds.

Sample processing, RNA isolation, and microarray hybridization

Five days after the blast procedure, mice were given an overdose of tribromoethanol and sacrificed by rapid cervical dislocation. Retinas were then dissected from eyes and directly placed into 160 U/mL Ribolock® (Thermo Scientific; Walton, MA) in Hank's Balanced Salt Solution (Sigma; St. Louis, MO) on ice. Tissue was immediately stored at −80°C. RNA was isolated using a Qiacube® and the RNeasy Mini Kit (Qiagen; Hilden, Germany) according to the manufacturer's instructions. The isolation included on-column DNase1 treatment to remove contaminating genomic DNA. All tissue was harvested between 10 a.m. and noon to minimize circadian differences in gene expression. RNA integrity was assessed on a Bioanalyzer 2100 (Agilent; Santa Clara, CA) and RNA integrity number (RIN) values for all animals ranged from 8.3 to 10 with a median of 9.5 (Supplementary Fig. 1; see online supplementary material at http://www.liebertpub.com). Each retina was hybridized to a separate GeneChip® Mouse Gene 2.0 ST (Affymetrix; Santa Clara, CA) according to the manufacturer's protocol. Microarray hybridization was performed by two different core laboratories: the Molecular Resource Center of Excellence at the University of Tennessee (Dr. William Taylor, Director) and the Emory Integrated Genomics Core (Dr. Michael E. Zwick, Director, and Robert B. Isett, Technical Director). In a separate experiment, we tested a set of arrays from C57BL/6J retinas at each facility to determine if there were batch effects or other confounding differences between core laboratories, but were not able to detect any. Therefore, data from both facilities were included in the analysis.

Quantitative PCR

For validation of microarray expression data, genes were randomly chosen from four BXD strains in both blast and normal situations. Exon-specific primers were designed using NCBI PrimerBlast and verified to be specific to the target by melting curve and gel analysis. Amplification efficiency for all primers was >90%. Primer sequences are given in Supplementary Figure 2 (see online supplementary material at http://www.liebertpub.com). First strand synthesis was carried out at 42°C using Quantitect Reverse Transcription Kit (Qiagen) and a mix of oligo(d)T primer and random hexamers. After incubation in genomic DNA (gDNA) eraser for 5 min, 350 μg of total RNA were retrotranscribed and diluted 10-fold with ultra-pure H2O. Quantitative polymerase chain reaction (PCR) was carried out in 10 μL reactions using QuantiTect SYBR Green Master Mix (Qiagen) according to the manufacturer's instructions on a Mastercycler realplex2 (Eppendorf; Hamburg, Germany) with annealing temperature set to 60°C. Technical triplicates were averaged and normalized against *Ppia*, which was identified to be a stably expressed housekeeping gene in the retina with the help of all retinal databases found on GeneNetwork. Fold-changes were calculated in $\log_2$ using the ddCt method and compared with the microarray results by linear regression models.

Data processing, statistical analysis, and WGCNA

Microarray data were normalized using the Robust Multi-array Average (RMA) method.[11] Expression levels were $\log_2$-transformed, z-scored, and multiplied by a factor of 2 before a constant of 8 was added to avoid negative expression values and make the data comparable on GeneNetwork (see GeneNetwork extended methods). Data from probes with a mean expression level lower than the fifth percentile and probes whose sequence did not have a unique BLAT hit were filtered out. Differential expression was assessed by pairwise comparison of expression values across all strains.[12] P-values were adjusted for multiple comparisons using the false discovery rate (FDR), and a stringent cutoff of 0.001 was used to decide on statistical significance. The following parameters were chosen for weighted gene co-expression network analysis (WGCNA): a thresholding soft power of 7, for which both networks approached approximate scale-free topology. Signed topological overlap matrices were created separately and scaled appropriately to make them comparable. Modules were assigned by applying adaptive branch pruning to hierarchical clustering dendrograms with the deepSplit parameter set to 2, a minimum module size of 100, and the cutHeight set at 0.995. All analyses were performed in the R 3.1.1 statistical programming environment. The ggplot2 package for the R environment was used for most plots.[13]

Gene enrichment analyses and network graphs

Gene Ontology (GO) and Kyoto Encyclopedia of Genes and Genomes (KEGG) pathway enrichment were assessed by submitting Affymetrix Probe IDs to WebGestalt.org.[14] Reported p-values were adjusted for multiple comparisons using Benjamini-Hochberg's FDR. Network graphs were created with Cytoscape version 3.4.

Immunostaining, microscopy, and lymphocyte quantification

For staining retinal flat mounts, C57BL/6J ($n=4$–5 per timepoint) mice were deeply anesthetized with tribromoethanol and perfused through the heart with 0.9% saline followed by 4% paraformaldehyde in phosphate buffer (pH 7.4). The retinas were dissected from the globe and washed 3 times in PBS with 1% Triton X-100 (Sigma) added. Tissue was then blocked in 5% BSA (Sigma) with 0.5% Triton X-100 for 1 h at room temperature. The retinas were then transferred into directly labeled primary antibodies: CD3 (HM3420, Life Technologies; 1:1000), CD4 (ab51467, Abcam; 1:1000), and CD8 (MCD0828TR, Life Technologies; 1:1000). After overnight incubation at 4°C, retinas were rinsed, placed on glass slides, and coverslipped. The whole mounts were examined with a NikonTi inverted microscope with C1 confocal scanner

(Nikon Instruments; Melville, NY) at 40× to identify labeled cells. Each retina was systematically scanned in the X–Y plain and Z-stacks were taken through the entire thickness of the retina. After merging all 40 × images together to one picture, lymphocytes were manually counted per whole retina.

Results

Experimental design and quality of the data

To define the changes in gene expression occurring 5 days after an over-pressure blast to the eye (Fig. 1A), the blast array dataset was compared with a previously published dataset from naive retina.[15] The changes in expression were relatively modest and ranged from –0.8 to +0.6-fold on a $\log_2$ scale. The magnitude of these changes is below the arbitrary two-fold difference accepted by many microarray studies. We made a conscious decision not to analyze our results using this arbitrary cutoff for biological relevance. Instead, we controlled for statistical outliers by setting a 100-fold more stringent FDR than is usual for these kinds of micorarray studies.[16]

We found that 13,971 genes were differentially expressed (Fig. 1B,C) with FDR <0.001. A subset of randomly chosen genes was used to validate the microarray results by quantitative PCR (Pearson *r* with microarray data = 0.90, Supplementary Fig. 2; see online supplementary material at htpp://www.liebertpub.com). We were able to detect these moderate changes due to the size of both datasets and the quality of RNA samples. The blast injury dataset (DoD Retina After **Blast**AffyMoGene 2.0 ST (Mar 16), **''Blast''**) contained 213 independent biological samples from 52 BXD strains plus the two parental strains. For these microarrays, care was taken to produce high-quality RNA. The average RIN score was 9.5 (± 0.03, standard error of the mean [SEM]; Supplementary Fig. 1). The normal retina dataset (DoD Retina Normal AffyMoGene 2.0 ST (May 15), ''**Normal**'') contained a total of 222 microarrays from 55 strains and had an average RIN score of 9.4 (± 0.03, SEM). An optimized RNA isolation protocol combined with the repeatability of tissue dissection results in consistency between each of the biological samples. Tissue surrounding the retina was easily excluded from the sample including the optic nerve, minimizing between-sample variation and contamination by extraneous tissues. Thus, the large number of microarrays in each dataset, the quality of the RNA used to generate the data, and the consistency of tissue isolation allow our group to identify changes in gene expression with a high degree of statistical confidence. These changes may not have been seen in a smaller-sized traditional microarray or RNA-sequencing study. Finally, both datasets are hosted on GeneNetwork.[17]

Blast injury affects the expression of distinct molecular pathways

The initial approach to the data was designed to identify differentially expressed genes and then perform functional analysis using gene enrichment profiling. GO and KEGG analysis were used to identify pathways associated with the changes observed following blast injury.[18,19] For the downregulated transcripts,we found significant enrichment of genes related to protein turnover and metabolic function. The largest number of significantly downregulated genes was associated with the GO term ''Mitochondrion'' (Fig. 2A, left panel), whereas for KEGG pathways, the biggest change fell in the ''metabolic pathways'' category (Fig 2A, right panel). Many genes encoding mitochondrial ribosomes (*Mrp**) were found within this cluster. The second largest change in GO enrichment was for the

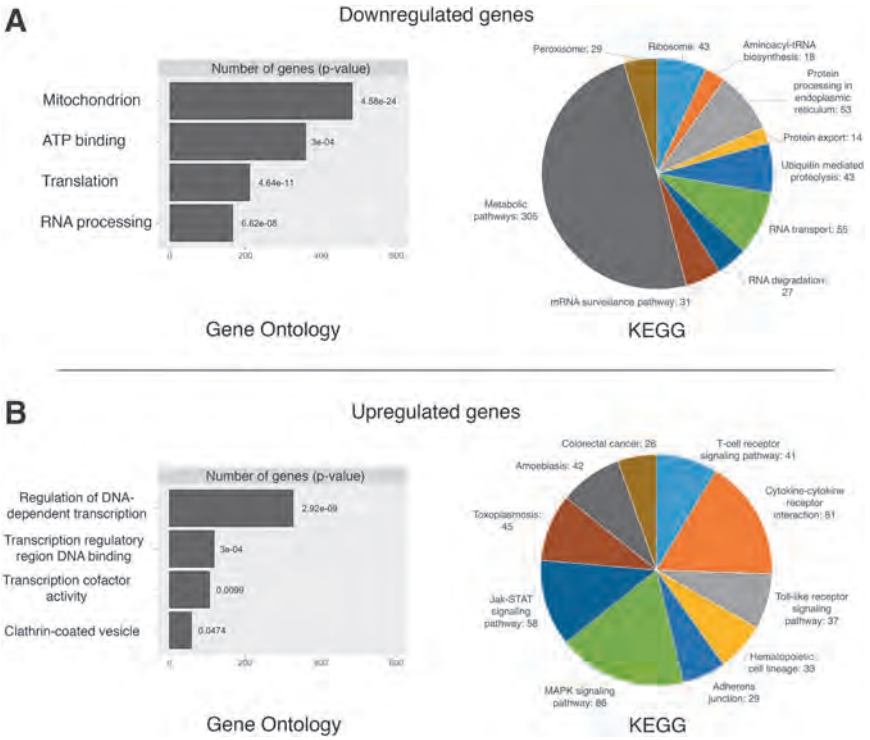

FIG. 2. **(A)** The left-hand plot shows the number and associated adjusted *p*-value of significantly downregulated genes and their top four Gene Ontology (GO) terms. The right-hand pie chart indicates significant Kyoto Encyclopedia of Genes and Genomes (KEGG) pathway enrichment for the same genes. **(B)** Identical to (A), but for significantly upregulated genes after blast injury. Color image is available online at www.liebertpub.com/neu

term ''ATP binding'' (see Supplementary Files 1 and 2 for the full list; see online supplementary material at htpp://www.liebertpub.com). The extent of the downregulation of genes associated with metabolic activity reflects a clear depression of metabolic capacity within the retina as a result of blast injury. The remaining categories for downregulated genes were primarily related to post-transcriptional molecular processes. For example, enrichment in GO terms such as ''Translation'' or KEGG pathways such as ''Ribosome,'' ''RNA transport,'' or ''tRNA biosynthesis'' collectively indicate protein synthesis dysregulation. Thus, at 5 days after blast injury, there is an overall decrease in genes regulating metabolic processes and genes associated with the production of finished protein products.

When we examined the genes that were upregulated following blast injury, a very different picture emerged. Most importantly and in contrast to downregulated genes, GO analysis was enriched in genes related to pre-transcriptional processes, such as transcriptional regulation (Fig. 2B, left panel). Additionally, upregulated genes were specific for diverse KEGG pathways, a good half of which were related to immune system processes (Fig. 2B, right panel). For example, the pathway ''Cytokine-cytokine interaction'' contained many cytokines from the CC and CXL subfamily as well as the transforming growth factor (TGF)-beta family. Additionally, Interferons (IFNs) alpha, beta, epsilon, and gamma were found upregulated within this category. These data point to a difference in transcriptional regulation as well as an increase in expression of immune response genes following blast injury, suggesting activation of the immune system similar to what our group had previously described following optic nerve crush (ONC).[20]

Network analysis of expression changes after blast injury

Gene enrichment profiling of significantly differentially expressed genes detected changes in several metabolic processes and revealed a role for the immune system following blast injury. Although it is known that isolated traumatic brain injury (TBI) in rodents and humans results in activation of an inflammatory cascade, we wondered if these transcriptional changes would be recapitulated in the mouse retina as well.[21] Because simply looking at gene expression changes between two conditions does not reveal any information about the inherently dynamic nature of gene networks, we expanded our analysis by using unbiased machine learning algorithms that compared gene co-expression patterns across the BXD strain set.

First, we performed hierarchical clustering of expression data using weighted gene co-expression network analysis, which partitioned our data into 25 modules. These modules can be thought of as functionally different compartments of the retinal transcriptome, forming groups of highly interconnected transcripts that may shape a pathway.[22,23] In general, there was very good preservation of modules between conditions (aggregate eigengene correlation = 0.86, see also Supplementary Fig. 3; see online supplementary material at htpp://www.liebertpub.com), suggesting that the general gene network architecture in the retina is well conserved after blast injury and the changes seen are due to dysregulation of a small number of genes only. Genes in each module were collected and subjected to GO profiling in order to reveal the module's closest functional annotation. Among the modules with the largest drop in preservation (or the biggest changes between conditions) were three modules whose top GO terms were significantly enriched in immune system and metabolic processes, mirroring the gene enrichment profiling results (the black, blue, and dark green module, Supplementary Fig. 3D). We then performed GO analysis separately for up- and downregulated genes in these three modules. This revealed a strong over-representation for the terms ''T-cell activation'' (adj. $p = 0.003$), ''Cytokine signaling'' (adj. $p = 0.02$), and ''regulation of gene expression'' (adj. $p < 1e\text{-}8$) for upregulated genes, whereas downregulated ones were enriched for ''primary metabolic process'' (adj. $p < 1e\text{-}4$) and ''cellular protein metabolic process'' (adj. $p = 0.004$).

Another way to examine gene network differences between conditions would be to look at changes of gene connectivity. This measure assigns an arbitrary number to a gene that represents how well its expression correlates to other genes.[24] Changes in connectivity mirror the dynamic nature of gene regulatory networks; an increase can be thought of as activation of a gene network and vice versa.[25] We performed GO analysis for the top percentile of genes with changes in connectivity. GO trees were very detailed, with genes having the highest increase in connectivity enriched in the terms ''cell adhesion'' (adj. $p = 0.025$), ''macrophage apoptotic process'' (adj. $p = 0.019$), ''extracellular region'' (adj. $p = 0.014$), ''regulation of immunoglobulin-mediated immune response'' (adj. $p < 0.001$), as well as ''isotype switching to IgG subtypes'' (adj. $p < 0.001$). On the other hand, genes whose connectivity dropped were associated with the GO terms ''axonogenesis,'' ''synaptic transmission,'' ''dendrite'' (all adj. $p < 1e\text{-}8$), ''synapse'' (adj. $p < 1e\text{-}12$), ''protein kinase activity,'' and ''ATP binding'' (both adj. $p < 0.001$), indicating that normal transcriptional regulation of these molecular processes or entities was impaired after blast injury.

In summary, these results suggest three dominating biologically relevant processes as a result of ocular blast injury: loss of synaptic transmission, impaired cell metabolism, as well as activation of the immune system.

Activation of innate and acquired immune system

Our analysis of the effects of blast injury on gene expression defined a series of differentially expressed genes and many of these genes clustered into GO categories and KEGG pathways associated with the innate immune system. Earlier work from our group has revealed an activation of the innate immune network following ONC.[20] Because ONC is a well-studied model of RGC damage, we wondered whether or not we would find activation of immune-system–related gene networks in the blast data as well. When we examined the blast injury dataset, we saw higher expression levels for many of the same genes (Table 1). Even though some of these genes did not reach significance regarding their differential expression, there was a dramatic increase in mutual correlations to genes involved in innate immunity processes (Fig. 3A). This suggested that the system is indeed activated. When we expanded this analysis for the top 200 correlates of *C4b* (a gene essential for the propagation of the classic complement cascade), we observed a strikingly strong mutual correlation in the blast but not in the normal condition (Fig. 3B). GO terms for these top 200 correlates of *C4b* revealed highly significant involvement in multiple immune-system–related biological processes and pathways (Fig. 3C), confirming the involvement of the innate immune system.

This acute activation also coincided with an increase in markers of the acquired immune system. There was a significant (adj. $p < 0.001$) increase in the gene expression levels of *Cd3* and *Cd8* (known markers of T-lymphocytes) in our microarray datasets. Others have shown infiltration of T-cells into the central nervous system (CNS) and retina under pathological conditions.[26,27] To determine if this was also the case after blast, we examined the retina at 7, 14, and 28 days following blast injury. At 7 days, CD3-

Table 1. Genes Associated with the Innate Immune System

Affymetrix probe	*Symbol*	*Description*	*Significant at FDR <0.001 (blast vs. normal)*	*Mean expression [log2]*		*Correlation: Pearson's* r		P-*values (Pearson)*	
				Normal	*Blast*	*Normal*	*Blast*	*Normal*	*Blast*
17343918	*C4b*	Complement component 4B	No	8.56	8.62	**1**	**1**		
17346528	*C3*	Complement component 3	No	7.81	7.95	0.56	0.80	0.000007	0
17387517	*Serping1*	Serine peptidase inhibitor, clade G, member 1	No	9.14	9.07	0.54	0.76	0.000014	0
17462492	*A2m*	Alpha-2-macroglobulin	No	8.85	8.83	0.32	0.75	0.015840	0
17417976	*Edn2*	Endothelin 2	No	8.03	8.14	0.43	0.75	0.001010	0
17212750	*Stat1*	Signal transducer and activator of transcription 1	No	10.31	10.33	0.40	0.71	0.002010	0.000002
17350982	*Cd74*	CD74 antigen	No	8.45	8.51	0.27	0.65	0.046220	0.000006
17269717	*Stat3*	Signal transducer and activator of transcription 3	**Yes**	10.92	11.10	0.54	0.65	0.000017	0
17546109	*Tlr7*	Toll-like receptor 7	No	6.36	6.32	0.09	0.63	0.379190	0.000013
17414836	*Tlr4*	Toll-like receptor 4	**Yes**	7.05	7.16	0.29	0.61	0.030960	0.000001
17515074	*Icam1*	Intercellular adhesion molecule 1	No	8.05	8.10	0.46	0.55	0.000370	0.000006

There is a slight increase of RNA expression and strong increase in correlation. Correlation values and their associated *p*-value are in relation to *C4b*.
FDR, false discovery rate; RNA, ribonucleic acid.

positive cells were observed invading the retina and most of these cells were found in the inner nuclear layer, in close proximity to the intraretinal vessels (Fig. 4A), and this increase was significant ($p < 0.0001$). At 14 days, there was an increase in the number of CD3/CD4 double-positive lymphocytes (T-helper cells). By 28 days after blast, many CD3-positive cells remained within the retina and in addition to the presence of CD3/CD4-positive T-helper cells, a few CD3/CD8 cytotoxic T-cells were observed (Fig. 4B). Our results are consistent with other research investigating lymphocyte invasion into the retina. For example, it was shown in a model of autoimmune uveitis that CD4+ T-cells predominate during the early phase, whereas CD8+ T-cells accumulate in later stages.[28] The identification of T-cells in the injured retina supports the view that cellular immune mechanisms could be responsible for the tissue damage caused by blast injury.

One potential link between the activation of the innate immune system and the infiltration of lymphocytes could be through a series of soluble factors such as pro-inflammatory cytokines *Cxcr3*, *Ccl4*, and IFN-gamma, all of which are expressed in the injured retina.[29–31] These cytokines and chemokines, which are released after injury by glial or endothelial cells, may play crucial roles in the recruitment of T-lymphocytes to the injured retina. Even though of these three cytokines only IFN-gamma was significantly upregulated after blast (adj. $p = 2.5$ e-06), this hypothesis is at least partially supported by increased correlations of all three cytokines to *Cd3* in our blast database (Fig. 4C).

Ocular blast injury leads to progressive vision loss associated with loss of retinal ganglion cells

The transcriptional changes observed at 5 days following a blast injury represent a small series of molecular cascades that may result in progressive loss of visual function and the death of RGCs. Because the functional changes that eventually lead to blindness may not be apparent as early as 5 days after blast, we assayed RGC features and function at different time points.

Many genes can serve as proxy for the identification of RGCs,[32] and when we investigated our data for changes in these markers, we surprisingly observed higher expression of many of these after blast (***Thy1***, ***Tubb3***, ***Pou4f2***, *Pou4f1*, *Rbpms*; bold ones are significant at $p < 0.001$). For example, the generic RGC marker *Thy1* showed a 0.2-fold $\log_2$ change (adj. $p = 2.16$e-6). We confirmed this upregulation by measuring the total fluorescence of flat-mounted retinas from *Thy1*-CFP transgenic animals at 1 week (Fig. 5A). At the same time-point, we also observed a significant increase in RGC soma size (Fig. 5B). Both total fluorescence and RGC soma size were significantly decreased at 6 weeks after blast. Functional measures at 6 weeks were also diminished in the same mice, as evidenced by a moderate drop in visual acuity and a dramatic drop in contrast sensitivity (Fig. 5C). Along with that, we observed an $\sim 16\%$ loss of *Thy1*-CFP-positive RGCs, ultimately identifying the culprit of ongoing vision loss (Fig. 5D). Taken together, these data demonstrate the devastating effects of what appears to be a relatively modest injury. They also reinforce the importance for early treatment, as the transcriptional events that are observable as early as 5 days after blast eventually lead to blindness.

Discussion

This study comprehensively characterized the in vivo effects of blast injury to the mouse retina and offers the first report on the systems genetics of ocular blast injury. A few other studies have previously investigated the molecular effects of ocular blast injury, and we note that the pressures used to inflict injury differ between models. Whereas one study reported globe rupture at pressures of 40 psi and more, this was not the case in our model.[6] In preliminary experiments using our gun, we did not see globe ruptures until pressures more than 70 psi were reached. One possible explanation for this difference could be variation in build of the models or placement of the pressure transducer (see Methods). It is likely that the effective pressure reaching the back of the eye is closer to the range previously reported (<30 psi), as there was an approximate 6-mm distance between the tip of the barrel and the eye. Nevertheless, calibration to 50 psi at the tip of the barrel was necessary to avoid technical variance in the blast apparatus. This pressure is comparable to the amount of pressure sustained at the epicenter of a

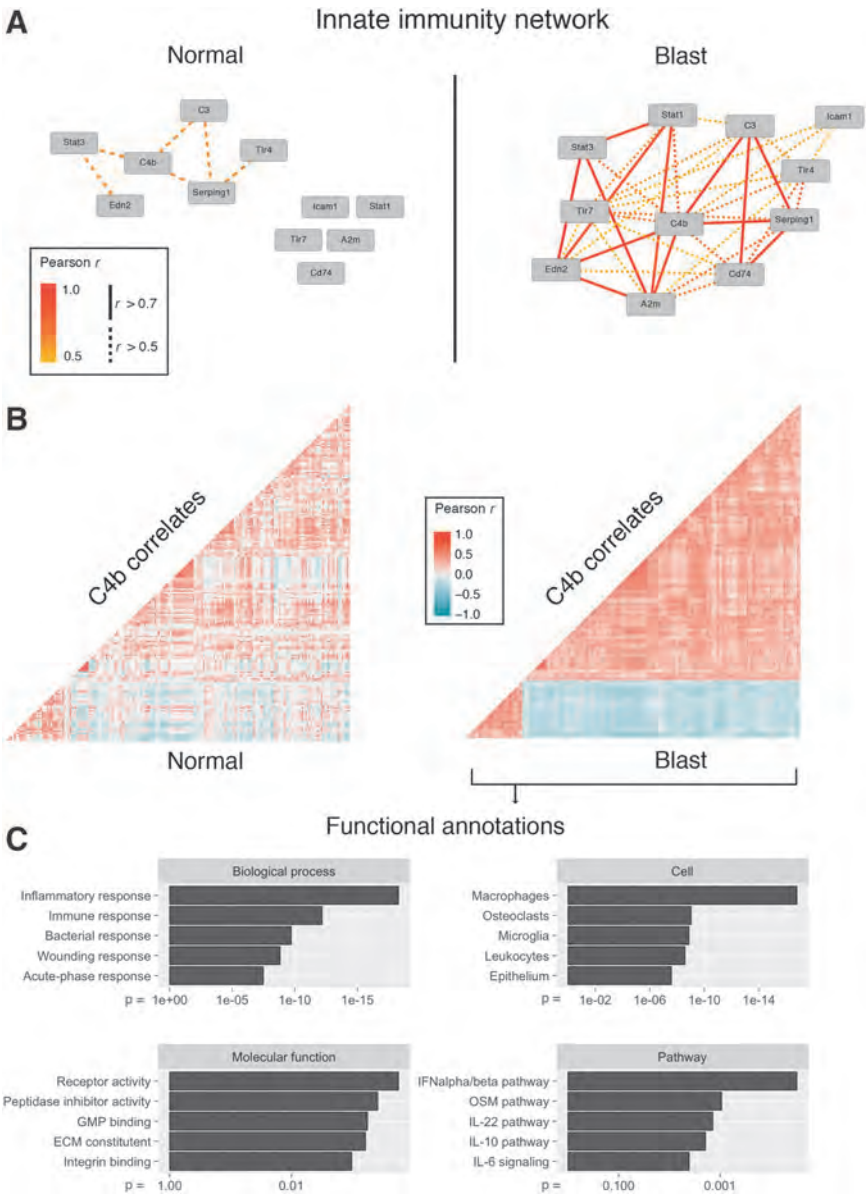

FIG. 3. **(A)** Network graph displaying Pearson's *r* for select innate immunity genes in the normal (left) and blast injury (right) situation. Although there is little correlation in the normal condition, the innate immunity network is activated after blast. **(B)** Correlation matrices showing mutual Pearson's *r* for the top 200 correlates of the gene *C4b*. Each dot represents one gene. Hierarchical clustering was applied to the blast matrix and genes did not change position between conditions. There is a strong increase in the mutual correlations indicating activation of a genetic network centered around *C4b* in the blast condition. **(C)** Top five Gene Ontology (GO) terms for the *C4b* correlates shown in (B). The adjusted *p*-value is indicated on the *x*-axis. GO enrichment demonstrates a strong relationship of *C4b* correlates to the immune system. ECM, extracellular matrix, \; GMP, guanosine monophosphate synthetase; IL, interleukin; OSM, oncostatin M.

grenade explosion, making this model roughly equivalent to being a few steps away from a grenade or bomb explosion (as pressure decreases with the cube of distance).[33] Here, we presented evidence that a single 50-psi ocular blast as measured at the tip of the airgun barrel was sufficient to lead to declining visual function. This progression was accompanied by a steady increase in the number of lymphocytes migrating into the retina (Fig. 6).

Although it is currently unknown whether this confers a regenerative or destructive effect, in many ways the pathology of ocular blast injury appears to be closely related to TBI. It is believed that in TBI, early-phase leukocyte-mediated breakdown of the blood–brain barrier eventually leads to vascular and synapse remodeling.[34] The ensuing neurodegeneration manifests itself as depression or anxiety in TBI or, in the case of ocular blast, as blindness. In mice, the negative neurological outcomes seen in TBI can be mitigated through inhibition of lymphocyte-mediated signaling, whereas the decline in visual function after ocular blast injury can be reduced through immediate-early administration of non-steroidal anti-inflammatory drugs (NSAIDs) such as meloxicam (P. Michael Iuvone, unpublished data).[35,36] Because this inflammatory response seems to occur in an acute and chronic phase over an extended period of time, treatment strategies have a wide therapeutic window. Early immunomodulatory treatments in the acute or subacute phase could have dramatic effects on the chronic response. Thus,it is appropriate to investigate

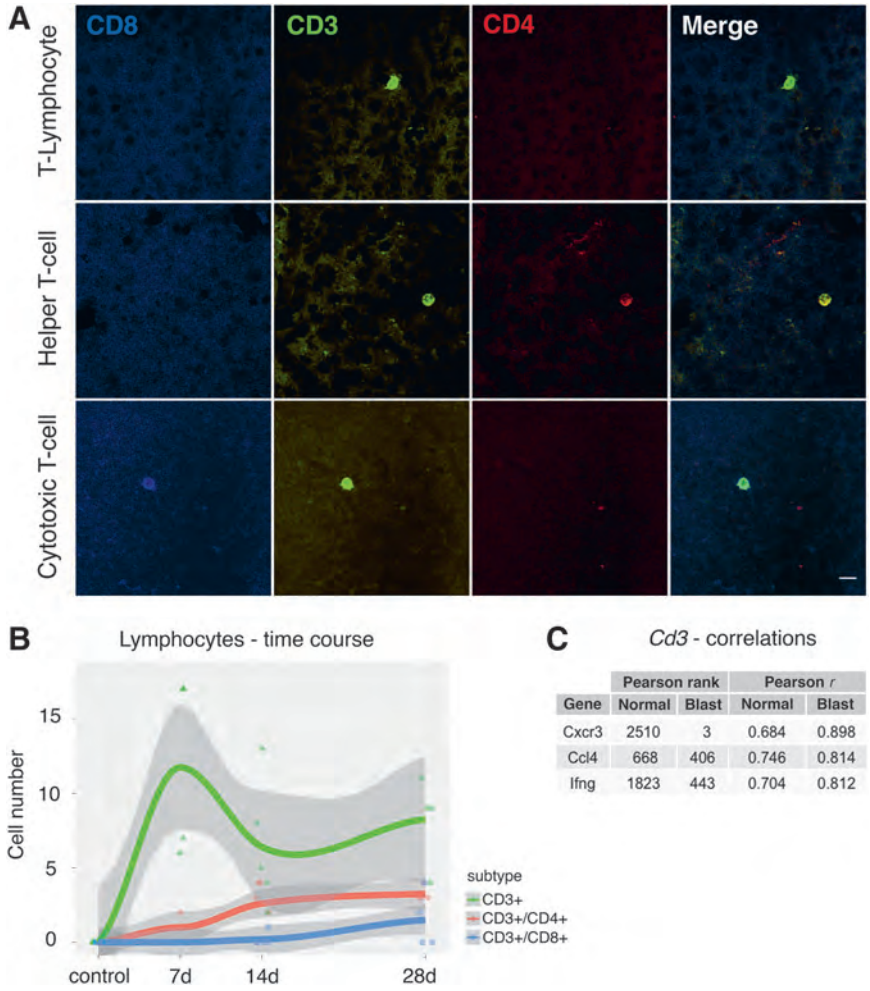

FIG. 4. **(A)** Micrographs of lymphocytes invading the retina. CD3 positivity identifies these cells as T-lymphocytes. Co-staining of CD3 and CD4 indicates Helper T-cells, and combined CD3/CD8 positivity identifies cytotoxic T-cells. Scale bar = 10μm. **(B)** Time course of lymphocyte counts in flat-mounted retinas. No lymphocytes were found in the control situation. There is an initial increase of CD3+ lymphocytes at 7 days after blast. As CD3+ cells decrease, the number of CD4+ and CD8+ cells increases over the course of a month. The gray shaded area denotes the 95% confidence interval per group. **(C)** Correlations of *Cd3* to the cytokine-related genes *Cxcr3* (chemokine receptor 3), *Ccl4* (chemokine ligand 4), and *Ifng* (interferon gamma). A drastic increase in ranked correlation and Pearson's correlation coefficient after blast can be seen. Color image is available online at www.liebertpub.com/neu

the transcriptional changes at the transition from an acute to a chronic state, as the invasion of lymphocytes into the retina likely marks an irreversibly damaging process.

Toward that end, we monitored the retinal transcriptome 5 days after blast injury, and found that a vast number of genes was differentially expressed at that time despite none of the changes exceeding two-fold. A potential reason for this is that we analyzed whole retina, which contains >7 cell types, but our and others' results indicate that the pathological changes mostly occur in fewer cell types (RGCs and glial cells), which together make up less than 1% of cells in the retina.[37] As such, most of the RNA that microarrays were normalized to is contributed by the likely unaffected photoreceptors, the most abundant cell type in the retina. Thus, even though it could be very possible that larger-fold changes exist in the affected cell populations, they are not seen in the whole retina data. Instead of focusing on a biologically relevant cutoff, we therefore strongly controlled for statistical outliers by setting a stringent FDR. Our results indicate that transcriptional changes originating from extracellular signaling pathways are dominating the ocular environment 5 days after blast, which comes at the expense of the cells' metabolic function, RNA processing, and protein production. It is not surprising that the largest number of downregulated genes after blast injury was associated with mitochondria, as dysregulated mitochondrial metabolism has long been known to play a significant role in TBI.[38] Whereas actual uncoupling of adenosine triphosphate (ATP) synthesis from the respiratory chain would result in mitochondrial stress and acute cell death, other more low-grade mechanisms of mitochondrial dysfunction must be responsible for the slow neurodegeneration that manifests itself after blast injury in the retina. It has very recently been shown that mitochondrial fission is strongly increased in TBI, and that the negative effects on learning and memory could be rescued through the administration of a fission inhibitor.[39] It would be interesting to investigate if similar improvements of metabolic function could be achieved in ocular blast injury.

Other changes in gene expression we observed between blasted and normal mice were seemingly related to the balance between transcription and translation. Along with a decrease in genes

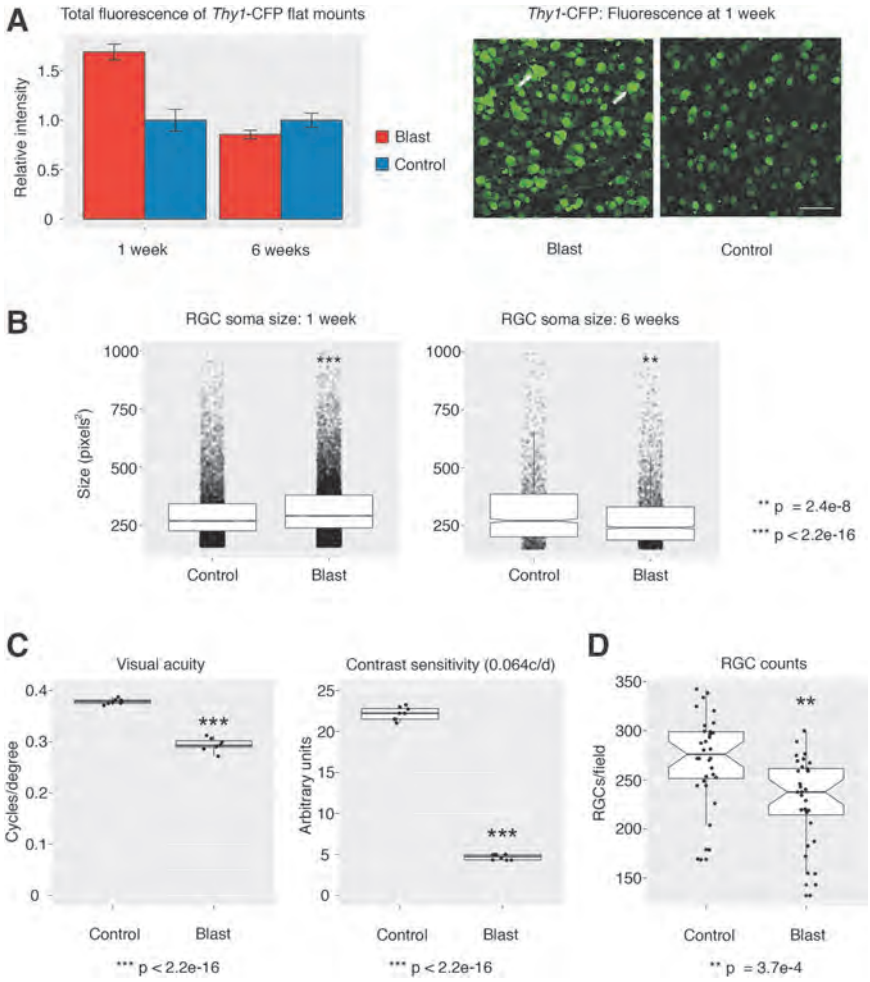

FIG. 5. **(A)** Measurements of *Thy1*-CFP fluorescence in retinal flat mounts at 1 and 6 weeks after blast. The micrographs on the right are representative of the hyper-fluorescence seen 1 week after blast. Arrows indicate *Thy1*-CFP positive cells with very large somata. Scale bar = 100 μm. Control versus Blast at 1 week, $p < 0.001$, $n = 3$ per condition. **(B)** Automated retinal ganglion cell (RGC) soma size measurements at 1 and 6 weeks after blast. Soma size is significantly larger at 1 week after blast but significantly smaller at 6 weeks after blast. **(C)** Visual acuity and contrast sensitivity 6 weeks after blast. Both measures drop significantly after compared with a control situation. **(D)** RGC counts in retinal *Thy1*-CFP flat mounts. There is a significant drop 6 weeks after mice have been subjected to blast injury. Color image is available online at www.liebertpub.com/neu

responsible for ribosomal or endoplasmic reticulum function, we found increased expression of many transcription factors and co-factors. This mirrors the dynamic nature of gene regulatory networks. Changes in RNA expression measured in total tissue are either due to one specific cell type adapting its transcriptional program to a stimulus, or additional new cells that became part of the whole cell population. Although it is likely that a small fraction of the changes seen are the result of lymphocyte invasion, a large part of the differentially expressed RNA will be contributed from retinal cells synthesizing regulatory molecules that prepare the cell for the changes to come.

Because ocular blast injury was previously associated with thinning of the retinal nerve fiber layer, we investigated RGC function as well as expression changes in RGC marker genes.[7] Interestingly, we saw statistically significant increased expression in genes such as *Thy1*, which also corresponded to an increase in RGC soma size and *Thy1*-CFP fluorescence. This could be related to a process termed ''neuronal chromatolysis,'' a cellular response after axonal damage resulting in the dissolution of Nissl bodies and redistribution of cytoskeletal proteins with an apparent increase in soma size.[40] As chromatolytic neurons are thought to still possess the ability to regenerate, it is interesting to speculate whether or not treatment at this time would stall neuronal apoptosis. We and others have observed that the decline in RCG number or nerve fiber layer thickness is gradual, suggesting a slow but constant underlying molecular process. It appears that this process is related to immune signaling, as our enrichment analysis identified the strongest positive change in expression in genes related to the immune system. Even when the changes in mRNA levels were not significant, increased correlation and connectivity of co-expressed genes was seen especially for immunity-related genes. This illustrates activation of genetic networks, which we have previously found to be the case in the same mouse population after ONC.[20] In ONC, a fixed amount of pressure is applied to the optic nerve without interrupting the blood flow to the retina, which leads to gradual decline in RGC number.[41] Therefore, both ONC and blast injury are models for RGC death, in which the immune signaling cascade appears to play a significant role. The exact molecular cascades leading to this have yet to be determined, but it is likely that cytokine signaling plays a significant role. Other studies suggest that

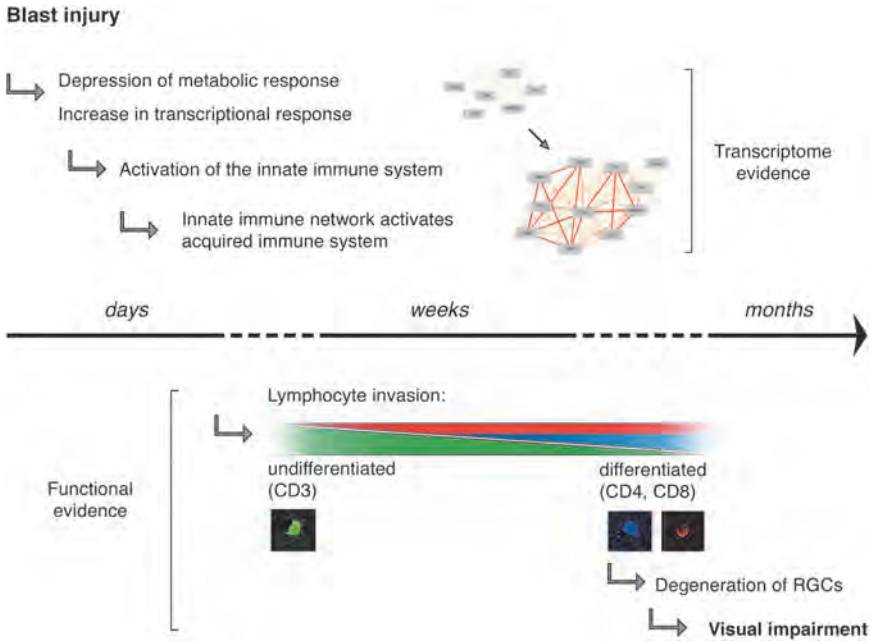

FIG. 6. Diagram summarizing the main findings of this study. Over the course of days and weeks, the moderate transcriptional changes seen in the retina lead to activation of the innate and the acquired immune networks, which in turn results in chronic neurodegeneration and visual impairment months after injury.

expression of cytokines in the retina is mediated by glial cells and that an increase in cytokine signaling results in activation of retinal microglia, astrocytes, and Müller glia on site.[42,43] In our analysis, we saw that *C4b* formed a genetic network after blast injury that was significantly enriched in the cellular GO terms ''Macrophages'' and ''Microglia.'' The parent protein of *C4b* is complement factor C4. It has been known now for about 20 years that microglia and astrocytes in mouse brains can synthesize complement factors[44] and it also has been shown that complement genes are expressed in the retina.[45] Whereas the exact origin of complement factor secretion in the retina remains unknown, our and others' results indicate a role for microglia in this process. It is interesting to note that *C4b* correlates were also enriched for the terms ''Epithelium,'' ''Extracellular Matrix,'' and ''Integrin Binding.'' This could suggest that one of the mechanisms that permit lymphocyte invasion through the otherwise tight blood–retina barrier after blast is mediated through breakdown of the blood–retina barrier by molecules secreted from microglia activated by complement factors. Similar processes have been observed in TBI as well.[46,47]

Ultimately, the DBA/2J mouse is known for having several immune-system–related defects compared with the C57BL/6J mouse.[48,49] Among these is a condition that abrogates ocular immune privilege associated with the anterior chamber, called a dysfunctional anterior chamber associated immune deviation (ACAID).[50] This syndrome was recently found to be at least in part due to a dysfunctional natural killer cell system resulting from *Cd94* deficiency in DBA/2J mice.[51] We examined our databases for correlations between the presence (B6 genotype) or absence (D2 genotype) of ACAID and inflammatory markers, but no significant correlation was found (data not shown). Whereas another study has detected greater influx of immune components into the anterior part of the eye in DBA/2J mice after blast injury, our data suggest no such connection for retina.[43] This indicates that lymphocyte infiltration into the retina is independent of a functional or dysfunctional ACAID.

In conclusion, our data reveal the genetic networks of ocular blast injury for the first time. Using a systems genetics approach, we show that the dysregulated transcriptional environment is reminiscent of the pathophysiology of TBI, with loss of metabolic function and activation of inflammatory cascades that eventually lead to decreases in visual function. Having used BXD strains for this study will potentially allow for identification of upstream modulators of this immune cascade as future work. To our knowledge, this is by far the largest microarray study on ocular blast injury, and it is our hope that the publically available data will be useful for fellow researchers who are interested in specific genes or pathways involved in the pathogenesis of blast injury.

Acknowledgments

This study was supported by the Department of Defense CDMRP Grants W81XWH1210255 and W81XWH-12-1-0436 from the U.S. Army Medical Research and Materiel Command and the Telemedicine and Advanced Technology (EEG, PMI), NEI grants R01EY178841 (EEG), R01EY004864 (PMI), P30EY06360 (Emory Vision Core, PMI), and unrestricted funds from Research to Prevent Blindness. FLS is supported by the institutional training grant T32EY007092-30 (PMI). Additional support was provided by the Emory Integrated Genomics Core (EIGC), which is subsidized by the Emory University School of Medicine as one of the Emory Integrated Core Facilities. We thank Dr. Robert Williams and Arthur Centeno (University of Tennessee Health Science Center) for maintaining the data on GeneNetwork, Dr. Xiangdi Wang and Dr. Justin Templeton for their technical assistance, as well as April Brooke Still for her help in breeding some BXD animals at Emory University.

Author Disclosure Statement

No competing financial interests exist. The study was conceived by EEG. RK collected and isolated RNA from most of the animals.

FLS performed the blast procedure and all statistical and bioinformatic analyses. YL was responsible for lymphocyte immunostaining and counting. MC compiled *Thy1*-CFP flat mounts and helped with animal breeding. CS and PL completed the OKT experiments overseen by PMI. FLS, EEG, and YL wrote the article with input from all other authors. All authors read and approved the final manuscript.

References

1. Weichel, E.D., and Colyer, M.H. (2008). Combat ocular trauma and systemic injury. Curr. Opin. Ophthalmol. 19, 519–525.
2. Cockerham, G.C., Rice, T.A., Hewes, E.H., Cockerham, K.P., Lemke, S., Wang, G., Lin, R.C., Glynn-Milley, C., and Zumhagen, L. (2011). Closed-eye ocular injuries in the Iraq and Afghanistan wars. N. Engl. J. Med. 364, 2172–2173.
3. Corrales, G., and Curreri, A. (2009). Eye trauma in boxing. Clin. Sports Med. 28, 591–607, vi.
4. Nemet, A.Y., Asalee, L., Lang, Y., Briscoe, D., and Assia, E.I. (2016). Ocular paintball injuries. Isr. Med. Assoc. J 18, 27–31.
5. Bricker-Anthony, C., Hines-Beard, J., and Rex, T.S. (2014). Molecular changes and vision loss in a mouse model of closed-globe blast trauma. Invest. Ophthalmol. Vis. Sci. 55, 4853–4862.
6. Hines-Beard, J., Marchetta, J., Gordon, S., Chaum, E., Geisert, E.E., and Rex, T.S. (2012). A mouse model of ocular blast injury that induces closed globe anterior and posterior pole damage. Exp. Eye Res. 99, 63–70.
7. Mohan, K., Kecova, H., Hernandez-Merino, E., Kardon, R.H., and Harper, M.M. (2013). Retinal ganglion cell damage in an experimental rodent model of blast-mediated traumatic brain injury. Invest. Ophthalmol. Vis. Sci. 54, 3440–3450.
8. Dougherty, A.L., MacGregor, A.J., Han, P.P., Heltemes, K.J., and Galarneau, M.R. (2011). Visual dysfunction following blast-related traumatic brain injury from the battlefield. Brain Inj. 25, 8–13.
9. Carpenter, A.E., Jones, T.R., Lamprecht, M.R., Clarke, C., Kang, I.H., Friman, O., Guertin, D.A., Chang, J.H., Lindquist, R.A., Moffat, J., Golland, P., and Sabatini, D.M., (2006). CellProfiler: image analysis software for identifying and quantifying cell phenotypes. Genome Biol. 7, R100.
10. Douglas, R.M., Alam, N.M., Silver, B.D., McGill, T.J., Tschetter, W.W., and Prusky, G.T. (2005). Independent visual threshold measurements in the two eyes of freely moving rats and mice using a virtual-reality optokinetic system. Vis. Neurosci. 22, 677–684.
11. Irizarry, R.A., Hobbs, B., Collin, F., Beazer-Barclay, Y.D., Antonellis, K.J., Scherf, U., and Speed, T.P. (2003). Exploration, normalization, and summaries of high density oligonucleotide array probe level data. Biostatistics 4, 249–264.
12. Cheadle, C., Vawter, M.P., Freed, W.J., and Becker, K.G. (2003). Analysis of microarray data using Z score transformation. J. Mol. Diagn. 5, 73–81.
13. Wickham, H. (2009). *Ggplot2: Elegant Graphics for Data Analysis. Use R! 2009.* Springer: New York, pps. viii, 212.
14. Wang, J., Duncan, D., Shi, Z., and Zhang, B. (2013). WEB-based GEne SeT AnaLysis Toolkit (WebGestalt): update 2013. Nucleic Acids Res. 41, W77–W83.
15. King, R., Lu, L., Williams, R.W., and Geisert, E.E. (2015). Transcriptome networks in the mouse retina: an exon level BXD RI database. Mol. Vis. 21, 1235–1251.
16. Gusnanto, A., Calza, S., and Pawitan, Y. (2007). Identification of differentially expressed genes and false discovery rate in microarray studies. Curr. Opin. Lipidol. 18, 187–193.
17. Mulligan, M.K., Mozhui, K., Prins, P., and Williams, R.W. (2017). GeneNetwork: a toolbox for systems genetics. Methods Mol. Biol. 1488, 75–120.
18. Gene Ontology Consortium. (2015). Gene Ontology Consortium: going forward. Nucleic Acids Res. 43, D1049–D1056.
19. Kanehisa, M., Sato, Y., Kawashima, M., Furumichi, M., and Tanabe, M. (2016). KEGG as a reference resource for gene and protein annotation. Nucleic Acids Res. 44, D457–D462.
20. Templeton, J.P., Freeman, N.E., Nickerson, J.M., Jablonski, M.M., Rex, T.S., Williams, R.W., and Geisert, E.E. (2013). Innate immune network in the retina activated by optic nerve crush. Invest. Ophthalmol. Vis. Sci. 54, 2599–2606.
21. Holmin, S., Mathiesen, T., Shetye, J., and Biberfeld, P. (1995). Intracerebral inflammatory response to experimental brain contusion. Acta Neurochir. (Wien) 132, 110–119.
22. Langfelder, P. and Horvath, S. (2008). WGCNA: an R package for weighted correlation network analysis. BMC Bioinformatics 9, 559.
23. Fuller, T.F., Ghazalpour, A., Aten, J.E., Drake, T.A., Lusis, A.J., and Horvath, S. (2007). Weighted gene coexpression network analysis strategies applied to mouse weight. Mamm. Genome 18, 463–472.
24. Langfelder, P., Mischel, P.S., and Horvath, S. (2013). When is hub gene selection better than standard meta-analysis? PLoS One 8, e61505.
25. Zhao, W., Langfelder, P., Fuller, T., Dong, J., Li, A., and Hovarth, S. (2010). Weighted gene coexpression network analysis: state of the art. J. Biopharm. Stat. 20, 281–300.
26. Charteris, D.G., Champ, C., Rosenthal, A.R., and Lightman, S.L. (1992). Behcet's disease: activated T lymphocytes in retinal perivasculitis. Br. J. Ophthalmol. 76, 499–501.
27. Imagawa, T., Kitagawa, H., and Uehara, M. (2003). Appearance of T cell subpopulations in the chicken and embryo retina. J. Vet. Med. Sci. 65, 23–28.
28. Richardson, P.R., Boulton, M.E., Duvall-Young, J., and McLeod, D. (1996). Immunocytochemical study of retinal diode laser photocoagulation in the rat. Br. J. Ophthalmol. 80, 1092–1098.
29. Ha, Y., Liu, H., Xu, Z., Yokota, H., Narayanan, S.P., Lemtalsi, T., Smith, S.B., Caldwell, R.W., Caldwell, R.B., and Zhang, W. (2015). Endoplasmic reticulum stress-regulated CXCR3 pathway mediates inflammation and neuronal injury in acute glaucoma. Cell Death Dis. 6, e1900.
30. Rutar, M., Natoli, R., Chia, R.X., Valter, K., and Provis, J.M. (2015). Chemokine-mediated inflammation in the degenerating retina is coordinated by Muller cells, activated microglia, and retinal pigment epithelium. J. Neuroinflammation 12, 8.
31. Zinkernagel, M.S., Chinnery, H.R., Ong, M.L., Petitjean, C., Voigt, V., McLenachan, S., McMenamin, P.G., Hill, G.R., Forrester, J.V., Wikstrom, M.E., and Degli-Esposti, M.A. (2013). Interferon gamma-dependent migration of microglial cells in the retina after systemic cytomegalovirus infection. Am. J. Pathol. 182, 875–885.
32. Struebing, F.L., Lee, R.K., Williams, R.W., and Geisert, E.E. (2016). Genetic Networks in Mouse Retinal Ganglion Cells. Front. Genet. 7, 169.
33. Glasstone, S., and Dolan, P. (1977). The effects of nuclear weapons. United States Department of Defense.
34. Schwarzmaier, S.M., Zimmermann, R., McGarry, N.B., Trabold, R., Kim, S.W., and Plesnila, N. (2013). In vivo temporal and spatial profile of leukocyte adhesion and migration after experimental traumatic brain injury in mice. J. Neuroinflammation 10, 32.
35. Wood, R.L., and Rutterford, N.A. (2006). Demographic and cognitive predictors of long-term psychosocial outcome following traumatic brain injury. J. Int. Neuropsychol. Soc. 12, 350–358.
36. Zhao, S., Yu, Z., Liu, Y., Bai, Y., Jiang, Y., van Leyen, K., Yang, Y.G., Lok, J.M., Whalen, M.J., Lo, E.H., and Wang, X. (2016). CD47 deficiency improves neurological outcomes of traumatic brain injury in mice. Neurosci. Lett. 643, 125–130.
37. Jeon, C.J., Strettoi, E., and Masland, R.H. (1998). The major cell populations of the mouse retina. J. Neurosci. 18, 8936–8946.
38. Vink, R., Head, V.A., Rogers, P.J., McIntosh, T.K., and Faden, A.I. (1990). Mitochondrial metabolism following traumatic brain injury in rats. J. Neurotrauma 7, 21–27.
39. Fischer, T.D., Hylin, M.J., Zhao, J., Moore, A.N., Waxham, M.N., and Dash, P.K. (2016). Altered mitochondrial dynamics and TBI pathophysiology. Front. Syst. Neurosci. 10, 29.
40. Chen, D.H. (1978). Qualitative and quantitative study of synaptic displacement in chromatolyzed spinal motoneurons of the cat. J. Comp. Neurol. 177, 635–664.
41. Templeton, J.P., and Geisert, E.E. (2012). A practical approach to optic nerve crush in the mouse. Mol. Vis. 18, 2147–2152.
42. Stahl, T., C. Mohr, C., Kacza, J., Reimers, C., Pannicke, T., Sauder, C., Reichenbach, A., and Seeger, J. (2003). Characterization of the acute immune response in the retina of Borna disease virus infected Lewis rats. J. Neuroimmunol. 137, 67–78.
43. Bricker-Anthony, C., Hines-Beard, J., D'Surney, L., and Rex, T.S. (2014). Exacerbation of blast-induced ocular trauma by an immune response. J. Neuroinflammation 11, 192.
44. Haga, S., Aizawa, T., Ishii, T., and Ikeda, K. (1996). Complement gene expression in mouse microglia and astrocytes in culture: com-

parisons with mouse peritoneal macrophages. Neurosci. Lett. 216, 191–194.
45. Luo, C., Chen, M., and Xu, H. (2011). Complement gene expression and regulation in mouse retina and retinal pigment epithelium/choroid. Mol. Vis. 17, 1588–1597.
46. Baskaya, M.K., Rao, A.M., Dogan, A., Donaldson, D., and Dempsey, R.J. (1997). The biphasic opening of the blood-brain barrier in the cortex and hippocampus after traumatic brain injury in rats. Neurosci. Lett. 226, 33–36.
47. Balu, R. (2014). Inflammation and immune system activation after traumatic brain injury. Curr. Neurol. Neurosci. Rep. 14, 484.
48. Casanova, T., Van de Paar, E., Desmecht, D., and Garigliany, M.M. (2015). Hyporeactivity of alveolar macrophages and higher respiratory cell permissivity characterize DBA/2J mice infected by influenza A virus. J. Interferon Cytokine Res. .35, 808–820.
49. Miyairi, I., Tatireddigari, V.R., Mahdi, O.S., Rose, L.A., Belland, R.J., Lu, L., Williams, R.W., and Byrne, G.I. (2007). The p47 GTPases Iigp2 and Irgb10 regulate innate immunity and inflammation to murine Chlamydia psittaci infection. J. Immunol. 179, 1814–1824.
50. Streilein, J.W., and Niederkorn, J.Y. (1981). Induction of anterior chamber-associated immune deviation requires an intact, functional spleen. J. Exp. Med. 153, 1058–1067.
51. Chattopadhyay, S., O'Rourke, J., and Cone, R.E. (2008). Implication for the CD94/NKG2A-Qa-1 system in the generation and function of ocular-induced splenic CD8+ regulatory T cells. Int. Immunol. 20, 509–516.

Address correspondence to:
Eldon E. Geisert, PhD
Department of Ophthalmology
Emory University
1365B Clifton Road NE
Room 5500
Atlanta, GA 30305

E-mail: egeiser@emory.edu

Appendix D

frontiers in Molecular Neuroscience

ORIGINAL RESEARCH
published: 02 November 2017
doi: 10.3389/fnmol.2017.00354

Differential Expression of *Sox11* and *Bdnf* mRNA Isoforms in the Injured and Regenerating Nervous Systems

*Felix L. Struebing[1], Jiaxing Wang[1,2], Ying Li[1], Rebecca King[1], Olivia C. Mistretta[3], Arthur W. English[3] and Eldon E. Geisert[1]**

[1] Department of Ophthalmology, Emory University, Atlanta, GA, United States, [2] Department of Ophthalmology, Tianjin Medical University General Hospital, Tianjin, China, [3] Department of Cell Biology, Emory University, Atlanta, GA, United States

In both the central nervous system (CNS) and the peripheral nervous system (PNS), axonal injury induces changes in neuronal gene expression. In the PNS, a relatively well-characterized alteration in transcriptional activation is known to promote axonal regeneration. This transcriptional cascade includes the neurotrophin *Bdnf* and the transcription factor *Sox11*. Although both molecules act to facilitate successful axon regeneration in the PNS, this process does not occur in the CNS. The present study examines the differential expression of *Sox11* and *Bdnf* mRNA isoforms in the PNS and CNS using three experimental paradigms at different time points: (i) the acutely injured CNS (retina after optic nerve crush) and PNS (dorsal root ganglion after sciatic nerve crush), (ii) a CNS regeneration model (retina after optic nerve crush and induced regeneration); and (iii) the retina during a chronic form of central neurodegeneration (the DBA/2J glaucoma model). We find an initial increase of *Sox11* in both PNS and CNS after injury; however, the expression of *Bdnf* isoforms is higher in the PNS relative to the CNS. Sustained upregulation of *Sox11* is seen in the injured retina following regeneration treatment, while the expression of two *Bdnf* mRNA isoforms is suppressed. Furthermore, two isoforms of *Sox11* with different 3′UTR lengths are present in the retina, and the long isoform is specifically upregulated in later stages of glaucoma. These results provide insight into the molecular cascades active during axonal injury and regeneration in mammalian neurons.

Keywords: axon injury, axon regeneration, gene expression, retinal ganglion cells, DRG neurons, glaucoma, epigenetic regulation, untranslated regions

OPEN ACCESS

Edited by:
Robert W. Burgess, Jackson Laboratory, United States

Reviewed by:
James Nicholas Sleigh, University College London, United Kingdom
John Svaren, University of Wisconsin-Madison, United States

***Correspondence:**
Eldon E. Geisert
egeiser@emory.edu

Received: *29 June 2017*
Accepted: *18 October 2017*
Published: *02 November 2017*

Citation:
Struebing FL, Wang J, Li Y, King R, Mistretta OC, English AW and Geisert EE (2017) Differential Expression of Sox11 and Bdnf mRNA Isoforms in the Injured and Regenerating Nervous Systems. Front. Mol. Neurosci. 10:354. doi: 10.3389/fnmol.2017.00354

INTRODUCTION

It is well known that neurons of the peripheral nervous system (PNS) have the ability to regrow damaged axons, while neurons of the central nervous system (CNS) often die following axonal injury (Young, 2014). This difference in regenerative capacity is partly attributed to the non-permissive growth environment of the CNS, with subsequent failure of neurons to re-myelinate their injured axons (Geisert et al., 1998; Yiu and He, 2006; Fernandes et al., 2016). The regeneration environment of the PNS is considered to be more permissive to axon regeneration. However, environment does not seem to be the only factor affecting regeneration differentially (Brosius Lutz and Barres, 2014). Neuron-specific transcriptional cascades are involved in promoting regeneration in the PNS and in the abrogative response in the CNS. The specific differences in these

transcription cascades are not fully defined (Venkatesh and Blackmore, 2017). Among the genes implicated in the differential capacity for axon regeneration is brain-derived neurotrophic factor (BDNF), known to play a prominent role in the developing and injured PNS (Richner et al., 2014). BDNF is not only secreted from muscles, but also from Schwann cells in the PNS and regenerating axons in the CNS. It can bind to axonal tropomyosin receptor kinase B (trkB) receptors, resulting in axon elongation (Segal et al., 1995), dendritic or synaptic growth, or neurogenesis (Lu et al., 2014). In line with a role for BDNF/trkB signaling in axon regeneration, application of small molecules acting as agonists on the trkB receptor were shown to increase axon growth after PNS injury, independent of endogenous BDNF expression (English et al., 2013). Inhibiting *Bdnf* expression in Schwann cells abolished axon regeneration, but the phenotype could be rescued by electrical stimulation or exercise. This rescue was the result of increased secretion of BDNF from neurons, suggesting that sustained neural activity can also lead to increased neuronal *Bdnf* expression that acts in an autocrine manner to promote axon regeneration (Wilhelm et al., 2012). Interestingly, *Bdnf* signaling is known to affect motor and sensory nerves differentially, as it was shown that mice lacking *Bdnf* expression developed sensory and not motor deficits (Ernfors et al., 1994), but high doses of exogenous BDNF could selectively promote motor axon outgrowth after sciatic nerve transection (Santos et al., 2016). Therefore, the molecular networks up- and downstream of the BDNF/trkB signaling pathway can partly mediate the regenerative response in neurons in a cell type-specific way.

One of the genes known to drive *Bdnf* expression is *Sox11*. This transcription factor is expressed in neuronal precursors and retinal ganglion cells (RGCs), making it indispensable for neuron differentiation (Mu et al., 2012; Salerno et al., 2012). Overexpression of *Sox11* after peripheral nerve injury resulted in enhanced regeneration and improvement of measurements of functional recovery (Jankowski et al., 2009; Jing et al., 2012). Conversely, overexpression of *Sox11* after spinal cord injury lead to impaired motor dexterity despite an enhanced regenerative capability of CNS axons (Wang et al., 2015). In the mouse retina, *Sox11* can activate transcripts associated with axon growth, while suppressing some genes involved in synapse formation (Norsworthy et al., 2017). *Sox11* also differentially affects survival and regeneration of distinct RGC subtypes and is a downstream effector of Dual Leucine Zipper Kinase (DLK/*Map3k12*) following axon injury (Welsbie et al., 2017). Furthermore, its overexpression results in substantial axonal regeneration (Norsworthy et al., 2017). These data suggest that *Sox11* acts as a regulatory switch between cell survival and axonal growth and that it selectively exploits a tissue- as well as cell-specific molecular environment to modulate gene expression and overall cell function.

Among other (epi)genetic mechanisms, this kind of specificity can be conferred by different mRNA isoforms. For example, it is now well established that in the mouse *Bdnf* gene, eight 5′ non-coding exons are alternatively spliced to create nine distinct mRNA isoforms (Aid et al., 2007). All of these different mRNAs include the same 3′ coding exon (exon IX), and thus encode the same protein, but they differ in regard to their subcellular location (Bishop et al., 1994; Aid et al., 2007). While no similar mRNA isoforms of *Sox11* have been described yet, this single-exon gene underwent a remarkable reannotation since its first discovery (Wright et al., 1993) primarily due to differences in 3′Untranslated Region (3′UTR) length. It is currently annotated with a 3′UTR length of almost 7 kb. Whereas this would be considered unusually long for a non-neural cell, 3′UTRs are frequently elongated in neurons (Miura et al., 2014). It was also shown that differences in UTR length can have functional effects. For example, expression of the same gene with different UTR lengths was recently observed in different cellular compartments (Berkovits and Mayr, 2015), implicating extended 3′UTRs in an RNA-binding protein mediated, post-transcriptional regulatory process. Similarly, expression of *Sox11* coding (exon) and non-coding (3′UTR) segments was found to be spatially separated in mouse neuronal tissue (Kocabas et al., 2015). Expression of its protein-coding region (CDS) was higher in hippocampal strati that underwent active neurogenesis, whereas expression of its 3′UTR was restricted to terminally differentiated cells. Therefore, the 3′UTR-to-CDS ratio of certain genes confers a distinct and tissue-specific regulatory mechanism.

Both *Bdnf* and *Sox11* are genes that play important roles in axon regeneration. Transcription of each gene is regulated in multiple ways. Thus, we began a series of experiments to compare and contrast the response of these genes under different conditions. The present study examines the transcriptional response of *Sox11* and *Bdnf* in the PNS and CNS in regenerating and non-regenerating paradigms.

MATERIALS AND METHODS

Animals

For each experimental group and time point, an equal number of male and female C57BL/6J mice ($n \geq 4$ per group) underwent the procedures described below (except for sciatic nerve crush where $m = 10$ and $f = 11$). Power analysis for this sample size and three pairwise comparisons demonstrated a 96% chance of detecting a true twofold change with a standard deviation of 25% and a Type I error rate of 5%. All C57BL/6J animals were between 60 and 100 days of age. Mice were maintained on a 12 h light – 12 h dark cycle in a parasite-free facility with food and water *ad libitum*. All procedures involving animals were approved by the Animal Care and Use Committee of Emory University and were in accordance with the ARVO Statement for the Use of Animals in Ophthalmic and Vision Research.

Optic Nerve Crush

Optic nerve crush was performed as described in Templeton and Geisert (2012). Briefly, C57BL/6J mice were anesthetized using Ketamine (100 mg/kg) and Xylazine (15 mg/kg). Under the binocular operating scope, a small incision was made in the conjunctiva. With micro-forceps (Dumont #5/45 Forceps, Roboz, cat. #RS-5005, Gaithersburg, MD, United States), the edge of the conjunctiva was grasped next to the globe. The globe was rotated nasally to allow visualization of its posterior aspect and optic nerve. The exposed optic nerve was then clamped 2 mm distal

from the optic nerve head with Dumont #N7 self-closing forceps (Roboz, cat. #RS-5027) for 10 s. At the end of the procedure, a drop of 0.5% proparacaine hydrochloride ophthalmic solution (Falcon Pharmaceuticals, Fort Worth TX, United States) was administered for pain control and a small amount of surgical lubricant (KY Jelly, McNeil-PPC, Skillman, NJ, United States) was applied to the eye to protect it from drying. Mice were allowed to recover on a heating pad while being monitored until fully awake.

Sciatic Nerve Crush

Ten male and 11 female mice were anesthetized with isoflurane (1%) and the sciatic nerve was exposed in the posterior mid-thigh. The nerve was then crushed midway between the sciatic foramen and the branching into common fibular, tibial, and sural nerves, using the same forceps used to crush optic nerves. Pressure on the forceps was held for 10 s. When pressure was released, a clear space in the nerve at the crush site, indicating an effective crush, could be observed in all cases. Surgical wounds were closed in layers and animals received a single dose of Meloxicam (5 mg/kg, po). Mice were allowed to recover on a heating pad while being monitored until fully awake. All procedures were performed bilaterally.

Regeneration Treatment and Vectors

Two weeks prior to optic nerve crush, mice were injected intravitreally with 2 μL of *Pten*-shRNA-GFP packaged into AAV2 backbone constructs (titer = $1.5*10^{12}$ vg/ml). The shRNA target sequence was previously validated and is described in (Zukor et al., 2013). PTEN knockdown was verified by immunostaining an AAV-transduced retina with a primary antibody against PTEN (Cell Signaling Technology Rabbit mAb 138G6) and a secondary antibody as described previously (Struebing et al., 2017). Intravitreal injection of an Alexa Fluor 647-conjugated anterograde neurite tracer Cholera toxin B (Invitrogen C34778) 2 days prior to sacrifice demonstrated successful axon regeneration past the optic nerve crush site using this model (**Supplementary Figure S3**). Fundus fluorescence (GFP) was monitored for successful retinal transfection on a Bioptigen SD-OCT. Mice without GFP fundus signal were excluded from the study. Two weeks after the AAV injection, eyes were injected with a mix of Zymosan and 8-CPT-cAMP (Sigma) (total volume 2 μL) which was immediately followed by ONC as described above. Co-delivery of Zymosan/8-CPT-cAMP and *Pten*-shRNA was previously shown to augment optic nerve regeneration more than 10-fold by induction of a low-grade inflammatory state (Kurimoto et al., 2010). GFP for both AAV-GFP and AAV-Pten-shRNA was under control of the CAG promoter. Both plasmids used the same pAAV backbone and AAV-GFP was titered to $1.2*10^{13}$ vg/ml.

DBA/2J Glaucoma Model

To study the effects of glaucoma, female DBA/2J mice ($n = 36$) were sacrificed between 280 and 320 days of age. The retina was quickly separated from the optic nerve and placed in RNA-inhibitor containing buffer as described below. Care was taken not to exert any force on the optic nerve, which was post-fixed in 2% Paraformaldehyde and 2% Glutaraldehyde in Phosphate Buffer. The optic nerve was then osmicated and embedded in plastic. Semi-thin (0.7 μm) sections were cut and stained with 1% p-phenylenediamine (Sigma) for 30 min. Optic nerve photographs were taken with an Olympus BX-51 microscope at 20× magnification and graded by two blinded reviewers according to the degree of damaged axons present in sections. PCR reactions for DBA/2J glaucoma samples were run individually, and the investigator was blinded to the optic nerve damage during analysis. Groups were then clustered by optic nerve damage after data normalization.

RNA Isolation

For each experimental time point, mice were deeply anesthetized with Ketamine/Xylazine as described above and sacrificed by rapid cervical dislocation. Retinas or L4 dorsal root ganglia were quickly dissected under a dissection microscope and directly placed into 160 U/ml Ribolock® (Thermo Scientific, Walton, MA, United States) in Hank's Balanced Salt Solution (Sigma, St. Louis, MO, United States) on ice. Tissue was stored at −80°C. RNA was isolated in batches using a Qiacube and the RNeasy Mini Kit (Qiagen, Hilden, Germany) according to the manufacturer's instructions. The isolation included on-column DNase1 treatment to remove contaminating genomic DNA. All tissue was harvested between 10 am and noon to minimize circadian differences in gene expression. RNA integrity was assessed on a Bioanalyzer 2100 (Agilent, Santa Clara, CA, United States). Samples with an RNA integrity score (RIN-score) less than 8.0 were not used in the study. For three DRG samples, a RIN-score could not be determined due to sub-threshold RNA concentrations. For these samples, RNA quality was assessed by 28S-18S rRNA gradient and only samples with a ratio ∼2 were used. RNA was then quantified by spectrophotometry and 260/280 ratios for all samples were >2.1.

Reverse Transcription

First strand synthesis was carried out using PrimeScript RT Kit (Takara Bio, Shiga, Japan). For each sample, 300 ng of total RNA were reverse transcribed following the manufacturer's instructions. To further decrease genomic DNA contamination, RNA was incubated for 5 min in gDNA eraser (Takara) at 42°C and then immediately cooled on ice. Reverse transcription took place at 42°C for 20 min and a mix of random hexamers and oligo-(d)T primers was used to prime the reactions. cDNA was diluted 100-fold to a final concentration of 0.3 ng/μL RNA equivalent with ultrapure H2O and stored at 4°C.

Primer Design and Validation

Primers for *Sox11* were designed using NCBI Primer Blast with targeted annealing temperature of 61–64°C after correction for 3.5 mM Mg^{2+}. For *Bdnf*, we used the primers previously validated and published in (Salerno et al., 2012). No *in silico* off-targets were found by BLASTing the primer sequences. All primers were checked for specificity by melting curve analysis and Sanger sequencing of amplicons. Primer sequences are given in **Supplementary Table S1**. All primers were evaluated in digital PCR reactions for linear amplification efficiency and

a clear separation between negative and positive fluorescent droplets. *Ppia* was used as a reference gene (Quantitect Primer Assay, Qiagen). We chose *Ppia* because (i) its expression level in DRG and retina is within the dynamic range of ddPCR and (ii) because its expression is very stable after crush procedure (**Supplementary Figure S4**). Additionally, this reference gene is used throughout the literature for qPCR of neuronal cells (He et al., 2015).

Digital Droplet PCR

A total of 1,038 20 μL reactions were distributed onto 96-well-plates using QX200 ddPCR EvaGreen Supermix (Bio-Rad, Hercules, CA, United States) according to the manufacturer's instructions. The final primer concentration was 200 nM and 5 μL of cDNA were used for each reaction. Droplets were generated automatically on a QX200 Droplet Generator (Bio-Rad). PCR was carried out on a C1000 Touch Thermal Cycler (Bio-Rad) with the following parameters: Initial activation at 95°C for 5 min, followed by 40 cycles of denaturation (95°C, 30 s) and combined annealing/elongation (60°C, 60 s) and a ramp rate of 2°C/sec. The droplet signal was stabilized for 5 min at 4°C followed by 5 min at 90°C according to the QX200 ddPCR EvaGreen Supermix protocol. Droplets were then read with a QX200 Droplet Reader (Bio-Rad).

Digital Droplet PCR Analysis

Absolute values of ddPCR products (copies/μL) including 95% confidence interval were calculated by QuantaSoft software (Bio-Rad) by fitting the fraction of positive droplets to a Poisson distribution (Gutierrez-Aguirre et al., 2015). The fluorescence threshold was adjusted manually and kept constant for each reaction that used the same primer to avoid batch effects. Normalization to *Ppia* was carried out by first calculating the average *Ppia* concentration (C_p) across all samples and then multiplying each sample concentration C_i by a calibrator $M = \frac{C_i}{(C_p)}$. Absolute levels were transformed to $\log_2$-based fold-changes for plotting purposes. Genomic DNA (gDNA) contamination was assessed with a primer pair (mVPA) designed to amplify only non-expressed genomic regions (Laurell et al., 2012). There were 11.4 copies of mVPA in 0.3 ng/μL gDNA, while all cDNA samples had mVPA concentrations < 0.25 copies for the same concentration throughout (more than 50% of the samples were completely free of gDNA according to this method). Thus, there was negligible gDNA contamination, contributing less than 2.5% to the total fluorescence signal after thermal cycling. Analysis of variance followed by Tukey's HSD *post hoc* test was used for statistical testing.

Rapid Amplification of cDNA Ends (RACE)

One μg of total RNA from normal C57BL/6J retinas and such that underwent ONC ($n = 6$ each) was isolated as described above and used for RACE experiments. 5′RACE was performed according to the manufacturers protocol (Ambion First Choice RLM-RACE Kit, #AM1700). For 3′ RACE, the protocol was adapted as follows: RNA was mixed with 150 nM custom 3′RACE adapter (DNA primer: 5′-CCTATAGTGAGTCGTATTAATTCTGTGCTC GC-3′) and 15 units of T4 RNA ligase 2 (New England Biolabs, M0239) in ligase buffer. Incubation for 1 h at 37°C resulted in ligation of free RNA 3′OH ends to the 5′ ends of the adapter primer. A reverse-complement 3′ RACE RT adapter (5′-GCGAGCACAGAATTAATACGACTCACTATAGG-3′ was then added and the reaction was heated for 5 min to 65°C to allow annealing. This was followed by random hexamer-dependent reverse transcription with Superscript IV RT enzyme (Invitrogen) according to the manufacturer's instructions and including an RNAse H digestion step at the end. Nested PCR was then carried out with a mix of gene-specific primers (**Supplementary Table S1**) and 3′RACE outer (5′-GCGAGCACAGAATTAATACGACT-3′), followed by 3′RACE inner primer (5′-CGCGGAT CCGAATTAATACGACTCACTATAGG) using AccuPrime High Fidelity Polymerase (Invitrogen) and the following cycling conditions: 94°C initial denaturation for 30 s, and 35 cycles of 20 s at 94°C, 30 s at 65°C, 8 min at 68°C. Amplicons were then separated by agarose gel electrophoresis and products were purified (NucleoSpin Gel and PCR Clean-up kit, Macherey-Nagel, Düren, Germany, #740609.10) for Sanger sequencing.

Data Sources and Bioinformatics

ChIP-Seq data were downloaded from the NCBI sequence read archive, mapped to 10 mm using bowtie2 and converted to genome coverage-normalized bigwig graphs with deeptools. Biological replicates were merged prior to conversion. All datasets were retina-specific and created using C57BL/6 mice. The following SRA accession IDs were used: SRX1365314, SRX1365315, SRX1365318, SRX1365319, SRX1365306, SRX1365307, SRX1365313, SRX1365312, SRX1365324, SRX 1365323, SRX1365329, SRX1365330 (Aldiri et al., 2015). CAGE data was downloaded from the FANTOM 5 consortium in tab-delimited format mapped to mm9 (Lizio et al., 2015).

RESULTS

Analysis of the *Sox11* Locus

The primary interest of the present study is the expression of specific mRNA isoforms of *Sox11* and *Bdnf*. In the mouse, the expression of specific mRNA isoforms of *Bdnf* is relatively well defined (Aid et al., 2007). This is not the case for *Sox11*. Therefore, the first step in our analysis was to re-evaluate the *Sox11* gene locus in adult mouse and the expression of isoforms in retinal tissue (**Figure 1A**). An earlier study using serial analysis of gene expression found evidence for alternative polyadenylation sites as well as antisense transcripts originating from this locus during mouse corticogenesis (Ling et al., 2009). We performed 5′- and 3′- rapid amplification of cDNA ends (RACE) assays in adult mice in an optic nerve crush (ONC) and a normal condition to specify transcription start (TSS) and end site, respectively. Because of the presence of at least 9 Poly-A stretches (defined as >8 consecutive A) within the main *Sox11* transcript, 3′RACE with the standard oligo(d)T

adapter primer resulted in false-positive 3′ tails terminating at one of these sites (Nam et al., 2002). We therefore modified the protocol so that it was independent of oligo(d)T priming. Using this method, we identified specific bands consistent with two different 3′UTR lengths that both aligned to the *Sox11* locus (verified by Sanger sequencing, **Figure 1B**). We observed no difference in mRNA isoforms between the ONC and the control situation, which was additionally validated by visually inspecting genome graphs of a published ONC RNA-seq dataset (Yasuda et al., 2014). Interestingly, the short *Sox11* isoform terminated just upstream of an intragenic CpG island that was only marginally conserved across species (**Figure 1A**). In comparison, the TSS-associated CpG-island was relatively conserved. Investigating the epigenomic profile of this locus using publically available data (Aldiri et al., 2015) suggested that both CpG islands possessed features reminiscent of developmentally regulated promoters. First, both were enriched in the promoter-associated histone mark H3K4me3 (Shen et al., 2012). While to a lesser degree, this mark was still present in adults. Second, the switch from Histone H3 Lysine 27 acetylation to trimethylation (H3K27ac → H2K27me3) between P0 and P21 likely represented gene silencing (Tie et al., 2016). This was consistent with the time course of *Sox11* expression during development, as the expression of this gene decreased rapidly after birth (Ling et al., 2009).

We then could confirm the previously established, canonical 5′ start site on the minus strand using cap-dependent 5′RACE. Other TSSs were not found and there was no difference between ONC and control; however, exploration of cap analysis of gene expression data (CAGE-seq) provided by the FANTOM consortium, a sequencing method that can detect TSSs (Hon et al., 2017), revealed intragenic sense and antisense transcription start sites at different development stages (**Supplementary Figure S1**). At the same time, CAGE data also confirmed the sole canonical 5′TSS in adult. It should be noted that we were not able to reliably amplify any message from the antisense strand. Based on these results, we suggest that *Sox11* in the adult retina is present in a long (7,812 nt) and a short (2,842 nt) isoform with identical TSSs but different 3′UTR lengths. Furthermore, the histone profile indicates that *Sox11* is epigenetically silenced in adults but may be reactivated when needed, as the promoter retains its active signature mark.

Expression of *Sox11* and *Bdnf* in the Injured CNS and PNS

To examine the role of the two *Sox11* isoforms in axon regenerating and non-regenerating scenarios, the temporal expression patterns of *Sox11* were defined after either ONC or sciatic nerve crush (SNC). Samples from the retina and the L4 dorsal root ganglion were taken at 2, 7, and 14 days after injury. For each control group at 0 days, we performed a sham surgery (identical anesthesia + surgical cuts less the crush). Each of the mRNA isoforms was targeted using primers specific for the short and long version of *Sox11* 3′UTR. In addition, primers were used to test whether or not differences in expression of the protein-coding region itself were found (**Figure 1A**). We observed almost equal upregulation (∼8-fold) of all *Sox11* isoforms between 0 and 2 days ($p < 0.01$) after crush in both tissues (**Figure 2A**). While mRNA levels remained elevated ∼4-fold at 14 days in DRGs, they returned to just above baseline in the retina at this time. Even though approximately equal fold *changes* between isoforms were found in both tissues, their starting (pre-injury) amount differed. For example, the long 3′UTR was expressed almost three times higher than short 3′UTR and CDS in retina control samples. This observation was corroborated by retinal microarray data taken 2 and 5 days after ONC, hosted on GeneNetwork and created previously by our group (**Supplementary Figure S2**). In DRGs, only the long 3′UTR was significantly increased between 0 and 2 days ($p = 0.03$), but the short *Sox11* 3′UTR was only expressed at half the concentration of CDS and long 3′UTR. These data argue for a non-linear relationship of CDS to UTR, suggesting differential regulation, post-transcriptional separation or selective degradation of mRNA isoforms, possibly in different cellular subtypes.

The next step in the analysis was to test the expression of *Bdnf* mRNA isoforms after ONC and SNC (**Figure 2B**). Each of the *Bdnf* mRNA isoforms is created by splicing one of its eight 5′ non-coding exons to a common 3′ protein-coding exon. Our numbering system reflects which of those exons is a part of the isoform; e.g., *Bdnf*-4 is the mRNA containing 5′ exon IV. For *Bdnf*-9a, the mRNA isoform does not contain a spliced 5′ exon; transcription is thought to be initiated in the intron before the protein-coding exon. For the purpose of this project, we used primers for five of its nine exons, which were previously determined to be specifically regulated by *Sox11* (Salerno et al., 2012). In control samples, *Bdnf*-4 was the most prevalent isoform in retina and DRG, followed by *Bdnf*-1 (**Figure 2B**). The remaining isoforms studied (*Bdnf*-7, *Bdnf*-8, and *Bdnf*-9a) were barely expressed in DRG and only slightly higher in retina. In DRG, there was a strong (>10-fold) increase of *Bdnf*-1 at 2 days ($p < 0.001$) and 14 days ($p < 0.001$) over the control situation, with a significant transient drop from 2 to 7 days ($p < 0.001$). A similar pattern was found for *Bdnf*-4 ($p = 0.04$, 0 days vs. 2 days, other comparisons n.s.), even though its expression only doubled. However, the opposite was true for *Bdnf*-4 expression in retina; here, *Bdnf*-4 expression was decreased at 2 and 14 days and increased at 7 days, even though this change did not reach statistical significance. Additionally, a transient upregulation of *Bdnf*-1 was found at 2 days ($p < 0.001$) and 7 days but dropped to baseline levels 14 days after ONC. Despite their relatively low absolute expression levels, other *Bdnf* isoforms were increased at all time points in the retina ($p > 0.05$), but either suppressed (*Bdnf*-7) or changed little in DRG. Thus, *Bdnf* isoform expression following axon injury varies decisively between DRG and retina.

Regeneration Treatment of the Injured Retina Influences *Bdnf* and *Sox11* Expression

The clear and distinct differences in the expression of *Sox11* and *Bdnf* in neurons whose axons regenerate well in the PNS and those that do not regenerate well in the CNS prompted us

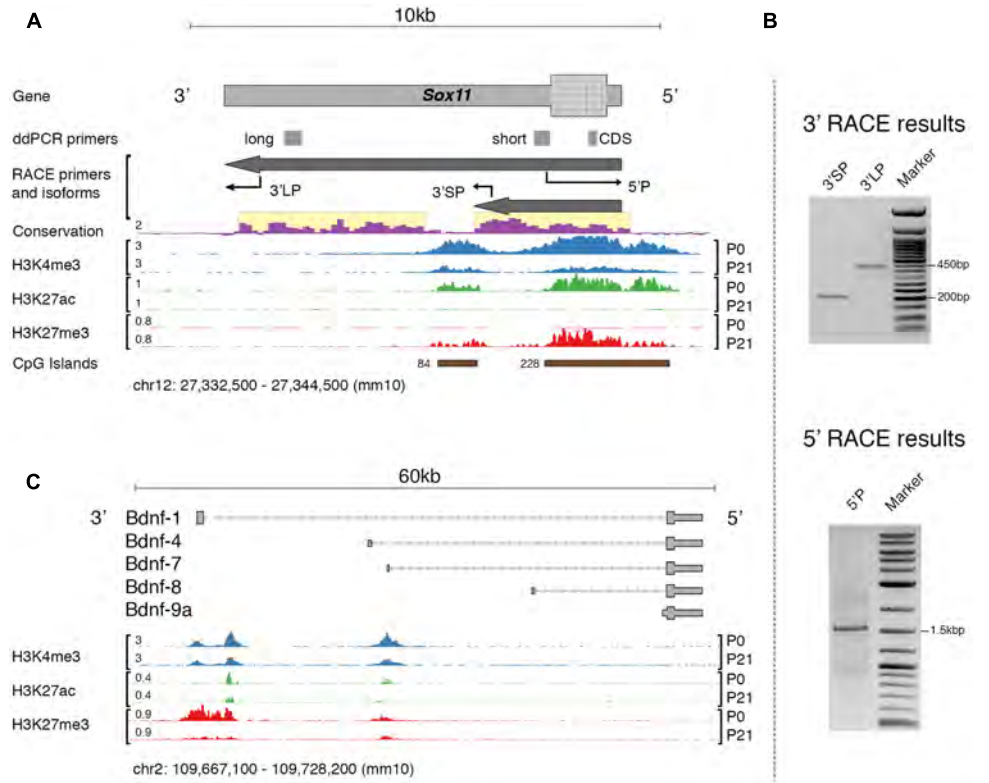

FIGURE 1 | (A) Overview of the mouse *Sox11* locus. The locations of primers for rapid amplification of cDNA ends (RACE) and gene expression testing (ddPCR primers) are shown together with the identified isoforms in the retina. Conservation score is given for multiple alignments of vertebrate genomes (conservation scoring by phylogenetic *p*-values from the PHAST package for multiple alignments of 59 vertebrate genomes to the mouse genome; phyloP60). Below, retina-specific ChIP-Seq coverage for three histone modifications is shown at P0 and P21, respectively. The number in 'CpG Islands' represents the max. number of consecutive CpG base pairs. Note the highly conserved 3′UTRs for both isoforms (highlighted in yellow). The histone features and concurrent CpG islands suggest the existence of two promoter-like states, one over the *Sox11* 5′UTR and CDS, and one within its 3′UTR. There is a switch from active (H3K27ac) to silenced (H3k27me3) chromatin between P0 and P21, and it appears that H3K27 trimethylation is increased over *Sox11* CDS compared to its 3′UTR. Similar data does not exist yet for adult mouse retina. **(B)** Agarose gel electrophoresis of RACE products using the primers described in **(A)**. Bands were purified and sequenced. Specificity was confirmed by aligning sequence results to the *Sox11* locus. Only the major band at ∼1.5 kb in the 5′RACE gel, but both bands in the 3′RACE gel resulted in specific products. **(C)** Overview of the mouse *Bdnf* locus and isoforms targeted during expression testing. The histone profile for this locus is shown for comparative reasons. Note the presence of 2–3 active promoters as indicated by positive H3K4me3 signal and the preferential silencing (H3K27me3) of the proximal promoter at P0.

to look at an experimental scenario in which CNS regeneration was enhanced (**Figure 3**). A GFP-tagged AAV vector containing short hairpin RNA (shRNA) targeting *Pten* was injected into the vitreous of the left eye. During the following 2 weeks, successful transfection was confirmed by monitoring fundus GFP fluorescence *in vivo* using an SD-OCT machine. After 2 weeks, ONC was performed, directly followed by injection of a Zymosan/cAMP analog mix, which is known to induce low-grade inflammation in the retina (Kurimoto et al., 2010). Tissue was harvested either 2, 7, or 14 days thereafter. Immunostaining for PTEN in a retinal flat mount demonstrated complete loss of PTEN expression in GFP-positive cells, and injection of an anterograde neurite tracer 2 days prior to sacrifice indicated strongly enhanced growth of retinal ganglion cell (RGC) axons past the crush site, verifying the efficacy of our approach (**Supplementary Figure S3**). We additionally performed two control experiments: One ONC experiment where only GFP and not *Pten* shRNA was delivered via AAV vectors ("ONC+GFP," **Figure 3**), and one where only the regeneration treatment was provided and the nerve was not crushed to assess the effect of regeneration treatment alone on gene expression ("REG," **Figure 3**). While REG resulted in only mild upregulation of *Sox11* isoforms, combined ONC+REG caused a >4-fold increase for the short *Sox11* isoform and CDS ($p < 0.02$) and a >2-fold increase for the long 3′UTR isoform ($p = 0.012$, **Figure 3B**). This increase also appeared to decay more slowly than in mice with ONC only (**Figure 2A**). We found an even stronger, almost 16-fold persistent upregulation of the *Sox11* CDS including its short 3′UTR in ONC eyes treated with the AAV-GFP control vector ($p < 0.001$), yet the expression levels of the long 3′UTR did not change significantly at any time under this situation ($p > 0.9$). While we expected to see no differences in gene expression between the ONC and ONC+GFP group, these results strongly argue for a dissociated regulation of *Sox11* short and long 3′UTR isoforms. They also further support the existing notion that either AAV, GFP or the combination of both can have unanticipated

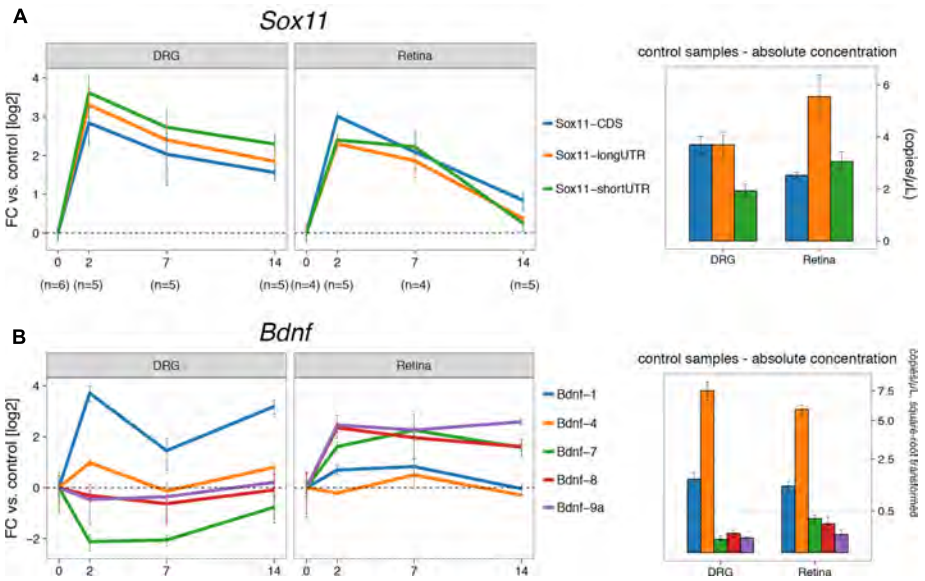

FIGURE 2 | Digital droplet PCR gene expression results for crush procedures. **(A)** The left part shows fold changes (log_2) for DRG and retina for the three *Sox11* primers used at 2, 7, and 14 days after the respective crush procedure. The control group (0 days) received a sham procedure. Absolute concentration in mRNA copies/µL for control samples ('starting amount') is given on the right-hand side. There is an overabundance of the *Sox11* long 3′UTR isoform in the retina, while the short 3′UTR is underrepresented in DRG ($p < 0.05$). Nevertheless, the fold-changes in both tissues suggest co-regulation of all transcripts. Notice the faster decay of *Sox11* in the retina compared to DRG. **(B)** Equivalent to **(A)**, but for *Bdnf* isoforms 1, 4, 7, 8, and 9a, among which *Bdnf-4* is the most abundant isoform in Retina and DRG, followed by *Bdnf-1*. Other isoforms are barely expressed. The y-scale on the right hand-side of the picture was square-root transformed to better show differences at lower concentrations. Error bars for fold-changes represent standard error, while the 95% CI is given for absolute concentrations.

consequences on gene expression (Ansari et al., 2016; Berns and Muzyczka, 2017).

In contrast to *Sox11*, we did not find any differences in the expression of *Bdnf* isoforms between the ONC and the ONC+GFP groups. REG alone caused virtually no change in *Bdnf*-1 or *Bdnf*-4 expression; however, combined ONC+REG treatment resulted in prolonged suppression of the expression of both of these mRNA isoforms ($p < 0.01$ for both, **Figure 3C**). *Bdnf*-7, *Bdnf*-8 and *Bdnf*-9a all showed consistent fourfold upregulation, but these isoforms were very lowly expressed to begin with (**Figure 2B**, right panel) and hence the difference was not statistically significant.

In summary, these data demonstrate that the expression of *Sox11* isoforms is modulated by AAV administration and ONC to a higher degree than the regeneration treatment alone. While silencing *Pten* combined with induction of low-grade inflammation in the adult retina after injury results in synchronized upregulation of all *Sox11* isoforms and decreased expression of *Bdnf-1* and *Bdnf-4,* injection of an AAV-GFP control vector leads to stronger activation of *Sox11* CDS and short 3′UTR.

Expression of *Sox11* and *Bdnf* during Chronic CNS Degeneration

Our results show that *Sox11* and *Bdnf* are reactive to acute injury in the CNS and PNS, and that their expression is influenced by regenerative treatment prior to injury. However, gene expression can differ markedly between chronic and acute injuries. In order to test whether this was the case for *Sox11* and *Bdnf*, we examined their mRNA levels at different stages of glaucoma, the most common neurodegenerative disease (Jutley et al., 2017). To examine the effects of low-grade chronic injury, we used the DBA/2J mouse model of glaucoma, in which mutations of two genes (*Tyrp1* and *Gpnmb150*) cause iris pigment dispersion and subsequent elevation of intraocular pressure beginning at approximately 6 months of age (Anderson et al., 2002). This elevation in intraocular pressure results in retinal ganglion cell death and optic nerve degeneration (Howell et al., 2007). We isolated retinal RNA from 36 aged DBA/2J mice. The severity of glaucoma in each eye was defined by examination of the corresponding optic nerve. The optic nerve damage was stratified by the number of degenerating axons and expression of *Sox11* and *Bdnf* isoforms was examined in all samples (**Figure 4A**). Interestingly, there was a significant and steady increase in levels of *Sox11* long 3′UTR message in moderate up to more than twofold in severe glaucoma stages (**Figure 4B**) ($p = 0.0012$). In contrast, we did not find significant differences for *Bdnf* at any glaucoma stage (**Figure 4C**). These data demonstrate that *Sox11* isoforms are specifically regulated in a chronic neurodegenerative context.

DISCUSSION

The present study examined the expression of two genes, *Sox11* and *Bdnf*, that are known to play significant roles in the response of neurons to injury. Both have distinct expression

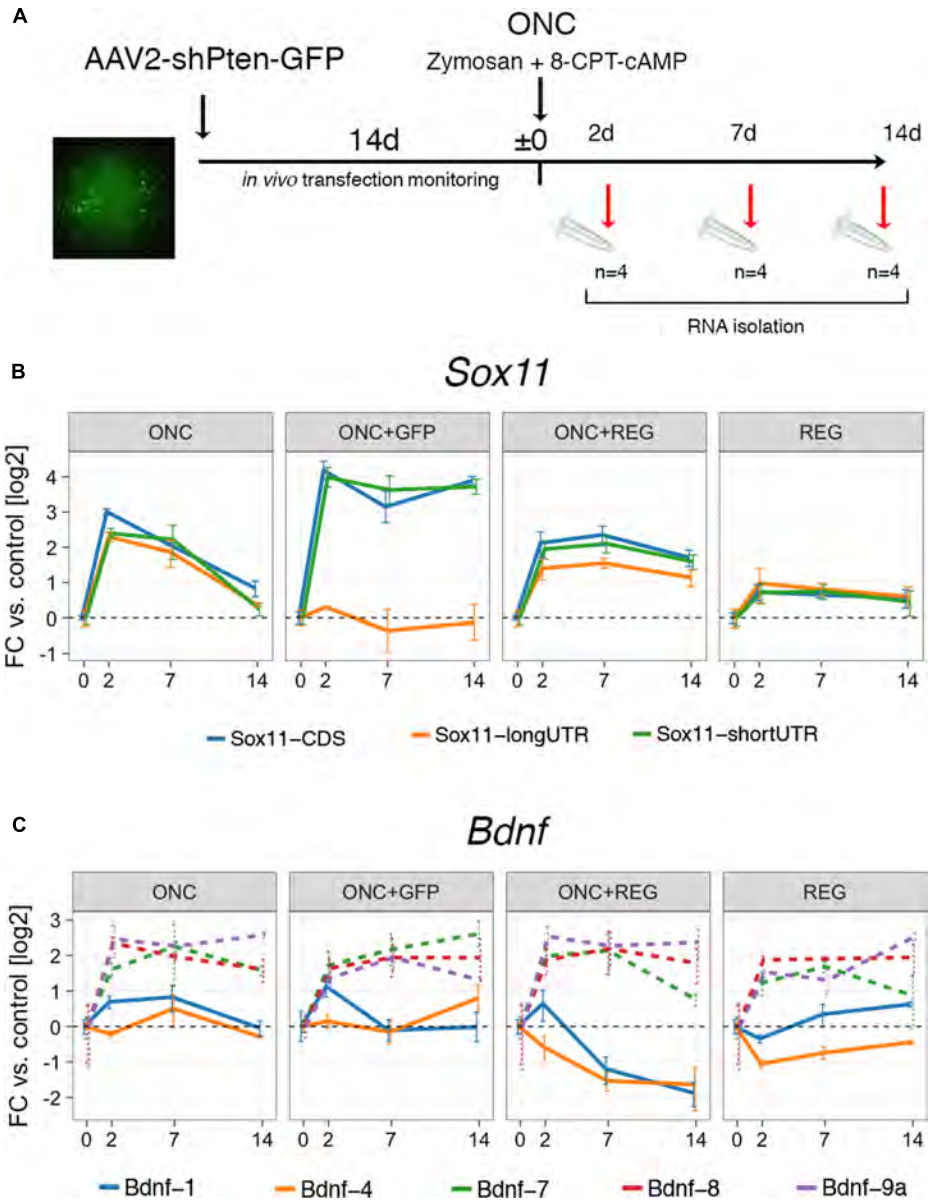

FIGURE 3 | Digital droplet PCR gene expression results for ONC after regeneration treatment. **(A)** Timeline of the experimental interventions for the regeneration protocol. *Pten* expression was silenced using shRNA delivered by GFP-tagged AAV via intravitreal injection and compared to an ONC + AAV-GFP control vector (ONC+GFP) and a regeneration treatment only (REG) group. After 2 weeks, eyes were injected with Zymosan-cAMP mix and subjected to ONC. Samples were collected at 2, 7, and 14 days. The fundus image on the left is an example of one of the animals used in the study. Bright green cells are successfully transfected retinal ganglion cells. **(B)** Gene expression results for *Sox11* in log2-transformed fold changes. The groups labeled "REG" and "ONC+REG" received the regeneration treatment (AAV-*Pten*-shRNA-GFP + Zymosan/cAMP analog mix). REG slightly increases global *Sox11* expression, which is exacerbated by additionally subjecting mice to ONC (ONC+REG). Treatment with the AAV-GFP control vector and ONC (ONC+GFP) result in dissociated expression changes for *Sox11* short 3′UTR and long 3′UTR isoforms ($p = 0.005$ at 14 days). **(C)** Same as in **(B)**, but for *Bdnf* isoforms. While there is little change in the prevalent isoforms (1 and 4) in the REG only group, REG plus ONC lead to a prolonged suppression in expression. *Bdnf* minor isoforms show little differences between conditions (all changes n.s. with $p > 0.05$, dashed lines). Error bars represent standard error.

patterns after axon damage and are directly involved in CNS and PNS regeneration. While peripheral and central neurons share about 90% of expressed genes, specific molecules are selectively expressed in both transcriptomes (Smith et al., 2011). This suggests that neurons in the CNS and PNS are not equal in their transcriptional program, which could explain their differing reactions to injury. Because the overexpression of either *Sox11* or *Bdnf* previously resulted in increased regenerative ability of CNS axons (Dawson et al., 2015; Wang et al., 2015; Santos et al., 2016; Norsworthy et al., 2017), we sought out to investigate their expression levels following crush injury in the regenerating PNS, the

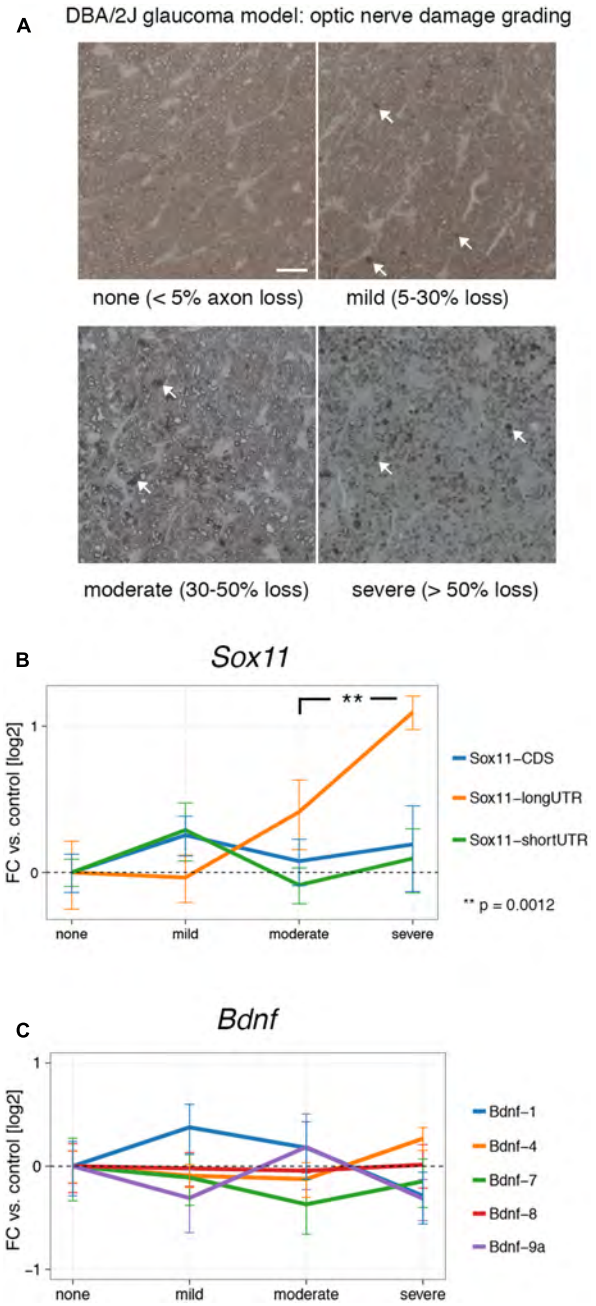

FIGURE 4 | Expression of *Sox11* and *Bdnf* at different stages of glaucoma. **(A)** Samples were staged by optic nerve damage as seen in PPD-stained thin sections according to the percentage of degenerating axons shown in parentheses. Arrows point to accumulated myelin, which represents degenerating axons. Scale bar = 25 μm. **(B)** Only the *Sox11* long 3′UTR changes significantly with increasing optic nerve damage. All $\log_2$ fold changes were calculated in relation to the "none" glaucoma sample. **(C)** No significant changes exist for *Bdnf* at different glaucoma stages.

non-regenerating CNS, and the regeneration-stimulated CNS.

While *Sox11* was strongly up-regulated after both sciatic nerve and optic nerve crush, distinct tissue-specific differences existed. First, *Sox11* expression dynamics were prolonged in DRG neurons compared to retina. Because this transcription factor is not only associated with neuron differentiation but also axon growth and synapse formation (Jayaprakash et al., 2016), prolonged *Sox11* expression appears to be necessary to activate genes that are needed for successful axon regeneration. When we stimulated optic nerve regeneration by inhibiting *Pten* and induced mild inflammation, we observed sustained, fourfold higher *Sox11* expression in the retina. While this upregulation of retinal *Sox11* was also observed in the regeneration treatment control group not subjected to ONC, it was enhanced by the crush procedure. These findings are consistent with a functional role of *Sox11* in affecting transcription of regeneration-associated genes. In a recent study, overexpression of *Sox11* and simultaneous deletion of *Pten* led to slightly decreased RGC survival after ONC compared to *Pten* deletion alone, but also resulted in strongly increased axon regeneration throughout the entire length of the optic nerve (Norsworthy et al., 2017). In the same study, *Sox11* overexpression resulted in the death of alpha-RGCs, a subtype that would normally survive and regenerate preferentially following *Pten* knockdown (Duan et al., 2015). However, overexpression of *Sox11* strongly enhanced the regeneration of RGC subtypes that would either die after injury or be resistant to regeneration after *Pten* knockdown. Thus, the choice between *Sox11*-induced axon regeneration or *Sox11*-induced cell death appears to be dependent upon the specific gene expression program of the host cell.

Unexpectedly, we detected an even stronger increase of the *Sox11* short 3′UTR isoform (including CDS) after ONC in animals treated with the AAV-GFP control vector (**Figure 3B**, ONC+GFP), when expression of the long 3′UTR did not change at all. This could be explained with selective AAV and/or GFP toxicity on *Sox11* regulation after ONC. In fact, some studies have reported immunogenic properties for both (Zhu et al., 2009; Ansari et al., 2016; Berns and Muzyczka, 2017), suggesting that the expression of genes related to immune system function is altered in response to AAV delivery. Even though little is known about the role of *Sox11* in immune cells, its overabundance is now well documented in mantle cell lymphoma, a subtype of B-cell lymphomas (Lu et al., 2013). While investigating the relationship between the regulation of *Sox11* mRNA isoforms, optic nerve injury and AAV/GFP toxicity was beyond the scope of our study, future experiments should be designed to investigate this phenomenon. Our finding also reaffirms that care should be taken when analyzing expression results from AAV- and/or GFP-treated samples.

Several non-coding *Bdnf* exons were previously established to be a transcriptional target of SOX11 (Salerno et al., 2012). Thus, we measured expression levels of those *Bdnf* mRNA isoforms known to be regulated by SOX11 to define the tissue-specific expression patterns. First, *Bdnf*-1 was increased 10-fold in DRG, decreased briefly at 7 days, and returned to increased expression at 14 days. This mRNA isoform was not even elevated twofold in the retina. Furthermore, *Bdnf*-4 expression was only minimally upregulated after nerve crush in DRG and not at all in retina. Three other isoforms, *Bdnf*-7, *Bdnf*-8, and *Bdnf*-9a, were expressed at much lower baseline levels

and trended toward injury-dependent suppression in DRG but toward an increase in retina. Because the low starting levels of these isoforms, the biological relevance of their fold-changes should be interpreted with caution. *Bdnf*-1 and *Bdnf*-4 were previously found to be the most reactive to depolarization in primary cortical neurons (Pruunsild et al., 2011), and both were reported to be retained in the neuron soma, while other isoforms were found to also be present in axons and dendrites (Chiaruttini et al., 2009). It is interesting to note that the promoters of both mRNA isoforms are repressed selectively at birth (positive H3K27me3, see **Figure 1C**) but that the most likely promoter for *Bdnf-4* is selectively acetylated (H3K27ac) at birth and in adolescence. This demonstrates the tight tissue-specific and spatiotemporal control of *Bdnf* expression. For example, a previous study demonstrated a phenotypic switch in DRG neuron subpopulations expressing BDNF one week after injury from medium-sized, trkA expressing neurons to large-sized, trkB/trkC-expressing neurons (Karchewski et al., 2002). This phenomenon may be the cause of the temporary dip in *Bdnf-1* and *Bdnf-4* expression 1 week after sciatic nerve crush as seen in our data, and could be related to the expression of distinct mRNA isoforms.

We observed a decrease in *Bdnf-4* and *Bdnf-1* expression in the retina after ONC and regeneration treatment. This was unexpected, for we anticipated these isoforms to show an increase similar to what we found in the regeneration-prone DRG following sciatic nerve crush (**Figure 2A**). In contrast, in a control group subjected to regeneration treatment but not ONC, no significant changes in expression were found, suggesting that only the combined effect of axon injury and *Pten* inhibition resulted in the suppression of *Bdnf-4* and *Bdnf-1*. This indicates that there is cell type-specific relationship between *Bdnf* mRNA levels and enhanced axon regeneration. PTEN is a known inhibitor of PI3K/AKT signaling, and this pathway is also known to be downstream of BDNF/trkB signaling (Christie et al., 2010). Thus, stimulating the downstream effects of BDNF/trkB signaling combined with injury might induce a negative feedback on *Bdnf* regulation, leading to lower expression levels.

In contrast to acute neuronal injury that can result in chromatolysis with subsequent apoptosis, chronic neurodegeneration is a slow-onset process with a different transcriptional environment (Struebing and Geisert, 2015). We therefore also examined *Sox11* and *Bdnf* mRNA isoform levels in different stages of glaucoma, a blinding disease associated with chronic degeneration of RGCs and optic nerve axons. The only marked change we saw was in the long 3′UTR isoform of *Sox11*, which gradually increased in moderate and severe stages up to twofold. Expression of *Sox11* CDS and short 3′UTR did not change in these aged mice, which was in complete contrast to the ONC+GFP results, where only the CDS and short 3′UTR but not the long 3′UTR showed differences. These results might seem counterintuitive if one assumes that short or long UTR and CDS should be co-expressed in a linear fashion on one RNA strand. However, the findings of expression of distinct RNAs from 3′UTRs or widespread spatial differences in the expression of 3′UTR and CDS of the same gene – which was reported for *Sox11* – may be a challenge to this notion (Mercer et al., 2011; Kocabas et al., 2015). The presence of intragenic histone modifications and CpG islands, as shown for *Sox11* in **Figure 1A**, could be related to this phenomenon. Furthermore, in our analysis of publicly available CAGE data (**Supplementary Figure S1**) we could detect the presence of at least nine mostly intragenic transcription start sites for *Sox11* during ocular development. Thus, *Sox11* 3′UTR and CDS are likely not co-regulated, as those transcripts are either spatially separated, post-transcriptionally modified or selectively degraded. While the biological function of 3′UTR-derived transcripts remains to be determined, based on our findings and those of others, we hypothesize that 3′UTR-derived transcripts could confer a regulatory effect on translation efficiency. In fact, preliminary results from our group suggest that despite a strong increase of *Sox11* mRNA after ONC, the amount of SOX11 protein does not change, and similar processes have been described for other genes (Szostak and Gebauer, 2013).

CONCLUSION

We have demonstrated differential expression of *Bdnf* and *Sox11* mRNA isoforms in the PNS and CNS after axon injury. Furthermore, we have shown that *Sox11* expression in the retina is non-linear in regard to its 3′UTR and CDS regions, and that the long 3′UTR and short 3′UTR isoforms are differentially regulated in disease or following experimental intervention. While beyond the scope of the present study, the molecular mechanisms and functional reasons for differential 3′UTR and CDS regulation and how they relate to neuron degeneration and regeneration deserve to be further studied.

AUTHOR CONTRIBUTIONS

FS and EG conceived the study in coordination with AE. JW performed all ONC procedures. YL was responsible for intravitreal injections. RK assisted with surgeries and animal breeding and isolated RNA for all samples. OM and AE conducted SCN and DRG isolation. FS performed and analyzed all ddPCR reactions and RACE assays, compiled figures and wrote the paper with input from EG and AE. All authors read and approved the final manuscript.

FUNDING

This study was supported by NEI grants R01EY017841 (EG), P30EY06360 (Emory Vision Core, P. Michael Iuvone), NINDS Grant NS057190 (AE), Unrestricted Funds from Research to Prevent Blindness and Department of Defense (DoD) Grant W81XWH12-1-0255 (EG). FS is supported by the institutional training grant T32EY007092-30 (P. Michael Iuvone, PI). The project was supported in part by the Viral Vector Core of the Emory Neuroscience NINDS Core Facilities grant, P30NS055077, and in part by the Emory Integrated Genomics Core (EIGC),

which is subsidized by the Emory University School of Medicine as one of the Emory Integrated Core Facilities. Additional support was provided by the National Center for Advancing Translational Sciences of the National Institutes of Health under Award Number UL1TR000454.

ACKNOWLEDGMENTS

We want to thank Oskar Laur for help with cloning and Xinping Huang for her assistance in virus packaging as well as April B. Still and Micah Chrenek for mouse colony management.

SUPPLEMENTARY MATERIAL

The Supplementary Material for this article can be found online at: https://www.frontiersin.org/articles/10.3389/fnmol.2017.00354/full#supplementary-material

FIGURE S1 | The *Sox11* locus is associated with dynamically regulated, intragenic transcription start sites during ocular development. CAGE data, which capture RNA start sites, were downloaded from the FANTOM database and aligned to the mouse genome (version mm9). There is an upstream antisense TSS during embryonic development stages, and in adulthood, only the canonical TSS is used. TPM, transcripts per million.

FIGURE S2 | The expression changes following optic nerve crush for four different microarray probes covering *Sox11* are shown in **(A)**. Data from GeneNetwork (G2 HEI ONC Retina April 2010). Mouse ages ranged from 60 to 90 days. The location of probes relative to the *Sox11* locus are pictured in **(B)**. Higher expression of *Sox11* distal 3′UTR (Probe D) parts are consistent with the ddPCR results from **Figure 2A**. Probes correspond to Illumina Mouse WG6 probe identifiers as follows: ILM610279 (Probe A), ILM106400717 (Probe B), ILM104010731 (Probe C), ILM104920446 (Probe D).

FIGURE S3 | Validation of regeneration treatment. Representative retinal flat mounts of animals transfected with either AAV-*Pten*-shRNA or AAV-GFP as control are shown in **(A)**. Staining with an antibody against PTEN demonstrates loss of signal in GFP-positive, successfully transfected retinal ganglion cells only in the AAV-*Pten*-shRNA group. Similarly, only animals having received the regeneration treatment regrow their axons past the optic nerve crush site, marked by an asterisk in **(B)**. Axons were visualized by intravitreal injection of fluorescence-conjugated Cholera toxin B 14 days after ONC. The scale bar represents 20 μm in **(A)** and 100 μm in **(B)**.

FIGURE S4 | *Ppia* expression 5 days after optic nerve crush is stable compared to the control situation. This microarray data from genenetwork.org. was created from whole retinas taken from BXD mice, a recombinant inbred mouse cross originating from DBA/2J and C57BL/6J parents.

TABLE S1 | Primers used for gene expression analysis were either taken from Salerno et al. (2012) or designed in house.

REFERENCES

Aid, T., Kazantseva, A., Piirsoo, M., Palm, K., and Timmusk, T. (2007). Mouse and rat BDNF gene structure and expression revisited. *J. Neurosci. Res.* 85, 525–535. doi: 10.1002/jnr.21139

Aldiri, I., Ajioka, I., Xu, B., Zhang, J., Chen, X., Benavente, C., et al. (2015). Brg1 coordinates multiple processes during retinogenesis and is a tumor suppressor in retinoblastoma. *Development* 142, 4092–4106. doi: 10.1242/dev.124800

Anderson, M. G., Smith, R. S., Hawes, N. L., Zabaleta, A., Chang, B., Wiggs, J. L., et al. (2002). Mutations in genes encoding melanosomal proteins cause pigmentary glaucoma in DBA/2J mice. *Nat. Genet.* 30, 81–85. doi: 10.1038/ng794

Ansari, A. M., Ahmed, A. K., Matsangos, A. E., Lay, F., Born, L. J., Marti, G., et al. (2016). Cellular GFP toxicity and immunogenicity: potential confounders in in vivo cell tracking experiments. *Stem Cell Rev.* 12, 553–559. doi: 10.1007/s12015-016-9670-8

Berkovits, B. D., and Mayr, C. (2015). Alternative 3′ UTRs act as scaffolds to regulate membrane protein localization. *Nature* 522, 363–367. doi: 10.1038/nature14321

Berns, K. I., and Muzyczka, N. (2017). AAV: an overview of unanswered questions. *Hum. Gene Ther.* 28, 308–313. doi: 10.1089/hum.2017.048

Bishop, J. F., Mueller, G. P., and Mouradian, M. M. (1994). Alternate 5′ exons in the rat brain-derived neurotrophic factor gene: differential patterns of expression across brain regions. *Brain Res. Mol. Brain Res.* 26, 225–232. doi: 10.1016/0169-328X(94)90094-9

Brosius Lutz, A., and Barres, B. A. (2014). Contrasting the glial response to axon injury in the central and peripheral nervous systems. *Dev. Cell* 28, 7–17. doi: 10.1016/j.devcel.2013.12.002

Chiaruttini, C., Vicario, A., Li, Z., Baj, G., Braiuca, P., Wu, Y., et al. (2009). Dendritic trafficking of BDNF mRNA is mediated by translin and blocked by the G196A (Val66Met) mutation. *Proc. Natl. Acad. Sci. U.S.A.* 106, 16481–16486. doi: 10.1073/pnas.0902833106

Christie, K. J., Webber, C. A., Martinez, J. A., Singh, B., and Zochodne, D. W. (2010). PTEN inhibition to facilitate intrinsic regenerative outgrowth of adult peripheral axons. *J. Neurosci.* 30, 9306–9315. doi: 10.1523/JNEUROSCI.6271-09.2010

Dawson, A. J., Miotke, J. A., and Meyer, R. L. (2015). Intraocular BDNF promotes ectopic branching, alters motility and stimulates abnormal collaterals in regenerating optic fibers. *Brain Res.* 1613, 13–26. doi: 10.1016/j.brainres.2015.03.045

Duan, X., Qiao, M., Bei, F., Kim, I. J., He, Z., and Sanes, J. R. (2015). Subtype-specific regeneration of retinal ganglion cells following axotomy: effects of osteopontin and mTOR signaling. *Neuron* 85, 1244–1256. doi: 10.1016/j.neuron.2015.02.017

English, A. W., Liu, K., Nicolini, J. M., Mulligan, A. M., and Ye, K. (2013). Small-molecule trkB agonists promote axon regeneration in cut peripheral nerves. *Proc. Natl. Acad. Sci. U.S.A.* 110, 16217–16222. doi: 10.1073/pnas.1303646110

Ernfors, P., Lee, K. F., and Jaenisch, R. (1994). Mice lacking brain-derived neurotrophic factor develop with sensory deficits. *Nature* 368, 147–150. doi: 10.1038/368147a0

Fernandes, K. A., Bloomsburg, S. J., Miller, C. J., Billingslea, S. A., Merrill, M. M., Burgess, R. W., et al. (2016). Novel axon projection after stress and degeneration in the Dscam mutant retina. *Mol. Cell. Neurosci.* 71, 1–12. doi: 10.1016/j.mcn.2015.12.003

Geisert, E. E. Jr., Seo, H., Sullivan, C. D., Yang, L. J., and Grefe, A. (1998). A novel approach to identify proteins associated with the inhibition of neurite growth. *J. Neurosci. Methods* 79, 21–29. doi: 10.1016/S0165-0270(97)00154-4

Gutierrez-Aguirre, I., Racki, N., Dreo, T., and Ravnikar, M. (2015). Droplet digital PCR for absolute quantification of pathogens. *Methods Mol. Biol.* 1302, 331–347. doi: 10.1007/978-1-4939-2620-6_24

He, Y. X., Zhang, Y., Yang, Q., Wang, C., and Su, G. (2015). Selection of suitable reference genes for reverse transcription-quantitative polymerase chain reaction analysis of neuronal cells differentiated from bone mesenchymal stem cells. *Mol. Med. Rep.* 12, 2291–2300. doi: 10.3892/mmr.2015.3671

Hon, C. C., Ramilowski, J. A., Harshbarger, J., Bertin, N., Rackham, O. J., Gough, J., et al. (2017). An atlas of human long non-coding RNAs with accurate 5′ ends. *Nature* 543, 199–204. doi: 10.1038/nature21374

Howell, G. R., Libby, R. T., Marchant, J. K., Wilson, L. A., Cosma, I. M., Smith, R. S., et al. (2007). Absence of glaucoma in DBA/2J mice homozygous for wild-type versions of Gpnmb and Tyrp1. *BMC Genet.* 8:45. doi: 10.1186/1471-2156-8-45

Jankowski, M. P., Mcilwrath, S. L., Jing, X., Cornuet, P. K., Salerno, K. M., Koerber, H. R., et al. (2009). Sox11 transcription factor modulates peripheral nerve regeneration in adult mice. *Brain Res.* 1256, 43–54. doi: 10.1016/j.brainres.2008.12.032

Jayaprakash, N., Wang, Z., Hoeynck, B., Krueger, N., Kramer, A., Balle, E., et al. (2016). Optogenetic interrogation of functional synapse formation by

corticospinal tract axons in the injured spinal cord. *J. Neurosci.* 36, 5877–5890. doi: 10.1523/JNEUROSCI.4203-15.2016

Jing, X., Wang, T., Huang, S., Glorioso, J. C., and Albers, K. M. (2012). The transcription factor Sox11 promotes nerve regeneration through activation of the regeneration-associated gene Sprr1a. *Exp. Neurol.* 233, 221–232. doi: 10.1016/j.expneurol.2011.10.005

Jutley, G., Luk, S. M., Dehabadi, M. H., and Cordeiro, M. F. (2017). Management of glaucoma as a neurodegenerative disease. *Neurodegener. Dis. Manag.* 7, 157–172. doi: 10.2217/nmt-2017-0004

Karchewski, L. A., Gratto, K. A., Wetmore, C., and Verge, V. M. (2002). Dynamic patterns of BDNF expression in injured sensory neurons: differential modulation by NGF and NT-3. *Eur. J. Neurosci.* 16, 1449–1462. doi: 10.1046/j.1460-9568.2002.02205.x

Kocabas, A., Duarte, T., Kumar, S., and Hynes, M. A. (2015). Widespread differential expression of coding region and 3′ UTR sequences in neurons and other tissues. *Neuron* 88, 1149–1156. doi: 10.1016/j.neuron.2015.10.048

Kurimoto, T., Yin, Y., Omura, K., Gilbert, H. Y., Kim, D., Cen, L. P., et al. (2010). Long-distance axon regeneration in the mature optic nerve: contributions of oncomodulin, cAMP, and pten gene deletion. *J. Neurosci.* 30, 15654–15663. doi: 10.1523/JNEUROSCI.4340-10.2010

Laurell, H., Iacovoni, J. S., Abot, A., Svec, D., Maoret, J. J., Arnal, J. F., et al. (2012). Correction of RT-qPCR data for genomic DNA-derived signals with ValidPrime. *Nucleic Acids Res.* 40, e51. doi: 10.1093/nar/gkr1259

Ling, K. H., Hewitt, C. A., Beissbarth, T., Hyde, L., Banerjee, K., Cheah, P. S., et al. (2009). Molecular networks involved in mouse cerebral corticogenesis and spatio-temporal regulation of Sox4 and Sox11 novel antisense transcripts revealed by transcriptome profiling. *Genome Biol.* 10:R104. doi: 10.1186/gb-2009-10-10-r104

Lizio, M., Harshbarger, J., Shimoji, H., Severin, J., Kasukawa, T., Sahin, S., et al. (2015). Gateways to the FANTOM5 promoter level mammalian expression atlas. *Genome Biol.* 16, 22. doi: 10.1186/s13059-014-0560-6

Lu, B., Nagappan, G., and Lu, Y. (2014). BDNF and synaptic plasticity, cognitive function, and dysfunction. *Handb. Exp. Pharmacol.* 220, 223–250. doi: 10.1007/978-3-642-45106-5_9

Lu, T. X., Li, J. Y., and Xu, W. (2013). The role of SOX11 in mantle cell lymphoma. *Leuk. Res.* 37, 1412–1419. doi: 10.1016/j.leukres.2013.07.039

Mercer, T. R., Wilhelm, D., Dinger, M. E., Solda, G., Korbie, D. J., Glazov, E. A., et al. (2011). Expression of distinct RNAs from 3′ untranslated regions. *Nucleic Acids Res.* 39, 2393–2403. doi: 10.1093/nar/gkq1158

Miura, P., Sanfilippo, P., Shenker, S., and Lai, E. C. (2014). Alternative polyadenylation in the nervous system: to what lengths will 3′ UTR extensions take us? *Bioessays* 36, 766–777. doi: 10.1002/bies.201300174

Mu, L., Berti, L., Masserdotti, G., Covic, M., Michaelidis, T. M., Doberauer, K., et al. (2012). SoxC transcription factors are required for neuronal differentiation in adult hippocampal neurogenesis. *J. Neurosci.* 32, 3067–3080. doi: 10.1523/JNEUROSCI.4679-11.2012

Nam, D. K., Lee, S., Zhou, G., Cao, X., Wang, C., Clark, T., et al. (2002). Oligo(dT) primer generates a high frequency of truncated cDNAs through internal poly(A) priming during reverse transcription. *Proc. Natl. Acad. Sci. U.S.A.* 99, 6152–6156. doi: 10.1073/pnas.092140899

Norsworthy, M. W., Bei, F., Kawaguchi, R., Wang, Q., Tran, N. M., Li, Y., et al. (2017). Sox11 expression promotes regeneration of some retinal ganglion cell types but kills others. *Neuron* 94, 1112.e4–1120.e4. doi: 10.1016/j.neuron.2017.05.035

Pruunsild, P., Sepp, M., Orav, E., Koppel, I., and Timmusk, T. (2011). Identification of cis-elements and transcription factors regulating neuronal activity-dependent transcription of human BDNF gene. *J. Neurosci.* 31, 3295–3308. doi: 10.1523/JNEUROSCI.4540-10.2011

Richner, M., Ulrichsen, M., Elmegaard, S. L., Dieu, R., Pallesen, L. T., and Vaegter, C. B. (2014). Peripheral nerve injury modulates neurotrophin signaling in the peripheral and central nervous system. *Mol. Neurobiol.* 50, 945–970. doi: 10.1007/s12035-014-8706-9

Salerno, K. M., Jing, X., Diges, C. M., Cornuet, P. K., Glorioso, J. C., and Albers, K. M. (2012). Sox11 modulates brain-derived neurotrophic factor expression in an exon promoter-specific manner. *J. Neurosci. Res.* 90, 1011–1019. doi: 10.1002/jnr.23010

Santos, D., Gonzalez-Perez, F., Navarro, X., and Del Valle, J. (2016). Dose-dependent differential effect of neurotrophic factors on in vitro and in vivo regeneration of motor and sensory neurons. *Neural Plast* 2016:4969523. doi: 10.1155/2016/4969523

Segal, R. A., Pomeroy, S. L., and Stiles, C. D. (1995). Axonal growth and fasciculation linked to differential expression of BDNF and NT3 receptors in developing cerebellar granule cells. *J. Neurosci.* 15, 4970–4981.

Shen, Y., Yue, F., Mccleary, D. F., Ye, Z., Edsall, L., Kuan, S., et al. (2012). A map of the cis-regulatory sequences in the mouse genome. *Nature* 488, 116–120. doi: 10.1038/nature11243

Smith, R. P., Lerch-Haner, J. K., Pardinas, J. R., Buchser, W. J., Bixby, J. L., and Lemmon, V. P. (2011). Transcriptional profiling of intrinsic PNS factors in the postnatal mouse. *Mol. Cell. Neurosci.* 46, 32–44. doi: 10.1016/j.mcn.2010.07.015

Struebing, F. L., and Geisert, E. E. (2015). What animal models can tell us about glaucoma. *Prog. Mol. Biol. Transl. Sci.* 134, 365–380. doi: 10.1016/bs.pmbts.2015.06.003

Struebing, F. L., King, R., Li, Y., Chrenek, M. A., Lyuboslavsky, P. N., Sidhu, C. S., et al. (2017). Transcriptional changes in the mouse retina following ocular blast injury: a role for the immune system. *J. Neurotrauma*. doi: 10.1089/neu.2017.5104 [Epub ahead of print].

Szostak, E., and Gebauer, F. (2013). Translational control by 3′-UTR-binding proteins. *Brief. Funct. Genomics* 12, 58–65. doi: 10.1093/bfgp/els056

Templeton, J. P., and Geisert, E. E. (2012). A practical approach to optic nerve crush in the mouse. *Mol. Vis.* 18, 2147–2152.

Tie, F., Banerjee, R., Fu, C., Stratton, C. A., Fang, M., and Harte, P. J. (2016). Polycomb inhibits histone acetylation by CBP by binding directly to its catalytic domain. *Proc. Natl. Acad. Sci. U.S.A.* 113, E744–E753. doi: 10.1073/pnas.1515465113

Venkatesh, I., and Blackmore, M. G. (2017). Selecting optimal combinations of transcription factors to promote axon regeneration: why mechanisms matter. *Neurosci. Lett.* 652, 64–73. doi: 10.1016/j.neulet.2016.12.032

Wang, Z., Reynolds, A., Kirry, A., Nienhaus, C., and Blackmore, M. G. (2015). Overexpression of Sox11 promotes corticospinal tract regeneration after spinal injury while interfering with functional recovery. *J. Neurosci.* 35, 3139–3145. doi: 10.1523/JNEUROSCI.2832-14.2015

Welsbie, D. S., Mitchell, K. L., Jaskula-Ranga, V., Sluch, V. M., Yang, Z., Kim, J., et al. (2017). Enhanced functional genomic screening identifies novel mediators of dual leucine zipper kinase-dependent injury signaling in neurons. *Neuron* 94, 1142.e6–1154.e6. doi: 10.1016/j.neuron.2017.06.008

Wilhelm, J. C., Xu, M., Cucoranu, D., Chmielewski, S., Holmes, T., Lau, K. S., et al. (2012). Cooperative roles of BDNF expression in neurons and Schwann cells are modulated by exercise to facilitate nerve regeneration. *J. Neurosci.* 32, 5002–5009. doi: 10.1523/JNEUROSCI.1411-11.2012

Wright, E. M., Snopek, B., and Koopman, P. (1993). Seven new members of the Sox gene family expressed during mouse development. *Nucleic Acids Res.* 21, 744. doi: 10.1093/nar/21.3.744

Yasuda, M., Tanaka, Y., Ryu, M., Tsuda, S., and Nakazawa, T. (2014). RNA sequence reveals mouse retinal transcriptome changes early after axonal injury. *PLOS ONE* 9:e93258. doi: 10.1371/journal.pone.0093258

Yiu, G., and He, Z. (2006). Glial inhibition of CNS axon regeneration. *Nat. Rev. Neurosci.* 7, 617–627. doi: 10.1038/nrn1956

Young, W. (2014). Spinal cord regeneration. *Cell Transplant.* 23, 573–611. doi: 10.3727/096368914X678427

Zhu, J., Huang, X., and Yang, Y. (2009). The TLR9-MyD88 pathway is critical for adaptive immune responses to adeno-associated virus gene therapy vectors in mice. *J. Clin. Invest.* 119, 2388–2398. doi: 10.1172/JCI37607

Zukor, K., Belin, S., Wang, C., Keelan, N., Wang, X., and He, Z. (2013). Short hairpin RNA against PTEN enhances regenerative growth of corticospinal tract axons after spinal cord injury. *J. Neurosci.* 33, 15350–15361. doi: 10.1523/JNEUROSCI.2510-13.2013

Conflict of Interest Statement: The authors declare that the research was conducted in the absence of any commercial or financial relationships that could be construed as a potential conflict of interest.

Appendix E

PLOS GENETICS

RESEARCH ARTICLE

Genomic locus modulating corneal thickness in the mouse identifies *POU6F2* as a potential risk of developing glaucoma

Rebecca King[1], Felix L. Struebing[1], Ying Li[1], Jiaxing Wang[1,2], Allison Ashley Koch[3], Jessica N. Cooke Bailey[4], Puya Gharahkhani[5], International Glaucoma Genetics Consortium[¶a], NEIGHBORHOOD Consortium[¶b], Stuart MacGregor[5], R. Rand Allingham[6], Michael A. Hauser[6], Janey L. Wiggs[7], Eldon E. Geisert[1]*

1 Department of Ophthalmology, Emory University, Atlanta, Georgia, United States of America, **2** Department of Ophthalmology, Tianjin Medical University General Hospital, Tianjin, China, **3** Duke Molecular Physiology Institute, Duke University, Durham, North Carolina, United States of America, **4** Department of Population and Quantitative Health Sciences, Case Western Reserve University, Cleveland, Ohio, United States of America, **5** Statistical Genetics, QIMR Berghofer Medical Research Institute, Brisbane, Queensland, Australia, **6** Department of Medicine and Ophthalmology, Duke University Medical Center, Durham, North Carolina, United States of America, **7** Department of Ophthalmology, Harvard Medical School of Medicine, Massachusetts Eye and Ear Infirmary, Boston, Massachusetts, United States of America

¶a The membership of the NEIGHBORHOOD Consortium can be found under the "Members of the NEIGHBORHOOD Consortium" heading
¶b The membership of the International Glaucoma Genetics Consortium can be found under the "Members of the International Glaucoma Genetics Consortium" heading
* egeiser@emory.edu

Citation: King R, Struebing FL, Li Y, Wang J, Koch AA, Cooke Bailey JN, et al. (2018) Genomic locus modulating corneal thickness in the mouse identifies *POU6F2* as a potential risk of developing glaucoma. PLoS Genet 14(1): e1007145. https://doi.org/10.1371/journal.pgen.1007145

Editor: Michael G. Anderson, University of Iowa, UNITED STATES

Received: January 5, 2017

Accepted: December 7, 2017

Published: January 25, 2018

Data Availability Statement: All of the relevant data are within the paper and supporting files.

Funding: This study was supported by an Unrestricted Grant from Research to Prevent Blindness, National Eye Institute grant R01EY017841 (EEG); Owens Family Glaucoma Research Fund (EEG), DoD Grant W81XWH-12-1-0255 (EEG), P30EY06360 (Emory Vision Core) R01 EY022305 (JLW), P30EY014104 (JLW), National Institutes of Health grants 1R01-EY023646 (MAH), 5R01 EY019126 (MAH), 5P30-

Abstract

Central corneal thickness (CCT) is one of the most heritable ocular traits and it is also a phenotypic risk factor for primary open angle glaucoma (POAG). The present study uses the BXD Recombinant Inbred (RI) strains to identify novel quantitative trait loci (QTLs) modulating CCT in the mouse with the potential of identifying a molecular link between CCT and risk of developing POAG. The BXD RI strain set was used to define mammalian genomic loci modulating CCT, with a total of 818 corneas measured from 61 BXD RI strains (between 60–100 days of age). The mice were anesthetized and the eyes were positioned in front of the lens of the Phoenix Micron IV Image-Guided OCT system or the Bioptigen OCT system. CCT data for each strain was averaged and used to QTLs modulating this phenotype using the bioinformatics tools on GeneNetwork (www.genenetwork.org). The candidate genes and genomic loci identified in the mouse were then directly compared with the summary data from a human POAG genome wide association study (NEIGHBORHOOD) to determine if any genomic elements modulating mouse CCT are also risk factors for POAG.This analysis revealed one significant QTL on Chr 13 and a suggestive QTL on Chr 7. The significant locus on Chr 13 (13 to 19 Mb) was examined further to define candidate genes modulating this eye phenotype. For the Chr 13 QTL in the mouse, only one gene in the region (*Pou6f2*) contained nonsynonymous SNPs. Of these five nonsynonymous SNPs in *Pou6f2*, two resulted in changes in the amino acid proline which could result in altered secondary structure affecting protein function. The 7 Mb region under the mouse Chr 13 peak

EY005722; Australian Research Council Future Fellowship (SM). NIH NCATS KL2TR000440 (JNCB). The funders of this research had no role in study design, data collection and analysis, decisions to publish or preparation of the manuscript.

Competing interests: The authors have declared that no competing interests exist.

distributes over 2 chromosomes in the human: Chr 1 and Chr 7. These genomic loci were examined in the NEIGHBORHOOD database to determine if they are potential risk factors for human glaucoma identified using meta-data from human GWAS. The top 50 hits all resided within one gene (*POU6F2*), with the highest significance level of $p = 10^{-6}$ for SNP rs76319873. POU6F2 is found in retinal ganglion cells and in corneal limbal stem cells. To test the effect of POU6F2 on CCT we examined the corneas of a *Pou6f2*-null mice and the corneas were thinner than those of wild-type littermates. In addition, these POU6F2 RGCs die early in the DBA/2J model of glaucoma than most RGCs. Using a mouse genetic reference panel, we identified a transcription factor, *Pou6f2*, that modulates CCT in the mouse. POU6F2 is also found in a subset of retinal ganglion cells and these RGCs are sensitive to injury.

Author summary

Glaucoma is a complex group of diseases with several known causal mutations and many known risk factors. One well-known risk factor for developing primary open angle glaucoma is the thickness of the central cornea. The present study leverages a unique blend of systems biology methods using BXD recombinant inbred mice and genome-wide association studies from humans to define a putative molecular link between a phenotypic risk factor (central corneal thickness) and glaucoma. We identified a transcription factor, POU6F2, that is found in the developing retinal ganglion cells and cornea. POU6F2 is also present in a subpopulation of retinal ganglion cells and in stem cells of the cornea. Functional studies reveal that POU6F2 is associated with the central corneal thickness and susceptibility of retinal ganglion cells to injury.

Introduction

Since the early Ocular Hypertension Treatment Studies (OHTS) [1] and subsequent independent findings of others [2, 3], central corneal thickness (CCT) was identified as a factor related to the risk for developing primary open angle glaucoma (POAG). In these studies, CCT was a powerful predictor for developing POAG, with thinner corneas being associated with an increased risk of developing POAG [1–3] and this risk was independent of the confounding effects of CCT on intraocular pressure measurements [1, 3]. The thinner CCT is also associated with an increased severity of visual field loss and a more rapid progression of the disease [4–6]. Furthermore, ethnic differences in CCT are correlated with increased risk of developing POAG and an increased severity of the disease[7]. Thus, there is a profound link between CCT and the risk of developing POAG.

In humans, there is a considerable variation in CCT, ranging from under 450 μm to over 650 μm [8–10] with a mean CCT of approximately 550 μm [8–13]. The variation in CCT is a highly heritable ocular trait, the genomic contribution of CCT is estimated to be near 90% [8, 9, 11, 14]. Two studies on monozygotic and dizygotic twins from two different human populations confirmed the heritability, with the Chinese population having a heritability of 0.88 [8] [9] and the population in Australia and the United Kingdom having a heritability of 0.95 [8]. In addition, there is considerable variation in CCT between different ethnic groups. Aghaian et al. [15] found that African-Americans (mean CCT of 524 μm) and Japanese (mean CCT of 538 μm) had significantly thinner corneas than the general population. Others [10] have not

observed the same differences for Japanese populations; however; thinner corneas are consistently observed in the African-American populations [10, 13].

Genome-wide association studies (GWAS) on different human populations have identified a number of human loci/genes [16–18] associated with CCT. Several of the loci contain genes associated with CCT that are risk factors for human diseases, including *ZNF496*, which is associated with brittle cornea syndrome [19], and *COL8A2*, causing Fuch's endothelial corneal dystrophy [20, 21]. A recent meta-analysis of over 20,000 individuals identified 16 additional loci associated with CCT [22]. Six of these loci conferred a significant risk for keratoconus, a disease characterized by an extremely thin cornea. This study of a large population successfully identified many different genes that contribute to the heritability of CCT and not surprisingly implicated collagens and extracellular matrix pathways in the regulation of CCT. Although this represents a significant increase in the number of genes involved in CCT, all of the loci only account for approximately 8% of the additive variance of CCT in the European population [22]. Taken together, these data reveal that this highly heritable trait, CCT, is a complex trait. In fact, it could be so complex that the contribution of many individual genomic elements would be difficult to prove, especially in a genetically heterogeneous species like humans.

Attempting to define the link between CCT and POAG in a human GWAS is complicated by the fact that one is comparing two complex traits. In this case, the effect size has to be very large. Many of the early studies specifically looked for a genetic/molecular association between CCT and POAG. The large GWAS meta-analysis of human CCT [22] identified many new loci associated with CCT. One of the loci that conferred a significant risk for keratoconus (*FNDC3B*), was also associated with POAG. Given the power of the study (20,0000 individuals) and the small effect of individual SNPs on CCT, it is clear that the association of individual SNPs with CCT and POAG will require an extremely larger (potentially unrealistic) sample size. Leveraging the unique genotype of recombinant inbred mouse strains can help to simplify such analysis.

The approach taken in the present study was to identify genomic loci modulating CCT using the largest recombinant inbred mouse strain set, the BXD strain set. The BXD RI strains were produced by crossing the C57BL/6J mouse with the DBA/2J mouse. The progeny were inbred (brother-sister matings) to produce over 80 inbred strains. The first 42 of these strains are from the Taylor series of BXD strains generated at the Jackson Laboratory by Benjamin Taylor [23]. BXD43 and higher were bred by the Williams group at the University of Tennessee (Peirce et al. 2004). The BXD RI strains offer a powerful tool to accurately identify genomic loci modulating phenotypes such as CCT. Among the strain set, there are over 7,000 breakpoints in the genome. All of the strains are fully mapped and the parental strains are fully sequenced. Thus, SNPs as well as insertions or deletions are known for every one of the BXD strains. With the aid of the bioinformatic tools present on GeneNetwork (Genenetwork.org), we were able to identify genomic loci and candidate genes modulating CCT in the mouse. We then used these data to interrogate human GWAS studies of corneal datasets [22] and glaucoma datasets [24, 25] to relate our findings in the mouse to the normal human cornea and disease states [26]. Ultimately, we examine genes that modify CCT in the mouse that may also be risk factors for human glaucoma.

Results

The BXD RI strains were used to define genomic loci that modulate CCT. The CCT was measured in a total of 818 mice across 61 members of the BXD strain set (Fig 1). For the purpose of the present study we examined the total thickness of the cornea and no attempt was made to measure the separate layers of the cornea (epithelium, stroma or endothelium). The mean and

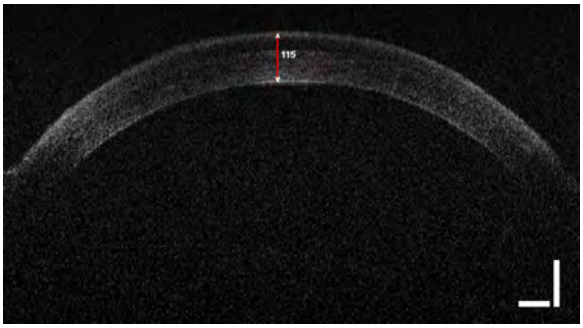

Fig 1. Image of the cornea and anterior chamber of the mouse eye scanned by the Phoenix Micron IV OCT System. The red bar shows the measurement of the central corneal thickness in microns.

https://doi.org/10.1371/journal.pgen.1007145.g001

standard error for each strain are shown in Fig 2. The mean central corneal thickness measured across 61 BXD strains was 100.9 μm with a standard deviation of 7.4 μm. The strain with the thinnest cornea was BXD 44 with an average corneal thickness of 85.3μm. The strain with the thickest cornea was BXD 74 with an average thickness of 124.6μm. The CCT for the parental strains is an intermediate value with the DBA2/J (D2) mouse having a CCT of 103.0μm and the C57BL/6J (B6) mouse having an average CCT of 93.1μm. Thus, there is considerable genetic transgression of CCT across the BXD RI strains with some BXD strains having corneas thinner than the parental strains and other strains having corneas thicker than the parental strains. This distribution of the CCT phenotype indicates that CCT is a complex trait, with multiple genomic loci segregating across the BXD RI strain set.

These data also demonstrate that CCT is a heritable trait. Fig 2 shows that there is considerable variability in the CCT from strain to strain and the standard error for each strain is rather small, which suggests that the genetic variability has a greater effect than the environmental variability. These data can be used to calculate the heritability of CCT in the BXD RI strains. Heritability (H^2) is the genetic variance (Vg) of the trait divided by the sum of genetic variance plus the environmental variance (Vg +Ve). The genetic variance can be estimated by calculating the standard deviation of the mean of the CCT for each strain (Vg = 10.054). The environmental variance can be estimated by taking the mean of the standard deviation across the

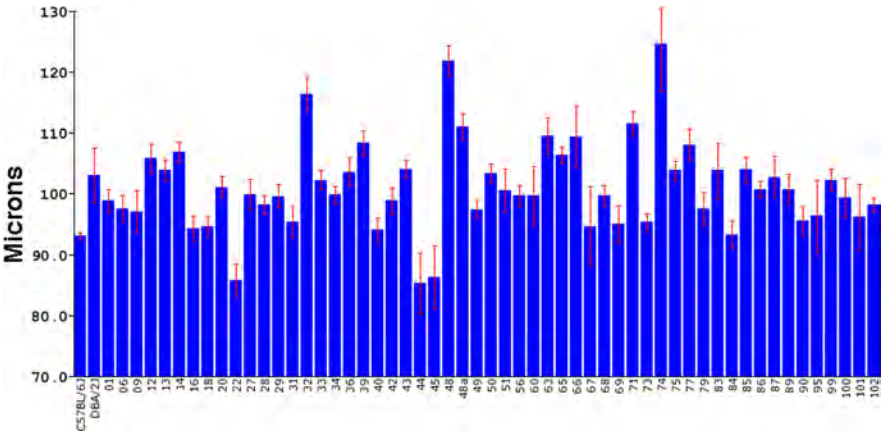

Fig 2. The CCT for 61 BXD strains is illustrated, with the mean indicated by the bar and standard error of the mean is presented by the red brackets. The specific BXD strains are indicated along the X-axis. The thickness of the cornea is shown to the right in microns.

https://doi.org/10.1371/journal.pgen.1007145.g002

strain (Ve = 2.92). Using the formula for heritability, $H^2 = Vg/(Vg + Ve)$, the calculation of 10.054/(10.054 + 2.92) reveals that $H^2 = 0.78$. Thus, CCT is a highly heritable trait across the BXD RI strains.

Using an unbiased forward genetic approach and the data collected from the cohort of 61 BXD strains, we performed a genome-wide scan in an effort to identify QTLs that modulate CCT. The genome-wide interval map (Fig 3) reveals one significant peak on chromosome 13 (13 to 19 Mb) and a suggestive peak on chromosome 7 (42 to 57 Mb). An expanded view of the peak on chromosome 13 is illustrated in Fig 4 along with a haplotype map of the BXD strains. The strains with the thicker corneas in general tend to have the D2 allele; while, strains with thinner corneas have the B6 allele. This is reflected in the genome wide map by the presence of the green line in the peak on chromosome 13 that indicates that higher phenotypic values are associated with the D2 allele (Fig 3). The QTL on Chr. 13 (Fig 4) rises above the significance level of $p<0.05$ as indicated by the pink line. The significant portion of the peak extends from 13Mb to 19Mb over Chr. 13. Genomic elements modulating CCT are located in this region. To identify candidates for modulating CCT in the BXD RI strains, we examined this 7Mb long region. The candidate genes can either be genomic elements with cis-QTLs or they can be genes with nonsynonymous SNPs changing protein sequence. Within this region are 29 traditional genes and one microRNA. In the Whole Eye Database (Eye M430V2 (Sep08) RMA) hosted on GeneNetwork.org we found two genes within this locus with cis-QTLs: *Cdk13* and *Mplkip*. We examined the expression of both of these genes in the cornea and the eye using quantitative PCR (S1 Data, S1 Appendix). Neither of the two genes were expressed at a high enough level in the cornea to be monitored by microarrays of the whole eye. Thus, both genes were discounted as potential candidates for modulating CCT. Within the significant QTL on Chr 13, only one gene (*Pou6f2)* had nonsynonymous SNPs. *Pou6f2* contained five separate nonsynonymous SNPs (rs29821949, rs52634762, wt37-13-18331131, rs29234524 and rs29250924). Three of these SNPs result in a change in the amino acid proline, which could cause a change in secondary structure of the protein and an alteration in protein function.

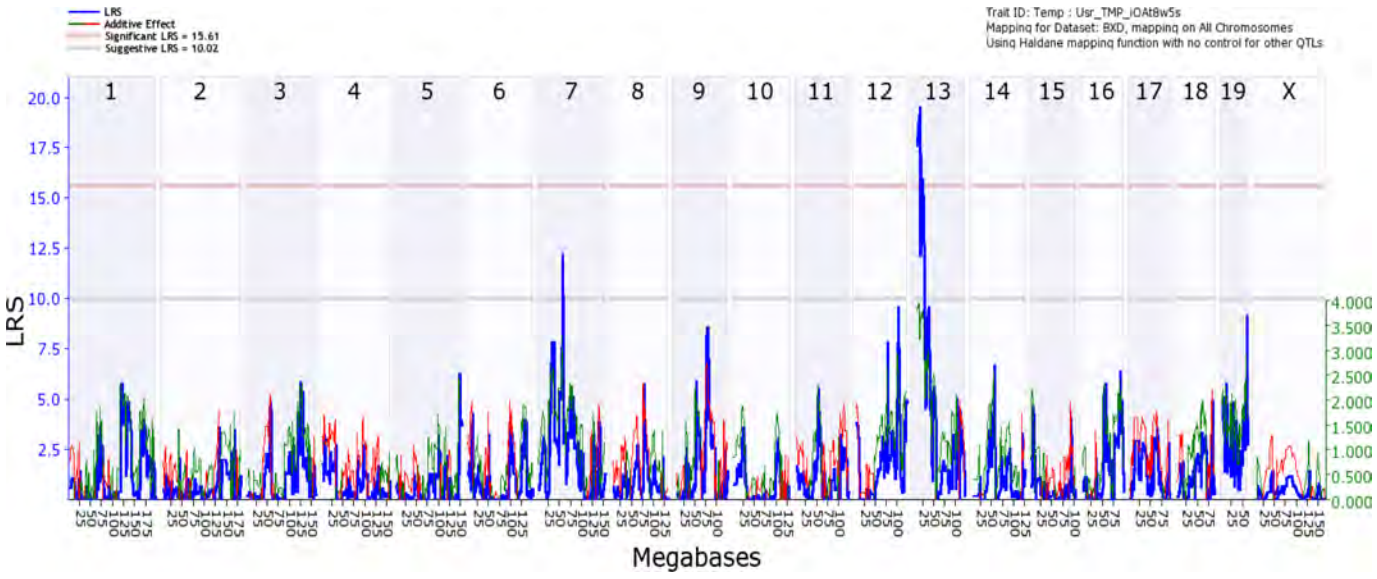

Fig 3. Interval map of CCT across the mouse genome is illustrated. The blue line indicates the total LRS score. The red line illustrates the contribution from the B6 allele and the green line the contribution from the D2 allele. The location across the genome is indicated on the top from chromosome 1 to chromosome X. On the y-axis is the linkage related score (LRS). Notice one significant QTL peak on Chr13 (above the pink Line, p = 0.05) and additional suggestive peaks (above the gray Line).

https://doi.org/10.1371/journal.pgen.1007145.g003

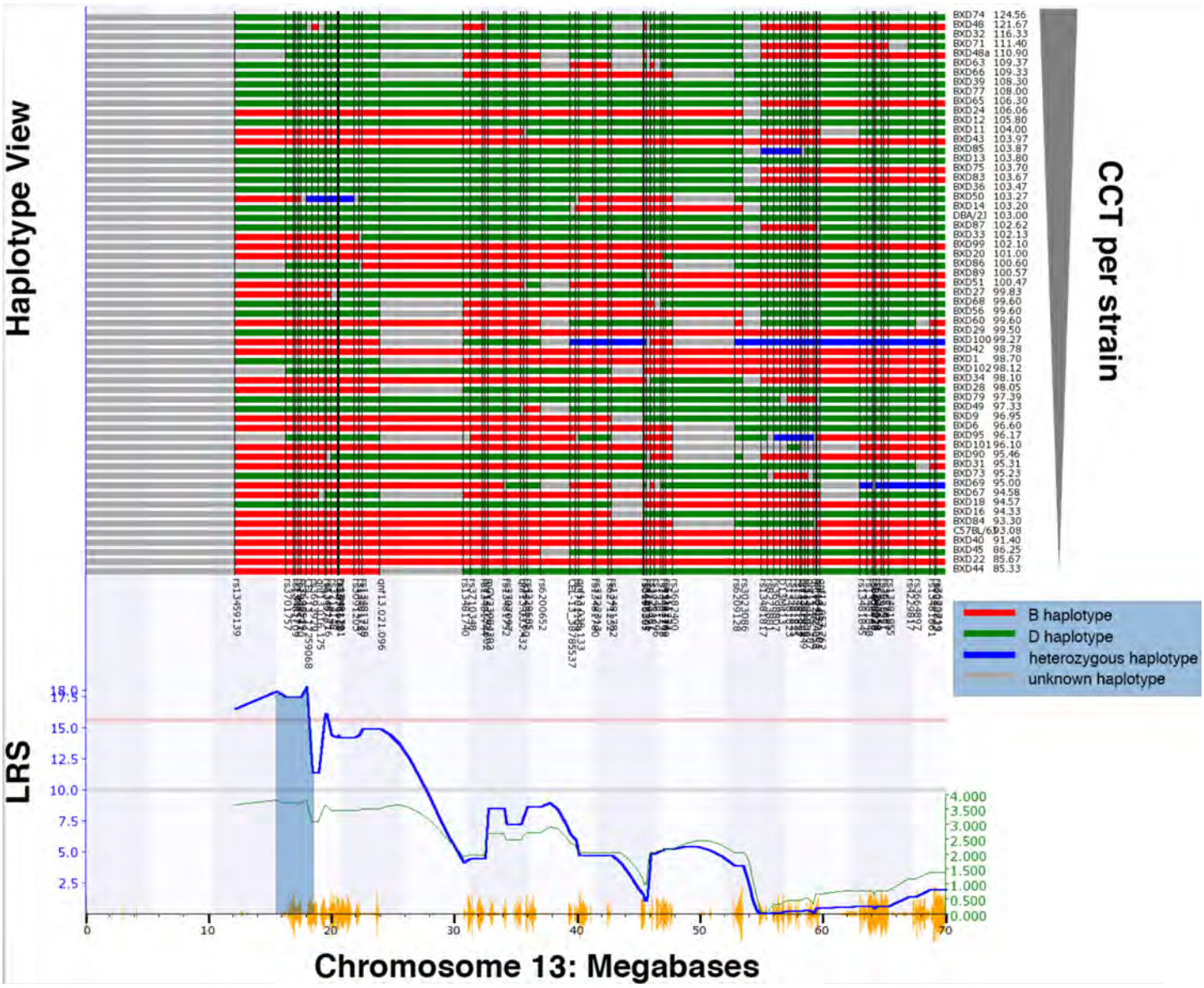

Fig 4. Map of gene locations across Chr. 13. The haplotype map for the 61 strains in the CCT dataset is shown in the top panel. As indicated at the key on the right, red represents the B6 alleles, green defines the D2 alleles, blue represents regions of the DNA that are heterozygotic and gray is unmapped. The genomic markers used in the mapping process are listed at the bottom of the haplotype map. At the far right is a list of the specific BXD RI strains and the associated CCT measurements going from thick corneas at the top to thin corneas at the bottom. QTL map of CCT on Chr. 13 is shown below the haplotype map. An LRS of above the pink line is statistically significant ($p<0.05$). A positive additive coefficient (green line) indicates that D2 alleles are associated with higher trait values. The light fill under the peak defines the genomic locus associated with the modulation of CCT. The significant peak for CCT is from 13 to 19 Mb (gray shaded area). Vertical orange lines at the bottom of the plot show the SNPs on Chr. 13.

https://doi.org/10.1371/journal.pgen.1007145.g004

Analyzing these changes using SIFT to predict functional changes in the protein structure [27], one SNP (rs29234524) was predicted to potentially alter the function of the protein. Based on this examination of the locus, there are no valid cis-QTLs and only one gene, *Pou6f2*, with nonsynonymous SNPs that could have biological effects.

The genomic elements within significant QTLs on mouse chromosome 13 (13 to 19 Mb) were examined to determine if there were specific associations in two human datasets: the International Glaucoma Genetics Consortium dataset for association with CCT [22], and the

NEIGHBORHOOD glaucoma dataset [28]. The syntenic regions on human chromosome 1 (235 to 238 Mb) and chromosome 7 (38 to 43 Mb) were queried for associations of genetic effects relative to human CCT and with genetic risk for human glaucoma. In the International Glaucoma Genetics Consortium dataset for CCT [22], there were a number of nominally significant associations; however, none of the markers remained significant after corrections for multiple testing. When we looked specifically for the candidate genes from the mouse, weak associations were found in both European populations (peak marker rs4723833; $P = 4.34x10^{-3}$ $\beta = -0.062\mu m$) and Asian populations (peak marker rs17619647; $P = 3.72x10^{-3}$; $\beta = -0.066\mu m$), both of these SNPs (rs4723833 and rs17619647) overlap *POU6F2*. However, the associations are not significant after correction for multiple testing of 482 SNPs in Europeans and 265 SNPs in Asians. The β values from this linear regression analysis reflect the quantitative change in CCT per associated allele. The mouse locus was also used to interrogate the NEIGHBORHOOD human POAG glaucoma dataset [28]. In the NEIGHBORHOOD dataset, the top 50 SNPs associated with glaucoma within the syntenic region were all found within the *POU6F2* locus. The most significant SNP (rs76319873) had a genome-wide p-value of 5.34^{-6} and the next top 3 SNPs had p-values less than 10^{-5} (Fig 5, Table 1). None of these SNPs reached genome-wide significance when corrected for multiple testing.

Distribution of POU6F2 in the mouse eye

Our data suggests that *Pou6f2* modulates central corneal thickness and it may also modulate risk for glaucoma in humans. To determine if *Pou6f2* could be a molecular link between CCT and glaucoma, we examined the distribution of POU6F2 protein and mRNA in the retina and cornea in mice. The first approach was to examine its absolute expression levels in adult retina and cornea using digital droplet PCR. We first confirmed the specificity of tissue dissection using the corneal marker Uroplakin 1[29], which was highly abundant in cornea but not retina (5760±260 copies/μL vs. 3.3±0.9 copies/μL). The expression levels of *Pou6f2* were relatively high in the retina (76.3±1.5 copies/μL); however, levels of *Pou6f2* message from cornea were just above the detection threshold of digital droplet PCR (0.5±0.2 copies/μL), suggesting that only few if any corneal cells express *Pou6f2*. These data indicate that *Pou6f2* was barely expressed in the adult cornea, while it was readily detectable in the adult retina.

Previous studies [30] demonstrated that POU6F2 is expressed in neuroblasts in the future ganglion cell layer of the developing eye and in retinal ganglion cells in the adult mouse, cat and monkey. To confirm these findings and to examine the potential for a link between RGCs and cornea, we immunostained sections from the embryonic mouse eye, the adult mouse eye and flat-mounts of mouse retina. In the embryonic eye, there is strong staining of the neuroblasts destined to become retinal ganglion cells (Fig 6). There is also notable staining of the epithelium of the developing cornea and what appears to be corneal stem cells (Fig 6). The distribution of POU6F2 in the developing eye indicates a clear association between the development of retinal ganglion cells and the cornea.

In sections through the adult mouse retina (C57BL/6J), POU6F2 is found to label the nuclei of many cells in the retinal ganglion cell layer. To fully explore the distribution of POU6F2 in the retinal ganglion cell layer, we examined flat mounts of the mouse retina (Fig 7) counterstained with RBPMS (a ganglion cell marker [31]) and a nuclear stain. We observed that POU6F2 labels only a small percentage of the total number of cells in the ganglion cell layer. When we quantified the number of cells labeled with POU6F2, only 17.4% of the total cells were heavily labeled with POU6F2. Virtually all of the POU6F2-positive cells were ganglion cells positive for RBPMS. There were a few cells in the inner nuclear layer that were positive for POU6F2 and these cells were also positive for RBPMS, identifying these cells as displaced

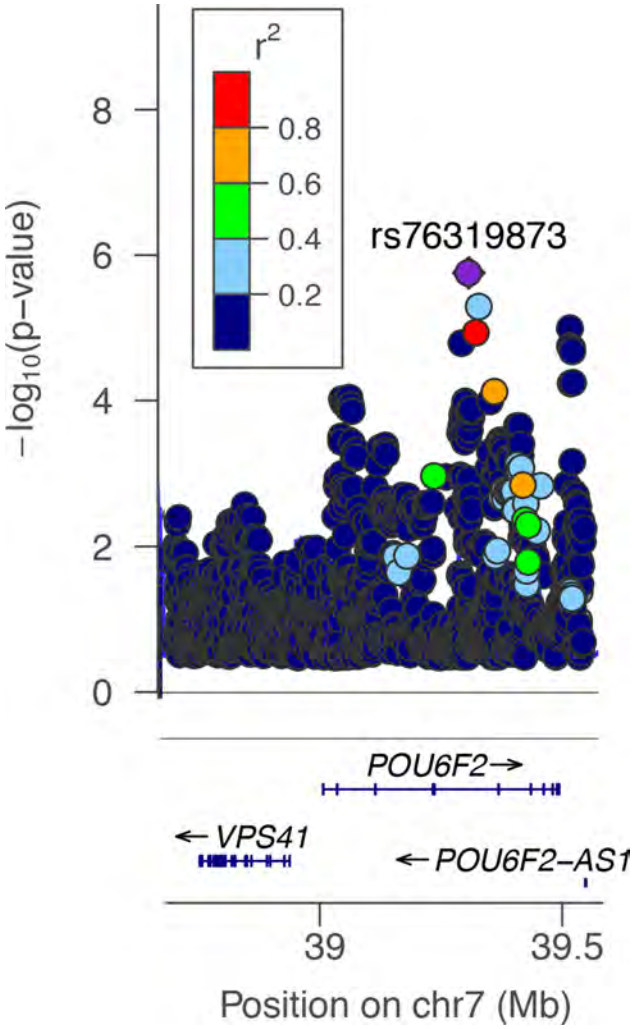

Fig 5. This is a Manhattan plot over the locus containing *POU6F2*. To the left is the p value related to glaucoma in a $\log_{10}$ scale. On the bottom portion of the panel the location of three human genes is shown: *VPA41*, *POU6F2* and *Pou6F2-AS1*. The SNP (rs76319873) with the highest association to POAG is colored purple. The panel insert denotes the imputed quality score (r^2) and the appropriate SNPs are colored in the plot.

https://doi.org/10.1371/journal.pgen.1007145.g005

ganglion cells. These data demonstrate that POU6F2 is expressed in a small subset of retinal ganglion cells. To provide additional evidence that the POU6F2 positive cells are ganglion cells, we crushed the optic nerve unilaterally in three mice and allowed them to survive for 28 days. The retinas were then examined for POU6F2 staining. No labeling was observed in the RGC layer, indicating that all POU6F2 cells were gone (Fig 1, S1 Appendix). Taken together,

Table 1. The four SNPs with the highest p values from the NEIGHBORHOOD Human GWAS Dataset. None of the SNPs reached genome-wide significance which is $6.4X10^{-8}$.

CHR	BP	SNP	P	Gene
7	39318083	rs76319873	5.34E-06	POU6F2
7	39339109	rs73130485	1.55E-05	POU6F2
7	39333177	rs75082513	3.52E-05	POU6F2
7	39304125	rs4302750	4.88E-05	POU6F2

https://doi.org/10.1371/journal.pgen.1007145.t001

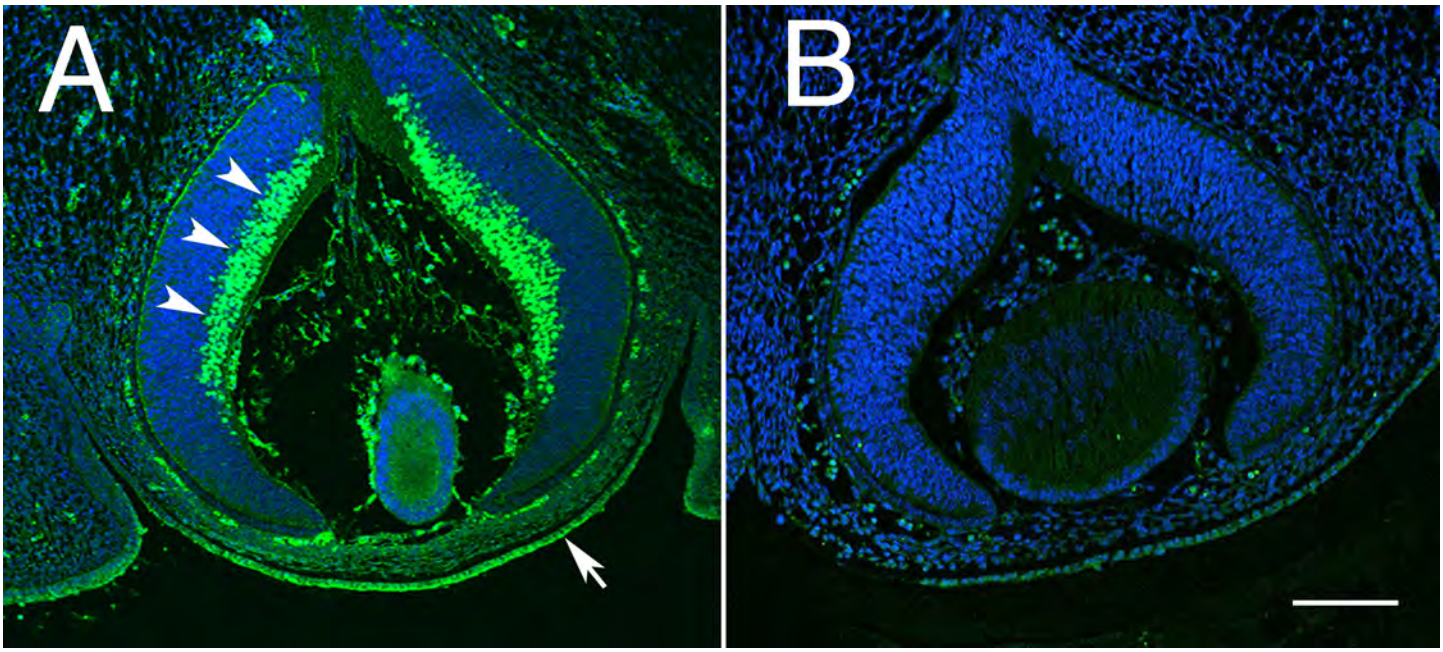

Fig 6. Distribution of POU6F2, in the embryonic eye P15 is illustrated. In sections stained for POU6F2 (A), there is prominent staining of neuroblasts destined to become retinal ganglion cells (arrow heads). There is also staining of the developing cornea and corneal epithelium (arrow). This staining is specific to the primary antibody for it is not present in sections in which the primary antibody was omitted (B) a secondary only control. Both sections are at the same magnification and the scale bar in B represents 100μm.

https://doi.org/10.1371/journal.pgen.1007145.g006

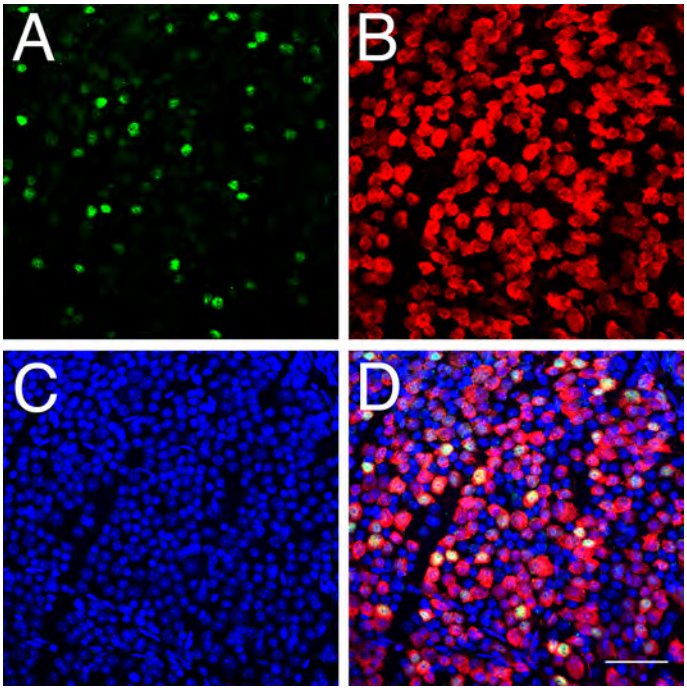

Fig 7. The labeling of RGCs with an antibody directed against POU6F2 is illustrated in a flat-mount of the mouse retina. Panel A is the staining within the retina (green) for POU6F2. The same area (panel B) was stained (red) for the ganglion cell marker Class III beta tubulin. Nuclei in the ganglion cell layer were stained blue with TOPRO-3 (panel C). The merged image is shown in D. Notice that many of the ganglion cells were heavily stained for POU6F2 and that others are lightly labeled. The scale bar in D represents 50μm.

https://doi.org/10.1371/journal.pgen.1007145.g007

these data reveal that POU6F2 is expressed in a subset of retinal ganglion cells in the ganglion cell layer. Finally, as previously observed by Zhou et al. [30] there were a few cells labeled with POU6F2 on the inner surface of the inner nuclear layer. These cells appeared to be displaced ganglion cells (Fig 2, S1 Appendix). Thus, POU62 labels a subset of RGCs within the mouse retina.

To determine if the POU6F2-positive RGCs are selectively sensitive to glaucoma, we double stained 4 young DBA/2J (2 months old) mice for POU6F2 and RBPMS and compared these values to 4 aged (8-month-old) DBA/2J mice (Fig 8). When we counted the cells in the 4 young mice there were an average of 460 (±81, SEM) RBPMS-labeled RGCs per 40X field. In the same sections, we observed an average of 74 POU6F2-labeled RGCs (±15). When these results were compared to 4 aged DBA/2J mice (8 months old) there was a significant decrease ($p<0.001$, student t test) in the total number of RGCs to an average of 361 RGCs (±21) per 40 X field. This represented a total decrease in RBPMS labeled ganglion cells of 22%. When we examined POU6F2-positive cells in the aged DBA/2J retinas there was a 73% loss of cells, a significant difference relative to young DBA/2J retinas ($p<0.0001$). The average number of POU6F2 cells in the young retina was 74 (±5), while in the aged retina this number decreased to 21 (±3). These data demonstrate that the POU6F2 RGC subtype is very sensitive to early phases of glaucoma in the DBA/2J model.

To examine the expression of POU6F2 in the cornea, we first examined sections through the cornea and limbus extending down into the sclera. There was no staining in the cornea or sclera. Occasionally, we observed individual cells stained in the limbal area. However, it was difficult to unequivocally identify these cells as limbal stem cells. As an alternative approach, we stained the surface of six eyes using extended antibody incubation times. When examining the junction between the cornea and sclera, a line of cells is stained at the junction between the cornea and sclera in the limbus (Fig 9). This line of cells was also positive for the stem cell

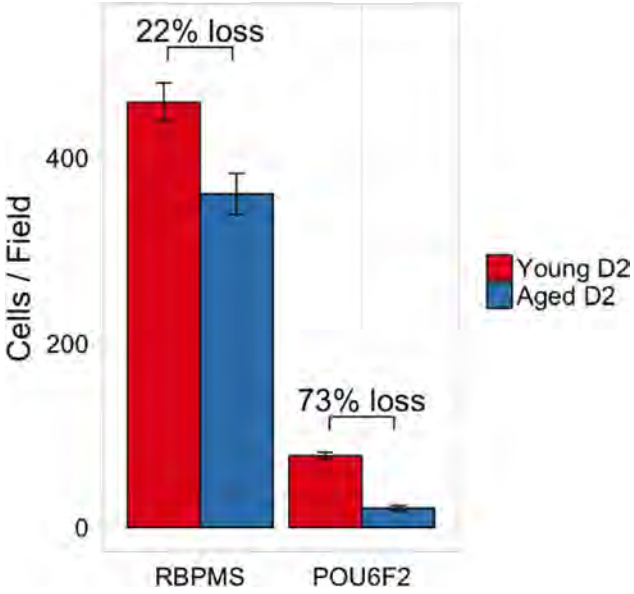

Fig 8. The selective sensitivity of POU6F2 RGC subtypes is demonstrated using the DBA/2J model of glaucoma. There was a 22% loss of RBPMS-labeled RGCs in aged DBA/2J mice (8 months of age, Aged D2) as compared to young DBA/2J mice (2 months of age, Young D2). There was a dramatic loss of 73% of the POU6F2-positive cells comparing the Young D2 mice to the Aged D2 mice. These data demonstrate the sensitivity of the POU6F2 RGC subtype to glaucoma.

https://doi.org/10.1371/journal.pgen.1007145.g008

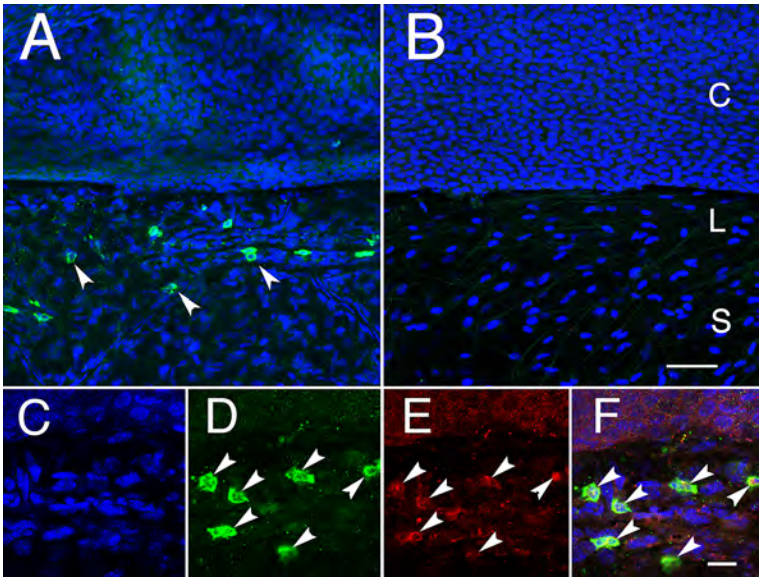

Fig 9. The surface of the eye was stained for POU6F2 and counter-stained with TOPRO-3 (A). The control section without primary antibody is shown in B. The limbus (L) is the transition between the cornea (C) and the sclera (S). In A, there are many cells stained for POU6F2 and all of these cells are localized to the limbus. C, D, E and F are higher magnification photomicrographs taken from the same region of a triple stained section. The section was stained with TOPRO-3, a nuclear marker (C), POU6F2 (D) and ABCB5 (E). F represents a merged image of the three channels. Stem cells are labeled by arrows in C, D and E. Photomicrographs in A and B are taken at the same magnification and the scale bar in B represents 50μm. Photomicrographs in C, D, E and F are taken at the same magnification and the scale bar in F represents 20 μm.

https://doi.org/10.1371/journal.pgen.1007145.g009

marker ABCB5 (Fig 9E). Thus, POU6F2 is not only a marker for limbal stem cells but it may be responsible in part for the maintenance of the corneal integrity in the adult mouse eye.

To determine if POU6F2 is directly involved in corneal development and maintenance affecting CCT, we examined the corneas of 8 *Pou6f2*-null mice and compared their CCT to that from 10 wild-type littermates (Fig 10). There was a significant difference ($p<0.01$, Wilcoxon signed-rank test) in CCT between the *Pou6f2*-null mice and the wild-type littermates. In the *Pou6f2*-null mice the mean CCT was 102.8μm (±1.8μm). The wild-type littermates had a mean CCT of 109.9μm (±1.8μm). Thus, abolishing *Pou6f2* expression has a significant effect on CCT in the adult mouse.

Discussion

The BXD RI strain set is particularly well suited for a systems genetic approach to study CCT. This relatively new branch of quantitative genetics has the goal of understanding networks of interactions across multiple levels that link DNA variation to phenotype [32]. The present approach involves an analysis of sets of causal interactions among classic traits such as CCT, together with networks of gene variants, and developmental/environmental factors. The main challenge is the need for a comparatively large sample size and the use of more advanced statistical and computational methods and models. The BXD strain set is sufficiently large to have adequate power for this approach [33, 34]. The genetic reference panel used in this study consisted of 62 strains of mice. The novel aspect of our current approach is the combination of phenotypic mouse data, mRNA expression data (baseline and experimental) from the same BXD RI strains and the interrogation of GWAS studies for glaucoma (NEIGHBORHOOD Study [24]) and for CCT [22]. Data that we generated throughout this experiment and data

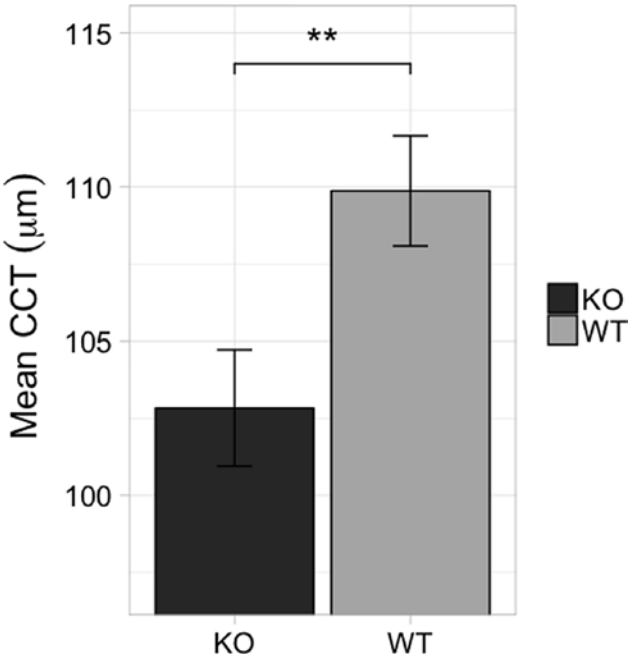

Fig 10. The effect of knocking out *Pou6f2* on CCT. The average CCT (bars represent SEM) from Wild-type (WT) mice and *Pou6f2*-null (KO) mice is shown. In the Wild-type littermates (n = 10) the cornea was on average significantly ($p < 0.01$) thicker than observed in the *Pou6f2*-null mice (n = 6).

https://doi.org/10.1371/journal.pgen.1007145.g010

already deposited in GeneNetwork (www.genenetwork.org) for gene expression in the eye [33] and retina [35–37] were used to test specific mechanisms and predictions.

In the present study, we have identified a significant QTL on Chr 13 (13–19 Mb) that modulates CCT in the BXD RI strain set. One suggestive QTL was also found on chromosome 7 (41 to 57 Mb). Previous studies from the Anderson group [38, 39] have found significant QTLs associated with CCT. Using a F2 cross between C57BLKS/J and SL/J F2 mice, Lively et al. [38] found a significant QTL on Chr. 7 at 105Mb that modulated CCT. This differs from the suggestive QTL identified on Chr. 7 in the present study. The QTL identified with the C57BLKS/J and SL/J F2 cross is located at 105Mb on Chr7, while the suggestive QTL from the present study was at 41 to 57Mb on Chr7. A second study by Koehn et al. [39], identified two significant QTLs associated with CCT in an F2 cross between BXD24/TyJ and CAST/EiJ. One was on Chr 3 at 104Mb, and the second was on Chr11 at 88Mb [39]. Neither of these loci demonstrated even suggestive associations with CCT in the BXD RI strains used in the present study.

In humans, CCT is a highly heritable trait affected by many genomic loci [16–22]. Comparing these human loci to those identified in the mouse reveals several genomic regions that are similar. For example, the mouse locus on Chr7 at 105Mb [38] could include previously identified human loci near several known genes: *TJP1, CHSY1, LRRK1* and *AKAP13* [22, 40]. Other than this region in the mouse, there does not appear to be any overlap between loci modulating CCT in the mouse and those identified in the human.

CCT is a phenotypic risk factor for glaucoma [1–3]. Glaucoma is a diverse set of diseases with heterogeneous phenotypic presentations associated with different risk factors. Untreated, glaucoma leads to permanent damage of axons in the optic nerve and visual field loss. Millions of people worldwide are affected [41, 42] and glaucoma is the second leading cause of blindness in the United States [43]. Adult-onset glaucoma is a complex collection of diseases. The

severity of glaucoma appears to be dependent on the interaction of multiple gene variants, age, and environmental factors [44]. These complex genetic risk factors are the focus of recent genome-wide association studies that are not only defining genetic risk factors but also aiding in our understanding of disease mechanisms [45–47]. These would include the identification of genes that could influence cerebral spinal fluid pressure [48] and ultimately the differential pressure observed across the optic nerve head [49]. Recent findings suggest that RGC number is also a risk factor for glaucoma. Several polymorphisms in the genes *SIX6* and *ATOH7* were identified that are responsible for thinner retinal nerve fiber layer due to fewer RGCs, suggesting that humans with fewer RGCs are at increased risk of developing glaucoma [25, 50, 51]. In addition, linkage analysis in families affected by glaucoma has led to an extensive list of genomic loci linked to POAG. The genes underlying some of the adult-onset glaucoma loci have been identified (*MYOC*, *OPTN*, *TBK1*, *CDKN2BAS* [52] [53] [54, 55].

Many studies in human and mouse have looked for a genetic link between CCT and glaucoma. Studies in the human cornea have found several SNPs that modulate corneal thickness. However, none of the genes in these studies appear to relate CCT to the risk of developing glaucoma with the exception of *FNDC3B* [22]. Several studies have examined the genomic loci in the mouse that modulate CCT and again none of the loci controlling CCT thickness relate to glaucoma risk. In the present study, we have identified a well-defined QTL associated with CCT in the mouse. Within this locus, there is a limited number of candidate genes. One gene, *Pou6f2*, is uniquely poised to modulate CCT, for we have shown that it is expressed in the developing cornea and in limbal stem cells. In addition, *Pou6f2* may also be associated with glaucoma risk. Interestingly, Zhou et al. [30] demonstrated that *Pou6f2 i*s present in the developing and adult retinal ganglion cells. This gene product is also associated with the regeneration of neurons in zebrafish [56].

Based on the distribution of POU6F2 in the cornea and retinal ganglion cells in the developing and adult mouse eye, it is tempting to suggest that *Pou6f2* may be a molecular link between CCT and the potential for RGC loss in glaucoma. A search of the normal mouse retina (DoD Normal Retina Affy MoGene 2.0 ST [36]) on GeneNetwork (genenetwork.org) reveals that *Pou6f2* forms a genetic network with retinal ganglion cells markers, including *Thy1*, *Pou4f1* (Brn3a) and *Rbfox3* (NeuN) [57]. This association suggests that *Pou6f2* could be commonly regulated in a specific subset of retinal ganglion cells. These RGC subtypes may be selectively sensitive to loss in mouse models of glaucoma. In the present study, we have also shown that *Pou6f2* is expressed in the developing cornea and corneal stem cells. When we examined the NEIGHBORHOOD database, *POU6F2* has an interesting association with POAG. However, for the International Glaucoma Genetics Consortium dataset for CCT [22] the P value was $p = 0.0037$, and when corrected for multiple testing it did not reach a significant level. Thus, we are not able to definitively say that *Pou6F2* is a molecular link between CCT and glaucoma. As discussed above, CCT is a highly heritable trait and it is the second highest risk factor for glaucoma, following IOP. If this is the case, then why do we not know the molecular link between CCT and POAG? Some phenotypic traits are very complex or even hyper-complex. A well-known example of a complex trait is height. It is estimated that there are over 2,000 genomic loci that may contribute to height and that the heritability is relatively high as much as 80% [58], although others estimate that the heritability is lower due to dependence on family-based studies indicating that the true heritability is between 60% to 70% [59]. Nonetheless, the weight of any one genomic locus influencing height in the human population is low and genetic components known to be associated with heritability can only be accounted for a portion of the heritability. That being said, CCT is a glaucoma risk factor and a highly heritable trait. The identification of molecular links connecting CCT to POAG may be complicated by the fact that both are complex traits, influenced by multiple genomic as well as

environmental factors. Using a mouse model like the BXD RI strain set (a restricted genetic reference panel) is an effective approach to identify genomic elements modulating phenotypes such as CCT. These data can now be used to design experiments that will attempt to link CCT to potential glaucoma risk.

POU6F2 appears to mark a subpopulation of RGCs that are selectively sensitive to injury in the DBA/2J mouse model of glaucoma. To understand the potential role of POU6F2 we examined data from a ChIP-chip experiment [60] in HEK293 cells. In this human cell line, POU6F2 bound to a number of different targets: CHD5, DACH1, ELAVL3, GFRA2, GRIN1, LHX1, MTSS1, NAP1L3, NEFH, NPTX1, NR4A2, NTNG2, PCDH7, ROBO2, SLC30A3, SLC7A8, SORCS2, UNC5A and VGF. If we examine these targets in the DoD Normal Retina Database [36] on GeneNetwork, all of the targets are expressed at relatively high levels in the retina, at least 2-fold above the mean expression of mRNA. In addition, their expression levels are highly correlated across the BXD strain set, with most probes having a Pearson's *r* value above 0.7. One of these down-stream targets, *Slc30a3*, encodes a zinc transporter (ZNT3). Recent studies from the Benowitz lab [61], reveal that ZNT3 plays an important role in injured ganglion cells and axon regeneration. Thus, it is tempting to hypothesize that POU6F2 exerts its effects on retinal ganglion cell survival in an injury and chronic neurodegeneration (glaucoma) context by modulation of Slc30a3.

In conclusion, we have shown that POU6F2 is involved in corneal development and modulates CCT. In retinal ganglion cells, POU6F2 is a transcription factor marking a subtype that is selectively sensitive to injury. POU6F2 is also known to be upstream of genes that play a critical role in ganglion cell death following injury and it is a potential glaucoma risk factor in humans.

Materials and methods

Ethical statement

All of the procedures involving mice were approved by IACUC at Emory University and the University of Tennessee Health Science Center. The study adhered to the ARVO Statement for the Use of Animals in Research. Mice were anesthetized via intraperitoneal injection of ketamine 100mg/kg and xylazine 15mg/kg. For euthanasia, mice were anesthetized via intraperitoneal injection of ketamine 100mg/kg and xylazine 15mg/kg, and perfused through the heart with saline followed by 4% paraformaldehyde in phosphate buffer.

Mice

All of the mice in this study were between 60 to 110 days of age, which is long before any significant elevation in IOP due to two gene mutations (*Tyrp1* and *Gpnmb*) carried by selected BXD strains originating from the DBA/2J mouse. We examined equivalent numbers of males and females for each of the strains. Mice were housed in a pathogen-free facility at UTHSC or at Emory University, maintained on a 12 hr light/dark cycle, and provided with food and water ad libitum. The B6.129-*Pou6f2*^{tm1Nat}/J mice were cryorecovered at Jackson Laboratory (Bar Harbor, ME) and bred at Emory. These mice were originally created in Jeremy Nathans' lab by replacing an approx. 3.5 kb long fragment of *Pou6f2* that encompasses exon and flanking intronic regions with a PGK-Neo positive selection cassette in 129 ES cells. Animals were back-crossed to the C57BL/6J strain for more than 10 generations. All mice were genotyped in-house and only homozygote null or wild-type littermates were used in the present study. All CCT measurements on the *Pou6f2*-null and wild-type mice were performed in a double-blind manner. The mice were genotyped after all CCT measurements were made. To our knowledge, this is the first publication using the mice generated by Dr. Nathans.

Measuring CCT

CCT was measured using two different Ocular Coherence Tomography (OCT) systems: a Bioptigen SD-OCT system (Morrisville, NC) and a Phoenix Micron IV OCT Imaging system (Pleasanton, CA). Mice were anesthetized using ketamine 100mg/kg and xylazine 15mg/kg. The eye was positioned in front of the lens. The entire anterior chamber was imaged. The corneal scans were saved to a portable hard drive for subsequent analysis. CCT was then measured three times for each eye using the Mouse Retina Program, InVivoVue Clinic, in the Bioptigen Software or the Micron OCT software. These data were stored and entered into an Excel spreadsheet. Repetitive measures were possible with the BXD RI strains since each strain has the identical genetic background allowing us to sample the developmental consequences of the same genetic background for all independent measures. For the BXD strains the corneas were measured between 60 and 90 days. In the *Pou6f2*-null mice the corneal thickness was measured at 30 days of age.

Optic nerve crush

Optic nerve crush was performed as described in Templeton and Geisert [62]. Briefly, three C57BL/6J mice were anesthetized using ketamine 100mg/kg and xylazine 15mg/kg. Under the binocular operating scope a small incision was made in the conjunctiva. With micro-forceps (Dumont #5/45 Forceps, Roboz, cat. #RS-5005, Gaithersburg, MD), the edge of the conjunctiva was grasped next to the globe. The globe was rotated nasally to allow visualization of the posterior aspect of the globe and optic nerve. The exposed optic nerve is then clamped 2 mm from the optic nerve head with Dumont #N7 self-closing forceps (Roboz, cat. #RS-5027) for 10 seconds. At the end of the procedure, a drop of 0.5% proparacaine hydrochloride ophthalmic solution (Falcon Pharmaceuticals, Fort Worth TX) was administered for pain control and a small amount of surgical lube (KY Jelly, McNeil-PPC, Skillman NJ) was applied to the eye to protect it from drying. The mouse was allowed to wake up on a heating pad and monitored until fully recovered.

Interval mapping for the traditional phenotypes

CCT data was subjected to conventional QTL analysis using simple and composite interval mapping and pair-scans for epistatic interactions. Genotypes were regressed against each trait using the Haley-Knott equations implemented in the WebQTL module of GeneNetwork [63, 64]. Empirical significance thresholds of linkage were determined by permutations [65]. We correlated phenotypes with expression data for whole eye and retina generated by Geisert, Lu and colleagues [33, 36]. Based on recent work with the enlarged set of BXDs, we expected all significant ($p < 0.05$) QTLs to be mapped with a precision of ± 2 Mb [34, 66–68]. To identify loci, and also to nominate candidate genes, we used the following approaches: interval mapping for the traditional phenotypes, candidate gene selection within the QTL region, cis-eQTL analysis of gene expression, trans-eQTL analysis, multi-trait and complex analysis of molecular, clinical, and laboratory traits.

NEIGHBORHOOD analysis

The peak area of association on mouse chromosome 13 was examined for associations in human datasets. Syntenic regions on human chromosomes 1 and 7 were queried for associations with POAG in the NEIGHBORHOOD [24] dataset. Subsequently, the POU6F2 locus was queried in the International Glaucoma Genetics Consortium dataset for association with CCT [22].

RNA isolation and digital PCR

In order to quantify Pou6f2 mRNA expression, C57BL/6J mice (n = 5) were deeply anesthetized with a mixture of 15 mg/kg of xylazine and 100 mg/kg of ketamine and sacrificed at 9am. Corneas and retinas were dissected separately and stored in Hank's Balanced Salt Solution and RiboLock (Thermo Scientific, Waltham MA) at -80˚C. RNA was isolated on a Qiacube with the RNeasy mini kit (both Qiagen, Hilden, Germany) according to the manufacturer's instructions with additional on-column DNase1 treatment. RNA integrity was assessed using an Agilent Bioanalyzer 2100 and RIN scores for both pooled tissues were >9.5. Takara PrimeScript (Clontech, Mountain View, CA) was used to retrotranscribe equal amounts of RNA for both tissues. Digital Droplet PCR was then carried out using 30ng of total RNA in 20μL reactions of EvaGreen ddPCR supermix supplying 2μM Mg^{2+}. Primers were designed using NCBI Primer-Blast to work at a combined annealing/extension temperature step of 60˚C and the sequences were as follows: Upk1b fwd (5-CAGGCAGCCGGTCTTTTAGAAA-3), Upk1b rev (5-ATCA TTGTTGGTGGCTTCGAGA-3), Pou6f2 fwd (5-CCCTCAATCAGCCAATCCTCAT-3), Pou6f2 rev (5-GTTCAGGGATGAGGTAGCTTGT-3). A combination of Ppia and Gapdh (Qiagen Quantitect primer assays) was used for ddPCR normalization.

Immunohistochemistry

Twelve C57BL/6J mice were deeply anesthetized with a mixture of 15 mg/kg of xylazine and 100 mg/kg of ketamine and perfused through the heart with saline followed by 4% paraformaldehyde in phosphate buffer (pH 7.3). The eyes were removed and embedded in paraffin and sectioned at 5μm. For the embryonic eyes, two timed-pregnant female mice were deeply anesthetized with tribromoethanol, decapitated and the E16 embryos were removed. The embryo heads were placed in 4% paraformaldehyde on ice for 1 hour, rinsed with PBS and dehydrated in stages of ethanol followed by xylenes, and then embedded in paraffin. The 5μm sections of retina and E16 mice had the paraffin removed and the sections were blocked with 5% normal donkey serum and stained with a rabbit antiserum directed against POU6F2 (MyBiosource, Cat. # MBS9402684) at 1:500 for 2 hours at room temperature (S2 Data, S1 Appendix). To demonstrate the specificity of the POU6F2 antibody, retinas from *Pou6f2*-null mice were stained and no nuclear labeling was observed. The sections were rinsed three times and transferred to secondary antibodies (Alexa Fluor 488 AffiniPure Donkey Anti-Rabbit, Jackson Immunoresearch, Cat. #715-545-152; at 1:1000 for two hours at room temperature. After three washes of 15 minutes each, To-PRO-3 Iodide (Molecular Probes, Cat. # T3605) was applied 1:1000 as a nuclear counterstain. After a final wash in PBS, coverslips were placed over the sections using Fluoromount -G (Southern Biotech, Cat. #0100–01) as a mounting medium. For the retinal flat mounts, the retinas were removed from the globe and rinsed in PBS, blocked in 5% normal donkey serum and placed in primary antibodies in primary rabbit antibody POU6F2 (MyBiosource, Cat. # MBS9402684) at 1:500 and to label RGCs, a primary guinea pig antiserum against RBPMS (Millipore, Cat # ABN1376) at 1:1000 overnight. The retinas were rinsed and placed in secondary antibodies, (Alexa Fluor 488 AffiniPure Donkey Anti-Rabbit, Jackson Immunoresearch, Cat. #715-545-152 and Alexa Fluor 594 AffiniPure Donkey Anti-Guinea pig, Jackson Immunoresearch, Cat. #706-585-148) at 1:1000 for two hours at room temperature. After three washes of 15 minutes each, To-PRO-3 Iodide (Molecular Probes, Cat. # T3605) was applied 1:1000 as a nuclear counterstain. After To-PRO3 has stained the section for 30 minutes, slides were washed twice with PBS for 10 minutes followed by a 5-minute wash with distilled water. Autofluorescence was decreased by treating the sections with cupric sulfate [69]. The 10mM cupric sulfate pH5 was applied to the section for 5 minutes. Slides were washed for 5 minutes with distilled water, then twice with PBS for 10 minutes and the slides were coverslipped.

Staining the surface of the limbus

Adult C57BL/6J mice were anesthetized with a mixture of 15 mg/kg of xylazine and 100 mg/kg of ketamine and perfused with saline followed by 4% paraformaldehyde in phosphate buffer (pH 7.4). The eyes were removed and post-fixed in 4% PFA for one hour at room temperature. The sclera along the ministry equator line was removed along with the posterior sclera and whole retina, vitreous body and lens. The remaining portion of the eye was rinsed three times in PBS containing 2% Triton X-100 for 10 minutes each. Dissected blocks the anterior hemisphere were placed in 10% donkey serum and 4% BSA overnight 4˚C. The tissue was incubated for two days in rabbit primary antiserum to POU6F2 (MBS9402684 MyBiosource, San Diego CA) and ABCB5 (Product ab126 Abcam, Cambridge MA) at 1:500 at 4˚C. The dissected limbal area was washed 3 times with PBS. Finally, the tissue was placed in secondary antibodies that included Donkey anti-Rabbit labeled with Alexa 488 (#711-545-152, Jackson ImmunoResearch Laboratories, West Gove CA) and Donkey anti-Goat IgG labeled with Alexa 594 (#705–585, Jackson ImmunoResearch Laboratories, West Gove CA) at 4˚C overnight. The tissue was cut into 5 pieces, radially mounted on a glass slide and a coverslip was placed over the tissue.

Members of the NEIGHBORHOOD consortium

Rand Allingham[1], Murray Brilliant[2], Don Budenz[3], Jessica Cooke Bailey[4] John Fingert[5], Douglas Gaasterland[6], Teresa Gaasterland[6], Jonathan L. Haines[4], Lisa Hark[7], Michael Hauser[1], Rob Igo[4], Jae Hee Kang[8], Peter Kraft[9], Richard Lee[10], Paul Lichter[11], Yutao Liu[12], Syoko Moroi[13], Louis R. Pasquale[8,14], Margaret Pericak-Vance[15], Anthony Realini[16],Doug Rhee[19], Julia R. Richards[13], Robert Ritch[20], Joel Schuman[21], William K. Scott[22], Kuldev Singh[23], Arthur Sit[24], Douglas Vollrath[25], Robert N. Weinreb[26] Janey L. Wiggs[14], Gadi Wollstein[21] & Don Zack[27]

[1]Department of Ophthalmology, Duke University Eye Center, Durham, NC 27705, USA. [2]University of Wisconsin Institute for Clinical and Translational Research, Madison, WI 53705, USA. [3]Department of Ophthalmology, UNC School of Medicine, Chapel Hill, NC 27517, USA. [4]Department of Population and Quantitative Health Sciences, Case Western Reserve University School of Medicine, Cleveland, OH 44106, USA [5]Department of Ophthalmology and Visual Sciences, University of Iowa, Iowa City, IA 52242, USA. [6]Scripps Genome Center, University of California at San Diego, San Diego, CA. [7]Glaucoma Research Center, Wills Eye Hospital, Philadelphia, PA 19107, USA. [8]Channing Division of Network Medicine, Brigham and Women's Hospital, Boston, MA 02115, USA. [9]Harvard T.H. Chan School of Public Health, Boston, MA 02115, USA. [10]Department of Ophthalmology, Bascom Palmer Eye Institute, University of Miami, Miami, FL 33136, USA. [11]Department of Ophthalmology, Kellogg Eye Center, University of Michigan, Ann Arbor, MI 48105, USA. [12]Department of Cellular Biology and Anatomy, Augusta University, Augusta, GA 30901, USA. [13]Department of Ophthalmology, Kellogg Eye Center, University of Michigan, Ann Arbor, MI 48105, USA, [14]Department of Ophthalmology, Harvard Medical School, Massachusetts Eye and Ear Infirmary, Boston, MA 02298, USA. [15]John P. Hussman Institute for Human Genomics, University of Miami, Miami, FL 33136, USA. [16]Department of Ophthalmology, West Virginia University, Morgantown, WV 26506, USA. [19]Department of Ophthalmology and Visual Sciences, Case Western Reserve University, Cleveland, OH 44106, USA. [20]Department of Ophthalmology, Einhorn Clinical Research Center, New York Eye and Ear Infirmary, New York, NY 10003, USA. [21]Department of Ophthalmology, NYU Langone Medical Center, New York, NY 10016, USA. [22]Dr. John T. Macdonald Foundation Department of Human Genetics, John P. Hussman Institute for Human Genomics, University of Miami Health System, Miami, FL 33136, USA. [23]Department of Ophthalmology, Stanford University Medical Center, Stanford, CA 94303, USA. [24]Department of Ophthalmology, Mayo Clinic, Rochester, MN 85259, USA.

[25]Department of Genetics, Stanford University Medical Center, Stanford, CA 94305, USA. [26]Hamilton Glaucoma Center, Shiley Eye Institute, University of California, San Diego, CA [27]Department of Ophthalmology, Wilmer Eye Institute, The Johns Hopkins University School of Medicine, Baltimore, MD 21287, USA.

Members of the International Glaucoma Genetics Consortium

Tin Aung[28, 29], Kathryn P. Burdon[30], Ching-Yu Cheng[28, 29], Jessica N. Cooke Bailey[31], Jamie E. Craig32, Angela J Cree[33], Puya Gharahkhani[34], Christopher J. Hammond[35], Alex W. Hewitt[36], René Höhn[37, 38], Pirro Hysi[35], Adriana I Iglesias Gonzalez[39], Jost Jonas[40], Anthony Khawaja[41, 42], Chiea-Cheun Khor[43], Caroline CW Klaver[44], Francesca Pasutto[45], Stuart MacGregor[34], David Mackey[46, 47], Paul Mitchell[48], Aniket Mishra[34], Calvin Pang[49], Louis R Pasquale, Henriette Springelkamp[44], Gudmar Thorleifsson[51], Unnur Thorsteinsdottir[51], Cornelia M van Duijn[39], Ananth Viswanathan[52], Veronique Vitart[53], Janey L Wiggs[50], Robert Wojciechowski[54-56], Tien Wong[28, 57], Terrri L Young[58], Tanja Zeller[59]

[28]Singapore Eye Research Institute, Singapore National Eye Centre and Eye ACP, Duke-National University of Singapore, Singapore. [29]Department of Ophthalmology, National University Health System, Yong Loo Lin School of Medicine, National University of Singapore, Singapore. [30]Menzies Institute for Medical Research, University of Tasmania, Hobart, Tasmania, Australia. [31]Department of Population and Quantitative Health Sciences Case Western Reserve University School of Medicine, Cleveland, OH. [32]Department of Ophthalmology, Flinders University, Adelaide, Australia. [33]Clinical & Experimental Sciences, Faculty of Medicine, University of Southampton, Southampton, UK. [34]Statistical Genetics, Queensland Institute of Medical Research, Brisbane 4029, Australia. [35]Department of Twin Research and Genetic Epidemiology, King's College London, St. Thomas' Hospital, London, UK. [36]Centre for Eye Research Australia, University of Melbourne, Royal Victorian Eye and Ear Hospital, Melbourne, Australia. [37]Department of Ophthalmology, University Medical Center Mainz, Mainz, Germany. [38]Department of Ophthalmology, Inselspital, University Hospital Bern, University of Bern, Switzerland. [39]Department of Epidemiology, Erasmus University Medical Center, Rotterdam, The Netherlands. [40]Department of Ophthalmology, Medical Faculty Mannheim of the Ruprecht-Karls-University of Heidelberg, Mannheim, Germany. [41]Department of Public Health and Primary Care, University of Cambridge, Cambridge, UK. [42]NIHR Biomedical Research Centre for Ophthalmology, Moorfields Eye Hospital and UCL Institute of Ophthalmology, London, UK. [43]Genome Institute of Singapore, Agency for Science Technology and Research, Singapore, Singapore. [44]Department of Epidemiology and Department of Ophthalmology, Erasmus Medical Center, Rotterdam, The Netherlands. [45]Institute of Human Genetics, Friedrich-Alexander-Universität Erlangen-Nürnberg (FAU), Erlangen, Germany. [46]Lions Eye Institute, Centre for Ophthalmology and Visual Science, University of Western Australia, Perth, WA, Australia. [47]Institute for Medical Research, School of Medicine, Menzies University of Tasmania, Hobart, TAS, Australia. [48]Centre for Vision Research, Department of Ophthalmology and Westmead Millennium Institute, University of Sydney, Sydney, Australia. [49]Department of Ophthalmology and Visual Sciences, Chinese University of Hong Kong, Hong Kong, China. [50]Department of Ophthalmology, Harvard Medical School, Massachusetts Eye and Ear, Boston, MA. [51]deCODE Genetics/Amgen, 101 Reykjavik, Iceland. [52]NIHR Biomedical Research Centre, Moorfields Eye Hospital NHS Foundation Trust, University College London, Institute of Ophthalmology, London, UK. [53]MRC Human Genetics Unit, IGMM, University of Edinburgh, Edinburgh EH4 2XU, UK. [54]Department of Epidemiology, Johns Hopkins Bloomberg School of Public Health, Baltimore, MD, USA. [55]Wilmer Eye Institute, Johns Hopkins School of Medicine, Baltimore, MD, USA. [56]National Human

Genome Research Institute (NIH), Baltimore, MD, USA. [57]Department of Ophthalmology, National University of Singapore and National University Health System, Singapore. [58]Department of Ophthalmology and Visual Sciences, School of Medicine and Public Health, University of Wisconsin, Madison, Wisconsin 53705, USA. [59]Clinic for General and Interventional Cardiology, University Heart Center Hamburg, Hamburg, Germany.

Supporting information

S1 Data. Expression of *Mplkip* and *Cdk13* in the cornea and the eye in the mouse. We examined the cornea and the eye cup for the expression of the transcripts monitored by three of the probes designated as cis-QTLs in the whole eye dataset. The expression level of *Mplkip* and *Cdk13* is considerably higher (3- to 5-fold) in the eye cup relative to the cornea per ng of cDNA. We next measured the RNA content of the cornea in six independent biological samples relative to the eye cup in four independent biological samples. The cornea contained approximately 1.92% of the total RNA in the eye. To determine the contribution of the RNA expression in the cornea to the signal monitored by microarrays in the whole eye dataset, we multiplied the signal by the relative amount of RNA. The total contribution of corneal signal for *Mplkip* and *Cdk13* to that monitored in the dataset is less than 1%. Thus, if the cis-QTL is real, then it does not represent a corneal QTL for there just is not enough expression in the cornea to be monitored in a whole eye sample (Figure A).
(DOCX)

S2 Data. To validate the specificity of rabbit antiserum directed against POU6F2 (MyBiosource, Cat. # MBS9402684) we used in the present study, we first ran an immunoblot and found one major band in the retina sample at approximately 73 kDa, the appropriate size for POU6F2 (lane A). There were no significant bands observed in blots of similar tissue that were stained with secondary antibody only (lane B). Next, we examined four different tissues by PCR, including: retina, brain, colon and salivary gland. We found significant levels of *Pou6f2* message in retina and brain, with virtually no *Pou6F2* mRNA detected in the other samples. When we examined protein samples from these tissues using immunoblot methods, we observed a 74 kDa band in retina and brain and no bands in colon or salivary gland. This confirmed that the antibody was specific for POU6F2.
(DOCX)

S1 Fig. We conducted a series of RNA isolations and quantitative PCR to determine the relative expression of *Mplkip* and *Cdk13* in the cornea and the eye. Based on ng of cDNA from the tissues, the expression within the cornea was less than 25% of the that in the eye. Almost no expression of the corneal marker Upk1b was found in the retina. The total amount of RNA from the cornea in a sample from the eye was only 1.92%. If we determine the relative contribution of corneal *Mplkip* and *Cdk13* to the signal coming from whole eye samples it is less than 1% and thus negligible. The corneal expression of *Mplkip* and *Cdk13* would not be reflected in the whole eye sample. For genes expressed at high levels in the cornea, this is not the case, as it can be seen that the majority of the signal from Upk1b in the whole eye sample originates form the cornea.
(TIF)

S2 Fig. Immunoblots of retina stained with POU6F2 (A) and with secondary antibody only (B). The molecular weights are shown to the left in kDa.
(TIF)

S3 Fig. Flat mounts of the retina from mice 28 days after optic nerve crush were stained for POU6F2 (B) and counterstained for TOPRO-3 (A). The two images are merged and presented

in C. Notice there is no nuclear labeling in the ganglion cell layer (B and C) and that there is a decreased number of nuclei following optic nerve crush (A and C). All photomicrographs are taken at the same magnification and the scale bar in C represents 50 μm.
(TIF)

S4 Fig. Flat mounts of the mouse retina were stained for POU6F2 and counter stained with TOPRO-3. The ganglion cell layer is shown in A and the top of the inner nuclear layer (amacrine cell layer) is shown in B. Notice that brightly labeled cells are observed in the ganglion cell layer and the amacrine cell layer (Arrows). There are also faintly labeled cells in both layers (arrow heads). These data strongly suggest that POU6F2 labels both ganglion cells and amacrine cells. Both A and B are taken at the same magnification and the scale bare in B represents 50 μm.
(TIF)

Acknowledgments

We would like to thank XiangDi Wang (Department of Ophthalmology, Hamilton Eye Institute) for her assistance in collecting data. We would like to thank Micah Chrenek for breeding and genotyping all of the *Pou6f2*-null mice. Chelsey Faircloth was responsible for the sectioning and staining of the adult and embryonic eyes. Xue Jun Qin Duke Molecular Physiology Institute, Duke University, Durham NC for his assistance in data analysis.

Author Contributions

Conceptualization: Janey L. Wiggs, Eldon E. Geisert.

Data curation: Rebecca King, Felix L. Struebing, Ying Li, Jiaxing Wang, Allison Ashley Koch, Jessica N. Cooke Bailey, Michael A. Hauser.

Formal analysis: Rebecca King, Felix L. Struebing, Ying Li, Jiaxing Wang, Eldon E. Geisert.

Funding acquisition: Eldon E. Geisert.

Investigation: Rebecca King, Felix L. Struebing.

Resources: Puya Gharahkhani, Stuart MacGregor, R. Rand Allingham, Michael A. Hauser, Janey L. Wiggs.

Supervision: Eldon E. Geisert.

Writing – original draft: Eldon E. Geisert.

Writing – review & editing: Rebecca King, Felix L. Struebing, Michael A. Hauser, Janey L. Wiggs.

References

1. Gordon MO, Beiser JA, Brandt JD, Heuer DK, Higginbotham EJ, Johnson CA, et al. The Ocular Hypertension Treatment Study: baseline factors that predict the onset of primary open-angle glaucoma. Arch Ophthalmol. 2002; 120(6):714–20; discussion 829–30. PMID: 12049575.
2. Medeiros FA, Sample PA, Weinreb RN. Corneal thickness measurements and visual function abnormalities in ocular hypertensive patients. Am J Ophthalmol. 2003; 135(2):131–7. PMID: 12566014.
3. European Glaucoma Prevention Study G, Miglior S, Pfeiffer N, Torri V, Zeyen T, Cunha-Vaz J, et al. Predictive factors for open-angle glaucoma among patients with ocular hypertension in the European Glaucoma Prevention Study. Ophthalmology. 2007; 114(1):3–9. https://doi.org/10.1016/j.ophtha.2006.05.075 PMID: 17070596.

4. Leske MC, Heijl A, Hyman L, Bengtsson B, Dong L, Yang Z, et al. Predictors of long-term progression in the early manifest glaucoma trial. Ophthalmology. 2007; 114(11):1965–72. https://doi.org/10.1016/j.ophtha.2007.03.016 PMID: 17628686.
5. Medeiros FA, Sample PA, Zangwill LM, Bowd C, Aihara M, Weinreb RN. Corneal thickness as a risk factor for visual field loss in patients with preperimetric glaucomatous optic neuropathy. Am J Ophthalmol. 2003; 136(5):805–13. PMID: 14597030.
6. Herndon LW, Weizer JS, Stinnett SS. Central corneal thickness as a risk factor for advanced glaucoma damage. Arch Ophthalmol. 2004; 122(1):17–21. https://doi.org/10.1001/archopht.122.1.17 PMID: 14718289.
7. Salowe R, Salinas J, Farbman NH, Mohammed A, Warren JZ, Rhodes A, et al. Primary Open-Angle Glaucoma in Individuals of African Descent: A Review of Risk Factors. J Clin Exp Ophthalmol. 2015; 6 (4). https://doi.org/10.4172/2155-9570.1000450 PMID: 26664770; PubMed Central PMCID: PMCPMC4671514.
8. Toh T, Liew SH, MacKinnon JR, Hewitt AW, Poulsen JL, Spector TD, et al. Central corneal thickness is highly heritable: the twin eye studies. Invest Ophthalmol Vis Sci. 2005; 46(10):3718–22. https://doi.org/10.1167/iovs.04-1497 PMID: 16186354.
9. Zheng Y, Ge J, Huang G, Zhang J, Liu B, Hur YM, et al. Heritability of central corneal thickness in Chinese: the Guangzhou Twin Eye Study. Invest Ophthalmol Vis Sci. 2008; 49(10):4303–7. https://doi.org/10.1167/iovs.08-1934 PMID: 18502994.
10. Wang SY, Melles R, Lin SC. The Impact of Central Corneal Thickness on the Risk for Glaucoma in a Large Multiethnic Population. J Glaucoma. 2014; 23(9):606–12. https://doi.org/10.1097/IJG.0000000000000088 WOS:000345865000005. PMID: 25055208
11. Dimasi DP, Burdon KP, Craig JE. The genetics of central corneal thickness. Br J Ophthalmol. 2010; 94 (8):971–6. https://doi.org/10.1136/bjo.2009.162735 PMID: 19556215.
12. Alsbirk PH. Corneal thickness. II. Environmental and genetic factors. Acta Ophthalmol (Copenh). 1978; 56(1):105–13. PMID: 580329.
13. Haseltine SJ, Pae J, Ehrlich JR, Shammas M, Radcliffe NM. Variation in corneal hysteresis and central corneal thickness among black, hispanic and white subjects. Acta Ophthalmol. 2012; 90(8):e626–e31. https://doi.org/10.1111/j.1755-3768.2012.02509.x WOS:000311852500009. PMID: 22938724
14. Alsbirk PH. Corneal thickness. I. Age variation, sex difference and oculometric correlations. Acta Ophthalmol (Copenh). 1978; 56(1):95–104. PMID: 580340.
15. Aghaian E, Choe JE, Lin S, Stamper RL. Central corneal thickness of Caucasians, Chinese, Hispanics, Filipinos, African Americans, and Japanese in a glaucoma clinic. Ophthalmology. 2004; 111(12):2211–9. https://doi.org/10.1016/j.ophtha.2004.06.013 WOS:000225512300011. PMID: 15582076
16. Ulmer M, Li J, Yaspan BL, Ozel AB, Richards JE, Moroi SE, et al. Genome-wide analysis of central corneal thickness in primary open-angle glaucoma cases in the NEIGHBOR and GLAUGEN consortia. Invest Ophthalmol Vis Sci. 2012; 53(8):4468–74. https://doi.org/10.1167/iovs.12-9784 PMID: 22661486; PubMed Central PMCID: PMCPMC3394688.
17. Vithana EN, Aung T, Khor CC, Cornes BK, Tay WT, Sim X, et al. Collagen-related genes influence the glaucoma risk factor, central corneal thickness. Hum Mol Genet. 2011; 20(4):649–58. https://doi.org/10.1093/hmg/ddq511 PMID: 21098505.
18. Vitart V, Bencic G, Hayward C, Skunca Herman J, Huffman J, Campbell S, et al. New loci associated with central cornea thickness include COL5A1, AKAP13 and AVGR8. Hum Mol Genet. 2010; 19 (21):4304–11. https://doi.org/10.1093/hmg/ddq349 PMID: 20719862.
19. Abu A, Frydman M, Marek D, Pras E, Nir U, Reznik-Wolf H, et al. Deleterious mutations in the Zinc-Finger 469 gene cause brittle cornea syndrome. Am J Hum Genet. 2008; 82(5):1217–22. https://doi.org/10.1016/j.ajhg.2008.04.001 PMID: 18452888; PubMed Central PMCID: PMCPMC2427192.
20. Gottsch JD, Sundin OH, Liu SH, Jun AS, Broman KW, Stark WJ, et al. Inheritance of a novel COL8A2 mutation defines a distinct early-onset subtype of fuchs corneal dystrophy. Invest Ophthalmol Vis Sci. 2005; 46(6):1934–9. https://doi.org/10.1167/iovs.04-0937 PMID: 15914606.
21. Biswas S, Munier FL, Yardley J, Hart-Holden N, Perveen R, Cousin P, et al. Missense mutations in COL8A2, the gene encoding the alpha2 chain of type VIII collagen, cause two forms of corneal endothelial dystrophy. Hum Mol Genet. 2001; 10(21):2415–23. PMID: 11689488.
22. Lu Y, Vitart V, Burdon KP, Khor CC, Bykhovskaya Y, Mirshahi A, et al. Genome-wide association analyses identify multiple loci associated with central corneal thickness and keratoconus. Nat Genet. 2013; 45(2): 155–63. https://doi.org/10.1038/ng.2506 PMID: 23291589; PubMed Central PMCID: PMCPMC3720123.
23. Taylor BA, Wnek C, Kotlus BS, Roemer N, MacTaggart T, Phillips SJ. Genotyping new BXD recombinant inbred mouse strains and comparison of BXD and consensus maps. Mamm Genome. 1999; 10 (4):335–48. PMID: 10087289.

24. Bailey JN, Loomis SJ, Kang JH, Allingham RR, Gharahkhani P, Khor CC, et al. Genome-wide association analysis identifies TXNRD2, ATXN2 and FOXC1 as susceptibility loci for primary open-angle glaucoma. Nat Genet. 2016; 48(2):189–94. https://doi.org/10.1038/ng.3482 PMID: 26752265; PubMed Central PMCID: PMCPMC4731307.

25. Carnes MU, Liu YP, Allingham RR, Whigham BT, Havens S, Garrett ME, et al. Discovery and functional annotation of SIX6 variants in primary open-angle glaucoma. PLoS Genet. 2014; 10(5):e1004372. https://doi.org/10.1371/journal.pgen.1004372 PMID: 24875647; PubMed Central PMCID: PMCPMC4038608.

26. Struebing FL, Geisert EE. What Animal Models Can Tell Us About Glaucoma. Prog Mol Biol Transl Sci. 2015; 134:365–80. https://doi.org/10.1016/bs.pmbts.2015.06.003 PMID: 26310165.

27. Choi Y, Sims GE, Murphy S, Miller JR, Chan AP. Predicting the functional effect of amino acid substitutions and indels. PLoS One. 2012; 7(10):e46688. https://doi.org/10.1371/journal.pone.0046688 PMID: 23056405; PubMed Central PMCID: PMCPMC3466303.

28. Lu Y, Dimasi DP, Hysi PG, Hewitt AW, Burdon KP, Toh T, et al. Common genetic variants near the Brittle Cornea Syndrome locus ZNF469 influence the blinding disease risk factor central corneal thickness. PLoS Genet. 2010; 6(5):e1000947. https://doi.org/10.1371/journal.pgen.1000947 PMID: 20485516; PubMed Central PMCID: PMCPMC2869325.

29. Adachi W, Okubo K, Kinoshita S. Human uroplakin Ib in ocular surface epithelium. Invest Ophthalmol Vis Sci. 2000; 41(10):2900–5. PMID: 10967043.

30. Zhou H, Yoshioka T, Nathans J. Retina-derived POU-domain factor-1: a complex POU-domain gene implicated in the development of retinal ganglion and amacrine cells. J Neurosci. 1996; 16(7):2261–74. PMID: 8601806.

31. Rodriguez AR, de Sevilla Muller LP, Brecha NC. The RNA binding protein RBPMS is a selective marker of ganglion cells in the mammalian retina. J Comp Neurol. 2014; 522(6):1411–43. https://doi.org/10.1002/cne.23521 PMID: 24318667; PubMed Central PMCID: PMCPMC3959221.

32. Cambien F, Tiret L. Atherosclerosis: from genetic polymorphisms to system genetics. Cardiovasc Toxicol. 2005; 5(2):143–52. PMID: 16046790.

33. Geisert EE, Lu L, Freeman-Anderson NE, Templeton JP, Nassr M, Wang X, et al. Gene expression in the mouse eye: an online resource for genetics using 103 strains of mice. Mol Vis. 2009; 15:1730–63. PMID: 19727342; PubMed Central PMCID: PMCPMC2736153.

34. Mozhui K, Ciobanu DC, Schikorski T, Wang X, Lu L, Williams RW. Dissection of a QTL hotspot on mouse distal chromosome 1 that modulates neurobehavioral phenotypes and gene expression. PLoS Genet. 2008; 4(11):e1000260. https://doi.org/10.1371/journal.pgen.1000260 PMID: 19008955; PubMed Central PMCID: PMCPMC2577893.

35. Templeton JP, Freeman NE, Nickerson JM, Jablonski MM, Rex TS, Williams RW, et al. Innate immune network in the retina activated by optic nerve crush. Invest Ophthalmol Vis Sci. 2013; 54(4):2599–606. https://doi.org/10.1167/iovs.12-11175 PMID: 23493296; PubMed Central PMCID: PMCPMC3629889.

36. King R, Lu L, Williams RW, Geisert EE. Transcriptome networks in the mouse retina: An exon level BXD RI database. Mol Vis. 2015; 21:1235–51. PMID: 26604663; PubMed Central PMCID: PMCPMC4626778.

37. Freeman NE, Templeton JP, Orr WE, Lu L, Williams RW, Geisert EE. Genetic networks in the mouse retina: growth associated protein 43 and phosphatase tensin homolog network. Mol Vis. 2011; 17:1355–72. PMID: 21655357; PubMed Central PMCID: PMCPMC3108897.

38. Lively GD, Koehn D, Hedberg-Buenz A, Wang K, Anderson MG. Quantitative trait loci associated with murine central corneal thickness. Physiol Genomics. 2010; 42(2):281–6. https://doi.org/10.1152/physiolgenomics.00140.2009 PMID: 20423963; PubMed Central PMCID: PMCPMC3032283.

39. Koehn DR, Meyer KJ, Anderson MG. Genetic Evidence for Differential Regulation of Corneal Epithelial and Stromal Thickness. Invest Ophthalmol Vis Sci. 2015; 56(9):5599–607. https://doi.org/10.1167/iovs.15-17179 PMID: 26305532; PubMed Central PMCID: PMCPMC4553932.

40. Cornes BK, Khor CC, Nongpiur ME, Xu L, Tay WT, Zheng Y, et al. Identification of four novel variants that influence central corneal thickness in multi-ethnic Asian populations. Hum Mol Genet. 2012; 21(2):437–45. https://doi.org/10.1093/hmg/ddr463 PMID: 21984434.

41. Quigley HA. Number of people with glaucoma worldwide. Br J Ophthalmol. 1996; 80(5):389–93. PMID: 8695555; PubMed Central PMCID: PMCPMC505485.

42. Thylefors B, Negrel AD. The global impact of glaucoma. Bull World Health Organ. 1994; 72(3):323–6. PMID: 8062393; PubMed Central PMCID: PMCPMC2486713.

43. Leske MC. The epidemiology of open-angle glaucoma: a review. Am J Epidemiol. 1983; 118(2):166–91. Epub 1983/08/01. PMID: 6349332.

44. Wiggs JL. Genetic etiologies of glaucoma. Arch Ophthalmol. 2007; 125(1):30–7. https://doi.org/10.1001/archopht.125.1.30 PMID: 17210849.

45. Ozel AB, Moroi SE, Reed DM, Nika M, Schmidt CM, Akbari S, et al. Genome-wide association study and meta-analysis of intraocular pressure. Hum Genet. 2014; 133(1):41–57. https://doi.org/10.1007/s00439-013-1349-5 PMID: 24002674; PubMed Central PMCID: PMCPMC3982323.

46. Wang R, Wiggs JL. Common and Rare Genetic Risk Factors for Glaucoma. Cold Spring Harbor perspectives in medicine. 2014. https://doi.org/10.1101/cshperspect.a017244 PMID: 25237143.

47. Wiggs JL, Hauser MA, Abdrabou W, Allingham RR, Budenz DL, Delbono E, et al. The NEIGHBOR consortium primary open-angle glaucoma genome-wide association study: rationale, study design, and clinical variables. J Glaucoma. 2013; 22(7):517–25. https://doi.org/10.1097/IJG.0b013e31824d4fd8 PMID: 22828004; PubMed Central PMCID: PMCPMC3485429.

48. Pasquale LR, Loomis SJ, Kang JH, Yaspan BL, Abdrabou W, Budenz DL, et al. CDKN2B-AS1 genotype-glaucoma feature correlations in primary open-angle glaucoma patients from the United States. Am J Ophthalmol. 2013; 155(2):342–53 e5. https://doi.org/10.1016/j.ajo.2012.07.023 PMID: 23111177; PubMed Central PMCID: PMCPMC3544983.

49. Fleischman D, Berdahl J, Stinnett SS, Fautsch MP, Allingham RR. Cerebrospinal fluid pressure trends in diseases associated with primary open-angle glaucoma. Acta ophthalmologica. 2014. https://doi.org/10.1111/aos.12551 PMID: 25209300.

50. Macgregor S, Hewitt AW, Hysi PG, Ruddle JB, Medland SE, Henders AK, et al. Genome-wide association identifies ATOH7 as a major gene determining human optic disc size. Hum Mol Genet. 2010; 19(13):2716–24. https://doi.org/10.1093/hmg/ddq144 PMID: 20395239; PubMed Central PMCID: PMCPMC2883339.

51. Prasov L, Nagy M, Rudolph DD, Glaser T. Math5 (Atoh7) gene dosage limits retinal ganglion cell genesis. Neuroreport. 2012; 23(10):631–4. https://doi.org/10.1097/WNR.0b013e328355f260 PMID: 22660169; PubMed Central PMCID: PMCPMC3733793.

52. Wiggs JL, Yaspan BL, Hauser MA, Kang JH, Allingham RR, Olson LM, et al. Common variants at 9p21 and 8q22 are associated with increased susceptibility to optic nerve degeneration in glaucoma. PLoS genetics. 2012; 8(4):e1002654. Epub 2012/05/10. https://doi.org/10.1371/journal.pgen.1002654 PMID: 22570617; PubMed Central PMCID: PMC3343074.

53. Kawase K, Allingham RR, Meguro A, Mizuki N, Roos B, Solivan-Timpe FM, et al. Confirmation of TBK1 duplication in normal tension glaucoma. Exp Eye Res. 2012; 96(1):178–80. https://doi.org/10.1016/j.exer.2011.12.021 PMID: 22306015; PubMed Central PMCID: PMCPMC3296819.

54. Hauser MA, Sena DF, Flor J, Walter J, Auguste J, Larocque-Abramson K, et al. Distribution of optineurin sequence variations in an ethnically diverse population of low-tension glaucoma patients from the United States. J Glaucoma. 2006; 15(5):358–63. https://doi.org/10.1097/01.ijg.0000212255.17950.42 PMID: 16988596.

55. Kubota R, Kudoh J, Mashima Y, Asakawa S, Minoshima S, Hejtmancik JF, et al. Genomic organization of the human myocilin gene (MYOC) responsible for primary open angle glaucoma (GLC1A). Biochem Biophys Res Commun. 1998; 242(2):396–400. https://doi.org/10.1006/bbrc.1997.7972 PMID: 9446806.

56. Powell C, Cornblath E, Goldman D. Zinc-binding domain-dependent, deaminase-independent actions of apolipoprotein B mRNA-editing enzyme, catalytic polypeptide 2 (Apobec2), mediate its effect on zebrafish retina regeneration. J Biol Chem. 2014; 289(42):28924–41. https://doi.org/10.1074/jbc.M114.603043 PMID: 25190811; PubMed Central PMCID: PMCPMC4200251.

57. Struebing FL, Lee RK, Williams RW, Geisert EE. Genetic Networks in Mouse Retinal Ganglion Cells. Front Genet. 2016; 7:169. https://doi.org/10.3389/fgene.2016.00169 PMID: 27733864; PubMed Central PMCID: PMCPMC5039302.

58. Wood AR, Esko T, Yang J, Vedantam S, Pers TH, Gustafsson S, et al. Defining the role of common variation in the genomic and biological architecture of adult human height. Nat Genet. 2014; 46(11):1173–86. https://doi.org/10.1038/ng.3097 PMID: 25282103; PubMed Central PMCID: PMCPMC4250049.

59. Yang J, Weedon MN, Purcell S, Lettre G, Estrada K, Willer CJ, et al. Genomic inflation factors under polygenic inheritance. Eur J Hum Genet. 2011; 19(7):807–12. https://doi.org/10.1038/ejhg.2011.39 PMID: 21407268; PubMed Central PMCID: PMCPMC3137506.

60. Fiorino A, Manenti G, Gamba B, Bucci G, De Cecco L, Sardella M, et al. Retina-derived POU domain factor 1 coordinates expression of genes relevant to renal and neuronal development. Int J Biochem Cell Biol. 2016; 78:162–72. https://doi.org/10.1016/j.biocel.2016.07.013 PMID: 27425396.

61. Li Y, Andereggen L, Yuki K, Omura K, Yin Y, Gilbert HY, et al. Mobile zinc increases rapidly in the retina after optic nerve injury and regulates ganglion cell survival and optic nerve regeneration. Proc Natl Acad Sci U S A. 2017; 114(2):E209–E18. https://doi.org/10.1073/pnas.1616811114 PMID: 28049831; PubMed Central PMCID: PMCPMC5240690.

62. Templeton JP, Geisert EE. A practical approach to optic nerve crush in the mouse. Mol Vis. 2012; 18:2147–52. PMID: 22876142; PubMed Central PMCID: PMCPMC3413441.

63. Wang J, Williams RW, Manly KF. WebQTL: web-based complex trait analysis. Neuroinformatics. 2003; 1(4):299–308. Epub 2004/03/27. NI:1:4:299 [pii] https://doi.org/10.1385/NI:1:4:299 PMID: 15043217.

64. Overall RW, Kempermann G, Peirce J, Lu L, Goldowitz D, Gage FH, et al. Genetics of the hippocampal transcriptome in mouse: a systematic survey and online neurogenomics resource. Front Neurosci. 2009; 3:55. Epub 2009/01/01. https://doi.org/10.3389/neuro.15.003.2009 PMID: 20582282; PubMed Central PMCID: PMCPMC2858614.

65. Churchill GA, Doerge RW. Empirical threshold values for quantitative trait mapping. Genetics. 1994; 138(3):963–71. Epub 1994/11/01. PMID: 7851788; PubMed Central PMCID: PMCPMC1206241.

66. Lu L, Wei L, Peirce JL, Wang X, Zhou J, Homayouni R, et al. Using gene expression databases for classical trait QTL candidate gene discovery in the BXD recombinant inbred genetic reference population: mouse forebrain weight. BMC Genomics. 2008; 9:444. Epub 2008/09/27. 1471-2164-9-444 [pii] https://doi.org/10.1186/1471-2164-9-444 PMID: 18817551; PubMed Central PMCID: PMCPMC2570693.

67. Rosen GD, Pung CJ, Owens CB, Caplow J, Kim H, Mozhui K, et al. Genetic modulation of striatal volume by loci on Chrs 6 and 17 in BXD recombinant inbred mice. Genes Brain Behav. 2009; 8(3):296–308. Epub 2009/02/05. GBB473 [pii] https://doi.org/10.1111/j.1601-183X.2009.00473.x PMID: 19191878; PubMed Central PMCID: PMCPMC2706028.

68. Philip VM, Duvvuru S, Gomero B, Ansah TA, Blaha CD, Cook MN, et al. High-throughput behavioral phenotyping in the expanded panel of BXD recombinant inbred strains. Genes Brain Behav. 2010; 9 (2):129–59. Epub 2009/12/05. GBB540 [pii] https://doi.org/10.1111/j.1601-183X.2009.00540.x PMID: 19958391; PubMed Central PMCID: PMCPMC2855868.

69. Watson J. Suppressing autofluorescence of erythrocytes. Biotech Histochem. 2011; 86(3):207. https://doi.org/10.3109/10520295.2011.568971 PMID: 21391776.

Appendix F

GENOMIC LOCI MODULATING RETINAL GANGLION CELL DEATH FOLLOWING ELEVATED IOP IN THE MOUSE

Felix L. Struebing[1], Rebecca King[1], Ying Li, Jessica N. Cooke Bailey[2], NEIGHBORHOOD consortium, Janey L. Wiggs[3], and Eldon E. Geisert[1*]

[1] Department of Ophthalmology, Emory University, 1365B Clifton Road NE Atlanta GA, 30322

[2] Department of Population and Quantitative Health Sciences, Case Western Reserve University School of Medicine

[3] Department of Ophthalmology, Harvard Medical School, Massachusetts Eye and Ear Infirmary

*Corresponding Author: Eldon E. Geisert
Professor of Ophthalmology
Emory University
1365B Clifton Road NE
Atlanta GA 30322
email: egeiser@emory.edu
Phone: 404-778-4239

Author Contribution Statement:

Felix L. Struebing had a primary role in the collection and analysis of data. He was directly involved in the planning and writing of the manuscript and ran PCR experiments.

Rebecca King maintained the animal colonies and aided all the surgeries. She also contributed to data analysis and immunohistochemistry.

Ying Li conducted all of the immunohistochemical stains of the retina and assisted in the writing of the manuscript.

Jessica N. Cooke Bailey analyzed the NEIGHBORHOOD glaucoma dataset.

Janey L. Wiggs was involved in the initial design of the experiments and analysis of the NEIGHBORHOOD glaucoma dataset.

Eldon E. Geisert had direct oversight of the BXD mouse study, designed the experiments and assisted in writing the manuscript.

All authors read and approved the final manuscript.

Abstract:

The present study was designed to identify genomic loci modulating the susceptibility of retinal ganglion cells (RGC) to elevated intraocular pressure (IOP) in the BXD recombinant inbred mouse strain set. IOP was elevated by injecting magnetic microspheres into the anterior chamber and blocking the trabecular meshwork using a handheld magnet to impede drainage. The IOP was then measured over the next 21 days. Only animals with IOP greater than 25 mmHg for two consecutive days or an IOP above 30 mmHg on a single day after microsphere-injection were used in this study. On day 21, mice were sacrificed and the optic nerve was processed for histology. Axons were counted for both the injected and the control eye in 49 BXD strains, totaling 181 normal counts and 191 counts associated with elevated IOP. The axon loss for each strain was calculated and the data were entered into genenetwork.org. The average number of normal axons in the optic nerve across all strains was 54,788 ± 16% (SD), which dropped to 49,545 ± 20% in animals with artificially elevated IOP. Interval mapping demonstrated a relatively similar genome-wide map for both conditions with a suggestive Quantitative Trait Locus (QTL) on proximal Chromosome 3. When the relative axon loss was used to generate a genome-wide interval map, we identified one significant QTL (p<0.05) on Chromosome 18 between 53.6 and 57 Mb. Within this region, the best candidate gene for modulating axon loss was *Aldh7a1*. Immunohistochemistry demonstrated ALDH7A1 expression in mouse RGCs. *ALDH7A1* variants were not significantly associated with glaucoma in the NEIGHBORHOOD GWAS dataset, but this enzyme was identified as part of the butanoate pathway previously associated with glaucoma risk. Our results suggest that genomic background influences susceptibility to RGC degeneration and death in an inducible glaucoma model.

Keywords: Glaucoma model, QTL mapping, systems genetics, butanoate pathway, GeneNetwork

78 Acknowledgements: We would like to thank XiangDi Wang (Department of
79 Ophthalmology, Hamilton Eye Institute) for her assistance in collecting data.
80
81 Disclosures: This study was supported by an Unrestricted Grand from Research to
82 Prevent Blindness, NEI grant R01EY178841 (E.E.G.), Owens Family Glaucoma
83 Research Fund, P30EY06360 (Emory Vision Core, to PM Iuvone) R01 EY022305
84 (JLW), PO30EY014104 (JLW),
85

Introduction

Glaucoma is a diverse set of diseases with heterogeneous phenotypic presentations. Untreated, glaucoma leads to permanent damage of axons in the optic nerve and visual field loss. Millions of people worldwide are affected (Quigley, 1996; Thylefors and Negrel, 1994), and in the United States glaucoma is the second leading cause of blindness (Leske, 1983). Adult-onset glaucoma is associated with multiple risk factors such as intraocular pressure (IOP), age, family history, ethnicity, central corneal thickness and axial length (Aboobakar et al., 2016; Liu and Allingham, 2011; Nickells, 2012; Springelkamp et al., 2017). Genetically, primary open angle glaucoma (POAG) and normal tension glaucoma (NTG), common forms of adult-onset glaucoma, are currently associated with 16 loci (Wiggs and Pasquale, 2017) and exhibit complex inheritance. The present set of POAG genetic risk factors explains only 3-6% of the genetic variance (Verma et al., 2016). Thus, fully defining the genetic basis of glaucoma will require advances in analytical approaches and experimental methods (Boyle et al., 2017).

Many investigators have turned to mouse models to identify causal events linking glaucomatous risk factors and the death of retinal ganglion cells (Struebing and Geisert, 2015). Compelled by the genetic simplicity that recombinant inbred (RI) mouse strains afford in mapping genotype to phenotype (Geisert et al., 2009), we designed a study investigating the variance of axon loss due to increased IOP in a large cohort of mice. For this purpose, we used the BXD RI strain set, which is particularly suited for the study of genetics and the effects on the severity of glaucoma. This genetic reference panel presently consists of over 200 strains. The original 36 strains were extensively studied by our group for more than 18 years. Over the last decade, the Williams group has greatly expanded the BXD family. Both parental strains (C57BL/6J and DBA/2J) are completely sequenced, and all BXD strains are fully mapped with more than 17,000 genetic markers. As a result, the current set of BXD strains is far larger than any other mature RI resource and allows for sub-megabase resolution QTL mapping. Furthermore, this strain set was previously used to develop several large data sets,

including numerous ocular phenotypes (RGC number, IOP, eye size, retinal area, etc.), global transcriptome data for the eye (HEIMED (Geisert et al., 2009)) and retina (HEI Normal Retina Database (Freeman et al., 2011), DoD Normal Retina database (King et al., 2015)), and experimental consequences of optic nerve crush (ONC Retina Database (Templeton et al., 2013)) along with the effects of blast injury (DoD Blast Dataset (Struebing et al., 2017)). Each data set consists of measurements for as many as 80 strains, making the BXD set extremely revealing in the analysis of QTLs and ocular disease networks.

Because we needed a consistent and predictable model to increase IOP with little technical variation, we have adopted a method developed by Samsel et al. (Samsel et al., 2010) to induce acute IOP elevation through the injection of magnetic microspheres and the migration of these microspheres into the trabecular meshwork using magnetic fields. This method of blocking the trabecular meshwork yields a reliable IOP increase, and allows us to define BXD strains with differing susceptibility to axon loss. We then use these data to define a genomic locus modulating axon loss across the BXD strains.

Methods

Animals

All animals used in this study were either bought from the Jackson laboratory (Bar Harbor, ME) or bred in-house in a parasite-free facility. All mice were between 60 and 100 days of age and maintained on a 12h light – 12h dark cycle with food and water *ad libitum*. All procedures involving animals were approved by the Animal Care and Use Committee of Emory University and were in accordance with the ARVO Statement for the Use of Animals in Ophthalmic and Vision Research.

Microsphere Injection and Elevation of IOP

To define the effect of elevated IOP on retinal ganglion cell loss, we examined axonal loss in 47 BXD RI strains. A total of 230 mice received an injection of magnetic

microspheres into the right eye, following a method developed by Samsel et al. (Samsel et al., 2010). Briefly, magnetic microbeads (Spherotech PM-40-10) with a diameter of 4.14µm were washed in sterile HBSS 3 times and diluted 3-fold. The animals were deeply anesthetized with Ketamine (100mg/kg) and Xylazine (15mg/kg) and 10-15 µL of microbead solution were slowly injected into the anterior chamber with a custom-made 30G needle. The needle was held in place while microspheres were pulled into the trabecular meshwork with the help of a handheld 0.5T magnet. After having selectively fixed the magnetic microbeads in the iridocorneal angle, the needle was retracted and carrier HBSS was allowed to drain from the anterior chamber. After the end of the surgery, a drop of topical antibiotic (Certi-Sporyn Neomycin sulfate) was applied to the cornea and mice were allowed to recover on a heating pad until fully awake. Left eyes of many animals served as non-injected controls, but were excluded when any axon damage was present. A total of 181 control eyes and 191 bead injected eyes were included in the study.

IOP Measurement

We measured IOP before the injection of magnetic microspheres to establish baseline values, and then at 2d, 4d, 7d, 9d, 14d, and 21d after the surgery. A rebound tonometer (Tonolab Colonial Medical Supply) was used to measure the IOP under anesthesia with 5% Isoflurane. Measured values are averaged values of 18 (3x6) repeated measurements per animal and time point. IOP readings obtained with the Tonolab instrument have been shown to be accurate and reproducible in various mouse strains, including DBA/2J (Nagaraju et al., 2007; Saleh et al., 2007). The visual axis of the injected eyes remained clear with no visible signs of inflammation. For a bead-injected eye to be included in the sample set, the IOP had to be above 25 mmHg in two consecutive measurements or above 30 mmHg in a single measurement. Bead injected eyes that did not meet this minimum criterion were excluded from the analysis.

Analysis of Optic Nerve Axon Damage

After a survival period of 21 days, the mice were anesthetized with Ketamine (100mg/kg) and Xylazine (15mg/kg) and perfused through the heart with saline followed by 2% paraformaldehyde and 2% glutaraldehyde in phosphate buffer (pH 7.4). The optic nerves were carefully dissected and post-fixed for 24 hours at 4°C. Nerves were dehydrated and embedded in plastic (Libby et al., 2005). Thin sections (0.7μm) were cut from each nerve and mounted on glass slides. Sections were stained using a modified paraphenylenediamine (PPD) staining protocol. Slides were photographed using an Olympus BX51 microscope and a Microfire camera (Optronix) at a final magnification of 1,200X. Healthy axons were counted using ImagePad software developed in our laboratory for the iPad as described previously (Templeton et al., 2014). To assure that all sections were sampled systematically, a grid overlay was placed on the image of the optic nerve and fields were counted every 10 cells along appropriately spaced rows. This resulted in a minimum of 20 fields evenly spaced across the optic nerve, assuring that all sectors of the nerve were included in our sample. The sample was then converted to the average number of axons per mm^2. The cross-sectional area of the section through the optic nerve was calculated from a low power photomicrograph using NIH ImageJ. These two measures were then used to provide an accurate estimate of the axons within each optic nerve.

Analysis of Axon Loss

To map the genomic loci modulating axon loss, we calculated the average number of axons per strain in the normal nerves and the average number of axons in each strain following elevated IOP. We then subtracted the average number of axons in the bead injected nerves from that of the normal nerves to define the axon loss for each strain. Calculated values were used to map QTLs modulating the changes that occur following elevated IOP.

Candidate Gene Selection Within the QTL Region

Our approach for identification of candidate genes involved the following steps: **1)** trait mapping and definition of the 95% confidence interval; **2)** haplotype analysis using our

new sequence data to restrict analysis to those parts of the QTL that are not identical-by-descent between the parental strains; **3)** identification and analysis of all polymorphisms, including SNPs, InDels, inversions, and CNVs in the QTL interval using D2 genome sequence and the reference genome sequence of B6; **4)** identification of genes whose expression is high in the eye, retina, or other ocular tissue; **5)** correlation between our phenotype data and gene expression data from the eye and/or retina to extract highly correlated genes in the QTL; and **6)** gene analysis from the literature and other external data resources.

Immunohistochemistry

For tissue preparation, mice were deeply anesthetized with Ketamine (100mg/kg) and Xylazine (15mg/kg) and perfused through the heart with saline followed by 4% paraformaldehyde in phosphate buffer (pH 7.3). The dissected eyeballs were post-fixed in 4% paraformaldehyde for an extra hour at room temperature. Eyeballs were incubated with 30% sucrose in phosphate buffered saline (PBS) at 4˚C overnight and embedded within Optimal Cutting Temperature compound (OCT). Cryosections, 12-15 µm thick, were cut on a Leica CM 1850 cryostat and kept in a -20^{o}C freezer until further processing. For whole mounts, retinas were removed from the globe and cut into quarters. Sections or whole retinas were rinsed in PBS with 1% Triton-X100 and blocked with 5% normal donkey serum and 5% BSA in PBS with 1% Triton-X100, and placed in primary antibodies ALDH7A1 (Abcam, ab154264, Cambridge, MA) at 1:1000 and TUJ1 (gift from Anthony Frankfurter) at 1:1000 overnight at 4˚C. The sections or whole mount retinas were rinsed in PBS and then placed in secondary antibodies (Alexa Fluor 488 AffiniPure Donkey Anti-Rabbit, Jackson Immunoresearch, Cat. #715-545-152 and Alexa Fluor 594 AffiniPure Donkey Anti-Mouse, Jackson Immunoresearch, Cat. #715-585-150, West Grove, PA) at 1:1000 and To-PRO-3 Iodide (Molecular Probes, Cat. # T3605, Waltham, MA) at 1:1000 as nuclear counterstain for two hours at room temperature. After 3 washes in PBS, cover slips were placed over the sections or retina whole mounts using Fluoromount – G (Southern Biotech, Cat. # 0100-01, Birmingham, AL). High-resolution Z-stacks were captured on a Nikon confocal

microscope with the Nikon C1 software. Z-stacks were collapsed using imageJ and the whole image was adjusted for contrast and brightness using Adobe Photoshop.

QTL validation using qPCR

Retinas from 4 B6 and 4 D2 mice were dissected on ice into Hank's Balanced Salt Solution (HBSS) with RiboLock Rnase inhibitor (Thermo Scientific). RNA was isolated using the RNeasy Mini Kit on a Qiacube (Qiagen) and including a DNase1 gDNA digestion step. First strand synthesis was carried out according to the manufacturer's instructions (Takara PrimeScript Real Time). Primers were designed using NCBI Primer Blast and validated for specificity by melting curve analysis and Sanger sequencing of amplicons. The sequences were Aldh7a1 fwd (5'-GGAGCTGTATTTCCGGGGCT-3') and Aldh7a1 rev (5'-CGCGTTTTGGGGCAGGAATA-3'), and the amplicon crossed an exon junction between exon 3 and 4 (NM_138600.4). Quantitative cycling was carried out on a realplex2 Mastercylcler (Eppendorf) for 40 cycles and 60° annealing temperature using SYBR Green qPCR Master Mix (Qiagen) following the manufacturer's protocol. Reactions were run in quadruple and *Ppia* served as housekeeping gene (Qiagen QuantiTect Primer assay). Reported values are dCT values.

Human glaucoma association analysis (NEIGHBORHOOD dataset)

The peak area of association on mouse chromosome 18 was examined for associations in human datasets, specifically looking for an association of ALDH7A1 with POAG. Liftover of mouse genomic coordinates resulted in one whole syntenic region located on human chromosome 5. This region was queried for associations with POAG in the NEIGHBORHOOD (Bailey et al., 2016) dataset.

Results

The IOP was elevated in 49 strains of mice by injection of magnetic beads into the anterior chamber and fixation thereof in the trabecular meshwork with a hand-held magnet (Samsel et al., 2010). In all cases, the right eye was injected, while the left eye

served as control except in a few cases where the left optic nerve contained damaged axons. Following the injection, IOP was measured in both eyes over the next 21 days. The IOP in the injected eye rose quickly to glaucomatous levels (typically defined by > 20mmHg in humans) and remained elevated for the duration of this experiment (Fig. 1). Thus, this method proved to be a reliable approach to acutely elevate IOP in the mouse eye, even though it was originally developed for the rat (Samsel et al., 2011).

The first step in the analysis was to generate a series of measures for the normal control eyes. After appropriate fixation and preparation of the optic nerve for microscopy, normal axons were quantified for 181 eyes in 49 strains. (Fig. 2, right panel). The number of axons ranged from a mean of 37,2277 axons in BXD36 to a mean of 78,159 in BXD97. The average number of axons per eye was 54,788 with a standard deviation of 8,622, demonstrating natural variation in the number of optic nerve axons across the BXD strain set. There was a significant difference between the strain with the highest and the lowest number of axons within the optic nerve ($p = 0.002$, Mann-Whitney U test).

When the IOP was artificially elevated, the average axon number decreased across the 49 strains to 49,545 axons per optic nerve with a standard error of 9,982 axons (Fig. 2b). Thus, elevation of IOP decreased the average number of axons in the optic nerve, while it increased the standard deviation. Within the bead injected eyes, axon number ranged from 29,720 axons in the lowest strain (BXD1) to 72,473 axons in the highest strain (BXD97). The difference between the lowest and highest strain was significant ($p=0.018$, Mann-Whitney U test). When the number of axons in the normal retina and the number of axons following elevated IOP were used to generate genome-wide interval maps, they both revealed the same suggestive quantitative trait loci (QTLs) on proximal chromosome 3 (Fig. 3). Neither dataset had QTLs that reached the significance level ($p > 0.05$).

To define genomic loci that could modulate the susceptibility of RGCs to death, axon loss per strain was calculated by subtracting the mean number of axons in the bead injected eyes from the mean number of axons in the normal eyes for each strain (Fig. 4). The eye with elevated IOP had an average axon loss of 9.6% relative to the non-injected control eye. There was considerable variability in axon loss across the 49 strains ranging from basically no axon loss in several strains to an average loss of 20,000 axons in BXD1 and BXD51. These data were used to generate a genome-wide interval map (Fig. 5), which revealed a suggestive QTL on chromosome 9 and a significant QTL on chromosome 18. The significant peak on chromosome 18 (Fig. 6) was found between two genomic markers, rs13483369 (54.614840 Mb, mm10) and rs215803889 (56.037647 Mb). Because the high BXD genotyping density with >17,000 segregating markers allows us to map with a precision of roughly ±1 Mb, we examined the region on chromosome 18 from 53.6 to 57 Mb to define potential candidate genes modulating axonal loss. Good candidates should either contain nonsynonymous SNPs altering their amino acid sequence, or they should be cis-eQTLs, meaning that their expression level segregates into two groups defined by the distribution of parental alleles (Struebing et al., 2016). Examining the sequences between B6 and D2 using the SNP browser on GeneNetwork did not reveal genes with nonsynonymous SNPs within this 2 Mb large region. We then queried our recently published BXD Normal Retina databases on GeneNetwork for cis-eQTLs (DoD Normal Retina Affy MoGene 2.0 ST (May 15) RMA Gene Level, (King et al., 2015)). Only one known gene, *Aldh7a1*, showed a significant LRS score ($p < 0.01$, Probe 17354434), suggesting that this gene is a single cis-eQTL within this interval. The differential expression between C57BL/6J and DBA/2J parents was then confirmed by quantitative PCR ($p = 0.028$, Wilcoxon rank-sum test, Supplemental Fig. 1).

We then examined the distribution of ALDH7A1 in the retina using immunohistochemical methods. We stained retinal sections or flat-mounts with antibodies against ALDH7A1 and the RGC markers TUJ1 or RBPMS (Figure 6). While TUJ1 is known to stain RGCs and a few other retinal neurons as well as axons, RBPMS expression was shown to be restricted to the RGC population (Rodriguez et al., 2014;

Struebing et al., 2016). ALDH7A1 co-localized with all TUJ1- and RBPMS-positive cells, while ALDH7A1 staining was also present throughout other retinal layers, including cone photoreceptors. Higher magnifications revealed that ALDH7A1 staining was relatively ubiquitous in cell body and axons but absent from the nucleus. These results are in line with other studies that have demonstrated mitochondrial and cytosolic localization of ALDH7A1 in humans and rodents (Brocker et al., 2011; Brocker et al., 2010; Wong et al., 2010).

In order to test whether variants in *ALDH7A1* influence primary open-angle glaucoma (POAG) susceptibility in humans, we interrogated results from the NEIGHBORHOOD GWAS glaucoma dataset from 3,853 cases and 33,480 controls in the human genomic region corresponding to the mouse *ALDH7A1* locus. The intronic variant rs62391530 showed the strongest relation to POAG with a nominal p-value of 0.02 and an effect size of -0.16. Even though ALDH7A1 variants did not reach the genome-wide significance threshold of $5x10^{-8}$, this gene is part of the KEGG "butanoate metabolic pathway", which was previously identified to be associated with both POAG and NTG (Bailey et al., 2014).

Discussion

Earlier work in glaucoma suggested a role for genetic background in the degeneration of RGCs. The best evidence for this comes from studies in inbred mice (Li et al., 2007). For example, Li et al. looked at the loss of retinal ganglion cells after optic nerve crush in 15 different inbred mouse strains. There was a considerable variability in ganglion cell loss among different strains, and the authors showed that this difference was heritable. In another study, Anderson et al. found that transferring the two known glaucoma-causing DBA/2J mutations onto a C57BL/6J wild-type background recapitulated the iris pigment disease without causing IOP elevation or a neurodegenerative optic nerve phenotype (Anderson et al., 2006). These studies clearly demonstrate a heritable component in the susceptibility of RGCs to cell death.

Here, we have shown that susceptibility to IOP-elevation induced RGC death is influenced by genetic background in the BXD RI mouse strain set. When we performed quantitative trait

mapping for this trait, we could identify a significant genomic interval on Chromosome 18, which likely modified axon loss. We only found one candidate gene within this locus, and we were able to confirm differential expression of this gene, *Aldh7a1*, between the B6 and D2 parents. Furthermore, immunohistochemistry demonstrated expression of ALDH7A1 protein in RGC somata and axons, consistent with its hypothesized role of influencing RGC death susceptibility.

Aldehyde dehydrogenase 7 family member 1 (ALDH7A1), also known as antiquitin, is an enzyme involved in lysine metabolism and protection of cells from hyperosmotic stress (Brocker et al., 2011; Brocker et al., 2010). Mutations in *Aldh7a1* are most prominently known to cause pyridoxine-dependent seizures, a very rare neurological disease characterized by intractable pre- and neonatal seizures that can be treated with large daily doses of Vitamin B6 (Mills et al., 2006). A lower concentration of ALDH7A1 mRNA and protein was also previously found in the brain of DBA/2J mice compared to C57Bl/6J mice, which is coherent with our results and suggests that this QTL is not only retina-specific (Bhave et al., 2006).

While GWAS have identified many genes associated with glaucoma risk, a recent analysis (Bailey et al., 2014) used a randomized analysis to take the single gene data and assign associated molecular pathways. One pathway involved butanoate metabolism (KEGG pathway hsa00650; see Figure 3 in (Bailey et al., 2014)). This pathway is associated with both POAG (8 genes with nominal association) and NTG (8 genes with nominal associations) Of the 5 enzymes (ALDH1B1, ALDH2, ALDH3A2 ALDH7A1 and ALDH9A1) associated with the conversion of Acetaldehyde to Acetyl-CoA, three (ALDH1B1, ALDH2 and ALDH3A2) have a nominal association with either POAG or NTG. Even though ALDH7A1 does not have a significant association with human glaucoma, it is a participant in a molecular pathway that is directly involved in POAG and NTG risk.

Since we used an inducible glaucoma model in this study, additional factors may have influenced our mapping results. For example, the scleral stiffness (compliance) may be different between BXD strains, which could lead to differential susceptibility to artificial IOP

elevation (Sigal and Ethier, 2009). Likewise, differences may exist in the clearance of magnetic beads from the iridocorneal angle. An interesting possibility for the difference in axon loss we have demonstrated in the BXD strain set is differential susceptibility of RGC subtypes to IOP elevation. It was previously shown that alpha-RGCs and melanopsin-containing RGCs were more resistant to axotomy-induced cell death (Duan et al., 2015; Struebing et al., 2016), and similar observations were made in a mouse model of chronically elevated IOP (Feng et al., 2013). These findings argue for the existence of distinct transcriptional programs within each RGC subtype (Struebing et al., 2016). Further developments in this area of research will certainly shed more light onto the molecular mechanisms leading to differential susceptibility of RGCs to death.

In summary, the present study examined the loss of RGCs following an elevation of IOP in the BXD mouse strain set. We identified a single locus on Chr. 18 that modulates the loss of RGCs. A good candidate gene within this locus is *Aldh7a1*. This gene may be important for RGC survival in the BXD mouse strains, and the ALDH7A1 enzymatic pathway is associated with both NTG and POAG (Bailey et al., 2014). These results underline how mouse models and systems genetics could be used to enhance the interpretability of human GWA studies.

References:

Aboobakar, I.F., Johnson, W.M., Stamer, W.D., Hauser, M.A., Allingham, R.R., 2016. Major review: Exfoliation syndrome; advances in disease genetics, molecular biology, and epidemiology. Exp Eye Res 154, 88-103.

Anderson, M.G., Libby, R.T., Mao, M., Cosma, I.M., Wilson, L.A., Smith, R.S., John, S.W., 2006. Genetic context determines susceptibility to intraocular pressure elevation in a mouse pigmentary glaucoma. BMC Biol 4, 20.

Bailey, J.N., Loomis, S.J., Kang, J.H., Allingham, R.R., Gharahkhani, P., Khor, C.C., Burdon, K.P., Aschard, H., Chasman, D.I., Igo, R.P., Jr., Hysi, P.G., Glastonbury, C.A., Ashley-Koch, A., Brilliant, M., Brown, A.A., Budenz, D.L., Buil, A., Cheng, C.Y., Choi, H., Christen, W.G., Curhan, G., De Vivo, I., Fingert, J.H., Foster, P.J., Fuchs, C., Gaasterland, D., Gaasterland, T., Hewitt, A.W., Hu, F., Hunter, D.J., Khawaja, A.P., Lee, R.K., Li, Z., Lichter, P.R., Mackey, D.A., McGuffin, P., Mitchell, P., Moroi, S.E., Perera, S.A., Pepper, K.W., Qi, Q., Realini, T., Richards, J.E., Ridker, P.M., Rimm, E., Ritch, R., Ritchie, M., Schuman, J.S., Scott, W.K., Singh, K., Sit, A.J., Song, Y.E., Tamimi, R.M., Topouzis, F., Viswanathan, A.C., Verma, S.S., Vollrath, D., Wang, J.J., Weisschuh, N., Wissinger, B., Wollstein, G., Wong, T.Y., Yaspan, B.L., Zack, D.J., Zhang, K., Study, E.N., Consortium, A., Weinreb, R.N., Pericak-Vance, M.A., Small, K., Hammond, C.J., Aung, T., Liu, Y., Vithana, E.N., MacGregor, S., Craig, J.E., Kraft, P., Howell, G., Hauser, M.A., Pasquale, L.R., Haines, J.L., Wiggs, J.L., 2016. Genome-wide association analysis identifies TXNRD2, ATXN2 and FOXC1 as susceptibility loci for primary open-angle glaucoma. Nat Genet 48, 189-194.

Bailey, J.N., Yaspan, B.L., Pasquale, L.R., Hauser, M.A., Kang, J.H., Loomis, S.J., Brilliant, M., Budenz, D.L., Christen, W.G., Fingert, J., Gaasterland, D., Gaasterland, T., Kraft, P., Lee, R.K., Lichter, P.R., Liu, Y., McCarty, C.A., Moroi, S.E., Richards, J.E., Realini, T., Schuman, J.S., Scott, W.K., Singh, K., Sit, A.J., Vollrath, D., Wollstein, G., Zack, D.J., Zhang, K., Pericak-Vance, M.A., Allingham, R.R., Weinreb, R.N., Haines, J.L., Wiggs, J.L., 2014. Hypothesis-independent pathway analysis implicates GABA and acetyl-CoA metabolism in primary open-angle glaucoma and normal-pressure glaucoma. Hum Genet 133, 1319-1330.

Bhave, S.V., Hoffman, P.L., Lassen, N., Vasiliou, V., Saba, L., Deitrich, R.A., Tabakoff, B., 2006. Gene array profiles of alcohol and aldehyde metabolizing enzymes in brains of C57BL/6 and DBA/2 mice. Alcohol Clin Exp Res 30, 1659-1669.

Boyle, E.A., Li, Y.I., Pritchard, J.K., 2017. An Expanded View of Complex Traits: From Polygenic to Omnigenic. Cell 169, 1177-1186.

Brocker, C., Cantore, M., Failli, P., Vasiliou, V., 2011. Aldehyde dehydrogenase 7A1 (ALDH7A1) attenuates reactive aldehyde and oxidative stress induced cytotoxicity. Chem Biol Interact 191, 269-277.

Brocker, C., Lassen, N., Estey, T., Pappa, A., Cantore, M., Orlova, V.V., Chavakis, T., Kavanagh, K.L., Oppermann, U., Vasiliou, V., 2010. Aldehyde dehydrogenase 7A1 (ALDH7A1) is a novel enzyme involved in cellular defense against hyperosmotic stress. J Biol Chem 285, 18452-18463.

Duan, X., Qiao, M., Bei, F., Kim, I.J., He, Z., Sanes, J.R., 2015. Subtype-specific regeneration of retinal ganglion cells following axotomy: effects of osteopontin and mTOR signaling. Neuron 85, 1244-1256.

Feng, L., Zhao, Y., Yoshida, M., Chen, H., Yang, J.F., Kim, T.S., Cang, J., Troy, J.B., Liu, X., 2013. Sustained ocular hypertension induces dendritic degeneration of mouse retinal ganglion cells that depends on cell type and location. Invest Ophthalmol Vis Sci 54, 1106-1117.

Freeman, N.E., Templeton, J.P., Orr, W.E., Lu, L., Williams, R.W., Geisert, E.E., 2011. Genetic networks in the mouse retina: growth associated protein 43 and phosphatase tensin homolog network. Molecular vision 17, 1355-1372.

Geisert, E.E., Lu, L., Freeman-Anderson, N.E., Templeton, J.P., Nassr, M., Wang, X., Gu, W., Jiao, Y., Williams, R.W., 2009. Gene expression in the mouse eye: an online resource for genetics using 103 strains of mice. Molecular vision 15, 1730-1763.
King, R., Lu, L., Williams, R.W., Geisert, E.E., 2015. Transcriptome networks in the mouse retina: An exon level BXD RI database. Molecular vision 21, 1235-1251.
Leske, M.C., 1983. The epidemiology of open-angle glaucoma: a review. Am J Epidemiol 118, 166-191.
Li, Y., Semaan, S.J., Schlamp, C.L., Nickells, R.W., 2007. Dominant inheritance of retinal ganglion cell resistance to optic nerve crush in mice. BMC Neurosci 8, 19.
Libby, R.T., Anderson, M.G., Pang, I.H., Robinson, Z.H., Savinova, O.V., Cosma, I.M., Snow, A., Wilson, L.A., Smith, R.S., Clark, A.F., John, S.W., 2005. Inherited glaucoma in DBA/2J mice: pertinent disease features for studying the neurodegeneration. Visual neuroscience 22, 637-648.
Liu, Y., Allingham, R.R., 2011. Molecular genetics in glaucoma. Exp Eye Res 93, 331-339.
Mills, P.B., Struys, E., Jakobs, C., Plecko, B., Baxter, P., Baumgartner, M., Willemsen, M.A., Omran, H., Tacke, U., Uhlenberg, B., Weschke, B., Clayton, P.T., 2006. Mutations in antiquitin in individuals with pyridoxine-dependent seizures. Nat Med 12, 307-309.
Nagaraju, M., Saleh, M., Porciatti, V., 2007. IOP-dependent retinal ganglion cell dysfunction in glaucomatous DBA/2J mice. Invest Ophthalmol Vis Sci 48, 4573-4579.
Nickells, R.W., 2012. The cell and molecular biology of glaucoma: mechanisms of retinal ganglion cell death. Invest Ophthalmol Vis Sci 53, 2476-2481.
Quigley, H.A., 1996. Number of people with glaucoma worldwide. Br J Ophthalmol 80, 389-393.
Rodriguez, A.R., de Sevilla Muller, L.P., Brecha, N.C., 2014. The RNA binding protein RBPMS is a selective marker of ganglion cells in the mammalian retina. The Journal of comparative neurology 522, 1411-1443.
Saleh, M., Nagaraju, M., Porciatti, V., 2007. Longitudinal evaluation of retinal ganglion cell function and IOP in the DBA/2J mouse model of glaucoma. Invest Ophthalmol Vis Sci 48, 4564-4572.
Samsel, P.A., Kisiswa, L., Erichsen, J.T., Cross, S.D., Morgan, J.E., 2010. A novel method for the induction of experimental glaucoma using magnetic microspheres. Invest Ophthalmol Vis Sci.
Samsel, P.A., Kisiswa, L., Erichsen, J.T., Cross, S.D., Morgan, J.E., 2011. A novel method for the induction of experimental glaucoma using magnetic microspheres. Investigative ophthalmology & visual science 52, 1671-1675.
Sigal, I.A., Ethier, C.R., 2009. Biomechanics of the optic nerve head. Exp Eye Res 88, 799-807.
Springelkamp, H., Iglesias, A.I., Mishra, A., Hohn, R., Wojciechowski, R., Khawaja, A.P., Nag, A., Wang, Y.X., Wang, J.J., Cuellar-Partida, G., Gibson, J., Cooke Bailey, J.N., Vithana, E.N., Gharahkhani, P., Boutin, T., Ramdas, W.D., Zeller, T., Luben, R.N., Yonova-Doing, E., Viswanathan, A.C., Yazar, S., Cree, A.J., Haines, J.L., Koh, J.Y., Souzeau, E., Wilson, J.F., Amin, N., Muller, C., Venturini, C., Kearns, L.S., Hee Kang, J., Consortium, N., Tham, Y.C., Zhou, T., van Leeuwen, E.M., Nickels, S., Sanfilippo, P., Liao, J., Linde, H.V., Zhao, W., van Koolwijk, L.M., Zheng, L., Rivadeneira, F., Baskaran, M., van der Lee, S.J., Perera, S., de Jong, P.T., Oostra, B.A., Uitterlinden, A.G., Fan, Q., Hofman, A., Shyong Tai, E., Vingerling, J.R., Sim, X., Wolfs, R.C., Teo, Y.Y., Lemij, H.G., Khor, C.C., Willemsen, R., Lackner, K.J., Aung, T., Jansonius, N.M., Montgomery, G., Wild, P.S., Young, T.L., Burdon, K.P., Hysi, P.G., Pasquale, L.R., Wong, T.Y., Klaver, C.C., Hewitt, A.W., Jonas, J.B., Mitchell, P., Lotery, A.J., Foster, P.J., Vitart, V., Pfeiffer, N., Craig, J.E., Mackey, D.A., Hammond, C.J., Wiggs, J.L., Cheng, C.Y., van Duijn, C.M., MacGregor, S., 2017. New insights into the genetics of primary open-angle glaucoma based on meta-analyses of intraocular pressure and optic disc characteristics. Hum Mol Genet.

Struebing, F.L., Geisert, E.E., 2015. What Animal Models Can Tell Us About Glaucoma. Prog Mol Biol Transl Sci 134, 365-380.
Struebing, F.L., King, R., Li, Y., Chrenek, M.A., Lyuboslavsky, P.N., Sidhu, C.S., Iuvone, P.M., Geisert, E.E., 2017. Transcriptional Changes in the Mouse Retina Following Ocular Blast Injury: A Role for the Immune System. J Neurotrauma.
Struebing, F.L., Lee, R.K., Williams, R.W., Geisert, E.E., 2016. Genetic Networks in Mouse Retinal Ganglion Cells. Front Genet 7, 169.
Templeton, J.P., Freeman, N.E., Nickerson, J.M., Jablonski, M.M., Rex, T.S., Williams, R.W., Geisert, E.E., 2013. Innate immune network in the retina activated by optic nerve crush. Invest Ophthalmol Vis Sci 54, 2599-2606.
Templeton, J.P., Struebing, F.L., Lemmon, A., Geisert, E.E., 2014. ImagePAD, a novel counting application for the Apple iPad, used to quantify axons in the Mouse Optic Nerve. Experimental eye research 128C, 102-108.
Thylefors, B., Negrel, A.D., 1994. The global impact of glaucoma. Bull World Health Organ 72, 323-326.
Verma, S.S., Cooke Bailey, J.N., Lucas, A., Bradford, Y., Linneman, J.G., Hauser, M.A., Pasquale, L.R., Peissig, P.L., Brilliant, M.H., McCarty, C.A., Haines, J.L., Wiggs, J.L., Vrabec, T.R., Tromp, G., Ritchie, M.D., e, M.N., Consortium, N., 2016. Epistatic Gene-Based Interaction Analyses for Glaucoma in eMERGE and NEIGHBOR Consortium. PLoS Genet 12, e1006186.
Wiggs, J.L., Pasquale, L.R., 2017. Genetics of Glaucoma. Hum Mol Genet.
Wong, J.W., Chan, C.L., Tang, W.K., Cheng, C.H., Fong, W.P., 2010. Is antiquitin a mitochondrial Enzyme? J Cell Biochem 109, 74-81.

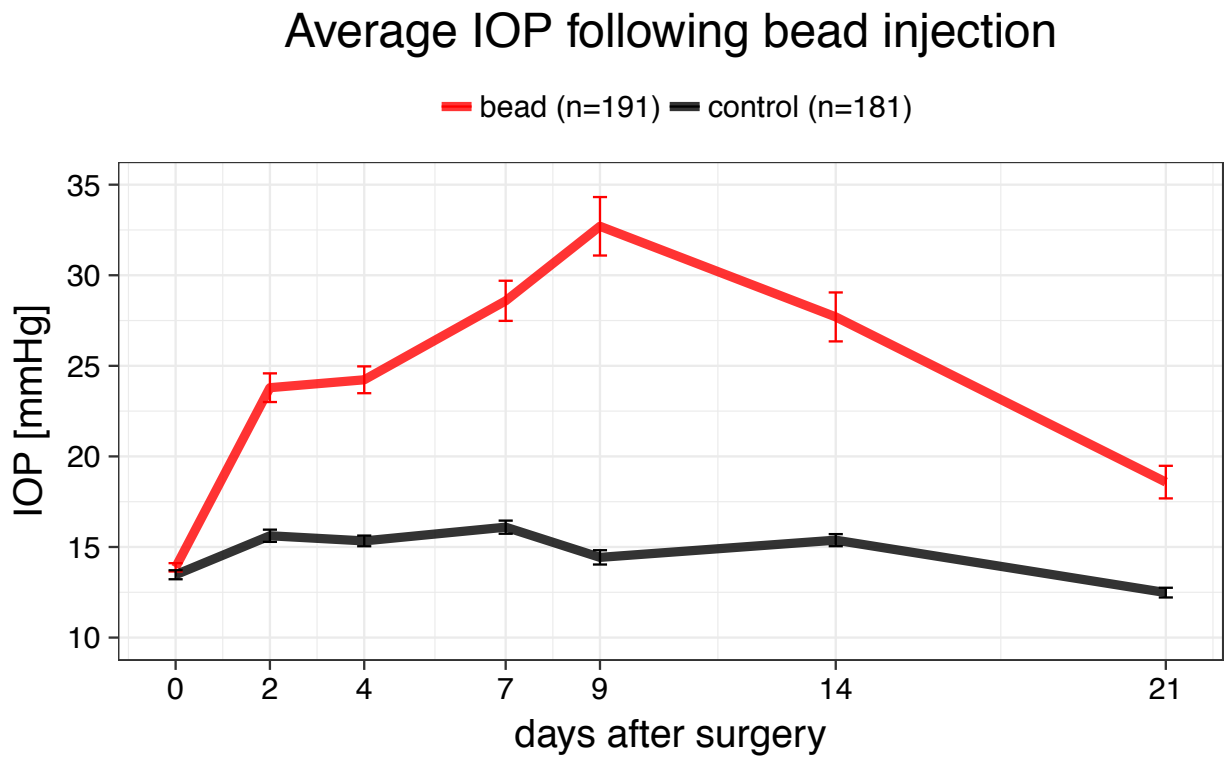

Figure 1. IOP development over 21 days after bead injection surgery. IOP was measured at the days given on the X-axis and averaged across all strains. IOP rises quickly on the second postoperative day, peaks at 9 days and stays elevated throughout the whole 3 weeks. Error bars show standard error.

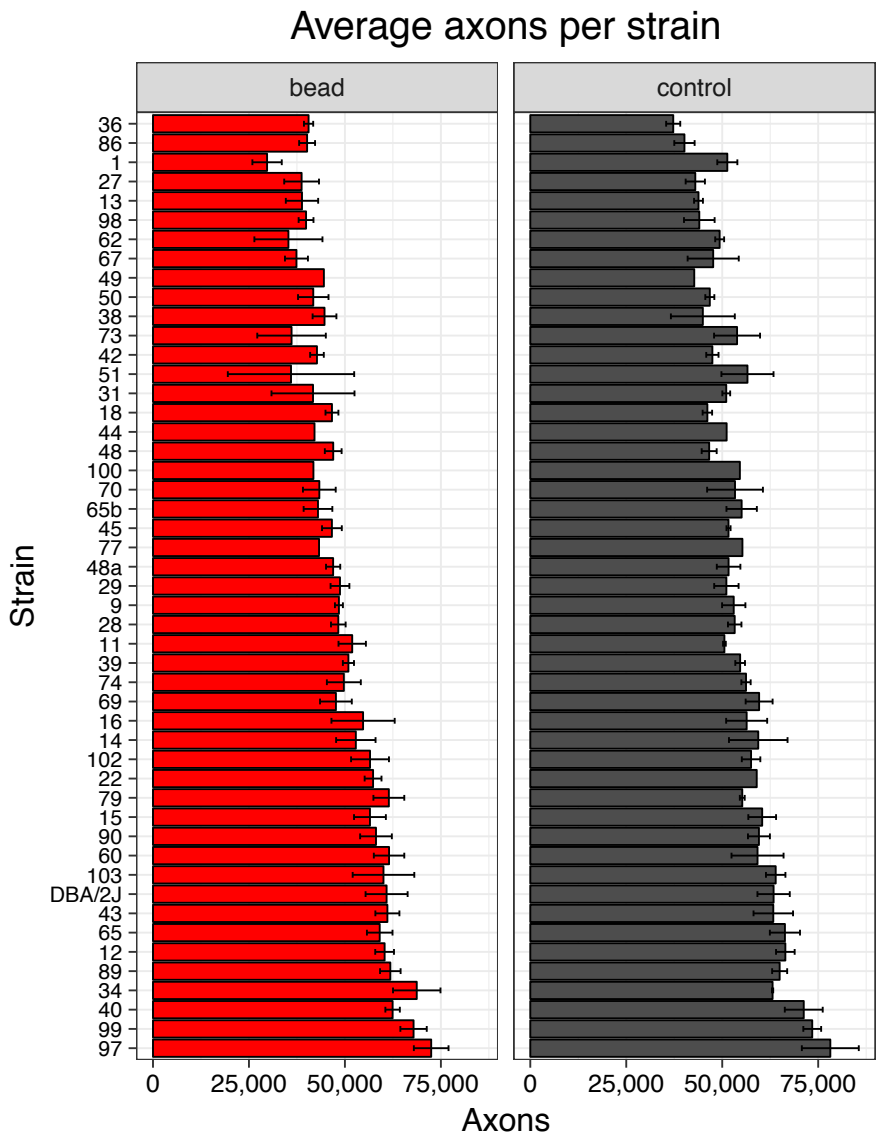

Figure 2. Axon counts for the normal eye ('control', grey) and for the eye 21 days after elevation of IOP ('bead', red). Error bars show standard error.

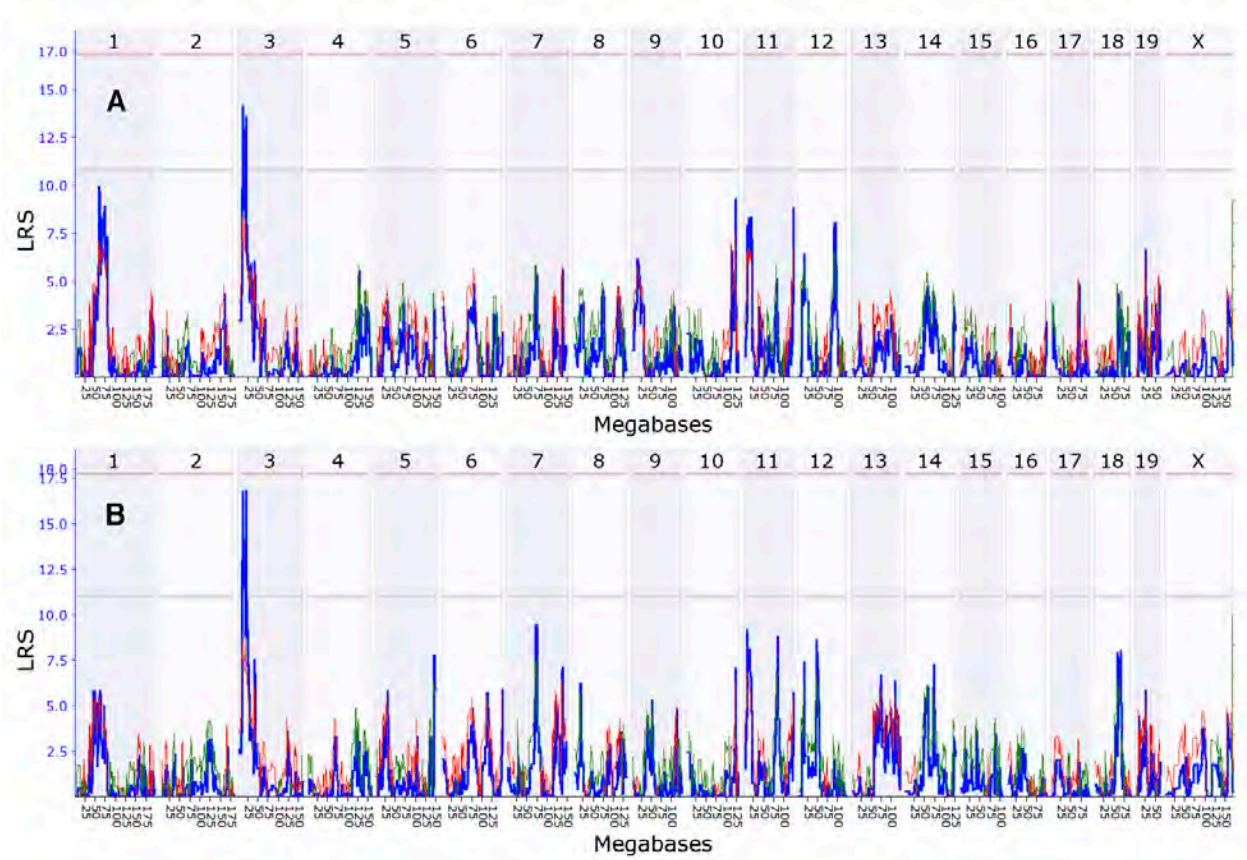

Figure 3. Interval map of axon number across the mouse genome is illustrated for the normal eye (A) and the eye 21 days following elevation of IOP (B). The blue line indicates the total likelihood ratio statistic (LRS) score as specified on the y-axis. The red line illustrates the contribution from the B6 allele and the green line the contribution from the D2 allele. The location across the genome is indicated on the top from chromosome 1 to chromosome X. Notice one suggestive QTL peak on Chr3 (exceeding the gray line, $p<0.63$).

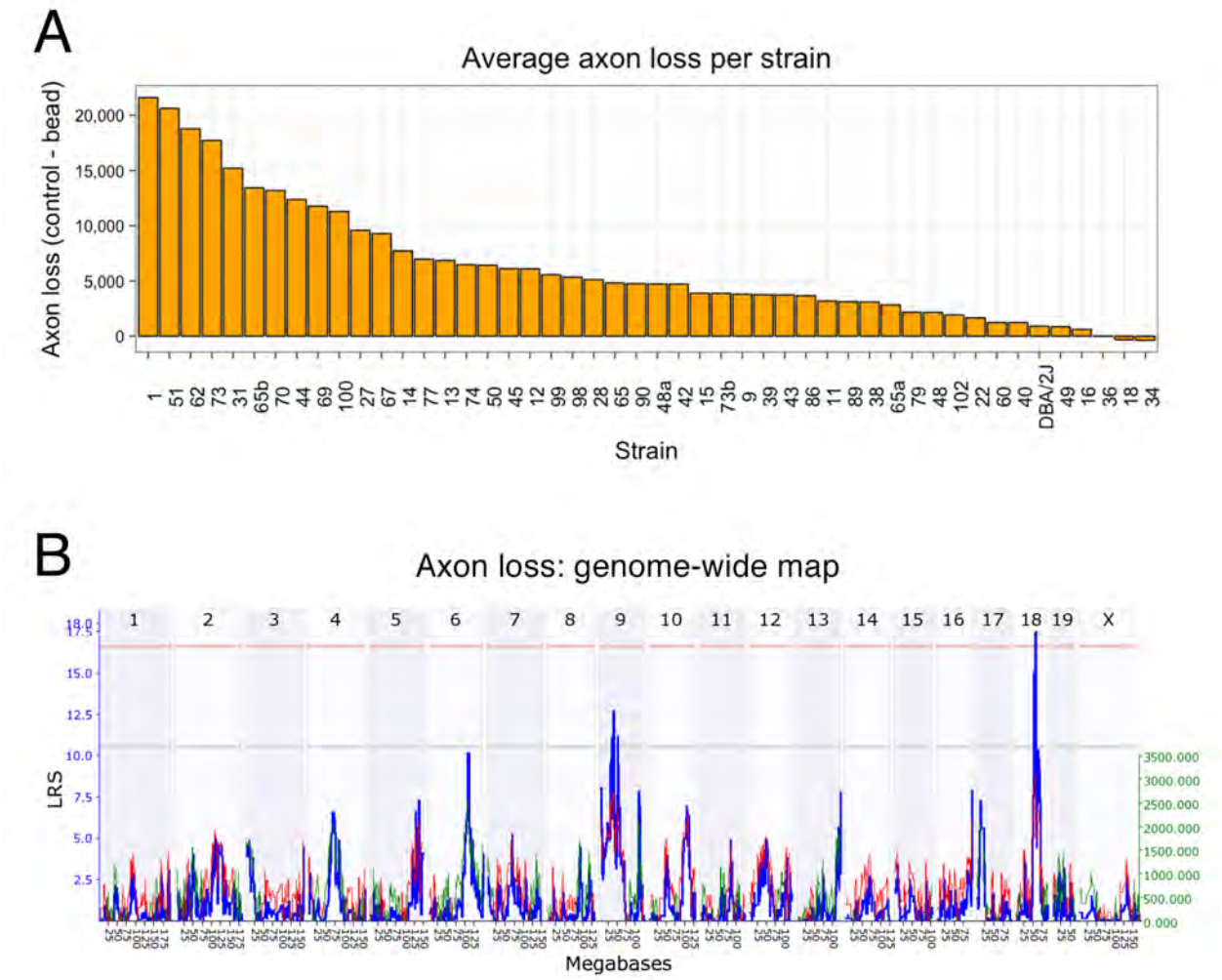

Figure 4: The average axon loss per strain is given in (A) in decreasing order. The genome-wide interval map is shown in (B). Here, chromosomes are displayed on the X axis, while the LRS score is plotted in blue along the Y axis. The light red line defines the genome-wide QTL significance interval of $p < 0.05$, while the light grey line identifies a suggestive QTL. Notice one significant LRS peak on chromosome 18 and one suggestive QTL on chromosome 9.

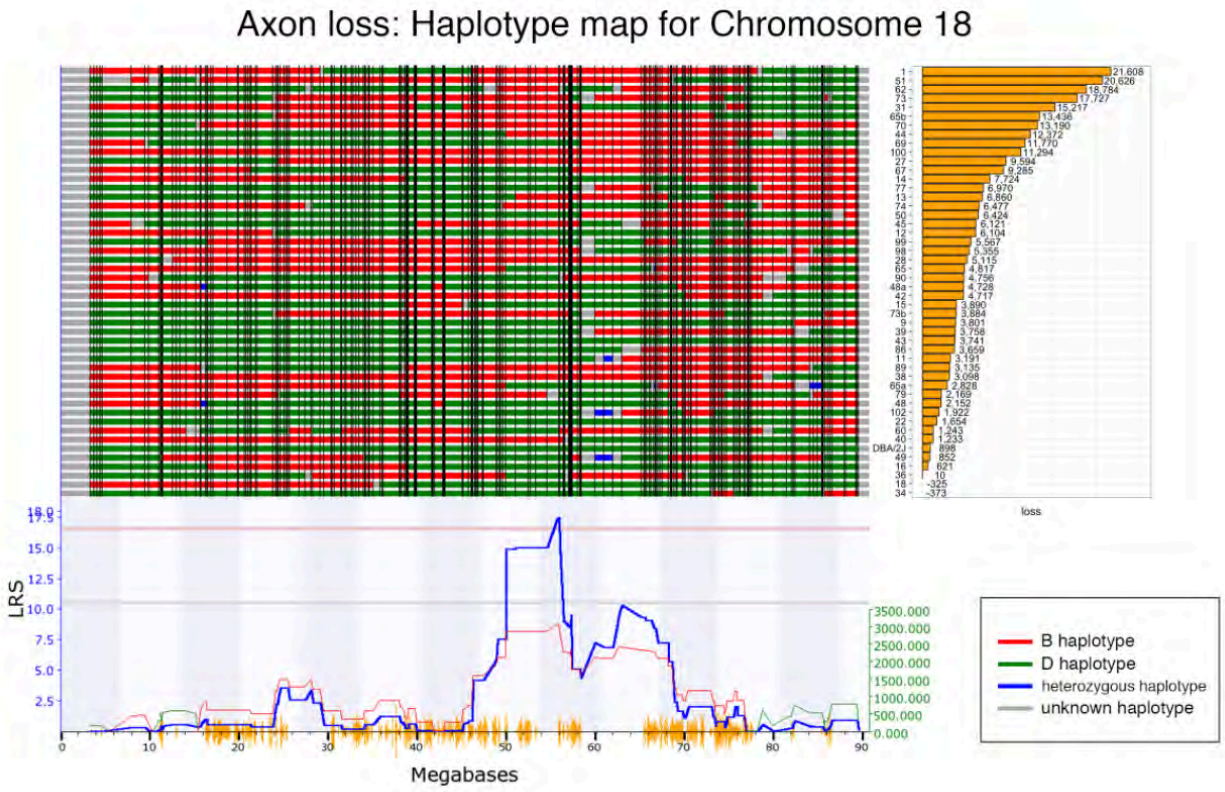

Figure 5. Map of gene locations across Chr. 18. The haplotype map for the 47 strains in the axon loss dataset is shown in the top panel. The haplotype map displays the contribution of each of the two parental strains. The red represents the B6 alleles, green defines the D2 alleles, blue represents regions of the DNA that are heterozygotic and gray is unmapped. At the far right is a list of the specific BXD RI strains with the associated axon loss in decreasing order from top to bottom. The QTL significance is indicated by the blueline below the haplotype map. A positive additive coefficient (red line) indicates that B6 alleles are associated with higher trait values. The QTL reaches significance from ~56 to ~58 Mb ($p<0.05$, light red line).

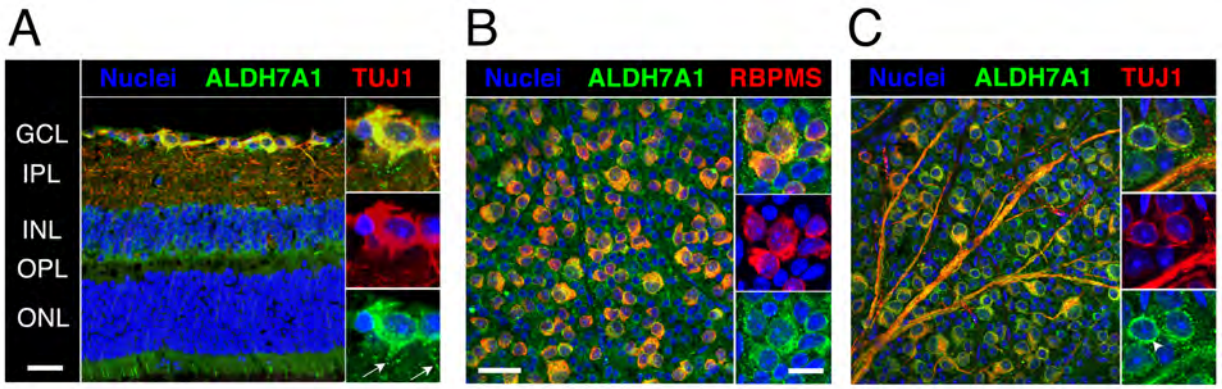

Figure 6. Cross section of a C57BL/6J retina stained for nuclei (blue), ALDH7A1 (green), and the neuronal marker TUJ1 (Class III beta-tubulin, red) is shown in (A). Notice the colocalization of ALDH7A1 with RGCs and its stippled distribution in RGC dendrites (white arrows, magnified section). In (B), a flat-mounted retina was stained with ALDH7A1 and RGC marker RBPMS and the ganglion cell layer (GCL) was imaged *en face*. While all RGCs are double labeled, some cells in the GCL stained exclusively for ALDH7A1 albeit in a less intense manner. (C) is analog to (B) except that it was stained for TUJ1, which also stains RGC axons. ALDH7A1 is most prominently distributed in a perinuclear fashion (arrowhead, magnified section). ALDH7A1 staining is absent in the nucleus, but slightly present in RGC axons. GCL = ganglion cell layer, IPL = inner plexiform layer, INL = inner nuclear layer, OPL = outer plexiform layer, ONL = outer nuclear layer. Low magnification scale bars = 50μm. High magnification scale bars = 20μm.

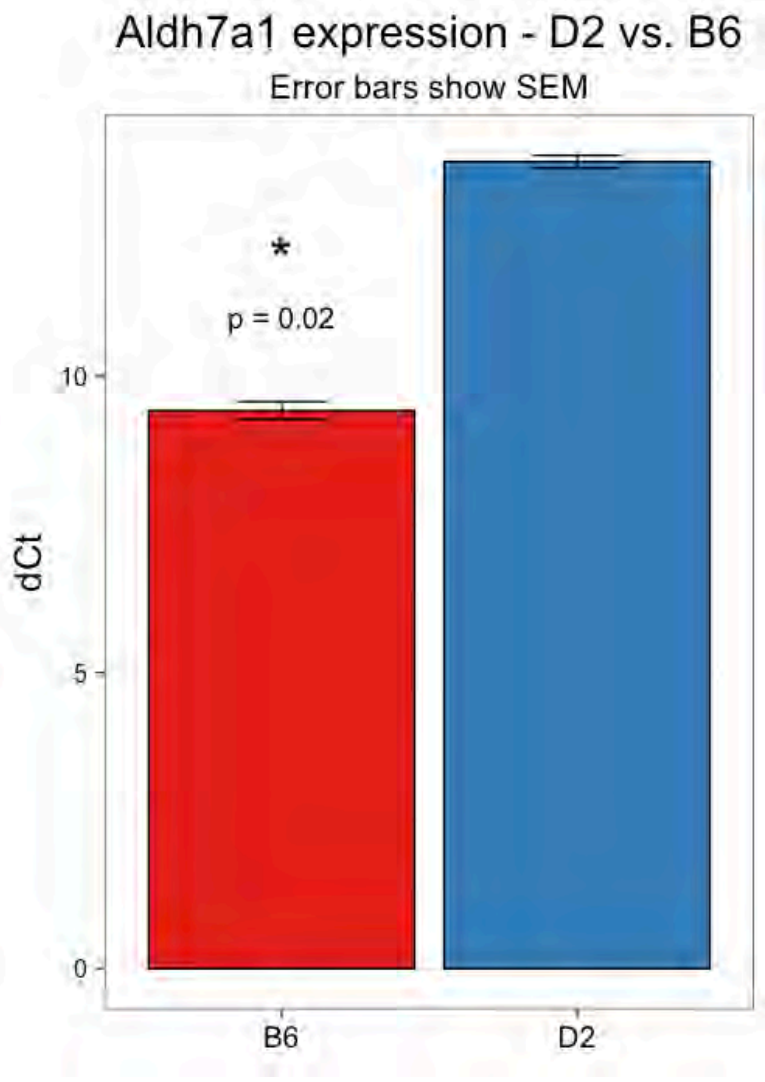

Supplemental Figure 1. Aldh7a1 expression measured by qPCR in D2 vs. B6 mice. The Y-scale shows dCt values on a $\log_2$ scale after normalization with the housekeeping gene Ppia. Expression is significantly higher in retinas of B6 mice ($p = 0.028$, Wilcoxon rank-sum test).

Appendix G

Optic Nerve Regeneration in the Mouse is a Complex Trait Modulated by Genetic Background

Jiaxing Wang[1,2], Ying Li[2], Rebecca King[2], Felix L. Struebing[2] and Eldon E. Geisert[2*]

[1]Department of Ophthalmology, Tianjin Medical University General Hospital, Tianjin, China.

[2]Department of Ophthalmology, Emory University, Atlanta, Georgia, United States of America 30322.

*Corresponding Author: Eldon E. Geisert
Professor of Ophthalmology
Emory University
1365B Clifton Road NE
Atlanta GA 30322
email: egeiser@emory.edu
Phone: 404-778-4239

Key Words:
Genomics; Complex Trait; Axon Regeneration; Optic Nerve; Mouse

Abstract

Purpose: The present study is designed to identify the influences of genetic background on optic nerve regeneration using the two parental strains C57BL/6J and DBA/2J and 7 BXD recombinant inbred strains.

Methods: To study regeneration in the optic nerve, *Pten* was knocked down in the retinal ganglion cells using AAV delivery of an shRNA, and the induction of a mild inflammatory response by an intravitreal injection of zymosan with CPT-cAMP. The axons of the retinal ganglion cells were damaged by optic nerve crush (ONC). Following a 12-day survival period, regenerating axons were labeled by Cholera Toxin B and two days later the regenerating axons within the optic nerve were examined. The number of axons at 0.5 mm and 1 mm from the crush site were counted. In addition, we measured the distance that 5 axons had grown down the nerve and the longest distance a single axon reached.

Results: The analysis revealed a considerable amount of differential axonal regeneration across all 9 BXD strains. There was a significant difference (P=0.014 Mann-Whitney U test) in the regenerative capacity in the number of axons reaching 0.5 mm from a low of 236.1 ± 24.4 axons in BXD102 to a high of 759.8 ± 79.2 axons in BXD29. There were also significant differences (P=0.014 Mann-Whitney U test) in the distance axons traveled, looking at a minimum of 5 axons with the shortest distance was 787.2 ± 46.5μm in BXD102 to a maximum distance of 2025.5 ± 223.3μm in BXD29.

Conclusion: Differences in genetic background can have a profound effect on axonal regeneration causing a 3-fold increase in the number of regenerating axons at 0.5 mm from the crush site and 2.5-fold increase in distance traveled by at least 5 axons in the damaged optic nerve.

INTRODUCTION

Over the last decade, significant advances have been made in approaches to induce regeneration of retinal ganglion cell (RGC) axons through the optic nerve[1-5] . The regeneration and survival of RGCs is influenced by interactions between multiple cellular processes (for review see [5-7]). The number of genes and molecular pathways that modulate the regenerative response in the mammalian optic nerve reveals that induced axonal regeneration (or the lack of regeneration in the normal adult CNS) is a complex trait[1, 2, 8-11]. Complex traits are controlled by multiple genomic elements, some of which are associated with specific molecular functions and others are believed to be associated with more generalized cellular functions[12-14]. This complexity of axonal regeneration could be predicted for we know that successful regeneration involves multiple cellular processes. The first is the survival on the injured retinal ganglion cell involving modulating apoptosis[15, 16], autophagy[1] and response to growth factors[11, 17-19]. The second necessity for axonal regeneration to occur is the growth of the axon itself down the optic nerve. This includes distinct pathways associated with the axon growth program[20]. The third series of events may be directly related to cellular elements that inhibit axonal growth in the adult CNS that are glial in origin, involving astrocytes[21, 22], oligodendrocytes[10] or the glial scar[21, 22]. One approach in studying regeneration is to use inbred mouse strains, identifying strains/genetic backgrounds that facilitate axonal regeneration**.** Omura et al. [8] tested 9 different inbred strains and found that one strain (CAST/Ei) was capable of considerable amount of axon regeneration on inhibitory substrates in tissue culture. The CAST/Ei strain also demonstrated a relative robust regeneration in vivo as compared to the C57BL/6J strain. Our goal in the present study is to take a similar systems biology approach to the study of optic nerve regeneration.

Our working hypothesis is that current regeneration treatments can be influenced by genetic background and within that genetic background are specific genomic elements that can be identified. Our group has used a systems biology approach working with the BXD recombinant inbred strains of mice to define genomic elements affecting the response of the retina to optic nerve damage[23] and to blast injury[24]. The power of the BXD strain set derives from the shuffled genomes of the parental strains (C57BL/6J mice and the DBA/2J mice). Both of the parental strains are fully sequenced and there are over 4.8 million known single nucleotide

polymorphisms, deletions, and insertions between them. In the first 102 BXD strains, there are over 7000 break-points in the genomes between the parental strains. All of the BXD strains are fully mapped. This allows for a rapid mapping of phenotypic data onto genomic elements to define loci modulating the phenotype in a quantitative trait analysis [25, 26]. All of these information and powerful bioinformatic tools are available on the GeneNetwork website (www.genenetwork.org) and are used to define the complex genetics underlying induced regeneration in the optic nerve.

We use the BXD recombinant inbred strains to examine the regeneration response 14 days after optic nerve crush in mice in which *Pten* (phosphatase and tensin homolog) knocked down and zymosan and CPT-cAMP were injected into the vitreous chamber [1, 3]. Regenerative response is determined by defining the number of axons regenerating as well as the distance these axons have traveled.

MATERIALS AND METHODS

Mice: Nine strains including seven BXD recombinant inbred strains and their parental strains – C57BL/6J and DBA/2J were used in this study. All of the mice were 60-70 days of age at the time of initial treatment (See supplemental Table 1). The mice were housed in a pathogen-free facility at Emory University, maintained on a 12-hour light/dark cycle, and provided with food and water ad libitum. All procedures involving animals were approved by the Animal Care and Use Committee of Emory University and were in accordance with the ARVO Statement for the Use of Animals in Ophthalmic and Vision Research. Controls were run with the C57BL/6J (n=6) and DBA/2J (n= 6) mice strains. For the studies of regeneration, we examined axon growth in the parental strains, C57BL/6J (n=5) and DBA/2J (n=8); along with, seven BXD strains: BXD11 (n=5), BXD29-*Tlr4*$^{lps\text{-}2J}$/J(n=4), BXD31(n=4), BXD38(n=4), BXD40(n=9), BXD75(n=5) and BXD102(n=5).

Surgery: The optic nerve regeneration protocol developed by others[1, 3, 4] was used to induce regeneration after optic nerve crush (ONC). The treatment included knocking down of *Pten* using AAV-shPTEN-GFP, and intravitreal injection of Zymosan plus CPT-cAMP. We followed a similar protocol with minor modifications. One is that we used AAV-shPTEN-GFP (*Pten* short hairpin RNA-GFP packaged into AAV2 backbone constructs, titer = $1.5x10^{12}$ vg/ml) to knock down *Pten* instead of cre recombinase-mediated knock-out in *Pten*-floxed mice. The shRNA target sequence is 5'-AGGTGAAGATATATTCCTCCAA-3' as described by Zukor K et al[27]. Our immunostaining also proved an efficient suppression of *Pten* expression in the retina ganglion cells by this *Pten* shRNA (Supplementary Figure 1). Two weeks prior to ONC, the mice were deeply anesthetized with 15 mg/kg of xylazine and 100 mg/kg of ketamine and intravitreal injection of 2μL of AAV-shPTEN-GFP. Optic nerve crush was performed as described by Templeton and Geisert[28]. Briefly, the mice were deeply anesthetized with a mixture of 15 mg/kg of xylazine and 100 mg/kg of ketamine. Under the binocular operating scope, a small incision was made in the conjunctiva, the optic nerve was visualized and then crushed 1 mm behind the eye with angled crossover tweezers (Dumont N7) for 5 seconds, avoiding injury to the ophthalmic artery. Immediately following ONC, Zymosan (Sigma, Z4250,

Lot#BCBQ8437V) along with the cAMP analog CPT-cAMP (Sigma, C3912, Lot#SLBH5204V) (total volume 2µL) were injected into the vitreous to induce an inflammatory response and augment regeneration. Mice were given buprenorphine SQ at 0.5mg/kg immediately following the optic nerve crush. When mice were fully recovered, they are returned to a clean cage and monitored for three days post-op. Mice showing signs of pain or distress are euthanized. Twelve days after ONC (2 days before sacrifice) the animals were deeply anesthetized and Alexa Fluor® 647-conjugated Cholera Toxin B (CTB) (ThermoFisher, C34778) was injected into the vitreous for retrograde labeling of the regenerated axons. All the intravitreal injections and optic nerve crushes were done by one well-trained postdoctoral fellow to avoid technical variation during the surgical procedure. At 14 days after ONC the mice were deeply anesthetized and perfused through the heart with phosphate buffered saline (pH 7.3) followed by 4% paraformaldehyde in phosphate buffer (pH 7.3).

Preparation of the optic nerve: Optic nerves along with optic chiasm, and brains were dissected and post fixed in 4% paraformaldehyde in phosphate buffer overnight. The optic nerve was cleared with FocusClear™ (CelExplorer, Hsinchu, Taiwan) for up to 4 hours until totally transparent. A small chamber was built on the slide to provide enough space for the whole nerve thickness and to keep the nerve from being damaged from flattening. The optic nerve was then mounted in the chamber using MountClear™ (CelExplorer, Hsinchu, Taiwan) and the slides were cover-slipped. FocusClear has been used to clear brain tissue for whole brain imaging [29] as well as clearing of the optic nerve of transgenic zebrafish to observe axon regeneration [30]. It allows us to scan the whole thickness of the optic nerve for better understanding of the status of axon regeneration. It provides clear imaging of regenerated axons from the optical slices scanned by confocal microscope for counting (Supplementary Movie 1). It also allowed us to determine the longest 5 axons or single axon growth along the nerve from z-stack of the whole nerve (Figure 1).

Quantitation of axon regeneration: Cleared optic nerves were examined on a confocal microscope by scanning through individual optical slices. Green pseudo-color was used for CTB-labeled axons in all the optic nerve images of this study for clear visual observation.

Stacked images were taken at 10µm increments, a total of 20-50 optical slices for each optic nerve.

The number of CTB labeled axons at 0.5 mm from the crush site were counted in at least 6 sections per case and calculated by the equation ($\Sigma ad = \pi r^2 * [\text{average axons/mm}]/t$) as described by Leon et al. in 2000 [31]. In this formular, the cross-sectional width of the nerve was measured at the point at which the counts were taken and was used to calculate the number of axons per millimeter of nerve width. The total number of axons extending distance *d* in a nerve having a radius of *r* (half of the biggest width of all optic sections), was estimated by summing over all sections. The virtual thickness of an optical slice from the confocal microscope were calculated using the formula $dz \cong \frac{0.64 \times \lambda exc}{n\text{-}\sqrt{n^2}\text{-}NA^2}$ we determined that the thickness of the optical section was 6µm where diffraction index (n) was 1.517, the numerical aperture (Na) was 0.45 and the excitation wavelength was 637nm. Since the optical section was 6µm and the spacing between optical sections was 10µm single axons were not counted multiple times. For quantifying the number of axons at 1mm from crush site, since there are very few axons observed in some strains, we used direct counts of axons as a measure of regeneration. We also measured the distance that 5 axons had grown down the nerve and the longest distance a single axon reached for each nerve from z-stack image of the whole nerve.

Transfection Efficiency of AAV-shPTEN-GFP: BXD102 mice (N=4) and BXD29 mice (N=4) were deeply anesthetized with a mixture of 15 mg/kg of xylazine and 100 mg/kg of ketamine and injected with 2 µl of AAV-shPTEN-GFP into the left eye. Two weeks later, they were deeply anesthetized as described above and perfused through the heart with saline followed by 4% paraformaldehyde in phosphate buffer (pH 7.3). For the retinal flat mounts, the retinas were removed from the globe and rinsed in PBS with 1% Triton X-100, blocked in 5% Bovine Serum Albumin (BSA) 1-hour room temperature and placed in primary antibodies RBPMS (Millipore, Cat. # ABN1376) at 1:1000 and GFP (Novus Biologicals, CAT #NB100-1770) at 1:1000 4°C overnight. The retinas were rinsed with PBS and placed in secondary antibodies, (Anti-Goat IgG(H+L) CFTM 488A, Sigma, Cat. #SAB4600032 and Alexa Fluor 594 AffiniPure Donkey Anti-Guinea, Jackson Immunoresearch, Cat. #706-585-1148) at 1:1000 for 1 hour at room temperature. After three washes of 15 minutes each, retinas were

flat mounted and cover-slipped using Fuoromount - G (Southern Biotech, Cat. #0100-01) as a mounting medium. Four confocal images were taken in each quadrant at 2 mm away from the optic nerve of each retina. Four retinas from 4 mice of each strain were included. Cell number were determined manually by using the cell counter in ImageJ. RBPMS was used as a marker to label the total number of RGCs [32, 33]. Transfection Efficiency are calculated as the number of AAV transfected RGCs (GFP^+RBPMS^+ cells) divided by total number of RGCs ($RBPMS^+$ cells).

Bioinformatic analysis of known regeneration genes in the BXD strain set: By searching the literature, we generated a list of genes that are known to have effects on optic nerve regeneration either directly or indirectly (Table 1). All those genes were examined for high Likelihood Ratio Statistics (LRS) scores and cis Quantitative Trait Loci (cis-QTLs) using the GeneNetwork database. They were then put into the SNP (Single Nucleotide Polymorphism) browser of GeneNetwork as well as UCSC genome browser (Mouse, GRCm38/mm10) to identify non-synonymous SNPs between C57BL/6J and DBA/2J. All the identified rsIDs of non-synonymous SNPs were then put into Ensembl (www.ensembl.org/) for SIFT analysis [34] to predict whether the SNP affects protein function.

Statistical Analysis: Data are presented as Mean ± SE (Standard Error of the Mean). Differences in axon counts, regeneration distance, and the differences in transfection efficiency were analyzed by Mann-Whitney U test using SPSS (Statistical Package for the Social Sciences) statistical package 24.0 (SPSS, IBM, Chicago, IL, USA). A value of $p<0.05$ was considered statistically significant.

RESULTS

Genetic Background Modulates RGC Axon Regeneration: In the present study, we examined the effects of genetic background on the regenerative response of retinal ganglion cells. The BXD recombinant inbred strains were chosen as a genetic reference panel due to distinct advantages these strains have to offer. The first advantage is there are over 80 well characterized strains of mice available through Jackson laboratories. The current set of strains is far larger than any other mature RI resource and will now allow for sub-megabase mapping resolution. The second benefit of the BXD strains are the large microarray datasets specifically for the eye (HEIMED database[14]; HEI Retina Database [35]; Optic Nerve Crush Database[23]; and the DoD Normal Retina Database[36]) along with the numerous ocular phenotypes RGC numbers, IOP, eye size, retinal area, etc[24]. GeneNetwork also offers an array of highly interactive series of bioinformatic tools that aid in the analysis of data generated with the BXD strains.

Regeneration of axons in the optic nerve was examined in nine strains of mice: the two parental strains (C57BL/6J and DBA/2J mice) and seven BXD strains (BXD11, BXD29, BXD31, BXD38, BXD40, BXD75 and BXD102) (Figure 2). As an internal control, we examined the ability of untreated retinas to regenerate following optic nerve crush in both the C57BL/6J mouse and the DBA/2J mouse (Figure 2). For all mice, the axonal regeneration was evaluated 14 days following optic nerve injury. In the two strains of the control group (C57BL/6J and DBA/2J) there was no detectable axonal regeneration; while in all of the strains receiving the regeneration treatment there was a significant regenerative response, both in the number of axons counted at 0.5mm and 1mm (Figure 4), as well in the distance the axons traveled (Figure 5). In the parental strains, the differences between treatment group and control group are statistically significance ($P<0.01$ for both C57BL/6J and DBA/2J). These data demonstrate that the regeneration treatment, knocking down *Pten* and inducing a mild inflammation by injecting of zymosan and CPT-cAMP, produces significantly more regenerating axons than observed in control animals that did not receive treatment.

The number of axons at 0.5mm and 1mm distal to the crush, is an estimate of the influence of genetic background on the total regenerative effect of the treatment. As can be seen in Figure 2 and Figure 4, there is a considerable difference between strains on the total number of axons reaching 0.5mm and 1.0mm. The strain with the least number of axons in both cases was BXD 102. At both distances from the crush site, the strain with the greatest number of axons was BXD29. The difference was significant (P=0.014 Mann-Whitney U test) in the number of regenerated axons reaching 0.5 mm (from a low of 236.1 ± 24.4 axons in BXD102 to a high of 759.8 ± 79.2 axons in BXD29, 3.2-fold difference) from the crush site. There was also a significant difference (P=0.007 Mann-Whitney U test, 12.6-fold difference) in the number of axons at 1mm, from a low of 1±0 axons in BXD102 to a high of 12.6 ± 0.6 axons in BXD29. The two strains that displayed the least and most robust (BXD102 and BXD29) regenerative response are illustrated in Figure 3.

The total length of a regenerating axon was also measured. This measure may provide an estimate of the rate at which the axon can grow down the injured optic nerve. When we examined axon length there was also a clear difference in growth across the BXD strains (Figure 2, Figure 5). In the control animals, virtually no regenerating axons were observed. When we examined the distance a minimum of 5 axons traveled, a significant difference was observed across the BXD strains. The strain with the shortest regenerating 5 axons was BXD102 with a mean distance of 787.2 ± 46.5µm, and the strain with the longest group of 5 axons was BXD29 with a mean distance of 2025.5 ± 223.3µm (P=0.014 Mann-Whitney U test, 2.5-fold difference). A similar result was observed when examining the distance of the longest single axon traveled in the nerve, with BXD102 having the shortest average distance (1107 ± 40.6µm) and BXD29 the longest (2386.8 ± 162.6µm, P=0.014 Mann-Whitney U test, 2.2-fold difference). Thus, the ability of axonal regeneration (both the number of regenerating axons and the distance traveled) is affected by the genetic backgrounds in the BXD strains with BXD102 having the least regeneration and BXD29 having the most robust regenerative response. These data revealed that genetic background can have a striking effect on the regenerative capacity of axons within the optic nerve.

Transfection Efficiency of AAV-shPTEN-GFP: One possible explanation for the difference is axonal regeneration is a differential transfection of the retinas from strain to strain by the AAV-shPTEN-GFP vector. To control for this possibility, we examined the transfection efficiency and level of *Pten* knock down in the strain with the most robust axon regeneration (BXD29) and another strain with least axon regeneration (BXD102). There was no statistically significant difference between the two strains. For the BXD29 strain (n=4) the mean transfection rates was 51.6%±1.3% and for the BXD102 strain (n=4) the mean transfection rate was 50.8% ± 1.4% (Figure 6), indicating that the difference of regeneration response is not due to different transfection efficiency.

Potential Contribution of Known Genes Affecting Axon Regeneration BXD Strains: Previous studies have identified a number of genes that affect the ability of axons to regenerate in the injured optic nerve (Table 1). Using the bioinformatic tools on GeneNetwork, it is possible to define any of the regeneration associated genes that are either differentially expressed forming a cis-QTL in the BXD strains or having non-synonymous SNPs between C57BL/6J and DBA/2J mice.

The cis-QTL is a QTL that maps to the location of the gene that produces the mRNA or protein. We usually use the LRS (Likelihood Ratio Statistic) score to represent the association or linkage between differences in traits and differences in particular genotype markers or specific genes. While a statistically significant cutoff can only be determined through permutation tests, LRS scores of >17 usually approximate the significance threshold of $p<0.05$ and are worthy of attention[14]. If a cis-QTL has a high LRS score, it is considered that this genetic locus is strongly linked to a certain phenotype and is able to influence the phenotype by regulating this locus. In other words, change of the expression level of this gene will have a higher chance to alter the phenotype, which in our case, is the axonal regeneration. In this process, two regeneration associated genes were identified with cis-QTLs, *Fgf2* and *Klf9* (Table 1). Only one of these cis-QTLs, *Fgf2*, is valid. The other, *Klf9,* contained a difference in the genetic sequences between C57BL/6J and DBA/2J mice at the exact site where the microarray probe binds. This difference in sequence will lead to differential binding of the

probe and a false positive LRS score. Thus, there was one cis-QTL (*Fgf2*) present in the BXD strains that could potentially affect the regenerative response.

We also examined the BXD strains to define genes with non-synonymous SNPs. A non-synonymous SNP between the parent strains (C57BL/6J and DBA/2J) is potentially able to alter the protein structure and function, ultimately leading to the different phenotype. The BXD strains that inherited different alleles may also have different phenotypes. There were eight genes (*Mapk10, Rtn4, Ctgf, Tlr2, Rock1, Rock2, Clec7a and Csf2)* with non-synonymous SNPs between C57BL/6J and DBA/2J. The SIFT analysis[34] revealed that only two of the eight genes, *Mapk10* (JNK3) and *Rtn4* (NOGO), had SNPs that was predicted to likely affect protein structure/function (rs36844177 in *Mapk10,* SIFT=0.01 and rs29465940 in *Rtn4*, SIFT=0.03). Thus, in the BXD strain set, only three genes known to be associated with axonal regeneration, *Fgf2, Mapk10* (JNK3)*,* and *Rtn4* (NOGO), are actively different between C57BL/6J and DBA/2J mice and potentially contribute to the different response of axonal regeneration across the BXD strains.

DISCUSSION

Over the past several years, advances in optic nerve axon regeneration have taken what was once thought of as an unachievable goal to the point where axonal regrowth after injury is a reality. Several different protocols are being used to promote axonal regeneration[2, 5, 37]. In the present study, we chose a popular protocol developed by others[3, 4] that involves knocking down *Pten* and causing a mild inflammatory response. The BXD recombinant strains are ideal for testing the effects of genetic background with the protocol of knocking down *Pten*, for there are not significant differences in *Pten* between the C57BL/6J strain and the DBA/2J strains. There are no non-synonymous SNPs found in the *Pten* gene between C57BL/6J and DBA/2J mice. Furthermore, there is a similar level of expression of *Pten* mRNA across all of the BXD strains in the DoD normal retina datasets housed on GeneNetwork. The injection of zymosan is believed to involve the activation of an inflammatory response and activation of macrophages[38], stimulating the release of oncomodulin[39]. When we examine the BXD RI

strains there is no significant difference in the levels of oncomodulin message and there are no nonsynonymous SNPs within the gene. That being said we do know that there is a significant immune network in the retina of the BXD RI strains and that this network is activated by optic nerve crush[23] and blast injury[24]**.** We also examined transfection efficiency in two strains (BXD29 and C57BL/6J) that respond differently to the regeneration treatment. There was no difference in transfection efficiency between these two strains. Thus, the difference in the axon regeneration we observed between the different BXD strains cannot be explained by the expression levels of *Pten* in the strains or a differential level of transfection by the AAV2 vector. This leaves only one possibility that the difference in axonal regeneration we observed is due to the specific segregation of genomic elements cross the BXD strains.

Using the BXD strains we were able to demonstrate the effect of genetic background on the regenerative capacity of axons in the optic nerve. In all strains tested, the amount of regeneration was considerably greater than that observed in mice that did not receive the *Pten*/Zymosan/cAMP treatment. The regeneration responses of C57BL/6J mice we observed were not as strong as described in other studies, a possible reason could be that we were using AAV-shPTEN-GFP to knock down *Pten* instead of cre recombinase-mediated *Pten* knock out. The other factor to be noticed is that the age of mice we used are over 60 days at the time of initial treatment, much older than reported in other studies[3, 4]. This also provides strong evidence that the regeneration response can happen not only in young adult mice but also in older mice. Among the strains treated to promote regeneration, some strains, like BXD102, showed a modest regenerative response; while other strains, like BXD 29, consistently demonstrated a high number of regenerating axons and axons that traveled longer distances down the injured optic nerve. When the response of the parental strains C57BL/6J and DBA/2J was compared to the BXD strains with extreme regenerative responses, there was a clear indication of genetic transgression. If we look at the number of axons at 0.5mm and 1mm from the crush site (Figure 4), there are BXD strains that have fewer axons and BXD strains that have more axons than the parental strains. This difference in regeneration is indicative of genetic transgression. These data reveal that it is not a single genomic locus causing the variability in the regenerative response, for if that were the case the extremes would be similar to the parental strains. This is a clear indication that multiple genomic loci are segregating across the BXD

strains to affect the regenerative response of the optic nerve axons. Thus, axon regeneration is a complex trait with multiple modulating genomic loci in the BXD strains.

Other studies have looked at multiple inbred strains of mice, identifying an increased regenerative capacity in the neurons of the CAST/Ei strain[8]. In this study, the authors identified *Inhba* as the contributing genetic element to the increased regenerative capacity. Interestingly, neurons form the BXD parental strains (C57BL/6 and DBA/2J mice) were also tested in this tissue culture system and neurons from these two strains did not grow well on inhibitory substrates. These data indicate that the genomic elements facilitating regeneration in the CAST/Ei strain is not present in the BXD strain set. In fact, when we examine *Inhba* in the DoD Normal Retinal database on GeneNetwork, this gene does not vary significantly across the strains and it does not display a significant QTL. Furthermore, there are no nonsynonymus SNPs in *Inhba* between the C57BL/6J and DBA/2J strains. These data suggest that novel elements are segregating across the BXD strain modulating regenerative capacity.

A complex trait could be driven by a handful of protein coding genes as well as noncoding variants that presumably affect gene regulation[40]. Multiple genes have been identified in recent years to have an impact on axon regeneration (Table 1). It is possible that some or all of these pathways are varying in the BXD strains and are influencing the outcome of the induced regeneration observed in the present study. With the DoD normal retina datasets[36] and the bioinformatic tools hosted on GeneNetwork, we examined all of the known regeneration-related genes to determine if they were able to modulate the regenerative response across the strains by having either cis-QTLs (differentially expressed genes) or non-synonymous SNPs that would affect protein function. Of all of the known genes known to alter the regenerative response of optic nerve axons, only two were potential candidates for modulating regeneration in the BXD strains. The only cis-QTL in the list of genes was *Fgf2* (LRS = 67.8). SNP analysis identified 8 genes with nonsynonymous SNPs in the list of regeneration genes (Table 1). All of the nonsynonymous SNPs were examined using a SIFT analysis and only 2 SNPs (rs36844177 in *Mapk10*(JNK3) and rs29465940 in *Rtn4*(NOGO)) was predicted to alter protein function. Therefore, three possible genomic elements that could be affecting regeneration in the BXD strains are *Fgf2* (Chr3, 37.3 Mb), *Mapk10* (Chr5, 102.9Mb) and *Rtn4* (Chr11, 29.7Mb). Beyond

all these, we believe that there are still unknown genomic elements modulating the regenerative response of the axons.

In conclusion, the ability of optic nerve regeneration response to injury is different across BXD strains given different genetic background. Quantitative trait analysis may provide us with new insights to axon regeneration, and maybe new loci of novel genes or non-coding elements that are involved in axon regeneration. Ongoing experiments are increasing the number of strains in the experimental dataset to define genomic loci modulating optic nerve regeneration.

Acknowledgements:

This study was supported by an Unrestricted Grand from Research to Prevent Blindness, NEI grant R01EY017841 (E.E.G.), W81XWH-12-1-0225 (E.E.G.) Owens Family Glaucoma Research Fund, P30EY06360 (Emory Vision Core). We would like to thank the Emory Viral Vector Core for the production of AAV (NINDS Core Facilities Grant P30NS055077) and the Emory Integrated Genomics Core (subsidized by the Emory University School of Medicine and NIH UL1TR002378). The content is solely the responsibility of the authors and does not necessarily reflect the official views of the National Institutes of Health.

Conflicts of Interest: The authors declare that they have no competing interests.

REFERENCES

1. Park KK, Liu K, Hu Y, Smith PD, Wang C, Cai B, Xu B, Connolly L, Kramvis I, Sahin M, He Z. Promoting axon regeneration in the adult CNS by modulation of the PTEN/mTOR pathway. Science 2008; 322(5903):963-6.
2. Moore DL, Blackmore MG, Hu Y, Kaestner KH, Bixby JL, Lemmon VP, Goldberg JL. KLF family members regulate intrinsic axon regeneration ability. Science 2009; 326(5950):298-301.
3. Kurimoto T, Yin Y, Omura K, Gilbert HY, Kim D, Cen LP, Moko L, Kugler S, Benowitz LI. Long-distance axon regeneration in the mature optic nerve: contributions of oncomodulin, cAMP, and pten gene deletion. J Neurosci 2010; 30(46):15654-63.
4. de Lima S, Koriyama Y, Kurimoto T, Oliveira JT, Yin Y, Li Y, Gilbert HY, Fagiolini M, Martinez AM, Benowitz L. Full-length axon regeneration in the adult mouse optic nerve and partial recovery of simple visual behaviors. Proc Natl Acad Sci U S A 2012; 109(23):9149-54.
5. Norsworthy MW, Bei F, Kawaguchi R, Wang Q, Tran NM, Li Y, Brommer B, Zhang Y, Wang C, Sanes JR, Coppola G, He Z. Sox11 Expression Promotes Regeneration of Some Retinal Ganglion Cell Types but Kills Others. Neuron 2017; 94(6):1112-20 e4.
6. Benowitz LI, He Z, Goldberg JL. Reaching the brain: Advances in optic nerve regeneration. Experimental neurology 2015.
7. Barber A, Farmer K, Martin KR, Smith PD. Retinal regeneration mechanisms linked to multiple cancer molecules: A therapeutic conundrum. Prog Retin Eye Res 2017; 56:19-31.
8. Omura T, Omura K, Tedeschi A, Riva P, Painter MW, Rojas L, Martin J, Lisi V, Huebner EA, Latremoliere A, Yin Y, Barrett LB, Singh B, Lee S, Crisman T, Gao F, Li S, Kapur K, Geschwind DH, Kosik KS, Coppola G, He Z, Carmichael ST, Benowitz LI, Costigan M, Woolf CJ. Robust Axonal Regeneration Occurs in the Injured CAST/Ei Mouse CNS. Neuron 2015; 86(5):1215-27.
9. Chen DF, Schneider GE, Martinou JC, Tonegawa S. Bcl-2 promotes regeneration of severed axons in mammalian CNS. Nature 1997; 385(6615):434-9.
10. Wang KC, Koprivica V, Kim JA, Sivasankaran R, Guo Y, Neve RL, He Z. Oligodendrocyte-myelin glycoprotein is a Nogo receptor ligand that inhibits neurite outgrowth. Nature 2002; 417(6892):941-4.
11. Williams PR, He Z. Building bridges to regenerate axons. Science 2016; 354(6312):544-5.
12. Solovieff N, Cotsapas C, Lee PH, Purcell SM, Smoller JW. Pleiotropy in complex traits: challenges and strategies. Nat Rev Genet 2013; 14(7):483-95.
13. Civelek M, Lusis AJ. Systems genetics approaches to understand complex traits. Nat Rev Genet 2014; 15(1):34-48.
14. Geisert EE, Lu L, Freeman-Anderson NE, Templeton JP, Nassr M, Wang X, Gu W, Jiao Y, Williams RW. Gene expression in the mouse eye: an online resource for genetics using 103 strains of mice. Mol Vis 2009; 15:1730-63.
15. Harder JM, Ding Q, Fernandes KA, Cherry JD, Gan L, Libby RT. BCL2L1 (BCL-X) promotes survival of adult and developing retinal ganglion cells. Mol Cell Neurosci 2012; 51(1-2):53-9.
16. Fernandes KA, Harder JM, Kim J, Libby RT. JUN regulates early transcriptional responses to axonal injury in retinal ganglion cells. Exp Eye Res 2013; 112:106-17.

17. Koprivica V, Cho KS, Park JB, Yiu G, Atwal J, Gore B, Kim JA, Lin E, Tessier-Lavigne M, Chen DF, He Z. EGFR activation mediates inhibition of axon regeneration by myelin and chondroitin sulfate proteoglycans. Science 2005; 310(5745):106-10.
18. Hoyng SA, De Winter F, Gnavi S, de Boer R, Boon LI, Korvers LM, Tannemaat MR, Malessy MJ, Verhaagen J. A comparative morphological, electrophysiological and functional analysis of axon regeneration through peripheral nerve autografts genetically modified to overexpress BDNF, CNTF, GDNF, NGF, NT3 or VEGF. Exp Neurol 2014; 261:578-93.
19. Cui Q, Lu Q, So KF, Yip HK. CNTF, not other trophic factors, promotes axonal regeneration of axotomized retinal ganglion cells in adult hamsters. Invest Ophthalmol Vis Sci 1999; 40(3):760-6.
20. Benowitz LI, He Z, Goldberg JL. Reaching the brain: Advances in optic nerve regeneration. Exp Neurol 2017; 287(Pt 3):365-73.
21. Yiu G, He Z. Glial inhibition of CNS axon regeneration. Nat Rev Neurosci 2006; 7(8):617-27.
22. Silver J, Miller JH. Regeneration beyond the glial scar. Nat Rev Neurosci 2004; 5(2):146-56.
23. Templeton JP, Freeman NE, Nickerson JM, Jablonski MM, Rex TS, Williams RW, Geisert EE. Innate immune network in the retina activated by optic nerve crush. Invest Ophthalmol Vis Sci 2013; 54(4):2599-606.
24. Struebing FL, King R, Li Y, Chrenek MA, Lyuboslavsky PN, Sidhu CS, Iuvone PM, Geisert EE. Transcriptional Changes in the Mouse Retina Following Ocular Blast Injury: A Role for the Immune System. J Neurotrauma 2017.
25. Williams RW, Williams EG. Resources for Systems Genetics. Methods Mol Biol 2017; 1488:3-29.
26. Mulligan MK, Mozhui K, Prins P, Williams RW. GeneNetwork: A Toolbox for Systems Genetics. Methods Mol Biol 2017; 1488:75-120.
27. Zukor K, Belin S, Wang C, Keelan N, Wang X, He Z. Short hairpin RNA against PTEN enhances regenerative growth of corticospinal tract axons after spinal cord injury. J Neurosci 2013; 33(39):15350-61.
28. Templeton JP, Geisert EE. A practical approach to optic nerve crush in the mouse. Mol Vis 2012; 18:2147-52.
29. Moy AJ, Capulong BV, Saager RB, Wiersma MP, Lo PC, Durkin AJ, Choi B. Optical properties of mouse brain tissue after optical clearing with FocusClear. J Biomed Opt 2015; 20(9):95010.
30. Diekmann H, Kalbhen P, Fischer D. Characterization of optic nerve regeneration using transgenic zebrafish. Front Cell Neurosci 2015; 9:118.
31. Leon S, Yin Y, Nguyen J, Irwin N, Benowitz LI. Lens injury stimulates axon regeneration in the mature rat optic nerve. J Neurosci 2000; 20(12):4615-26.
32. Kwong JM, Caprioli J, Piri N. RNA binding protein with multiple splicing: a new marker for retinal ganglion cells. Invest Ophthalmol Vis Sci 2010; 51(2):1052-8.
33. Rodriguez AR, de Sevilla Muller LP, Brecha NC. The RNA binding protein RBPMS is a selective marker of ganglion cells in the mammalian retina. J Comp Neurol 2014; 522(6):1411-43.

34. Kumar P, Henikoff S, Ng PC. Predicting the effects of coding non-synonymous variants on protein function using the SIFT algorithm. Nat Protoc 2009; 4(7):1073-81.
35. Freeman NE, Templeton JP, Orr WE, Lu L, Williams RW, Geisert EE. Genetic networks in the mouse retina: growth associated protein 43 and phosphatase tensin homolog network. Mol Vis 2011; 17:1355-72.
36. King R, Lu L, Williams RW, Geisert EE. Transcriptome networks in the mouse retina: An exon level BXD RI database. Mol Vis 2015; 21:1235-51.
37. Smith PD, Sun F, Park KK, Cai B, Wang C, Kuwako K, Martinez-Carrasco I, Connolly L, He Z. SOCS3 deletion promotes optic nerve regeneration in vivo. Neuron 2009; 64(5):617-23.
38. Yin Y, Cui Q, Li Y, Irwin N, Fischer D, Harvey AR, Benowitz LI. Macrophage-derived factors stimulate optic nerve regeneration. J Neurosci 2003; 23(6):2284-93.
39. Yin Y, Henzl MT, Lorber B, Nakazawa T, Thomas TT, Jiang F, Langer R, Benowitz LI. Oncomodulin is a macrophage-derived signal for axon regeneration in retinal ganglion cells. Nat Neurosci 2006; 9(6):843-52.
40. Boyle EA, Li YI, Pritchard JK. An Expanded View of Complex Traits: From Polygenic to Omnigenic. Cell 2017; 169(7):1177-86.
41. Sapieha PS, Peltier M, Rendahl KG, Manning WC, Di Polo A. Fibroblast growth factor-2 gene delivery stimulates axon growth by adult retinal ganglion cells after acute optic nerve injury. Mol Cell Neurosci 2003; 24(3):656-72.
42. Apara A, Galvao J, Wang Y, Blackmore M, Trillo A, Iwao K, Brown DP, Jr., Fernandes KA, Huang A, Nguyen T, Ashouri M, Zhang X, Shaw PX, Kunzevitzky NJ, Moore DL, Libby RT, Goldberg JL. KLF9 and JNK3 Interact to Suppress Axon Regeneration in the Adult CNS. J Neurosci 2017; 37(40):9632-44.
43. Geoffroy CG, Lorenzana AO, Kwan JP, Lin K, Ghassemi O, Ma A, Xu N, Creger D, Liu K, He Z, Zheng B. Effects of PTEN and Nogo Codeletion on Corticospinal Axon Sprouting and Regeneration in Mice. J Neurosci 2015; 35(16):6413-28.
44. Bodrikov V, Welte C, Wiechers M, Weschenfelder M, Kaur G, Shypitsyna A, Pinzon-Olejua A, Bastmeyer M, Stuermer CAO. Substrate properties of zebrafish Rtn4b/Nogo and axon regeneration in the zebrafish optic nerve. J Comp Neurol 2017.
45. Baldwin KT, Carbajal KS, Segal BM, Giger RJ. Neuroinflammation triggered by beta-glucan/dectin-1 signaling enables CNS axon regeneration. Proc Natl Acad Sci U S A 2015; 112(8):2581-6.
46. Sagawa H, Terasaki H, Nakamura M, Ichikawa M, Yata T, Tokita Y, Watanabe M. A novel ROCK inhibitor, Y-39983, promotes regeneration of crushed axons of retinal ganglion cells into the optic nerve of adult cats. Exp Neurol 2007; 205(1):230-40.
47. Koch JC, Tonges L, Barski E, Michel U, Bahr M, Lingor P. ROCK2 is a major regulator of axonal degeneration, neuronal death and axonal regeneration in the CNS. Cell Death Dis 2014; 5:e1225.
48. Legacy J, Hanea S, Theoret J, Smith PD. Granulocyte macrophage colony-stimulating factor promotes regeneration of retinal ganglion cells in vitro through a mammalian target of rapamycin-dependent mechanism. J Neurosci Res 2013; 91(6):771-9.
49. Cavalli V, Holtzman DM. B-RAF unlocks axon regeneration. J Exp Med 2014; 211(5):746.

50. O'Donovan KJ, Ma K, Guo H, Wang C, Sun F, Han SB, Kim H, Wong JK, Charron J, Zou H, Son YJ, He Z, Zhong J. B-RAF kinase drives developmental axon growth and promotes axon regeneration in the injured mature CNS. J Exp Med 2014; 211(5):801-14.
51. Belin S, Nawabi H, Wang C, Tang S, Latremoliere A, Warren P, Schorle H, Uncu C, Woolf CJ, He Z, Steen JA. Injury-induced decline of intrinsic regenerative ability revealed by quantitative proteomics. Neuron 2015; 86(4):1000-14.
52. Leibinger M, Muller A, Andreadaki A, Hauk TG, Kirsch M, Fischer D. Neuroprotective and axon growth-promoting effects following inflammatory stimulation on mature retinal ganglion cells in mice depend on ciliary neurotrophic factor and leukemia inhibitory factor. J Neurosci 2009; 29(45):14334-41.
53. Zhang JN, Koch JC. Collapsin response mediator protein-2 plays a major protective role in acute axonal degeneration. Neural Regen Res 2017; 12(5):692-5.
54. Kaneko A, Kiryu-Seo S, Matsumoto S, Kiyama H. Damage-induced neuronal endopeptidase (DINE) enhances axonal regeneration potential of retinal ganglion cells after optic nerve injury. Cell Death Dis 2017; 8(6):e2847.
55. Watkins TA, Wang B, Huntwork-Rodriguez S, Yang J, Jiang Z, Eastham-Anderson J, Modrusan Z, Kaminker JS, Tessier-Lavigne M, Lewcock JW. DLK initiates a transcriptional program that couples apoptotic and regenerative responses to axonal injury. Proc Natl Acad Sci U S A 2013; 110(10):4039-44.
56. Leibinger M, Andreadaki A, Golla R, Levin E, Hilla AM, Diekmann H, Fischer D. Boosting CNS axon regeneration by harnessing antagonistic effects of GSK3 activity. Proc Natl Acad Sci U S A 2017; 114(27):E5454-E63.
57. Miao L, Yang L, Huang H, Liang F, Ling C, Hu Y. mTORC1 is necessary but mTORC2 and GSK3beta are inhibitory for AKT3-induced axon regeneration in the central nervous system. Elife 2016; 5:e14908.
58. Simpson MT, Venkatesh I, Callif BL, Thiel LK, Coley DM, Winsor KN, Wang Z, Kramer AA, Lerch JK, Blackmore MG. The tumor suppressor HHEX inhibits axon growth when prematurely expressed in developing central nervous system neurons. Mol Cell Neurosci 2015; 68:272-83.
59. Liu Y, Yu H, Deaton SK, Szaro BG. Heterogeneous nuclear ribonucleoprotein K, an RNA-binding protein, is required for optic axon regeneration in Xenopus laevis. J Neurosci 2012; 32(10):3563-74.
60. Duan X, Qiao M, Bei F, Kim IJ, He Z, Sanes JR. Subtype-specific regeneration of retinal ganglion cells following axotomy: effects of osteopontin and mTOR signaling. Neuron 2015; 85(6):1244-56.
61. Elsaeidi F, Bemben MA, Zhao XF, Goldman D. Jak/Stat signaling stimulates zebrafish optic nerve regeneration and overcomes the inhibitory actions of Socs3 and Sfpq. J Neurosci 2014; 34(7):2632-44.
62. Qin S, Zou Y, Zhang CL. Cross-talk between KLF4 and STAT3 regulates axon regeneration. Nat Commun 2013; 4:2633.
63. Apara A, Goldberg JL. Molecular mechanisms of the suppression of axon regeneration by KLF transcription factors. Neural Regen Res 2014; 9(15):1418-21.
64. Veldman MB, Bemben MA, Thompson RC, Goldman D. Gene expression analysis of zebrafish retinal ganglion cells during optic nerve regeneration identifies KLF6a and KLF7a as important regulators of axon regeneration. Dev Biol 2007; 312(2):596-612.

65. Ogai K, Kuwana A, Hisano S, Nagashima M, Koriyama Y, Sugitani K, Mawatari K, Nakashima H, Kato S. Upregulation of leukemia inhibitory factor (LIF) during the early stage of optic nerve regeneration in zebrafish. PLoS One 2014; 9(8):e106010.
66. Fischer D, He Z, Benowitz LI. Counteracting the Nogo receptor enhances optic nerve regeneration if retinal ganglion cells are in an active growth state. J Neurosci 2004; 24(7):1646-51.
67. Chen C, Chen X, Yin X, Yuan R, Wang B, Ye J. NgR RNA interference, combined with zymosan intravitreal injection, enhances optic nerve regeneration. J Neurochem 2009; 110(5):1628-34.
68. Deiner MS, Kennedy TE, Fazeli A, Serafini T, Tessier-Lavigne M, Sretavan DW. Netrin-1 and DCC mediate axon guidance locally at the optic disc: loss of function leads to optic nerve hypoplasia. Neuron 1997; 19(3):575-89.
69. Dun XP, Parkinson DB. Role of Netrin-1 Signaling in Nerve Regeneration. Int J Mol Sci 2017; 18(3).
70. Shen Y, Tenney AP, Busch SA, Horn KP, Cuascut FX, Liu K, He Z, Silver J, Flanagan JG. PTPsigma is a receptor for chondroitin sulfate proteoglycan, an inhibitor of neural regeneration. Science 2009; 326(5952):592-6.
71. Fischer D, Petkova V, Thanos S, Benowitz LI. Switching mature retinal ganglion cells to a robust growth state in vivo: gene expression and synergy with RhoA inactivation. J Neurosci 2004; 24(40):8726-40.
72. Koch JC, Tonges L, Michel U, Bahr M, Lingor P. Viral vector-mediated downregulation of RhoA increases survival and axonal regeneration of retinal ganglion cells. Front Cell Neurosci 2014; 8:273.
73. Bertrand J, Winton MJ, Rodriguez-Hernandez N, Campenot RB, McKerracher L. Application of Rho antagonist to neuronal cell bodies promotes neurite growth in compartmented cultures and regeneration of retinal ganglion cell axons in the optic nerve of adult rats. J Neurosci 2005; 25(5):1113-21.
74. Heskamp A, Leibinger M, Andreadaki A, Gobrecht P, Diekmann H, Fischer D. CXCL12/SDF-1 facilitates optic nerve regeneration. Neurobiol Dis 2013; 55:76-86.
75. Trakhtenberg EF, Wang Y, Morkin MI, Fernandez SG, Mlacker GM, Shechter JM, Liu X, Patel KH, Lapins A, Yang S, Dombrowski SM, Goldberg JL. Regulating Set-beta's Subcellular Localization Toggles Its Function between Inhibiting and Promoting Axon Growth and Regeneration. J Neurosci 2014; 34(21):7361-74.
76. Sun F, Park KK, Belin S, Wang D, Lu T, Chen G, Zhang K, Yeung C, Feng G, Yankner BA, He Z. Sustained axon regeneration induced by co-deletion of PTEN and SOCS3. Nature 2011; 480(7377):372-5.
77. Welsbie DS, Mitchell KL, Jaskula-Ranga V, Sluch VM, Yang Z, Kim J, Buehler E, Patel A, Martin SE, Zhang PW, Ge Y, Duan Y, Fuller J, Kim BJ, Hamed E, Chamling X, Lei L, Fraser IDC, Ronai ZA, Berlinicke CA, Zack DJ. Enhanced Functional Genomic Screening Identifies Novel Mediators of Dual Leucine Zipper Kinase-Dependent Injury Signaling in Neurons. Neuron 2017; 94(6):1142-54 e6.
78. Weng YL, An R, Cassin J, Joseph J, Mi R, Wang C, Zhong C, Jin SG, Pfeifer GP, Bellacosa A, Dong X, Hoke A, He Z, Song H, Ming GL. An Intrinsic Epigenetic Barrier for Functional Axon Regeneration. Neuron 2017; 94(2):337-46 e6.

79. Tassew NG, Charish J, Shabanzadeh AP, Luga V, Harada H, Farhani N, D'Onofrio P, Choi B, Ellabban A, Nickerson PEB, Wallace VA, Koeberle PD, Wrana JL, Monnier PP. Exosomes Mediate Mobilization of Autocrine Wnt10b to Promote Axonal Regeneration in the Injured CNS. Cell Rep 2017; 20(1):99-111.
80. Li Y, Andereggen L, Yuki K, Omura K, Yin Y, Gilbert HY, Erdogan B, Asdourian MS, Shrock C, de Lima S, Apfel UP, Zhuo Y, Hershfinkel M, Lippard SJ, Rosenberg PA, Benowitz L. Mobile zinc increases rapidly in the retina after optic nerve injury and regulates ganglion cell survival and optic nerve regeneration. Proc Natl Acad Sci U S A 2017; 114(2):E209-E18.
81. Planchamp V, Bermel C, Tonges L, Ostendorf T, Kugler S, Reed JC, Kermer P, Bahr M, Lingor P. BAG1 promotes axonal outgrowth and regeneration in vivo via Raf-1 and reduction of ROCK activity. Brain 2008; 131(Pt 10):2606-19.

643
644

645 Table 1. Genetic characteristics of genes that are known to affect optic nerve regeneration
646 between C57BL/6J and DBA/2J mice.

Gene with cis-QTL	*Fgf2***[41]**
Genes with Non-synonymous SNPs	*Mapk10* [42], *Rtn4*[43, 44], *Ctgf*[11], *Tlr2*[45], *Rock1*[46], *Rock2*[46, 47], *Clec7a*[45], *Csf2*[48]
Other investigated genes (Genes that are found to have neither cis-QTL nor Non-synonymous SNPs)	*Braf[49, 50], Bcl2[9], Myc[51], Cntf[52] ,Dpysl2[53], Ecel1[54], Map3k12[55], Egfr [17], Gsk3b[56, 57], Hhex [58], Hnrnpk [59], Spp1[60], Stat3[2, 61, 62], Klf4[2, 62, 63], Klf6[2, 63, 64], Klf7[2, 63, 64], Klf9[2, 63], Lif[52, 65], Rtn4r[10, 66, 67], Ntn1[68, 69], Pten[1], Ptprs[70], Rhoa[71-73], Cxcl12[74], Set[75], Socs3[37, 76], Sox11[5, 77], Tet1[78], Tet3[78], Wnt10b[79], Slc30a3[80], Bag1 [81] Inhba[8]*

647

Figures:

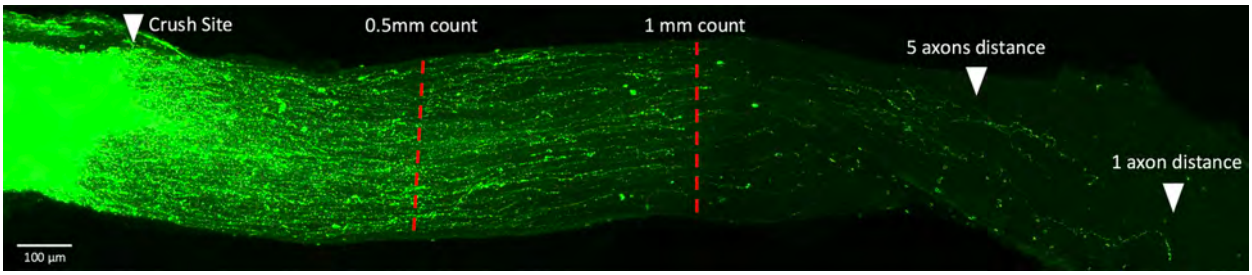

Figure 1. The regenerating axons in the optic nerve 14 days after optic nerve crush. We have indicated the regions of the nerve where axons were counted as well as the distance that 5 axons or 1 axon regenerated down the nerve. Scale bar represents 100 µm.

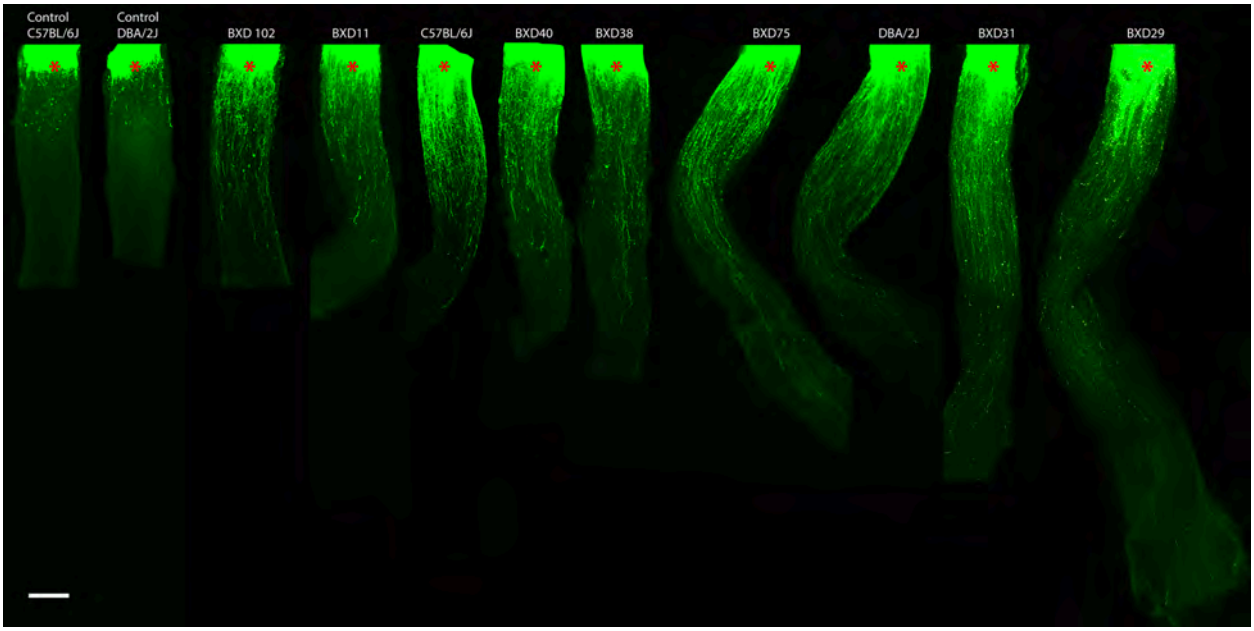

Figure 2 Genetic background affects regenerating axons in the optic nerve following crush. The figure is a series of photomicrographs from 11 optic nerves selected from 9 different strains of mice. The first two images on the far left are from control mice that did not receive the regeneration treatment prior to optic nerve crush (Control C57BL/6J and Control DBA/2J). All of the remaining nerves were from animals in which *Pten* was knocked-down and a mild inflammatory response was induced. The strain with the least regeneration was BXD102 and the strain with the greatest regeneration was BXD29. Red asterisks represent the crush site. The scale bar represents 200µm.

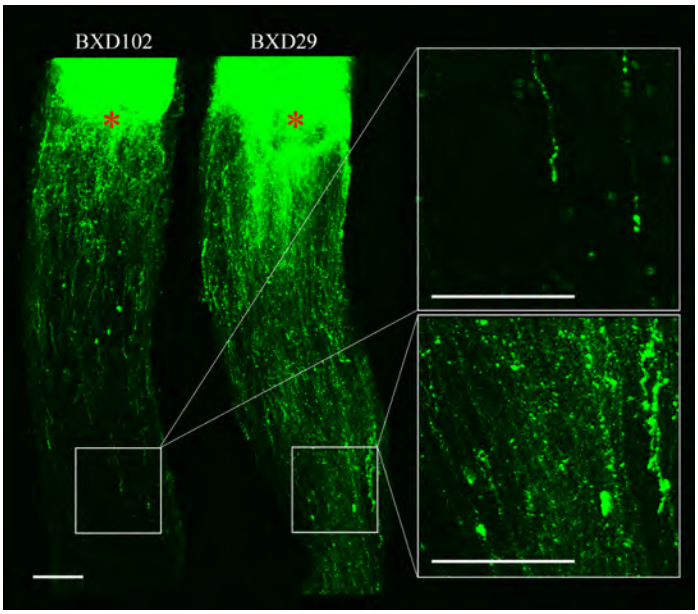

Figure 3. Comparison of regenerated axons in strains with the least regeneration (BXD102) and the greatest regeneration (BXD29). Higher magnification of axons at 1mm (Boxed region) from crush site were shown relatively. The scale bar represents 100μm.

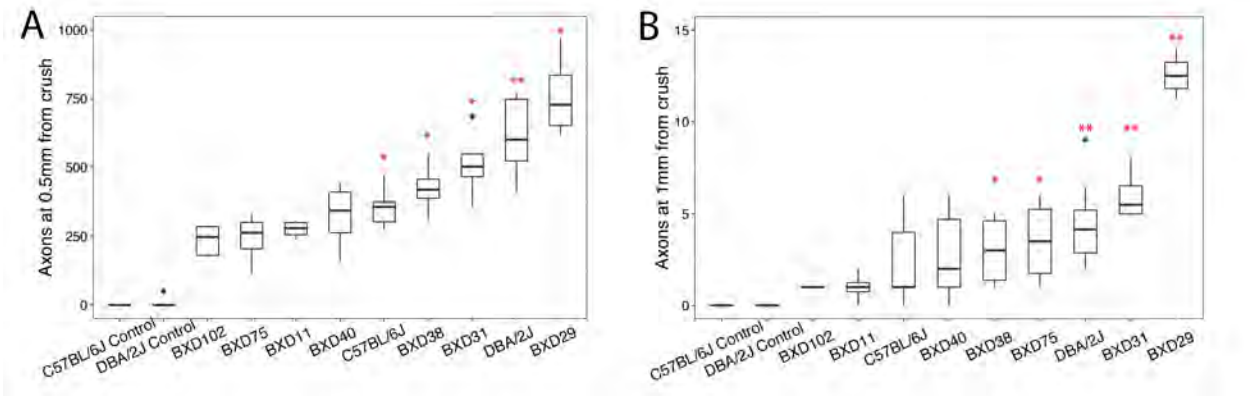

Figure 4: The number of axons at 0.5mm (A) and 1mm (B) from the crush site in two control strains (DBA/2J and C57BL/6J untreated mice) and in 9 strains treated with the regeneration protocol. Boxplots show median, 25th and 75th percentile, maximum, and minimum values for each BXD RI strain. Black dots: outliers. *: P<0.05 when compared with BXD102. **: P<0.01 when compared with BXD102.

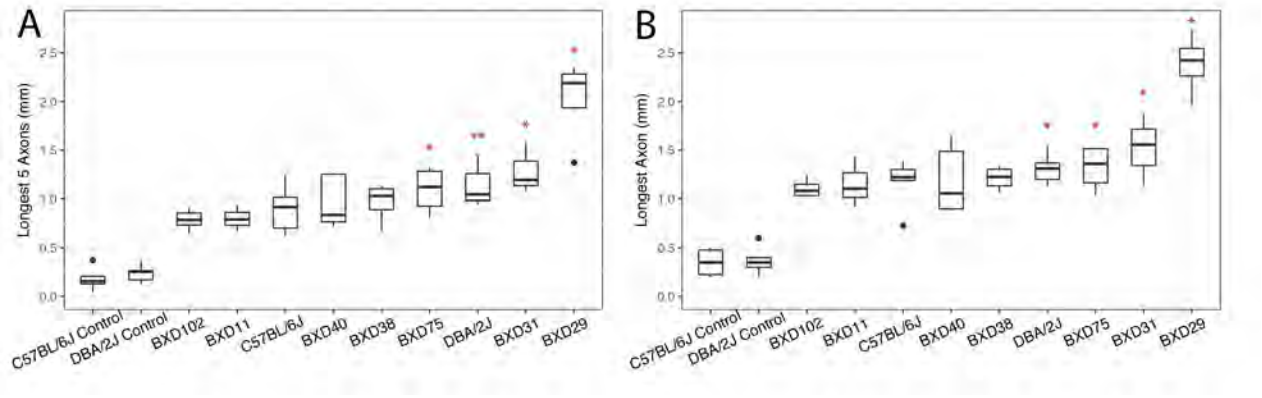

Figure 5: The longest distance that 5 axons regenerated (A) and the longest regeneration for a single axon (B) are shown for the two control strains (DBA/2J and C57BL/6J untreated mice) and in 9 strains treated with the regeneration protocol. Boxplots show median, 25th and 75th percentile, maximum, and minimum values for each BXD RI strain. Black dots: outliers. *: P<0.05 when compared with BXD102. **: P<0.01 when compared with BXD102.

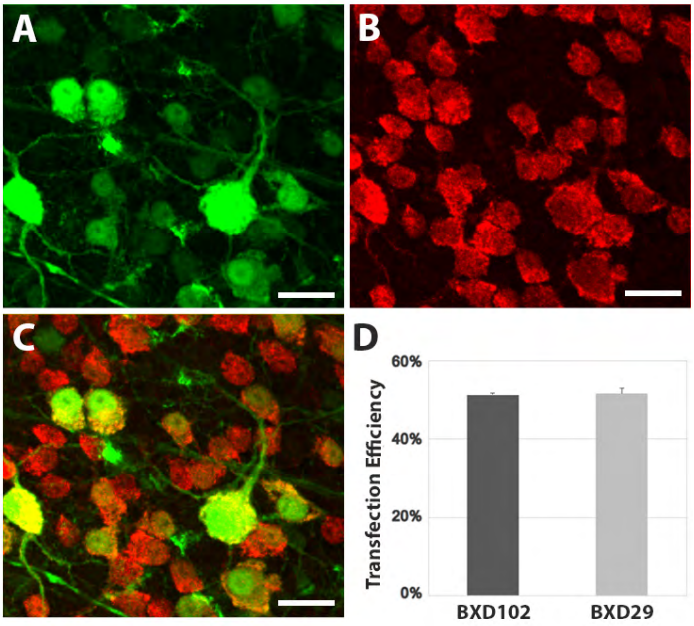

Figure 6. Transfection Efficiency of AAV-shPTEN-GFP. AAV transfected cells are labeled by GFP in green (A) and total number of RGCs are labeled by RBPMS in red (B). Merged channel shown in (C). No statistical difference of transfection efficiency was found between BXD102 mice and BXD29 mice (D). Scale bar represents 10 μm.

Supplementary data:

Supplementary Method:

Evaluation of *Pten* knock down by immunofluorescence staining

Six C57BL/6J mice were deeply anesthetized with a mixture of 15 mg/kg of xylazine and 100 mg/kg of ketamine and perfused through the heart with saline followed by 4% paraformaldehyde in phosphate buffer (pH 7.3). For the retinal flat mounts, the retinas were removed from the globe and rinsed in PBS with 1% Triton X-100, blocked in 5% Bovine Serum Albumin (BSA) 1 hour room temperature and placed in primary antibodies *Pten* (Cell Signaling, Cat. # 9559) at 1:200 and GFP (Novus Biologicals, CAT #NB100-1770) at 1:1000 4°C overnight. The retinas were rinsed with PBS and placed in secondary antibodies, (Anti-Goat IgG(H+L) CFTM 488A, Sigma, Cat. #SAB4600032 and Alexa Fluor 594 AffiniPure Donkey Anti-Rabbit, Jackson Immunoresearch, Cat. #711-585-152) at 1:1000 and To-PRO-3 Iodide (Molecular Probes, Cat. # T3605) was applied 1:1000 as a nuclear counterstain for 1 hour at room temperature. After three washes of 15 minutes each, retinas were flat mounted and cover-slipped using Fuoromount - G (Southern Biotech, Cat. #0100-01) as a mounting medium.

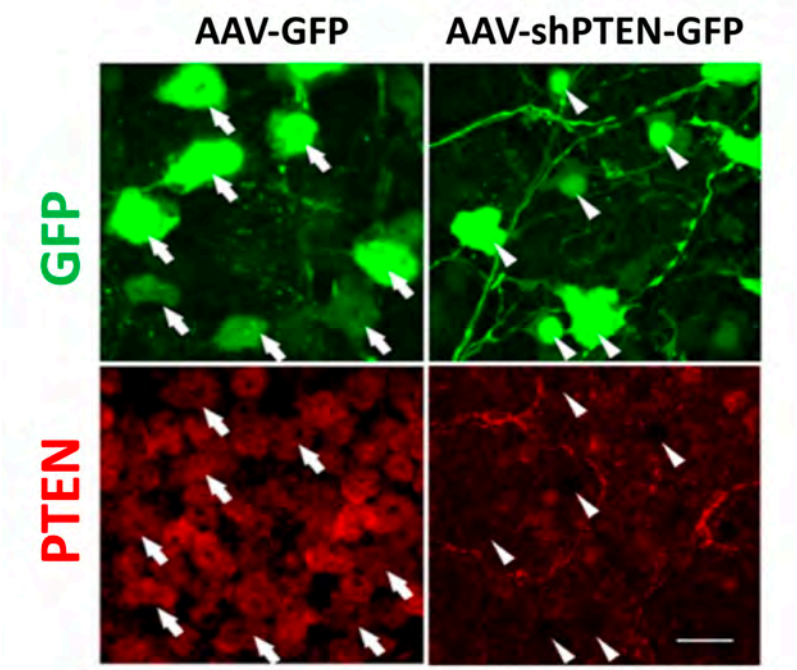

Supplemental figure 1. To determine if *Pten* was knocked down by our AAV treatment, we stained the retina for *Pten* (Red) in retinas injected with the AAV-GFP vector (control) or AAV-shPTEN-GFP to knock down *Pten*. In the control retina. all of the GFP positive cells were also well labeled for *Pten*. In the retinas that received the AAV-shPTEN-GFP, the transfected cells (GFP positive) had low levels of *Pten* staining indicating that the vector had in fact decreased the expression of *Pten*.

Supplementary Table 1. Summary of optic nerve regeneration in the BXD strains

Strains	N	Age (Days)*	Axons at 0.5mm from crush	Axons at 1mm from crush	Longest 5 Axons (µm)	Longest 1 Axon (µm)
C57BL/6J Control	6	67	0±0	0±0	179.2±45	350±56.3
DBA/2J Control	6	63	0±0	0±0	235.3±36.8	366.7±55.8
BXD102/RwwJ	5	61	236.1±24.4	1±0	787.2±46.5	1107±40.6
BXD11/TyJ	5	60	276.5±16.1	1±0.6	801.3±77.5	1152.7±149
C57BL/6J	5	67	356.3±34.0	2.4±1.1	902.2±110.9	1165.2±114.8
BXD40 /TyJ	9	62	321.5±39.2	2.7±0.8	962.1±87.5	1184.8±116.6
BXD38/TyJ	4	67	424.9±50.0	3±1	966.8±103.1	1210.5±63.2
BXD75/RwwJ	5	65	242.8±47.8	3.5±1.2	1090.8±122.8	1318±120.3
DBA/2J	8	63	612.5±48.8	4.5±0.8	1125.5±66.4	1298.1±49.2
BXD31/TyJ	4	61	511.4±67.2	6±1	1283.7±152.9	1519.3±216.7
BXD29 -Tlr4$^{lps\text{-}2J}$/J	4	65	759.8 ± 79.2	12.6±0.6	2025.5±223.3	2386.8±162.6

*: Ages of mice at the initial regeneration treatment (Day 0)

Supplementary Movie 1

Appendix H

PUBLIC RELEASE: 25-JAN-2018

Study finds genetic link between thinner corneas and increased risk of glaucoma

Studies in mice identify POU6F2 as important protein involved in corneal development and thickness

PLOS

Genetic studies in mice point to a protein called POU6F2, which can modulate corneal thickness, as a possible risk factor for glaucoma in humans, report Eldon Geisert of Emory University, and colleagues, January 25th in *PLOS Genetics*.

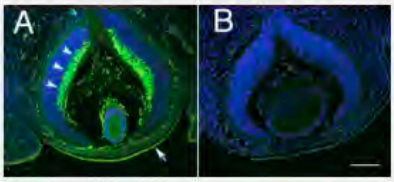

IMAGE: DISTRIBUTION OF POU6F2, IN THE EMBRYONIC EYE P15 IS ILLUSTRATED. IN SECTIONS STAINED FOR POU6F2 (A), THERE IS PROMINENT STAINING OF NEUROBLASTS DESTINED TO BECOME RETINAL GANGLION CELLS (ARROW HEADS).... view more ›

CREDIT: REBECCA KING AND COLLEAGUES

Glaucoma comprises a group of eye diseases that cause pressure to build up in the eye, which damages the optic nerve and ultimately leads to blindness. Multiple risk factors and underlying mutations contribute to glaucoma, but the best-known risk factor is having a thin cornea. Geisert and colleagues investigated genes that affect corneal thickness using strains of specially bred mice. They then compared genetic variants that lead to thin corneas in mice, to genes that increase a person's risk of a common type of glaucoma, called primary open angle glaucoma. The researchers identified a transcription factor called POU6F2, which is found in developing nerve cells in the retina and corneal cells in mice.

When they removed the gene that codes for POU6F2, the affected mice had thinner corneas than normal mice. Additionally, POU6F2 appears to help regulate the developing cornea and may also be responsible, in part, for the keeping the cornea healthy by regulating corneal stem cells in adult mice.

Overall, the new study suggests that genetic variations in the gene that codes for POU6F2 may affect the structure of the eye and increase a person's risk of glaucoma, but additional studies will be needed to describe the exact mechanism. Finding a genetic link between glaucoma and thin corneas has been difficult because while both traits run in families, a complicated mix of multiple genes and environmental conditions contribute to these complex traits. The role of POU6F2 in corneal development and thickness in mice, however, points to the gene as a possible risk factor for glaucoma in humans that deserves further investigation.

When they removed the gene that codes for POU6F2, the affected mice had thinner corneas than normal mice. Additionally, POU6F2 appears to help regulate the developing cornea and may also be responsible, in part, for the keeping the cornea healthy by regulating corneal stem cells in adult mice.

Overall, the new study suggests that genetic variations in the gene that codes for POU6F2 may affect the structure of the eye and increase a person's risk of glaucoma, but additional studies will be needed to describe the exact mechanism. Finding a genetic link between glaucoma and thin corneas has been difficult because while both traits run in families, a complicated mix of multiple genes and environmental conditions contribute to these complex traits. The role of POU6F2 in corneal development and thickness in mice, however, points to the gene as a possible risk factor for glaucoma in humans that deserves further investigation.

Eldon E. Geisert adds: "Glaucoma is a complex disease with many genetic and environmental factor influencing the patient population. Previous work by collaborators at Harvard and Duke identified many of these genetic factors; however, we currently only can account for approximately 7% of the genetic risk for glaucoma. We chose to use a well-defined mouse system to define genetic elements that can be directly related to human disease. It is our hope that defining this link between central corneal thickness and glaucoma will aid in early detection of glaucoma and eventually treatments to halt the progression of this disease."

###

In your coverage please use this URL to provide access to the freely available article in *PLOS Genetics*: http://journals.plos.org/plosgenetics/article?id=10.1371/journal.pgen.1007145

Citation: King R, Struebing FL, Li Y, Wang J, Koch AA, Cooke Bailey JN, et al. (2018) Genomic locus modulating corneal thickness in the mouse identifies POU6F2 as a potential risk of developing glaucoma. *PLoS Genet* 14(1): e1007145. https://doi.org/10.1371/journal.pgen.1007145

Funding: This study was supported by an Unrestricted Grant from Research to Prevent Blindness, National Eye Institute grant R01EY017841 (EEG); Owens Family Glaucoma Research Fund (EEG), DoD Grant W81XWH-12-1-0255 (EEG), P30EY06360 (Emory Vision Core) R01 EY022305 (JLW), P30EY014104 (JLW), National Institutes of Health grants 1R01-EY023646 (MAH), 5R01 EY019126 (MAH), 5P30-EY005722; Australian Research Council Future Fellowship (SM). NIH NCATS KL2TR000440 (JNCB). The funders of this research had no role in study design, data collection and analysis, decisions to publish or preparation of the manuscript.

Competing Interests: The authors have declared that no competing interests exist.

Genetic link between thinner corneas and increased risk of glaucoma

Studies in mice identify POU6F2 as important protein involved in corneal development and thickness

Date: January 25, 2018

Source: PLOS

Summary: Genetic studies in mice point to a protein called POU6F2, which can modulate corneal thickness, as a possible risk factor for glaucoma in humans, researchers report.

RELATED TOPICS

Health & Medicine

- Eye Care
- Genes
- Gene Therapy
- Personalized Medicine
- Asthma
- Workplace Health
- Multiple Sclerosis Research

FULL STORY

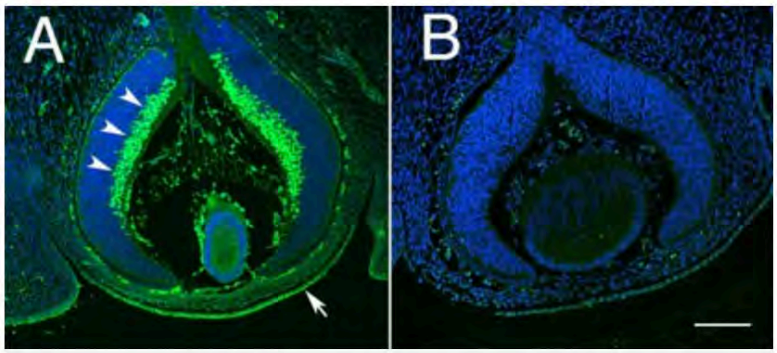

Distribution of POU6F2, in the embryonic eye P15 is illustrated. In sections stained for POU6F2 (A), there is prominent staining of neuroblasts destined to become retinal ganglion cells (arrow

Genetic link between thinner corneas and increased risk of glaucoma

Studies in mice identify POU6F2 as important protein involved in corneal development and thickness

Date: January 25, 2018

Source: PLOS

Summary: Genetic studies in mice point to a protein called POU6F2, which can modulate corneal thickness, as a possible risk factor for glaucoma in humans, researchers report.

Share:

RELATED TOPICS

Health & Medicine
- Eye Care
- Genes
- Gene Therapy
- Personalized Medicine
- Asthma
- Workplace Health
- Multiple Sclerosis Research
- Diseases and Conditions

FULL STORY

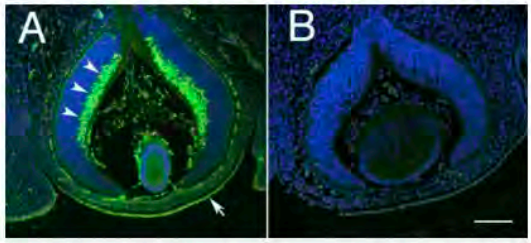

Distribution of POU6F2, in the embryonic eye P15 is illustrated. In sections stained for POU6F2 (A), there is prominent staining of neuroblasts destined to become retinal ganglion cells (arrow heads). There is also staining of the developing cornea and corneal epithelium (arrow). This staining is specific to the primary antibody for it is not present in sections in which the primary antibody was omitted (B) a secondary only control. Both sections are at the same magnification and the scale bar in B represents 100?m.

Credit: Rebecca King and colleagues

Genetic studies in mice point to a protein called POU6F2, which can modulate corneal thickness, as a possible risk factor for glaucoma in humans, report Eldon Geisert of Emory University, and colleagues, January 25th in *PLOS Genetics*.

Most Popular this week

HEALTH & MEDICINE


Researchers Create First Stem Cells Using CRISPR Genome Activation

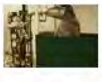
Flu May Be Spread Just by Breathing

Curcumin Improves Memory and

Genetic Link Between Corneal Thickness and Risk of Glaucoma

Posted on January 24, 2018

MedicalResearch.com Interview with:

— Dr. Geisert

Eldon E. Geisert, PhD
Professor of Ophthalmology
Emory School of Medicine

MedicalResearch.com: What is the background for this study? What are the main findings?

Response: In the late 1990s a group of doctors began a study of glaucoma patients to determine if there were phenotypes that are predictive for developing glaucoma.

In this Ocular Hypertension Treatment Study (OHTS) one of the highly correlated ocular traits was central corneal thickness (CCT). The early clinical studies found that people with thinner corneas were at a higher risk of developing glaucoma. In two large studies, examining thousands of people a number of genes were identified that were risk factors for glaucoma or that controlled CCT in humans. In both cases the identified genes accounted for less than 10% of the genetic risk for glaucoma and less than for 10% of the genetic control for CCT. There was little data linking the genetic control of CCT to the glaucoma risk.

Our group has taken an indirect approach to the question, using well-defined mouse genetic system to identify genes modulating CCT and then interrogating human glaucoma data to determine if these genes are associated with glaucoma risk.

MedicalResearch.com: What should readers take away from your report?

Response: Our group has identified a genetic link between corneal thickness and the risk for developing glaucoma. The gene encodes a transcription factor (POU6F2) that is involved in corneal development and that is expressed in a retinal cell type particularly susceptible to injury in the mouse. The identification of this link is a wonderful example of the use of mouse genetics to aid in understanding human disease.

MedicalResearch.com: What recommendations do you have for future research as a result of this work?

Response: Future studies will examine the role of POU6F2 in the retina following injury, identifying the molecular cascade that leads to the susceptibility of retinal ganglion cells to injury.

The identification of these molecular pathways may provide unique insights into methods to treat early phases of the glaucoma

MedicalResearch.com: Is there anything else you would like to add?

Response: Our studies hold the potential for improving human health, by providing a marker for early detection of glaucoma and potentially understanding why some of the cells in the retina are particularly sensitive to injury.

Finally, this study represents a true collaborative effort, involving many laboratories around the world including Emory University, Harvard University and Duke University. Our collaborative research efforts would not be possible without the Federal Funding from the National Eye Institute and a group of researchers willing to sit down and work together.

Citations:

Genomic Locus Modulating Corneal Thickness in the Mouse Identifies POU6F2 as a Potential Risk of Developing Glaucoma

Rebecca King, Felix L. Struebing, Ying Li, Jiaxing Wang, Allison Ashley Koch, Jessica Cooke Bailey, Puya Gharahkhan, Stuart MacGregor, R. Rand Allingham, Michael A. Hauser, Janey L. Wiggs, Eldon E. Geisert

doi: https://doi.org/10.1101/212605

eyewiretoday

FEATURED STORY JANUARY 26, 2018

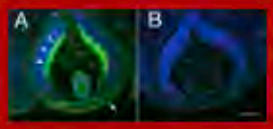

Study Finds Genetic Link Between Thinner Corneas and Increased Risk of Glaucoma

Genetic studies in mice point to a protein called POU6F2, which can modulate corneal thickness, as a possible risk factor for glaucoma in humans, report Eldon Geisert of Emory University, and colleagu...

Read More

Novartis Licenses Spark Therapeutics' Gene Therapy in All Markets Outside the US

Novartis announced a licensing agreement with Spark Therapeutics covering development, registration, and commercialization rights to voretigene neparvovec in markets outside the United States. Voretig…

Read More

Topcon's DRI OCT Triton Series Receives 510(k) Clearance

Topcon Medical Systems has announced that its DRI OCT Triton Series has received 510(k) clearance from the FDA. The DRI OCT Triton features easy image capture and a 1-micron, 1050nm-light source …

Study Finds Genetic Link Between Thinner Corneas and Increased Risk of Glaucoma

Source: PLOS Genetics

FRIDAY, JANUARY 26, 2018 | CORNEA , MEDICAL STUDIES

Genetic studies in mice point to a protein called POU6F2, which can modulate corneal thickness, as a possible risk factor for glaucoma in humans, report Eldon Geisert of Emory University, and colleagues, January 25 in *PLOS Genetics*.

Multiple risk factors and underlying mutations contribute to glaucoma, but the best-known risk factor is having a thin cornea. Geisert and colleagues investigated genes that affect corneal thickness using strains of specially bred mice. They then compared genetic variants that lead to thin corneas in mice, to genes that increase a person's risk of primary open angle glaucoma. The researchers identified a transcription factor called POU6F2, which is found in developing nerve cells in the retina and corneal cells in mice.

When they removed the gene that codes for POU6F2, the affected mice had thinner corneas than normal mice. Additionally, POU6F2 appears to help regulate the developing cornea and may also be responsible, in part, for the keeping the cornea healthy by regulating corneal stem cells in adult mice.

Overall, the new study suggests that genetic variations in the gene that codes for POU6F2 may affect the structure of the eye and increase a person's risk of glaucoma, but additional studies will be needed to describe the exact mechanism. Finding a genetic link between glaucoma and thin corneas has been difficult because while both traits run in families, a complicated mix of multiple genes and environmental conditions contribute to these complex traits. The role of POU6F2 in corneal development and thickness in mice, however, points to the gene as a possible risk factor for glaucoma in humans that deserves further investigation.

"Glaucoma is a complex disease with many genetic and environmental factor influencing the patient population. Previous work by collaborators at Harvard and Duke identified many of these genetic factors; however, we currently only can account for approximately 7% of the genetic risk for glaucoma," Eldon E. Geisert, said in a PLOS news release. "We chose to use a well-defined mouse system to define genetic elements that can be directly related to human disease. It is our hope that defining this link between central corneal thickness and glaucoma will aid in early detection of glaucoma and eventually treatments to halt the progression of this disease."

To read the PLOS Genetics study, click here.

Life Style | Health & Fitness

Thinner Corneas Linked To High Risk Of Eye Disease

The researchers found that while a complicated mix of multiple genes and alterations, as well as environmental conditions all, contribute to glaucoma, the most common risk factor among all is having a thin cornea

By **NewsGram Staff** - January 29, 2018// 6 0

The study, conducted on mice, found that genetic variations in the genes that codes for protein POU6F2 may affect the structure of the eye and increase a person's risk of glaucoma. Pixabay

- A protein that modulates corneal thickness can also act as a possible risk factor for a type of eye disease, a study has found
- The team investigated genes that affect corneal thickness using strains of specially bred mice
- The study was published in published in the journal Plos Genetics

A protein that modulates corneal thickness can also act as a possible risk factor for a type of eye disease, a study has found.

Glaucoma comprises of a group of eye diseases that builds up a pressure in the eye

RECENT POSTS

Firm Selling Fake Twitter Followers To Be Probed
January 29, 2018

Thinner Corneas Linked To High Risk Of Eye Disease
January 29, 2018

All You Need To Know About Kailash Satyarthi
January 29, 2018

Is Hindi The National Language of India?
January 29, 2018

Thinner corneas linked to high risk of eye disease

7 hours ago | 29-01-2018 | IANS

New York, Jan 29 : A protein that modulates corneal thickness can also act as a possible risk factor for a type of eye disease, a study has found.

Glaucoma comprises of a group of eye diseases that builds up pressure in the eye and damages the optic nerves, leading to blindness.

The study, conducted on mice, found that genetic variations in the genes that codes for protein POU6F2 may affect the structure of the eye and increase a person's risk of glaucoma.

When the researchers removed the genes carrying POU6F2, the affected mice had thinner corneas than normal mice.

The researchers found that while a complicated mix of multiple genes and alterations as well as environmental conditions all contribute to glaucoma, the most common risk factor among all is having a thin cornea.

"We hope that defining this link between central corneal thickness and glaucoma will aid in early detection of glaucoma and eventually treatments to halt the progression of this disease," said Eldon E. Geisert, Professor at the Emory University in Atlanta, US.

For the study, published in the journal Plos Genetics, the team investigated genes that affect corneal thickness using strains of specially bred mice.

They then compared genetic variants that lead to thin corneas in mice, to genes that increase a person's risk of a common type of glaucoma, called primary open angle glaucoma.

Additionally, POU6F2 was found to help regulate the developing cornea and may also be responsible, in part, for keeping the cornea healthy by regulating corneal stem cells in adult mice, the researchers said.

RECENT | POPULAR | RANDOM

General Mills Cereal Brings Invention and Creativity to the Breakfast Table through Rube Goldberg Partnership

THE DEAD DAISIES announce new Album "BURN IT DOWN" on April 6th, 2018

Royal Caribbean And CPP-The Myers-Briggs Company Team Up To Help Travelers Discover Their Adventure Personality

Monster Gathering of Rare Book Lovers Will Celebrate the 200th Anniversary of the Publication of Mary Shelley's Frankenstein

Is Word Processing As We Know It Over? This Startup Says Yes

Stella Artois And Water.org Team Up To Encourage Beer Lovers To Make Your Super Bowl Party Matter

PHOTO GALLERY

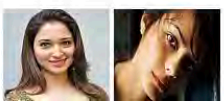

Thinner corneas linked to high risk of eye disease

January 29, 2018

New York, January 29 (IANS) A protein that modulates corneal thickness can also act as a possible risk factor for a type of eye disease, a study has found.

Glaucoma comprises of a group of eye diseases that builds up pressure in the eye and damages the optic nerves, leading to blindness.

The study, conducted on mice, found that genetic variations in the genes that codes for protein POU6F2 may affect the structure of the eye and increase a person's risk of glaucoma.

When the researchers removed the genes carrying POU6F2, the affected mice had thinner corneas than normal mice.

The researchers found that while a complicated mix of multiple genes and alterations as well as environmental conditions all contribute to glaucoma, the most common risk factor among all is having a thin cornea.

"We hope that defining this link between central corneal thickness and glaucoma will aid in early detection of glaucoma and eventually treatments to halt the progression of this disease," said Eldon E. Geisert, Professor at the Emory University in Atlanta, US.

For the study, published in the journal Plos Genetics, the team investigated genes that affect corneal thickness using strains of specially bred mice.

They then compared genetic variants that lead to thin corneas in mice, to genes that increase a person's risk of a common type of glaucoma, called primary open angle glaucoma.

Additionally, POU6F2 was found to help regulate the developing cornea and may also be responsible, in part, for keeping the cornea healthy by regulating corneal stem cells in adult mice, the researchers said.

Related post

Recent Post

Journalists celebrate 238th anniversary of India's first newspaper
Agra, January 29 (IANS) Journalists and social activists in the Taj city celebrated Hicky's... more»

No case for impeaching Chief Justice Misra, say former SC judges
New Delhi, January 29 (IANS) Former Supreme Court judges and legal luminaries have taken a dim view... more»

Tripura Governor's 'rail tracks sabotage' claim irks parties
Agartala, January 29 (IANS) Tripura Governor Tathagata Roy's "railway tracks... more»

Well within rights to build facility in Doklam: China
Beijing, January 29 (IANS) China on Monday said it is building military infrastructure in Doklam... more»

Modi's 'humble request' to MPs: Pass triple talaq Bill
New Delhi, January 29 (IANS) Prime Minister Narendra Modi on Monday made a "humble... more»

President pitches hard for Modi's pet theme of simultaneous polls
Prime Minister Narendra Modi and

Thinner corneas linked to high risk of eye disease

IANS **Indo Asian News Service**
IANS India Private Limited 29 January 2018

New York, Jan 29 (IANS) A protein that modulates corneal thickness can also act as a possible risk factor for a type of eye disease, a study has found.

Glaucoma comprises of a group of eye diseases that builds up pressure in the eye and damages the optic nerves, leading to blindness.

The study, conducted on mice, found that genetic variations in the genes that codes for protein POU6F2 may affect the structure of the eye and increase a person's risk of glaucoma.

When the researchers removed the genes carrying POU6F2, the affected mice had thinner corneas than normal mice.

The researchers found that while a complicated mix of multiple genes and alterations as well as environmental conditions all contribute to glaucoma, the most common risk factor among all is having a thin cornea.

"We hope that defining this link between central corneal thickness and glaucoma will aid in early detection of glaucoma and eventually treatments to halt the progression of this disease," said Eldon E. Geisert, Professor at the Emory University in Atlanta, US.

For the study, published in the journal Plos Genetics, the team investigated genes that affect corneal thickness using strains of specially bred mice.

They then compared genetic variants that lead to thin corneas in mice, to genes that increase a person's risk of a common type of glaucoma, called primary open angle glaucoma.

Additionally, POU6F2 was found to help regulate the developing cornea and may also be responsible, in part, for keeping the cornea healthy by regulating corneal stem cells in adult mice, the researchers said.

--IANS

ng/rt/him/vm

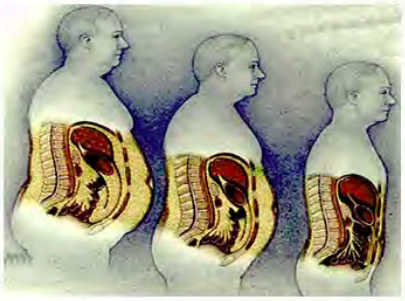

Thinner corneas linked to high risk of eye disease

IANS | New York
Last Updated at January 29, 2018 16:00 IST

Life & Style Health

Thinner corneas linked to high risk of eye disease

January 29, 2018

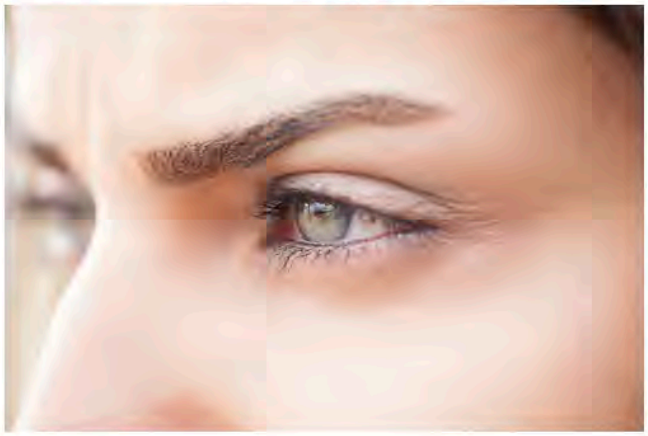

A protein that modulates corneal thickness can also act as a possible risk factor for a type of eye disease, a study has found. Glaucoma comprises of a group of eye diseases that builds up pressure in the eye and damages the optic nerves, leading to blindness.

The study, conducted on mice, found that genetic variations in the genes that codes for protein POU6F2 may affect the structure of the eye and increase a person's risk of glaucoma. When the researchers removed the genes carrying POU6F2, the affected mice had thinner corneas than normal mice.

The researchers found that while a complicated mix of multiple genes and alterations as well as environmental conditions all contribute to glaucoma, the most common risk factor among all is having a thin cornea.

"We hope that defining this link between central corneal thickness and glaucoma will aid in early detection of glaucoma and eventually treatments to halt the progression of this disease," said Eldon E. Geisert, Professor at the Emory University in Atlanta, US.

For the study, published in the journal Plos Genetics, the team investigated genes that affect corneal thickness using strains of specially bred mice.

They then compared genetic variants that lead to thin corneas in mice, to genes that increase a person's risk of a common type of glaucoma, called primary open angle glaucoma.

Additionally, POU6F2 was found to help regulate the developing cornea and may also be responsible, in part, for keeping the cornea healthy by regulating corneal stem cells in adult mice, the researchers said.

MOST POPULAR


IPL auction 2018: Chris Gayle bought by Kings XI Punjab in...
January 29, 2018

Archibald London is the New Age Luxury Brand that Should Be...
January 29, 2018

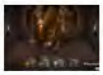
Lost Sphear Review: Short Of The Mark
January 29, 2018


Gerard Pique extends Barcelona contract until 2022
January 29, 2018

Load more

LATEST


Cricket
IPL auction 2018: Chris Gayle bought by Kings XI Punjab in...

Aviation
Archibald London is the New Age Luxury Brand that Should Be...

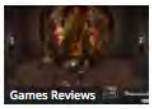
Games Reviews
Lost Sphear Review: Short Of The Mark

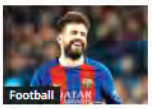
Football
Gerard Pique extends Barcelona contract until 2022

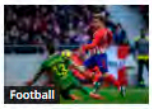
Football
Atletico Griezmann gets back on track with win over Las Palmas

Thinner corneas linked to high risk of eye disease

Posted By: news on: January 29, 2018 In: Lifestyle No Comments Print Email

A protein that modulates corneal thickness can also act as a possible risk factor for a type of eye disease, a study has found

A protein that modulates corneal thickness can also act as a possible risk factor for a type of eye disease, a study has found. Glaucoma comprises of a group of eye diseases that builds up pressure in the eye and damages the optic nerves, leading to blindness.

The study, conducted on mice, found that genetic variations in the genes that codes for protein POU6F2 may affect the structure of the eye and increase a person's risk of glaucoma.

When the researchers removed the genes carrying POU6F2, the affected mice had thinner corneas than normal mice.

The researchers found that while a complicated mix of multiple genes and alterations as well as environmental conditions all contribute to glaucoma, the most common risk factor among all is having a thin cornea.

"We hope that defining this link between central corneal thickness and glaucoma will aid in early detection of glaucoma and eventually treatments to halt the progression of this disease," said Eldon E. Geisert, Professor at the Emory University in Atlanta, US.

For the study, published in the journal Plos Genetics, the team investigated genes that affect corneal thickness using strains of specially bred mice.

They then compared genetic variants that lead to thin corneas in mice, to genes that increase a person's risk of a common type of glaucoma, called primary open angle glaucoma.

Additionally, POU6F2 was found to help regulate the developing cornea and may also be responsible, in part, for keeping the cornea healthy by regulating corneal stem cells in adult mice, the researchers said.

Catch up on all the latest Mumbai, National and International news here

WEATHER

Enter City...

Goa — Jan29 11:26 — NOW

Humidity 98%
Pressure 1014
Winds 2.81mph

23°C

TUE Jan30	Light Rain	
WED Jan31	Scattered Clouds	
THU Feb01	Light Rain	
FRI Feb02	Sky Is Clear	
SAT Feb03	Sky Is Clear	
SUN Feb04	Sky Is Clear	